Strengthening Steel Bridge Girders Using CFRP

By

Dr. Talat Salama and Mr. Ahmed Abd-El-Meguid
Department of Civil, Construction, and Environmental Engineering
The University of Alabama at Birmingham
Birmingham, AL

UTCA Theme: Management and Safety of Transportation Systems

Strengthening Steel Bridge Girders Using CFRP

By

Dr. Talat Salama and Mr. Ahmed Abd-El-Meguid
Department of Civil, Construction, and Environmental Engineering
The University of Alabama at Birmingham
Birmingham, AL

Prepared by

UTCA

University Transportation Center for Alabama
The University of Alabama, The University of Alabama at Birmingham, and
The University of Alabama in Huntsville

Technical Report Documentation Page

1. Report No. (FHWA/CA/OR-)	**2. Government Accession No.**	**3. Recipient's Catalog No.**
4. Title and Subtitle Strengthening Steel Bridge Girders Using CFRP		**5. Report Date:** Submitted June 2009; Published June 2010.
		6. Performing Organization Code
7. Author(s) Dr. Talat Salama and Mr. Ahmed Abd-El-Meguid		**8. Performing Organization Report No.** UTCA #06217
9. Performing Organization Name and Address Dept. of Civil, Construction, and Environmental Engineering The University of Alabama at Birmingham Birmingham, AL		**10. Work Unit No. (TRAIS)**
		11. Contract or Grant No.
12. Sponsoring Agency Name and Address University Transportation Center for Alabama The University of Alabama; P. O. Box 870205 Tuscaloosa, AL 35487-0205		**13. Type of Report and Period Covered** Final Report of Research Conducted June 1, 2006 – December 30, 2008.
		14. Sponsoring Agency Code
15. Supplementary Notes		

16. Abstract

While traditional retrofitting methods for steel bridge girders could be time consuming and uneconomical, an alternative repair method is suggested using Carbon Fiber Reinforced Polymers (CFRP) laminate strips, providing engineers with a competitive solution that will increase the life-cycle of repaired bridges. This study investigated its feasibility as an option to strengthen and rehabilitate steel bridges. The main advantages of using CFRP laminates are their light weight and durability, which results in ease of handling and maintenance.

The research conducted experimental and analytical work to evaluate the effectiveness of strengthening steel beams by the use of novel CFRP laminate strips configurations. The research involved the testing of five experimental composite beams, in addition to the development of approximately 100 finite element models. The results showed a significant gain in the beam's elastic and ultimate capacities. The conclusion is that there are specific sensitive parameters controlling the effectiveness of the CFRP laminate rehabilitation technique. An adequate AASHTO design of the rehabilitation method, which takes into consideration the effective parameters, would result in an effective bridge structure

17. Key Word(s) CFRP, Steel Beams, Bridge Girders, Rehabilitation, Strengthening, Finite Element Modeling, ABAQUS, SAP 2000, Design Guidelines	**18. Distribution Statement**

19. Security Classif. (of this report)	**20. Security Classif. (of this page)**	**21. No. of Pages** 184	**22. Price**

Form DOT F 1700.7 (8-72)

Contents

List of Tables

List of Figures

Executive Summary

While traditional retrofitting methods for steel bridge girders could be time consuming and uneconomical, an alternative repair method is suggested using Carbon Fiber Reinforced Polymers (CFRP) laminate strips, providing engineers with a competitive solution that will increase the life-cycle of repaired bridges. This study investigated its feasibility as an option to strengthen and rehabilitate steel bridges. The main advantages of using CFRP laminates are their light weight and durability, which results in ease of handling and maintenance.

The research conducted experimental and analytical work to evaluate the effectiveness of strengthening steel beams by the use of novel CFRP laminate strips configurations. The research involved the testing of five experimental composite beams, in addition to the development of approximately 100 finite element models. The results showed a significant gain in the beam's elastic and ultimate capacities. The conclusion is that there are specific sensitive parameters controlling the effectiveness of the CFRP laminate rehabilitation technique. An adequate AASHTO design of the rehabilitation method, which takes into consideration the effective parameters, would result in an effective bridge structure.

Section 1
Introduction

1.1 Background

Throughout the U.S., there are thousands of steel bridges that are at various levels of advanced deterioration due to many years of service and exposure to the environment (Liu, Silva, & Nanni, 2001). Rehabilitation can involve various strategies and application methods. These strategies include adding steel plates to the girders in order to increase the girder capacity, adding new girders between the old ones (McRae & Ramey, 2003), or replacing the whole bridge superstructure. Moreover, load ratings decrease as bridges deteriorate, which affects truck routing and loading limits and in turn affects freight costs dramatically. CFRP materials have been predominantly used by the aerospace industry, where cost is generally a secondary consideration to weight (Jones R. , 1998). Carbon fibers were first used in civil applications at Swiss Federal Testing Laboratories (Burgoyne, 1999).

The bridge collapse in Minnesota in 2007 was a wakeup call for bridge engineers and departments of transportation. Current bridge inspection is mainly visual and lacks in-depth inspection, such as strain and stress evaluation of different structural elements.

Besides the rehabilitation method using carbon fiber reinforced polymers (CFRP) laminates discussed in the report, modeling techniques using FE to verify the usefulness of the method are also presented.

1.2 Problem Statement

Corroded steel bridge girders cause the severe reduction of cross section, hence the inertia of the cross section needed to sustain truck loads. Moreover, the increased demand on goods and gas prices lead some truck companies to drastically increase truck loads beyond the legal weight limits designated for bridges. This causes a significant increase in both live load stresses in the short term and the fatigue stress range over the long term. Drops in section inertia also cause increases in live load deflections. According to the American Association of State Highway and Transportation Officials (AASHTO), limits are set for live load stresses, fatigue stresses, and deflections. Exceeding these limits leads to the non-adequacy of bridges in the short or long term. Traditional repair solutions include adding steel plates or adding external prestressed tendons at the steel girders.

The proposed rehabilitation and strengthening methodology for steel girder bridges is to install CFRP plates to the bottom flange of the girders.

The hypothesis of this research is that CFRP laminates are significantly effective strengthening and rehabilitating technique for steel girder bridges. CFRP laminates added to the tension flange of steel girders will enhance their flexural capacity.

1.3 Research Objectives

The objective of this research is to quantify the load improvement using novel CFRP configurations and develop design guidelines for using CFRP laminates to strengthen steel bridge girders.

1.4 Methodology and Approach

In order to achieve the outlined objectives, a detailed plan was developed. Five steel beam specimens having CFRP laminate configuration variations were tested. Bending testing was conducted on the simply supported beams via four-point loading. Nonlinear finite element analysis software, ABAQUS (*Abaqus Analysis User Manual,* 2007), was used to verify the experimental results. The report describes the tasks performed and the design process of steel beam strengthened using CFRP. Discussion of the FE models built to simulate the experimental beams is also presented. Evaluation of the rehabilitation technique is performed utilizing FE models.

The list of tasks accomplished is as follows:

- Experimental plan for the steel beams: this task was mainly focused on the preliminary design of steel beams to choose a suitable beam for laboratory experimentation given certain restrictions of the laboratory testing frame and equipment, such as length, depth, weight, and load capacity.
- Excel design spreadsheet utilizing Visual Basic programming: an Excel spreadsheet that incorporated Visual Basic programming was developed to predict the failure load of various experimental beams. The experimental beam was chosen using this spreadsheet.
- Steel beam purchase / fabrication: steel beams were fabricated and purchased from Garrison Steel Company. The bottom flange of the steel beams was sand blasted for proper attachment of the CFRP plate. Steel specimens for the tension tests were also provided.
- Experimental setup and testing: tension testing was performed on steel and CFRP specimens. Test setup for the beams involved the attachment of the CFRP laminates to the steel flange. The beam was equipped with strain gages at various locations, and a load cell and LVDT were placed at the midspan of the beam. All instruments were then connected to the data acquisition system, and testing followed. Analysis of experimental results: this task included graphing load deflection, load strain, and strain variation along the depth of the beam for all tested beams. Comparison of the results was performed.

- Parametric study using finite element (FE) analysis: a parametric study was conducted to test several parameters, such as CFRP laminate length, thickness, configuration, and material properties, and the steel beam section. ABAQUS was the software package used for the FE modeling, which involved special bonding elements, contact surfaces, constraints, and material properties.
- Analysis of parametric study results: load-deflection graphs were plotted to compare the effect of various parameters. A tabular form was then utilized to calculate elastic and plastic percentage gains.
- Performing structural evaluation of bridges strengthened using CFRP: FE models were developed using SAP2000 software.
- Developing design guidelines for rehabilitating bridges using CFRP laminates.

1.5   Scope of Study

The scope of this research is limited to the strengthening of steel beams in flexure only. No shear strengthening is included. Steel beams for the experimental work were chosen to have enough shear-carrying capacity throughout the loading process. The main focus was to increase the load carrying capacity of the beams using CFRP plates' configurations. Only laboratory strengthening was performed.

1.6   Organization of the Report

This report consists of seven chapters. Chapter 1, Introduction, discusses the research problem background. It also presents the objective of the research work performed and the methodology utilized to approach the objectives. Chapter 1 concludes with the report organization, a brief summary of the rest of the chapters.

Chapter 2, Literature Review, reviews the previous research conducted on rehabilitating bridges. A historical background is presented on the evolution of rehabilitation methods and when FRP, specifically CFRP, came into use in bridge rehabilitations.

Chapter 3, The Experimental Program; is concerned with the experimental work performed during the course of this study, starting with the tension tests performed on steel and CFRP specimens to obtain stiffness and strength properties. The bulk of the experimental work was performed on five steel W200 x 19.3 (W8 x 13) beams topped by a steel plate that replaced the reinforced concrete deck. The chapter describes the steps executed in order to perform the tests. A summary of the results concludes this chapter.

Chapter 4, Verification of FE Model, mainly describes the FE model built to simulate the steel beams tested experimentally in Chapter 3. Results from the verification models and the experimental results are compared in this chapter.

Chapter 5, Parametric Study, utilizes the FE model built in Chapter 4 to perform an extensive parametric study to evaluate the sensitivity of each parameter of the CFRP rehabilitation process.

Around a hundred models have been developed and executed using the ABAQUS FE program. Parameters investigated were CFRP laminate length, thickness, and configuration, and loading, and the steel beam section. Results are presented in the form of load deflection graphs and tables showing the strength gain in both the elastic and plastic load range. An Excel spreadsheet utilizing Visual Basic programming was developed for the design of steel beams strengthened with CFRP laminates. The Visual Basic modules were embedded in the spreadsheet and used as built-in functions to calculate the elastic and plastic neutral axis location, the plastic moment capacity, and the beam's deflection.

In chapter 6, Bridge Design: Rehabilitation Guidelines, two main topics are discussed: first, simulation work of a typical composite steel concrete bridge; second to evaluate the strengthening of steel girder bridges using CFRP plates through solved AASHTO bridge examples. This includes the gain in strength, section modulus, and stiffness of the bridge girders. The reduction of the deflections and the fatigue stress ranges are also discussed. Design guidelines for rehabilitating steel bridges using CFRP are introduced at the end of the chapter.

Chapter 7, Conclusions, presents conclusions regarding the effectiveness of CFRP laminates in the rehabilitation of steel bridge girders. Recommendations for future work are also presented.

1.7   Study Contribution and Innovation

This research conducts both experimental and analytical testing on various novel CFRP laminate configurations used in the rehabilitation and strengthening of steel bridge girders. The tested CFRP configurations presented here were not presented previously in any of the research.

Section 2
Literature Review

2.1 Introduction

Many state and local agencies are faced with deteriorating bridge infrastructure composed of relatively short to medium-span bridges. In many cases, these older structures are hot-rolled or welded longitudinal steel stringers acting compositely with a reinforced concrete deck (Wipf T. J., Phares, Klaiber, & Lee, 2003). Bridge deterioration rates, durability and longevity performance have been discussed thoroughly during the last few decades. A factor that receives too little consideration in bridge work is durability (Ramey & Wright, 1997). This leads to the huge number of structurally deficient and functionally obsolete bridges all over the United States.

2.2 Common Rehabilitation Field Applications

Conventional rehabilitation, such as welding steel plates to structural members has been the traditional method for a long time but induces high thermal stresses in the steel members. The induced stress reduces the member fatigue resistance. A rehabilitation design using conventional methods is discussed by Farhey (Farhey, et al., 2000), as applied to an existing historic bridge crossing Sandusky River in Fremont, Ohio. Although the conventional restoration methods are still applicable and preferred in some structural elements, such as the gusset plates, the CFRP method is on the rise as a rehabilitation technique to be used with bridge elements, such as main girders.

When total replacement is not an option and traditional retrofit methods are uneconomical and time consuming, an alternative retrofit method using CFRP composite material provide engineers with an effective solution that can increase the life cycle of these bridges. Research recently conducted on the use of CFRP for strengthening and repair of steel beams has been investigated (Mertz & Gillespie, 1996), (Tavakkolizadeh & Saadatmanesh, 2003) and (Al-Saidy, Klaiber, & Wipf, 2004). A number of different approaches have been studied to assess the effectiveness of various CFRP materials for the strengthening and repair of steel bridges, including the repair of overloaded girders (Sen, Libby, & Mullins, 2001).

A proposed solution to strengthen the damaged reinforced concrete headstock of the Tenthill Creeks Bridge, Queensland, Australia, using FRP composites was presented by Nezamian (Nezamian & Setunge, 2007). A decision was made to consider strengthening the headstock using bonded carbon FRP laminates to increase the load-carrying capacity of the headstock in shear and bending.

A reliability analysis of reinforced concrete bridge girders strengthened by CFRP laminates was developed by Okeil (Okeil, El-Tawil, & Shahawy, 2002). A resistance model is used to calculate the probability of failure and the reliability index of CFRP-strengthened cross sections. The reliability method is employed to calibrate the flexural resistance factor for a broad range of design variables. The study shows that the addition of CFRP improves reliability somewhat because the strength of CFRP laminates has a lower coefficient of variation than steel or concrete.

The rehabilitation of an existing concrete bridge in Alabama through external bonding of FRP plates to the bridge girders was performed by Stallings (Stallings, Tedesco, El-Mihilmy, & McCauley, 2000). Field load tests were conducted before and after application of the FRP plates to evaluate the advance in structural response.

2.3   Guidelines of Using FRP Reinforcement in the United States

Design guidelines and testing protocols for FRP reinforcement are nationally defined for concrete structures. The American Concrete Institute (ACI) presents a number of technical reports for the design, construction, and repair of concrete structures using FRP reinforcement. Recommendations for the design and construction of FRP reinforcement based knowledge gained from worldwide research can be found in ACI 440.1R-03 (ACI Committee, 2003). Flexure and shear design procedures, and FRP reinforcement detailing are presented in this report. The report also includes material characteristics of commercially available FRP.

Although FRP design, construction, and rehabilitation guidelines are available for concrete structures, similar guidelines are not available for steel structures.

2.4   Guidelines of Using FRP Reinforcement Worldwide

Limited literature was found for design guidelines of FRP worldwide. Deeks and Hao, (2004) mention some design guidelines and safety factors. Based on BS 8110 (1997), the guidelines identify critical areas to be assessed along the length of the beam. These are the areas of maximum moment and the ends of the FRP. It is recommended that internal steel reinforcement yield before failure from either concrete crushing or FRP rupture. BS 8110 (1997) also recommends that the characteristic material properties be divided by appropriate partial safety factors. The partial safety factors for concrete in flexure, γ_c, and steel reinforcement, γ_s, are 1.50 and 1.15, respectively. The partial safety factor for strength of FRP is equal to the type of fiber, γ_{mf}, multiplied by the stage in the manufacturing route in which the FRP samples were taken for testing, γ_{mm}, (e.g. in-situ or factory). CFRP, GFRP, and AFRP (C: carbon, G: glass, and A: aramid) have γ_{mf} values of 1.40, 3.50, and 1.50, respectively, while γ_{mm} varies from 1.10 to 2.0. The recommended partial safety factors for modulus of elasticity, γ_{mE}, are 1.10, 1.80, and 1.80, for CFRP, GFRP, and AFRP, respectively. To avoid any possibility of brittle failure, the ultimate moment capacity may be increased by 1.15.

2.5   FRP Types and Applications

Fiber reinforced plastic (FRP), also known as fiber reinforced polymer, is a composite material consisting of a polymer matrix reinforced with fibers. Fibers are usually aramid, fiberglass, or carbon, while the polymer is usually a vinylester, polyester thermosetting plastic, or epoxy.

Figure 2-1 shows a stress-strain comparison between steel and various FRPs. It shows that CFRP have similar stiffness to steel, while AFRP and GFRP have lower stiffness compared to steel. Both CFRP and AFRP have high strength compared to GFRP. Comparing the FRP modes of failure against steel, it is clear that all FRP have a brittle failure mode, while steel has its well-known ductile behavior.
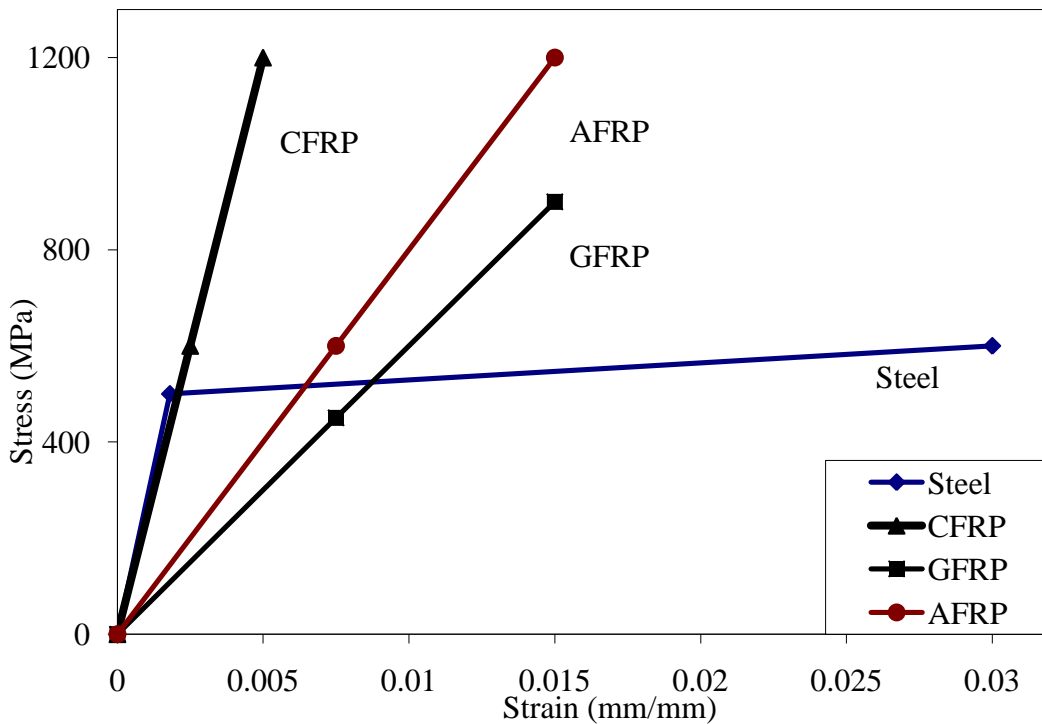
Figure 2-1. Comparison of stress-strain behavior of steel and FRPs (QuakeWrap, 2008).

FRP composites have a history of extensive successful use in the aerospace, defense, marine, and automotive sectors, particularly in corrosion resistant equipment. However, until recently they were largely considered to be of limited value in civil infrastructure beyond use in facades, aesthetic additions, and for architectural purposes. Nonetheless, over the past two decades these materials have made a rapid transition from being subjects of academic research to being increasingly considered for use in the renewal of civil infrastructure (Karbhari, 2005). FRP used as jackets for bridge piers in seismic zones showed great impact for rehabilitation and construction. FRP with reinforcement primarily in the hoop direction not only provides an efficient means of confinement but also enables rapid fabrication of cost-effective and durable jackets with little or no traffic disruption (Karbhari, 2005) and (Atadero, Lee, & Karbhari, 2005).

A new spun concrete pole reinforced with CFRP bars has proven to be of great importance, where poles usually serve in severe salt water, resulting in the deterioration of conventional concrete poles due to steel corrosion (Shalaby, 2007). Beyond their use in seismic retrofit, FRP composites have found great applicability in the rehabilitation of bridge girders and decks through their use as externally bonded reinforcements (Karbhari, 2005) and (Atadero, Lee, & Karbhari, 2005).

The use of FRP as reinforcement for concrete bridge decks was extensively studied and proved to be an effective, corrosion-resistant, flexible, and electromagnetic resistant (Boyd, 1997). Furthermore, anchorage of concrete parapets on GFRP bridge decks was investigated experimentally to develop an effective means of connecting glass fiber-reinforced polymer bridge decks to conventional reinforced concrete parapets (Naito, 2005).

Application of GFRP to enhance the flexural capacity of composite steel girders using heavy-duty adhesive systems is subject to ongoing research (El Damatty, Abushagur, & Youssef, 2005). The excellent performance of a W-shaped steel beam strengthened using GFRP sheets has encouraged the research at hand to assess the applicability of this technique to composite steel bridges.

A seismic retrofit design that was developed using CFRP composites was implemented in the summers of 2000 and 2001 to improve the displacement ductility of the U.S. Interstate 80 Bridge over State Street in Salt Lake City which is very close to the Wasatch fault. The seismic retrofit included column jacketing, as well as wrapping of the bent cap and bent cap-column joints for confinement, flexural, and shear strength increase (Pantelides, Cercone, & Policelli, 2004).

The study of composite (steel-CFRP) members were tested both experimentally and analytically (Al-Emrani & Kliger, 2006) to find different types of fracture modes that could be examined by testing composite elements with different combinations of CFRP-laminates and adhesives. The tested composite elements displayed different behavior, and a large difference in strength and ductility could be observed (Al-Emrani & Kliger, 2006).

Composite materials find extensive use in modern engineering applications due to their high strength-to-weight ratio coupled with favorable mechanical and thermal properties (Swaminathan, Pagano, & Ghosh, 2006). The main advantages of CFRP laminates are their light weight and durability, which results in ease of handling and maintenance (Nozaka, Sheild, & Hajjar, 2005). Moreover, FRP products are non-corrosive and light weight compared to traditional steel members (Stoll, Saliba, & Laura, 2000). However, the ultimate strength gain and elastic response depend heavily on the configuration of the CFRP laminates and the application technique to the steel beam, which in turn depends on the epoxy used. The global mechanical properties of the material are affected by local failures that include particle or fiber splitting, interfacial debonding and matrix cracking. The occurrence of a failure mechanism depends on such factors like matrix, particle and interface strength, and loading mode, as well as such morphological parameters as fiber volume fraction, reinforcement size and shape, orientation, and the spatial dispersion of the fibers in the matrix (Swaminathan, Pagano, & Ghosh, 2006).

2.5.1 AFRP

Aramid fiber reinforced plastic (AFRP) is a composite material made of plastic reinforced with fine aramid fibers. Like any reinforced plastic, the composite material is commonly referred to by its reinforcing fibers, aramid in this case. AFRP filaments are produced by extrusion of the precursor through a spinnert. Extrusion imparts anisotropy (increased strength in the lengthwise direction) to the filaments. The most popular matrix materials for manufacturing AFRP are thermosets (polymers which do not melt when heated) such as epoxies, vinylester, and phenolics. Aramid may protect carbon fibers and improve their properties. Hybrid fabric (Aramid + carbon fibers) combines very high tensile strength with high impact and abrasion resistance.

Aramid fibers were originally developed as a replacement for steel in automotive tires. The distinctive features of Aramid are high impact resistance and low density. The disadvantages of Aramid are ability to absorb moisture, difficulties in cutting, and low compressive strength. Aramid fibers possess the following properties:

- High tensile strength (five times stronger per weight unite than steel);
- High modulus of elasticity;
- Very low elongation up to breaking point;
- Low weight;
- High chemical inertness;
- Very low coefficient of thermal expansion;
- High fracture toughness (impact resistance);
- High cut resistance;
- Textile processibility;
- Flame resistance.

2.5.2 GFRP

Glass fiber reinforced plastic (GFRP) is a composite material made of plastic reinforced with fine glass fibers. Like graphite-reinforced plastic, the composite material is commonly referred to by the name of its reinforcing fibers (fiberglass). The plastic is thermosetting (polymer materials that irreversibly cure form), most often polyester or vinylester, but other plastics, such as epoxy are also used. The glass is mostly in the form of chopped strand mat (CSM), but woven fabrics are also used. CSM is a form of reinforcement used in glass-reinforced plastics. It consists of glass-fibers laid randomly across each other and held together by a binder.

An individual structural glass fiber is both stiff and strong in tension and compression, along its longitudinal axis. Although one might intuitively imagine the fiber to be weak in compression, it is actually only the long aspect ratio of the fiber which makes it seem so; i.e., because a typical fiber is long and narrow, it buckles easily. On the other hand, the glass fiber is relatively unstiff and weak in shear. In other words, the fiber is stiff and strong in the preferred direction, namely, along its length. Therefore if a collection of fibers can be arranged permanently in the preferred direction within a material, and if the fibers can be prevented from buckling in compression, then the material will become preferentially strong in that direction. Furthermore, by laying multiple

layers of fiber on top of one another, with each layer oriented in various preferred directions, the stiffness and strength properties of the overall material can be controlled in an efficient manner. In the case of glass-reinforced plastic, it is the plastic matrix that permanently constrains the structural glass fibers to directions chosen by the designer. With chopped strand mat, this directionality is essentially an entire two-dimensional plane; with woven fabrics or unidirectional layers, directionality of stiffness and strength can be more precisely controlled within the plane. A glass-reinforced plastic component is typically of a thin "shell" construction, sometimes filled on the inside with structural foam, as in the case of surfboards. The component may be of nearly arbitrary shape, limited only by the complexity and tolerances of the mold used for manufacturing the shell.

2.5.3 CFRP

Carbon fiber reinforced polymer (CFRP) is a kind of polymer matrix composite material reinforced by carbon fibers. The reinforcing dispersed phase may be in the form of either continuous or discontinuous carbon fibers, commonly woven into a cloth. Carbon fibers are expensive but they possess the highest specific mechanical properties per weight, such as modulus of elasticity and ultimate strength. Carbon fibers are used for reinforcing the polymer matrix due to their following properties:

- Very high modulus of elasticity, exceeding that of steel;
- High tensile strength, which may reach 1000 ksi (7 GPa);
- Low density: 114 lb/ft³ (1800 kg/m³);
- High chemical inertness.

Carbon fiber materials are commonly produced as dry fiber tow sheets. The sheets can be impregnated with a saturating resin on-site using a wet lay-up technique and are well suited for curved applications or highly irregular surfaces. For applications requiring a higher degree of strengthening, the carbon fibers can also be pultruded into a precured laminate, which can subsequently be bonded to the surface of the structure using a structural adhesive. The main disadvantage of carbon fibers is their catastrophic mode of failure, since carbon fibers exhibit a brittle mode of failure.

Carbon fiber reinforced plastic has over the past two decades become an increasingly notable material in structural engineering applications and been studied in an academic context for its potential benefits in construction. It has also been shown to be a cost-effective material in field applications to strengthen concrete, masonry, steel, and timber structures. Its use in industry can be either for retrofitting to strengthen an existing structure or as an alternative reinforcing (or prestressing material) to steel from the outset of a project.

Retrofitting has become the dominant use of the material in civil engineering, and applications include increasing the load capacity of old structures (such as bridges) that were designed to tolerate lower service loads than they are experiencing today, as well as seismic retrofitting and repair of damaged structures. Retrofitting is popular in many instances as the cost of replacing the deficient structural elements can greatly exceed its strengthening using CFRP. Due to the

high stiffness of CFRP, it can be used underneath bridge spans to help prevent excessive deflections or wrapped around beams to limit shear stresses.

When used as a replacement for reinforcing steel, CFRP bars are also used to reinforce concrete structures. More commonly they are used as prestressing tendons due to their high stiffness and strength. The advantages of CFRP over steel as a prestressing material are its light weight and corrosion resistance, enabling the material to be used in highly corrosive environments, such as offshore structures.

CFRP is a more costly material than its counterparts GFRP and AFRP, though CFRP is generally regarded as having superior properties. Much research continues to be done on using CFRP both for retrofitting and as an alternative to steel as a reinforcing or prestressing material. Cost remains an issue and long-term durability questions remain. Though design codes have been drawn up by institutions such as the American Concrete Institute, there remains some hesitation among the engineering community in regards to implementing these alternative materials. In part this is due to a lack of standardization and the proprietary nature of the fiber and resin combinations on the market, though this in itself is advantageous in that the material properties can be tailored to the desired application requirements.

2.6   CFRP Structural Characteristics

The material properties of the CFRP laminates have been greatly improved over the last few years, with a wide variety of dimensions and strengths required to achieve significant stiffness increases. More recently, CFRP materials with a modulus of elasticity approximately twice that of structural steel have become available. Several researchers have indicated that these materials can be used to increase the strength and stiffness of steel-concrete composite beams. Consideration of the CFRP plate end debonding as critical failure mode should be avoided to prevent an undesirable failure of the system. Debonding strength of steel beams strengthened with CFRP plates were discussed by Lenwari (Lenwari, Thepchatri, & Albrecht, 2006) and Nozaka (Nozaka, Sheild, & Hajjar, 2005). Spliced connections were further discussed by other researchers (Schnerch D. , 2005) and (Dawood, 2005).

2.7   CFRP in Steel Beam Applications

Several researches were performed on strengthening steel beams and steel girders using CFRP. Due to the great development in CFRP material properties, and due to the development of epoxies used, the gain in stiffness and strength in steel structures is still in the research phase. Two main CFRP products are used by structural engineer researchers in strengthening steel structures. These are CFRP laminates (plates) and CFRP tendons. CFRP laminates are available in a wide variety of thicknesses, widths, and lengths. The coming sections will focus on both CFRP products and review some of the research performed using these products.

Recent work was performed on the use of CFRP plates on steel girders (Phares, Wipf, Klaiber, Abu-Hawash, & Lee, 2003). The bridge was 45.72 m x 9.14 m three-span continuous I-beam

girders. Furthermore, research by Al-Saidy (2001) showed the effectiveness of CFRP plates for improving the strength of steel composite beams. Research that involved laboratory and field study, in which CFRP plates were used to strengthen composite steel stringers, was performed (Wipf T. , Phares, Klaiber, Al-Saidy, & Lee, 2005). The study showed a potential enhancement in the bridge live load capacity through the addition of CFRP plates to the bottom flange. Conclusions as to the performance and behavior of the strengthened bridge will be made as a follow-up tests takes place.

2.8   CFRP Bond Behavior

Similar to the way stresses develop in reinforcement bars or plates, high concentrated stresses develop at the reinforcement ends. Several details were investigated by Schnerch (2007) to help reduce the bond stress concentration near the ends of the splice plate, including increasing the length of the splice cover plate, implementing a reverse taper near the plate ends, and applying a transverse CFRP wrap around the splice plate. It was found that increasing the length of the splice plate beyond the maximum moment region did not significantly increase the total capacity of the CFRP system but may be necessary to avoid sequential failure in unreinforced regions. Similarly, the presence of the transverse CFRP wrap did not increase the ultimate capacity of the spliced connection.

The debonding strength of partial-length adhesively bonded CFRP plates that are used to strengthen steel beams was studied by Lenwari, Thepchatri, & Albrecht (2006). CFRP plates only covered a partial length of the steel beams. Bonded CFRP plates tend to debond under static and fatigue loadings because of the very high stress field at the plate ends. CFRP plate length was also studied, and research concluded that the hybrid beams had two failure modes: plate debonding in beams with short plates, and plate rupture at midspan in beams with long plates (Lenwari, Thepchatri, & Albrecht, 2005).

2.9   Fatigue Behavior of Steel Beams Reinforced with CFRP

Repairing fatigue cracks in older structures especially, with bridges designed prior to the AASHTO fatigue detailing provisions, is an ongoing problem. The use of CFRP has shown significant promise in bridge rehabilitation and strengthening. In addition to all of the previously mentioned advantages, CFRP has a very good resistance to fatigue in fiber-dominated materials (Jones & Civjan, 2003). Researchers proved that composite laminates can extend the fatigue life of aluminum specimens (Baker, 1997). An investigation of the use of prestressed CFRP to repair fatigue cracks and prevent future cracks from propagating showed a good impact on structures (Basseti, 2000). An experimental and analytical study was conducted to investigate the effectiveness of applying CFRP overlays to steel fatigue tension coupons to prolong fatigue life (Jones & Civjan, 2003). Specimens were either notched or center hole specimens and tested in uniaxial tension. Variables studied were CFRP system, bond length, bond area, one and two sided applications, and applications prior or subsequent to crack propagation. Two-sided applications were very effective, prolonging fatigue life by as much as 115%. The method

therefore showed promise as both a preventive technique and repair method (Jones & Civjan, 2003).

2.10 Summary

Based on the literature review, concrete and steel structures reinforced with CFRP have proven to have a satisfactory behavioral improvement, including enhancements in strength and ductility. The literature review also pointed out the great significance of CFRP bonding. Even though there are limited uses of CFRP plates to strengthen and rehabilitate structures, further research is needed to provide confidence in the usefulness of the materials, as illustrated by this research.

Section 3
The Experimental Program

This chapter describes the various tests conducted in the laboratory to evaluate the CFRP laminate strengthening system performance. Tension tests were performed to evaluate the tensile strength properties of the steel and CFRP used. Scaled four-point loading tests were performed on five steel beams to evaluate the flexural enhancement gained by strengthening the beams with CFRP laminates.

3.1 Specimen Details

Five scaled steel beams were tested in the lab to investigate the effectiveness of using different configurations of CFRP laminates to increase the strength and stiffness of steel highway bridge girders. The details of the testing program are presented in Table 3-1. All of the beams had a length of 4.3 m and were loaded monotonically to failure using a four-point bending configuration separated equally. A schematic diagram of the cross-section of a typical test beam and the corresponding strain gages location is shown in Figure 3-1.

Table 3-1. Test Matrix for the Large-Scale Steel-CFRP Composite Beam Tests

Beam Designation	CFRP Configuration	CFRP Strip Length (mm)	CFRP Strip Width (mm)
Beam 1 (control beam)	None	---	---
Beam 2	One strip on lower face of bottom flange	3200	100
Beam 3	One bottom face of lower flange + one strip on upper face of bottom flange	3200	100 & 50
Beam 4	Two strips on lower face of bottom flange	3200	100 & 100
Beam 5	One strip on lower face of bottom flange	3200	50
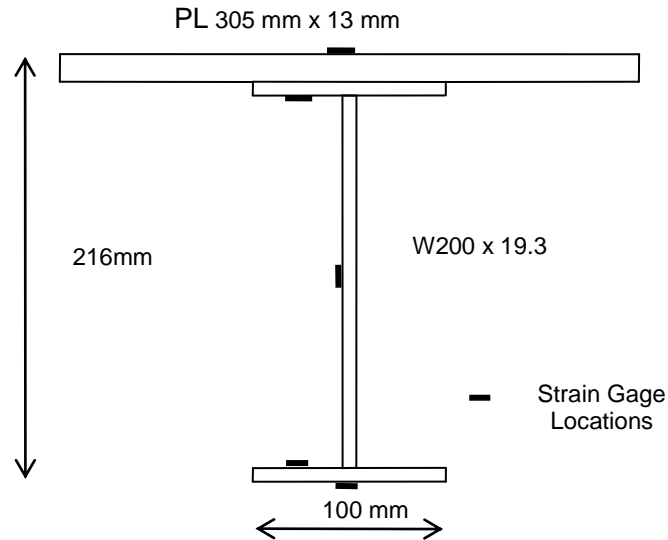
Figure 3-1. Beam dimensions and strain gage locations.

The beam's cross-section was chosen based on several factors and limitations. The first factor was that the span-to-depth ratio had to be representative of a typical bridge girder. Due to laboratory restrictions, the beam's length was limited to a maximum of 4.5 m, which affected the design of the beam's depth. The CFRP laminate was designed accordingly. Furthermore, the weight of the beam was restricted to the lightest possible section for ease of handling in the lab using the mechanical crane. Through the development of an Excel spreadsheet, various W-shaped steel beams were evaluated. The W200 x 19.3 (W8 x 13) steel beam proved to be the most appropriate, based on the limitations and design criteria. Bridge decks are commonly composed of steel girders attached by shear connectors to an overlaying concrete slab. In this experimental setup, the concrete deck was replaced by a steel plate to avoid the results from being influenced by varying concrete strength produced by different batches for each beam. This would insure a controlled experiment with the CFRP laminates being the only variable. The steel plate was designed to have the neutral axis at the top flange of the steel beam, therefore causing the beam to be mainly in tension and the plate in compression. The steel plate's width provided the beam with sufficient lateral support to avoid any lateral torsional buckling. A top plate with cross-sectional dimensions of 305 mm by 13 mm was welded to the I-beam (Figure 3-1). The arc-weld strength used was 483 MPa, with a size of 9.5 mm (3/8 in) and length 76 mm (3.0 in) at 152 mm separation center-to-center (6.0 in). Steel beams were purchased from Garrison Steel, a steel manufacturing company in Pell City, Alabama. Figure 3-2 shows the steel beam and steel plate before welding in the manufacturing yard of Garrison steel. Figure 3-3 shows the spot welding size being requested from the technician and measurement mark-ups on the beam. The automatic arc-welding machine used to weld the steel beam to the plate is shown in Figure 3-4, and the welding process is shown in Figure 3-5. Beams were then transported to the UAB structural laboratory.

Figure 3-2. Steel beam and steel plate centered before welding.

Figure 3-3. Weld size and spacing dictated.

Figure 3-4. Automatic welding machine used.

Figure 3-5. Steel beam and steel plate during the welding process.

Several CFRP configurations were tested, all having CFRP strips covering 75% of the beam's span. Figure 3-6 (a, b, c, & d) shows the different CFRP configurations for the four strengthened beams, Beams 2 through 5. Beam 1 is the unstrengthened beam, which is considered the control beam.

CFRP configurations varied from covering the whole flange width as in Beam 2, to covering both the top and bottom faces of the flange, as in Beam 3, adding two CFRP layers to the bottom face of the bottom flange, as in Beam 4, or covering the bottom face of the bottom flange partially, which is the case with Beam 5. The CFRP configurations tested are the novelty of this research work. Adding CFRP to both faces of the bottom flange was first tested in this research. Throughout the literature review, no CFRP configurations were discussed.

a) Beam 2   b) Beam 3   c) Beam 4   d) Beam 5
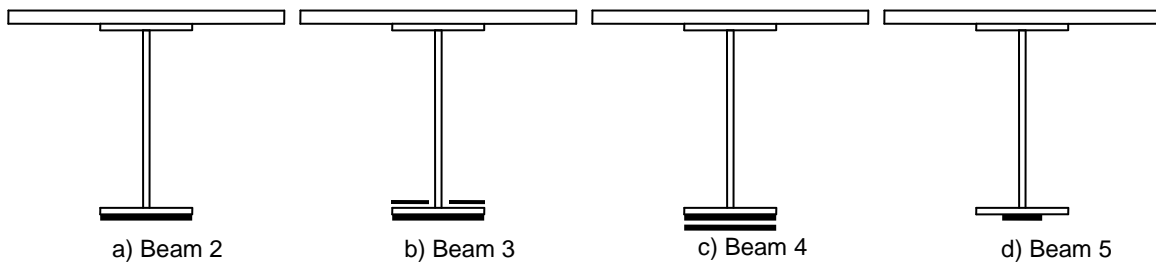
Figure 3-6. Different CFRP configurations.

CFRP strips for this experimental work were obtained from FYFE Company, the manufacturer of Tyfo® UC Composite Laminate Strip System. The laminate was compromised of a high modulus, high tensile strength, pull-formed advanced composite. Epoxy used in the experimentation was Tyfo® MB high performance-adhesive. The epoxy is a two-component acrylic adhesive, which bonds a wide variety of metals and fiber-reinforced polymers. It provides high peel and impact strengths even in low temperature environments and has an average of 20 to 30 minutes pot life at room temperature. The laminate strip system comes with a fiber wrap that is mainly placed to act as an insulator between the CFRP and steel to prevent the galvanic action that may cause quick steel corrosion. The CFRP, fiber wrap, and epoxy used are shown in Figure 3-7.
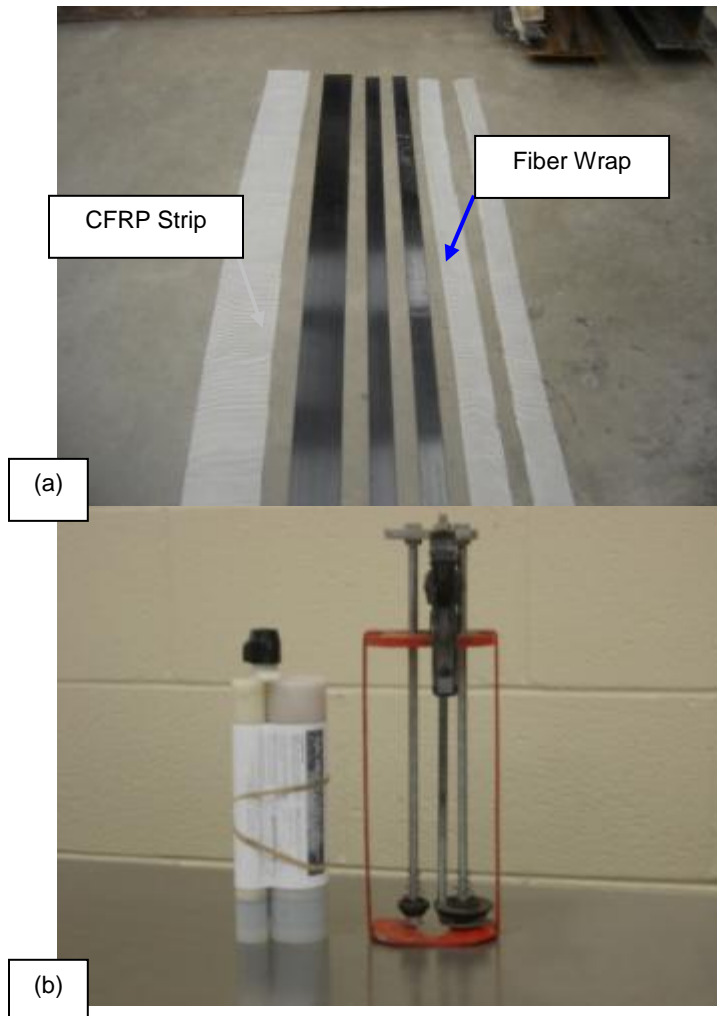
Figure 3-7. (a) CFRP & fiber wraps, (b) Epoxy and gun applicator.

The beam preparation process included surface preparation, installing CFRP laminates and strain gages, positioning the beam on the testing frame, and placing the LVDT (Linear Variable Differential Transformer) at the midpoint. All of the measurement devices were then connected to the data acquisition system. To install the CFRP strips, the bottom flange's surface had to be prepared by abrasive methods, typically light sandblasting and grinding (Figure 3-8). Fine abrasion of the surface was performed using sandpaper grades ranging from 100 to 400. The CFRP laminates and the fiber wraps were then cut to the required lengths. Figure 3-7 (a) shows the CFRP and fiber wraps cut down to the required lengths. The epoxy was spread on the surface using the gun applicator shown in Figure 3-7 (b). The installation sequence was started by turning over the steel beam, spreading the epoxy on the steel beam's flange (Figure 3-9), placing the fiber wrap onto the epoxy, and finally installing the CFRP plate (Figure 3-10). To ensure proper bonding between the laminate and the steel beam, a uniform pressure was applied by steel clamps through 25 mm x 100 mm pieces of wood (Figure 3-11). A minimum of eight pressure points was used over the length of the CFRP to ensure equal distribution of pressure. Complete curing was achieved within one week. Figure 3-12 shows a typical beam ready for testing.

Figure 3-8. Roughening the surface of CFRP.
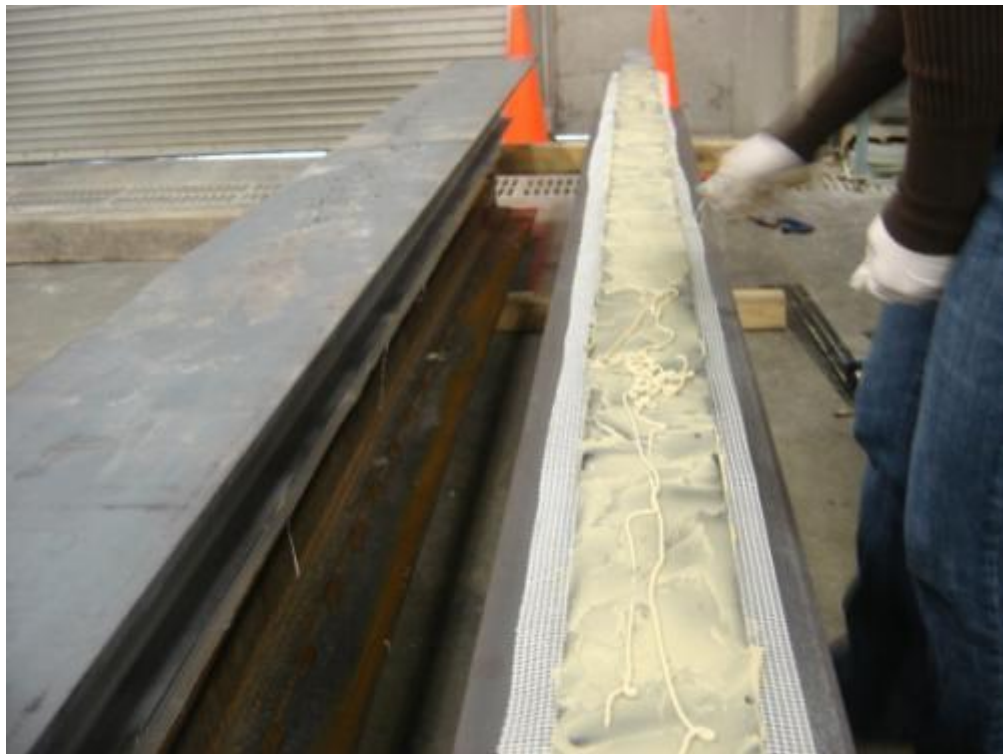
Figure 3-9. Adding Epoxy and spreading it on the prepared surface.

Figure 3-10. The strengthened beam after adding the CFRP layer.

Figure 3-11. Applying pressure on the CFRP layer using clamps.
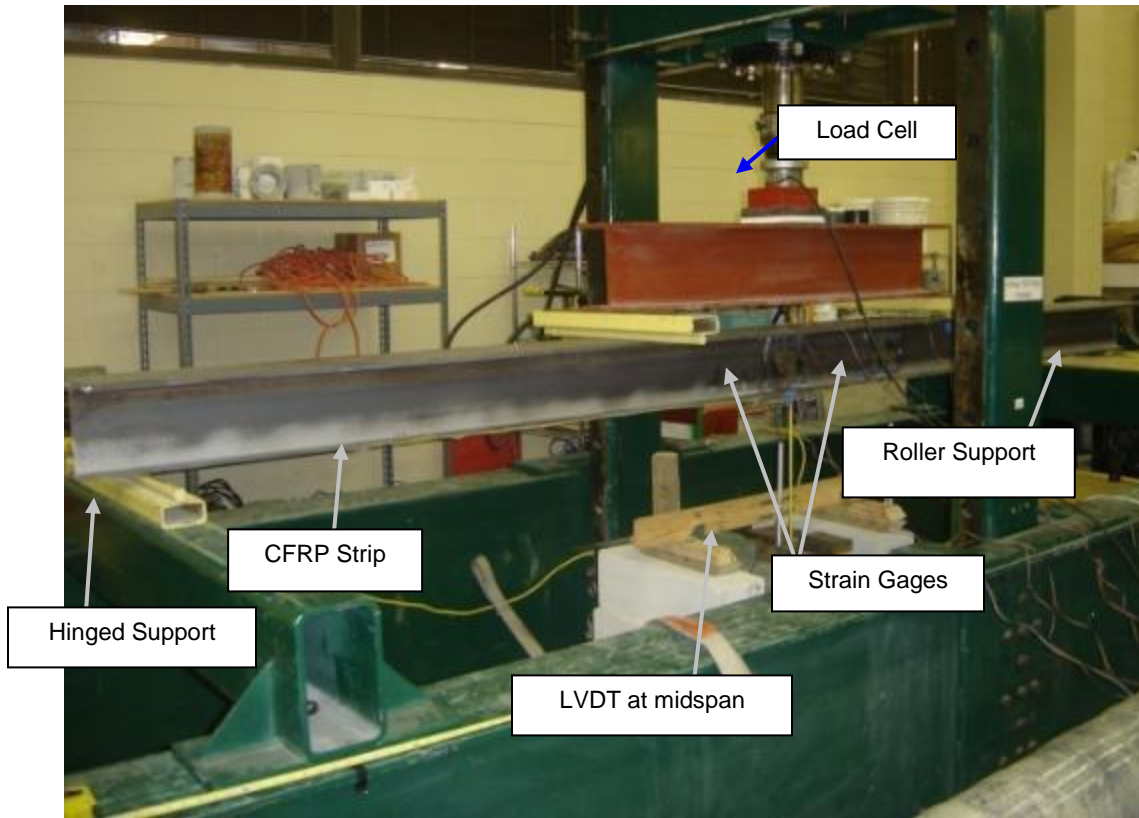
Figure 3-12. Experimental setup of steel beam strengthened by CFRP.

3.2 Instrumentation

Several outputs were required for the experiment. First, load readings were required; a load cell was installed to read them. Second, strain values were required at various points, and strain gages were used. Third, displacement at various points was required. Instrumentation for this consisted of two LVDTs.

3.2.1 Strain Gages

Strain gages used in the project were purchased from Vishay® Micro-Measurements. Strain gages had a resistance of $350.0 \pm 0.3\%$ ohms, which are adequate for measuring strain for steel and CFRP. The high-resistance gage is preferable in that it reduces the heat generation rate by a factor of three for the same applied voltage across the gage.

Because the strain gage is an extremely sensitive device capable of registering the smallest effects of an imperfect bond, considerable attention to detail must be taken to assure stable, creep-free installations. Strain gages were installed using M-Bond 200 adhesive. Strain gage application consists of several steps: surface preparation, strain gage bonding, and attaching the gages to the data acquisition system (Figure 3-13).

Figure 3-13. Installation of strain gages.

3.2.2 Load Cell and LVDT Sensor

A load cell is an electronic device used to measure forces. It converts the applied forces to an electrical signal that is captured by the data acquisition system. The load cell in this experimental setup was used to measure the applied load on the beam.

The LVDT, a transformer used to measure linear displacements, was used in this experimental program. Two LVDTs were used to measure vertical displacement at the midspan and the third point. Data recorded by the load cell and the LVDT at the midspan was used to develop the load deflection diagrams for the beams.

3.2.3 Data Acquisition System

The data acquisition system used was a VISHAY model 5100B. The most important specification for this model is that it scans and digitizes 20 channels of input within 1 ms. This data acquisition model also provided stable, high-accuracy data for fast static performance. The maximum number of channels needed in any of the performed experiments was 19 channels (16 strain gages, 2 LVDTs, and a load cell). Wiring strain gages to the data acquisition system is shown in Figure 3-14.

Figure 3-14. Wiring strain gages to the data acquisition system.

3.3 Experimental Testing

After the beam was placed in the testing frame and equipped with all measurement devices, the testing phase of the experimental program started. It took an hour for each beam to be tested and the data to be correctly acquired and saved. A minimum of two persons were needed to perform a successful loading test for per beam. The first person was needed to physically perform the loading, which is done by means of a hydraulic pump, and the second person was mainly responsible of monitoring the data acquisition system and making sure that all data was recorded continuously.

Figure 3-15 shows Beam 4 after completion of the experimental test. It can be seen that the CFRP has debonded from the beam and, on closer observation, that some rupture has also occurred.

Figure 3-15. A view of Beam 4 showing the deflection at the end of the experiment.

3.4   Results

Data collected from the experimental phase is displayed and summarized in this section of the chapter. Data acquired were mainly strain readings at different locations on the beam, displacement readings at the midspan and the third point, and load readings from the load cell.

Charts were constructed for the load–strain diagrams for each of the tested beams. Figure 3-16 shows the load strain curves for five strain gages attached at the midspan of Beam 1. Positive strain represents tension, as opposed to negative strain representing compression. Strain gages located at the extreme bottom fibers read the most tension strain, while the strain gages located at the extreme top fibers read the maximum compression.

Figure 3-17 shows the load strain curves for five strain gages attached at the midspan of Beam 2. The strain variation was similar to that of Beam 1, except for the debonding behavior, which is observed at the two strain readings in the extreme tension zone, where a drop of strain readings indicated the CFRP debonding point. Figure 3-18 shows the load strain curves for five strain gages attached at the midspan of Beam 3. The strain variation is similar to that of Beam 2. Figure 3-19 and Figure 3-20 shows the load strain curves for five strain gages attached at the midspans of Beam 4 and Beam 5, respectively. The strain variations are similar to those of Beam 2.
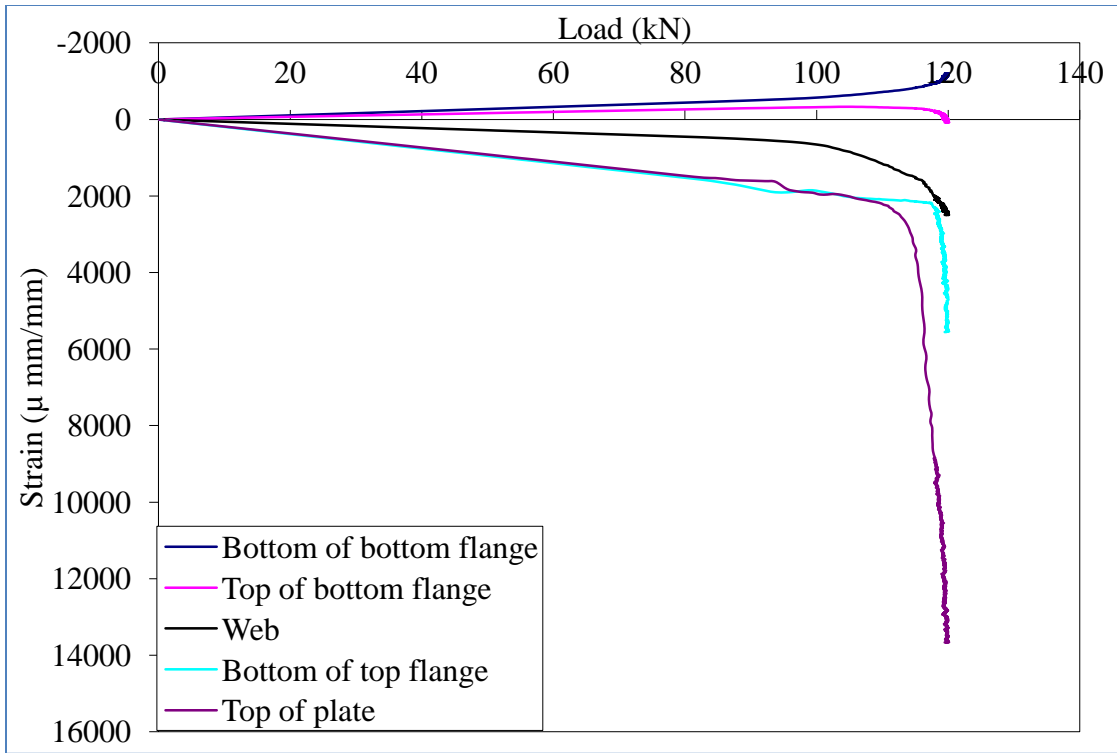
Figure 3-16. Load-strain curve for Beam 1.
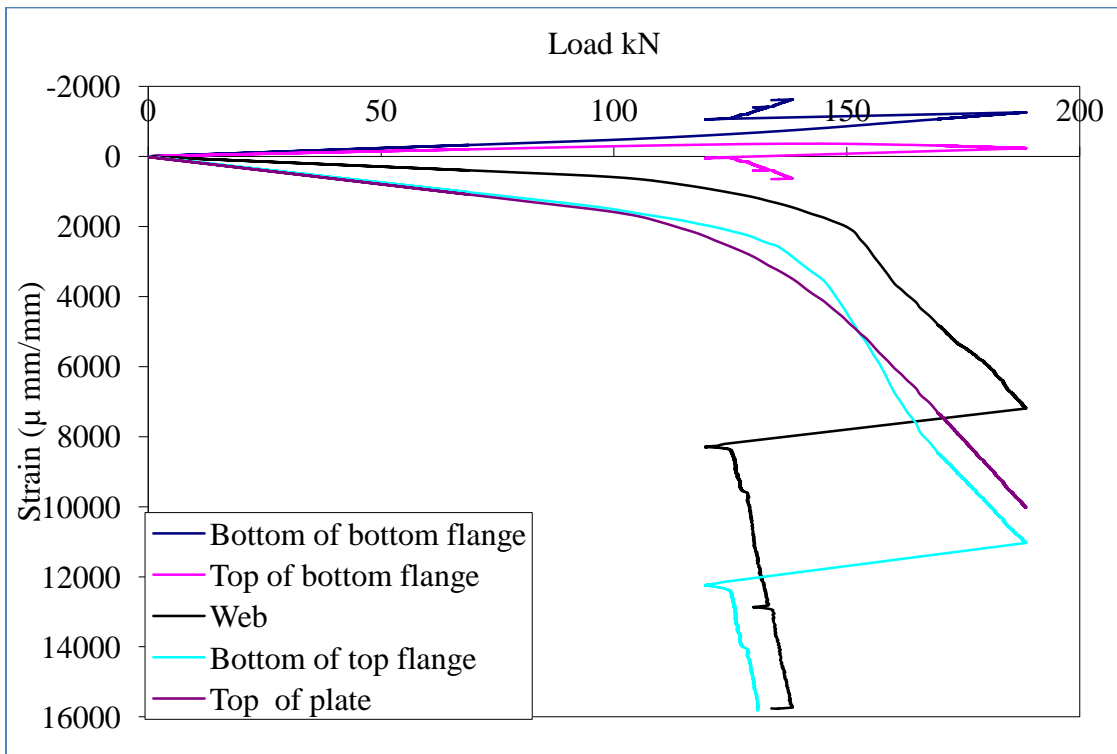
Figure 3-17. Load-strain curve for Beam 2.
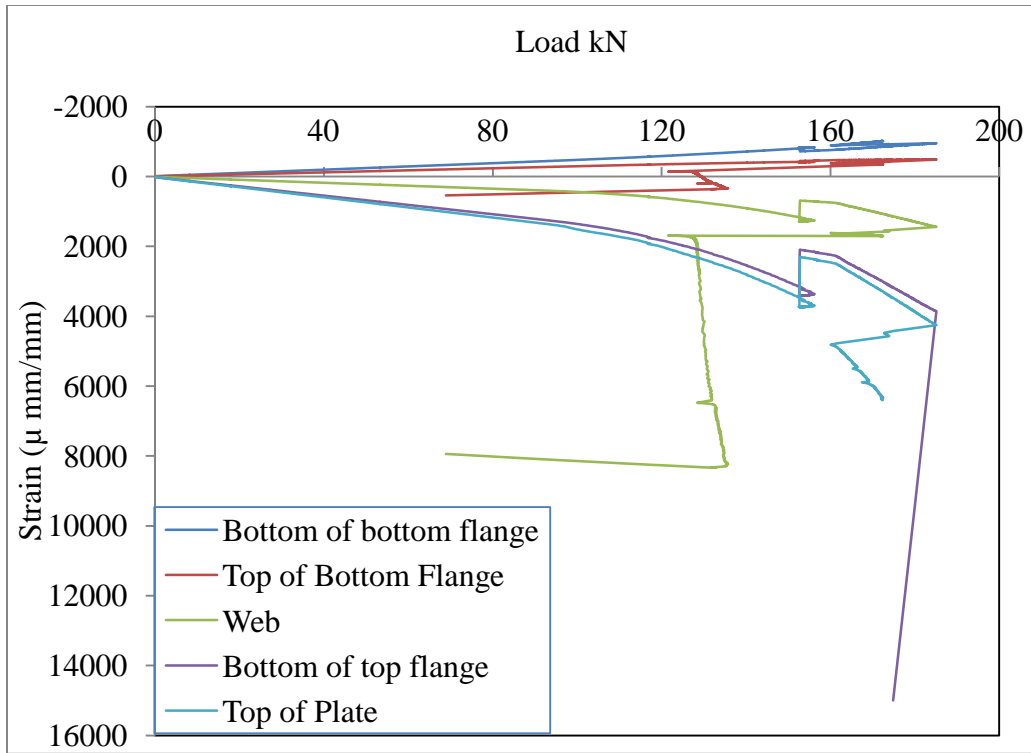
Figure 3-18. Load-strain curve for Beam 3.
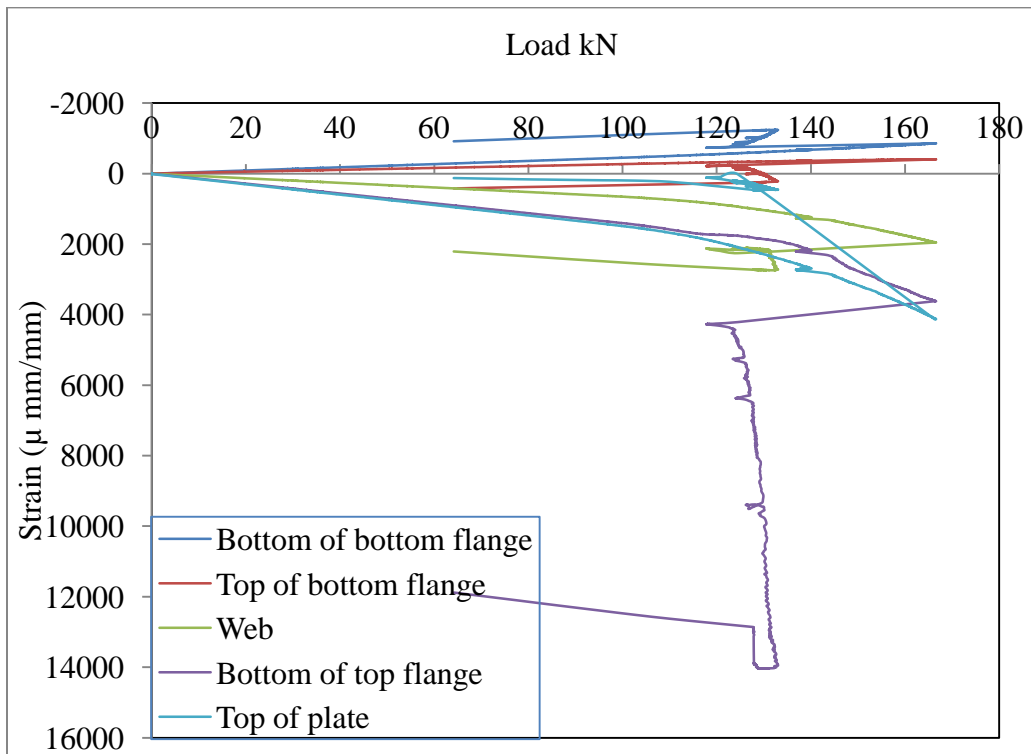
Figure 3-19. Load-strain curve for Beam 4.

27
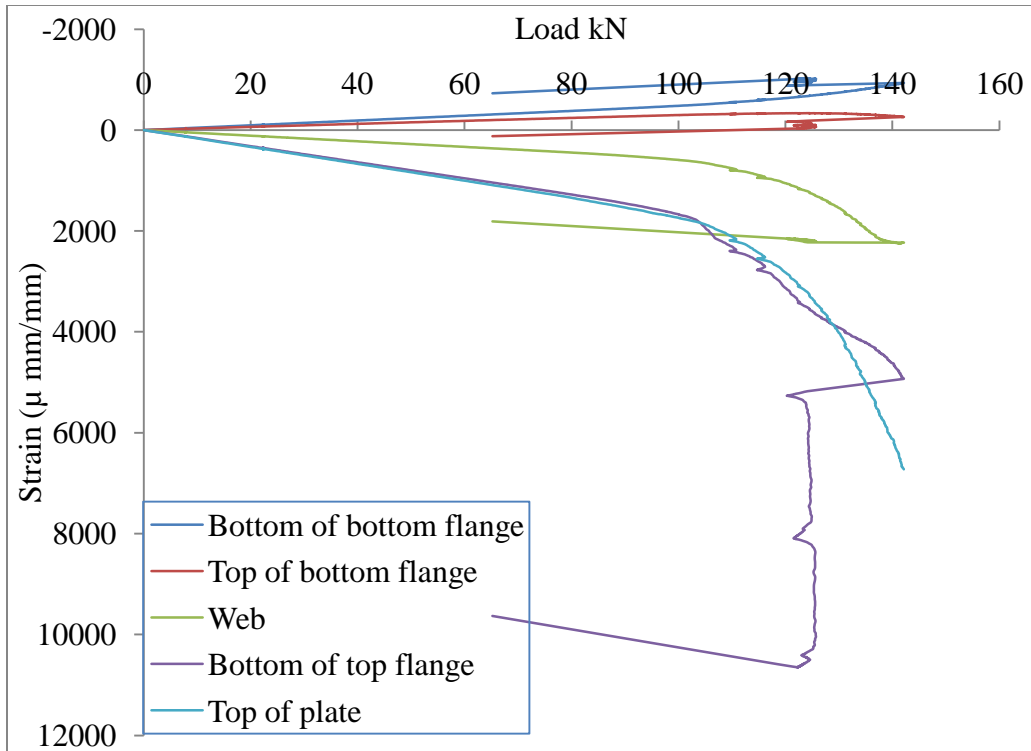
Figure 3-20. Load-strain curve for Beam 5.

Data acquired and displayed in Figure 3-16 to Figure 3-20 was manipulated to read three different loading stages; i.e., 30%, 60%, and the 90% of the beam's ultimate load. The three loading stages are named Stage 1, Stage 2, and Stage 3 to reflect the 30%, 60%, and the 90% of the ultimate beam load, respectively. Charts developed represent the strain variation across the beam's depth. Figure 3-21 shows the strain variation across the depth of Beam 1. It can be seen that the strain variation was almost linear throughout stages 1 and 2. Debonding of the CFRP could be observed at Stage 3. Figure 3-22 shows the strain variation across the depth of Beam 2. It can be seen that the strain variation was almost linear throughout Stages 1, 2, and 3. This indicates that the CFRP was strongly bonded and kept bearing the load until the final loading stages without significant slippage. Figure 3-23, Figure 3-24, and Figure 3-25 show the strain variation across the depth of Beam 3, Beam 4, and Beam 5, respectively. The main characteristic of the curves is that the beams have a linear strain variation during the early stages, while high tensile strains are observed towards the higher loading stages.
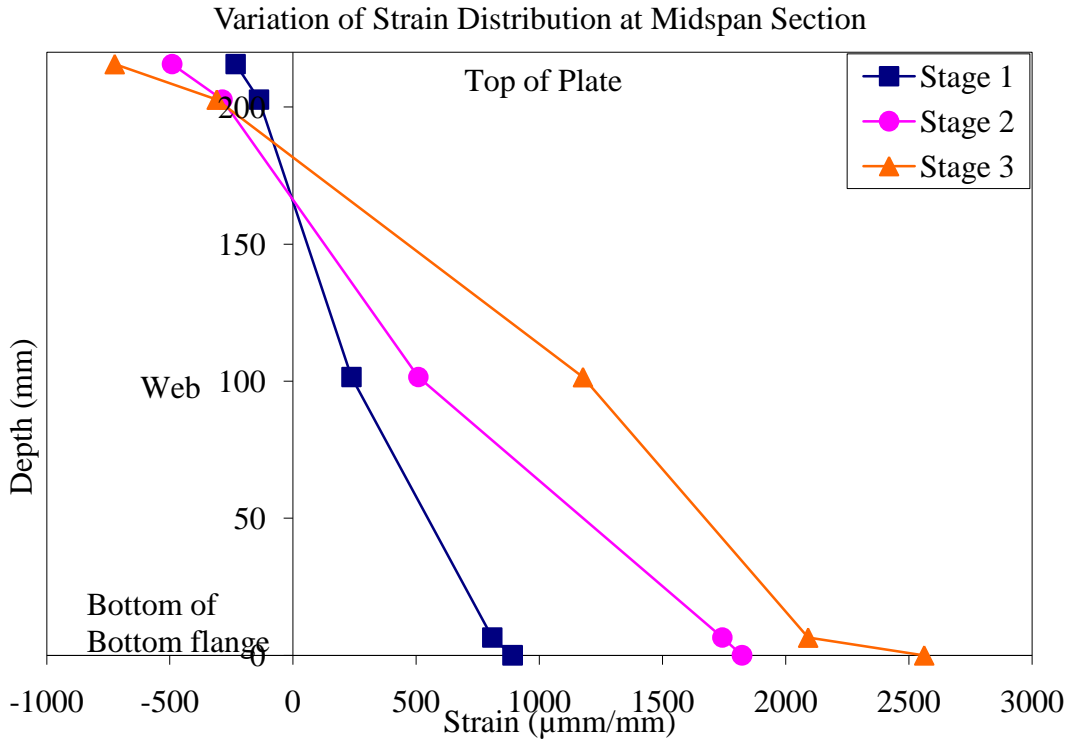
Figure 3-21. Strain-depth curve for Beam 1.
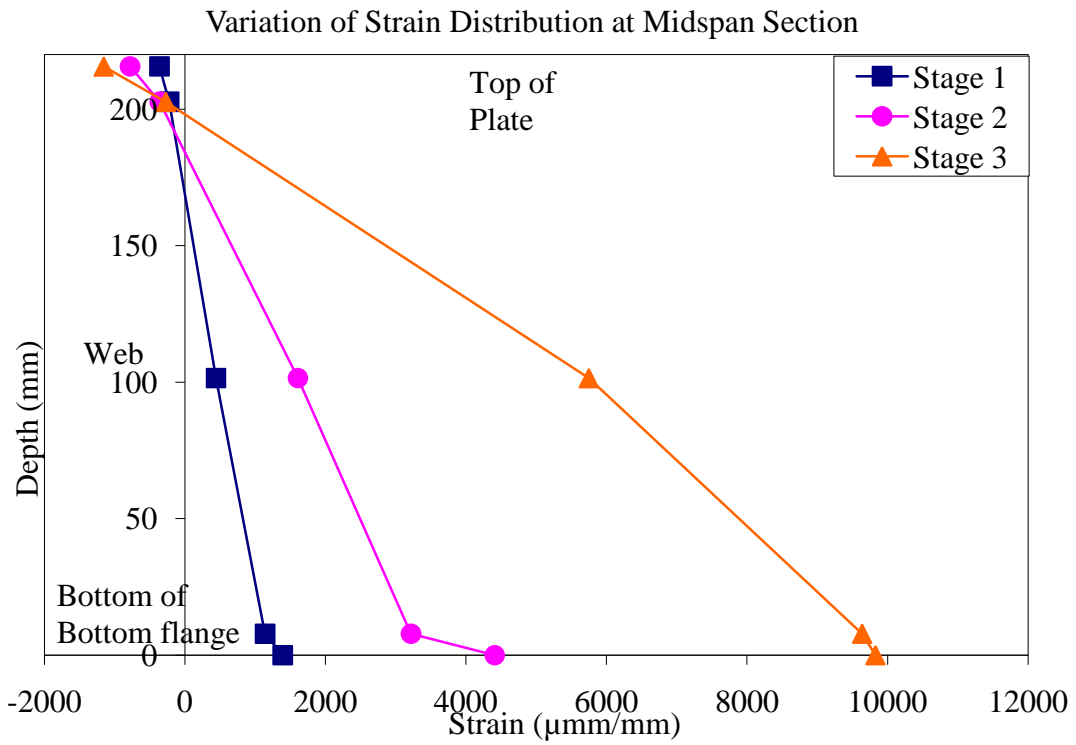
Figure 3-22. Strain-depth curve for Beam 2.

29
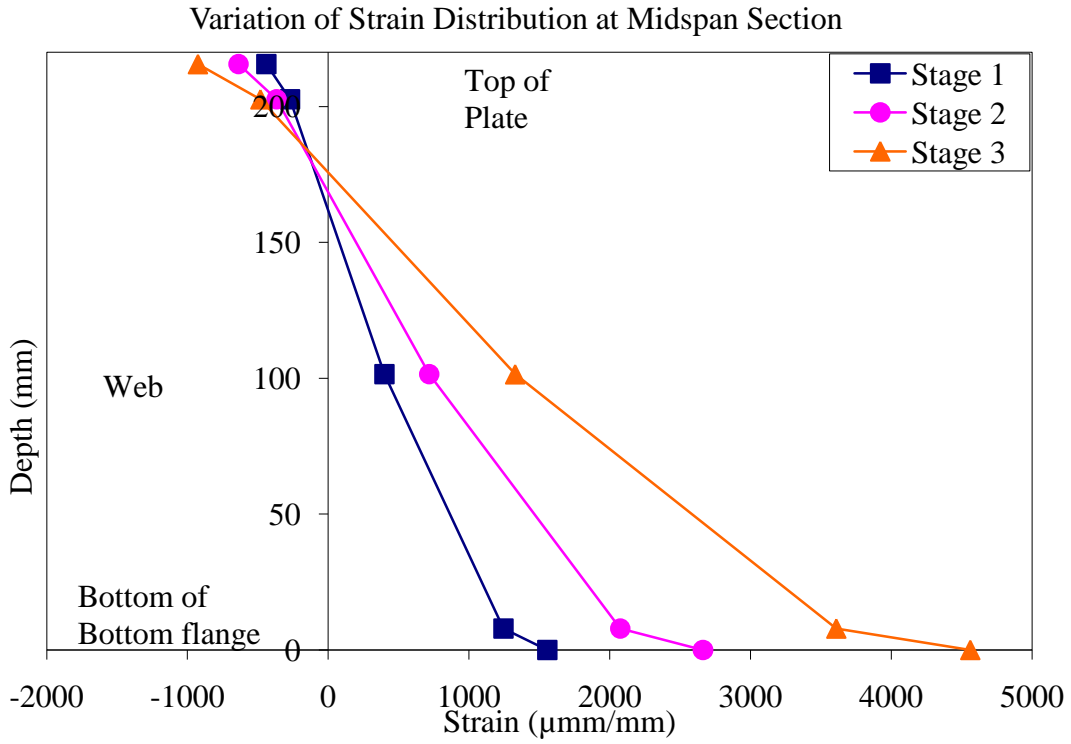
Figure 3-23. Strain-depth curve for Beam 3.
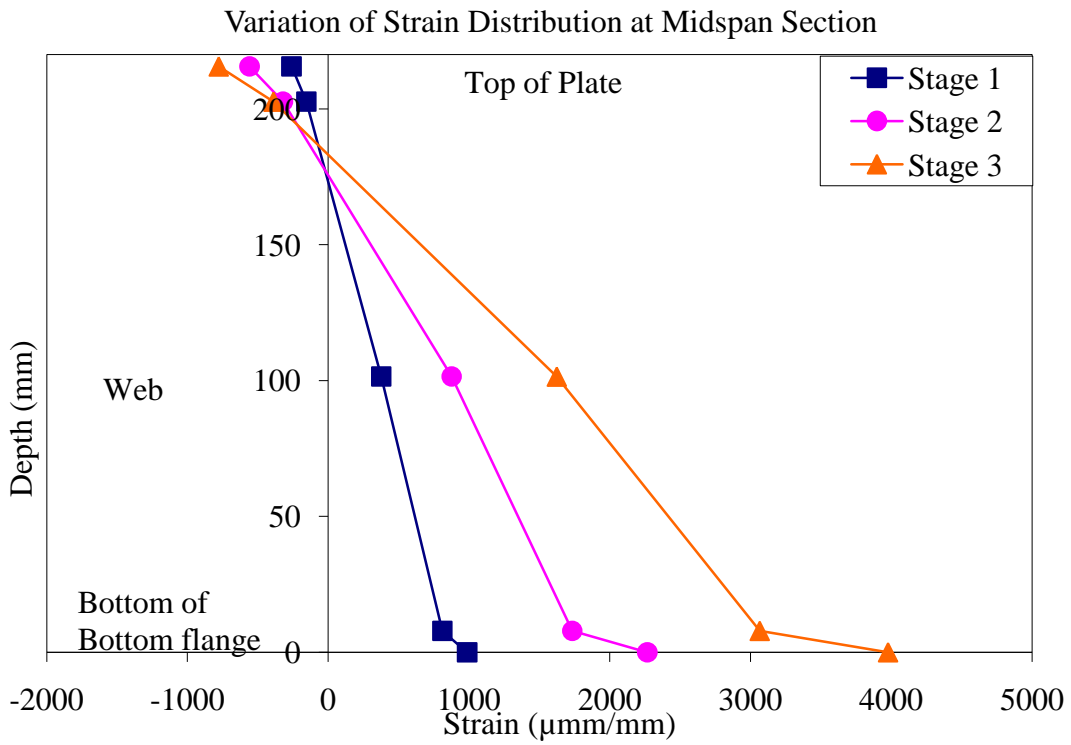
Figure 3-24. Strain-depth curve for Beam 4.

Variation of Strain Distribution at Midspan Section
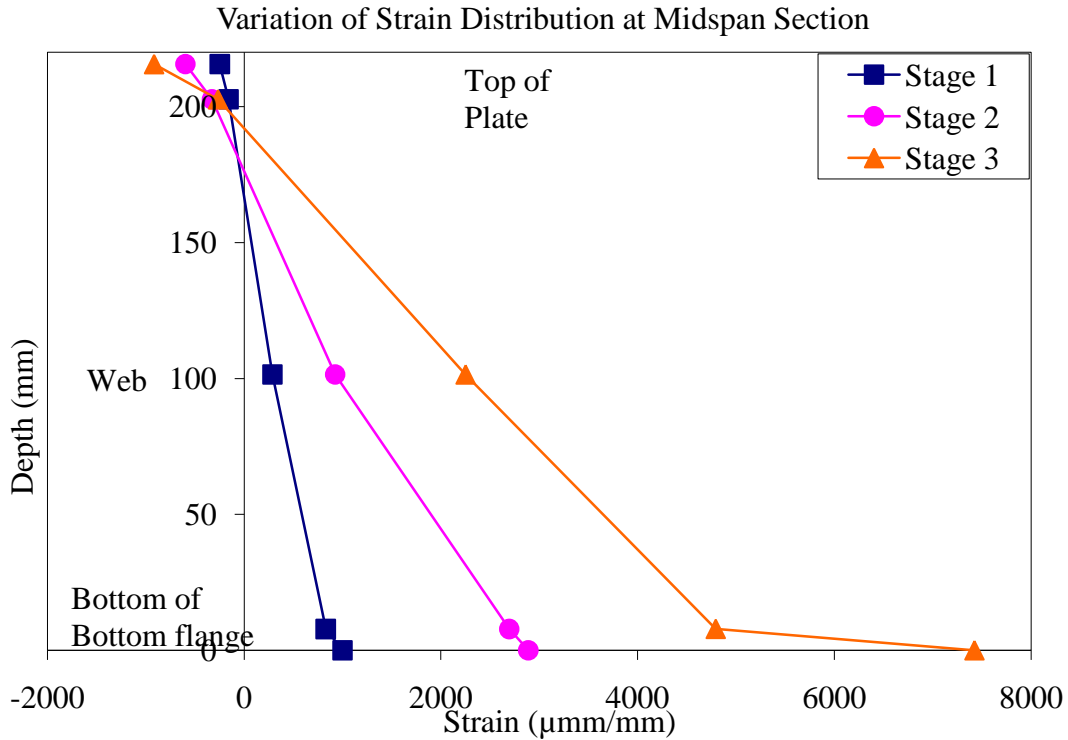
Figure 3-25. Strain-depth curve for Beam 5.

The load-deflection behavior of the four strengthened beams was essentially linear up to the yielding point of the steel. The behavior then became increasingly non-linear until debonding of the CFRP occurred (Figure 3-15), after which the beams followed a close trend to that of Beam 1 (the control beam) until failure occurred due to plastification of the beam's middle region. After debonding, the strengthened beams had more capacity than Beam 1 due to the presence of the epoxy layer that was still attached to the flanges. The load-deflection behavior obtained from the experiments on the five beams is presented in Figure 3-26.

Figure 3-26 shows the load deflection diagram for all five beams tested. The debonding behavior can be seen clearly in the sudden drop in load capacity. Whenever the debonding behavior occurs, the beam capacity is reduced to the original control beam capacity. The maximum load gain was observed to be 22% at the end of the elastic range compared to the unstrengthened control beam. The maximum load gain observed at the plastic load range was found to be 62% compared to the unstrengthened control beam. The experimental program shows the significant effect of CFRP plates on steel beams.

Experimental test results are summarized in Table 3-2. Load gain for both elastic and plastic stages are presented. The ductility ratio is calculated by dividing the deflection at debonding by the deflection at the end of the elastic load range. The ductility ratio is also presented in the table.

31

Table 3-2. Experimental Beam Results

Beam #	Elastic		Ultimate		Ductility ratio	Load Gain	
	Deflection (mm)	Load (kN)	Deflection (mm)	Load (kN)		Elastic	Plastic
Beam 1	27	103	0	119	0.0		
Beam 2	27	116	97	193	3.6	13%	62%
Beam 3	27	124	60	187	2.2	20%	57%
Beam 4	27	126	54	177	2.0	22%	48%
Beam 5	27	109	62	145	2.3	6%	22%
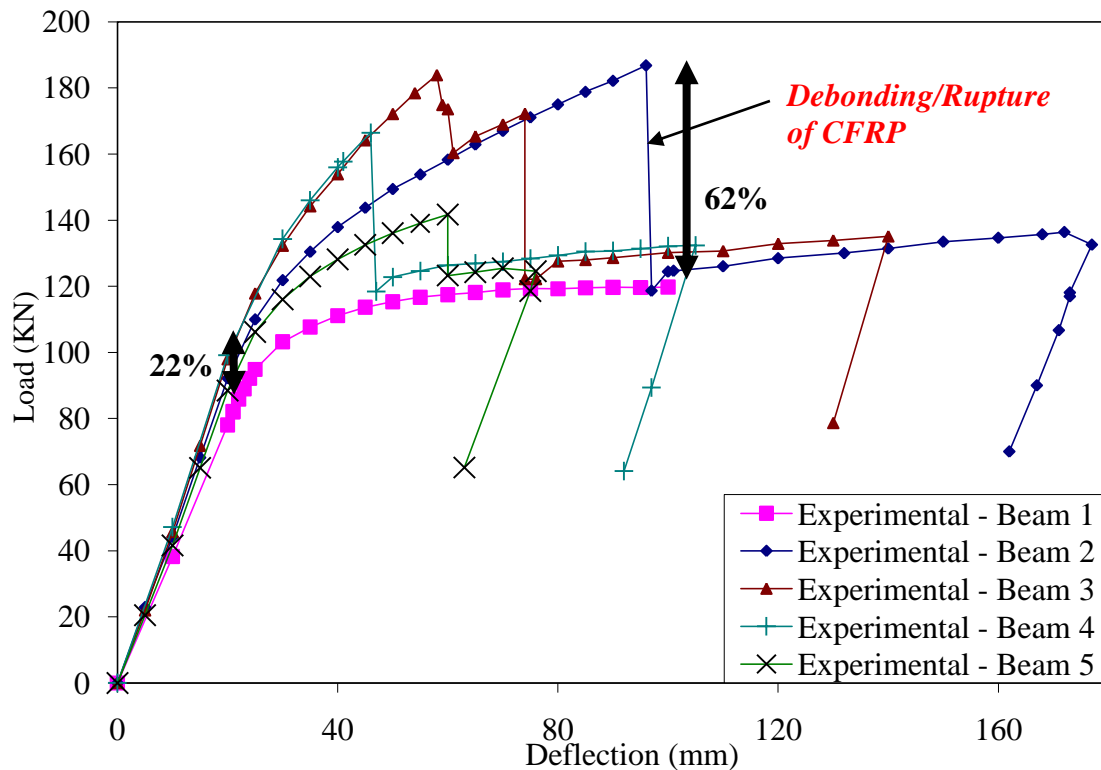
Figure 3-26. Experimental load-deflection curves for the five Beams.

Comparing the five experimental beams, the only variable was the CFRP configuration. Beam 3 and Beam 4 showed the highest stiffness among the beams tested. Beam 2 and Beam 3 showed the highest beam strength. Beam 2 was the only beam showing significant deflection before debonding. This configuration (CFRP on bottom face only) proved to be the best CFRP configuration among all tested beams. This configuration is used throughout the design chapters later in the report.

3.5   Material Properties of Steel and CFRP Plates

Tension tests were performed experimentally to obtain accurate material properties of the beams used. Steel tension testing as well as CFRP tension testing was performed. Stress-strain curves were used later as modeling input parameters.

3.5.1   Steel Tension Testing

Several tension tests were performed on steel plate specimens to test for the stiffness and strength of the steel used in the experimentation program. Steel specimen dimensions were 50 mm x 6.47 mm (2.0 in x 0.255 in) obtained from the same steel plates as the tested I-beams. Similar steel specimens were obtained from the top plates having the dimensions of 50 mm x 12.7 mm (2.0 in x 0.50 in).

The steel plate specimens were mounted in the Tinius Olsen Universal Testing machine and equipped with a strain gage in order to plot the stress-strain relationship (Figure 3-27). The machine has a capacity of 272 kN (600 kips) and was connected to a data acquisition system, where loads applied, crosshead movement, and loading rate are displayed and stored. Figure 3-28 shows the steel plate after testing where it is observed that the plate rupturing near the midpoint. Figure 3-29 shows the steel stress-strain graph obtained from the tension tests. It is observed that steel specimens tested from the steel beam had higher strength than that of the steel plate used on top of the beam. These results were verified by more tension tests, where all specimens gave the same values for both kinds of steel. Results obtained from this test were very useful in the accurate development of the FE model developed and used later and discussed.

Figure 3-27. Steel specimen mounted for a tension test – strain gage installed.

Figure 3-28. Steel specimen after the tension test.
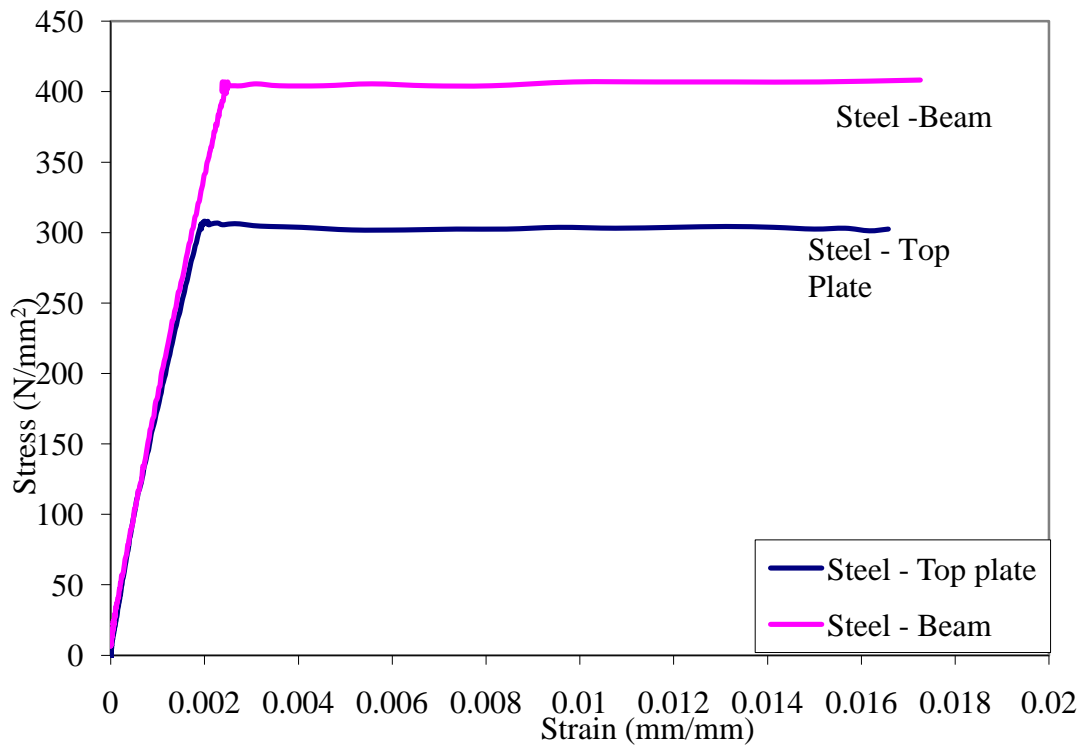
Figure 3-29. Stress-strain curve for steel from tension test results.

3.5.2 CFRP Tension Testing

The typical material properties of the dry fibers and pultruded laminate CFRP materials are presented in Table 3-3, as specified by the producing company, Fyfe. To verify the values of the modulus of elasticity and yield strength, several tension tests were performed on CFRP laminate specimens. CFRP laminate specimen cross-sectional dimensions were 100 mm x 1.40 mm (4.0 in x 0.055 in), and 50 mm x 1.40 mm (2.0 in x 0.055 in). The specimen total length was 1000 mm. A length of 160 mm was clamped from each side.

Table 3-3. Carbon Fiber Material Properties

	Fiber Properties (Fyfe, 2006)	Laminate Properties
Tensile modulus, E	231 GPa	155 GPa
Tensile strength, f_u	3790 MPa	2790 MPa
Rupture strain, ε_u	0.015	0.018
Volumetric fiber content	-	68%

CFRP laminate specimens were equipped with a strain gage in order to plot the stress-strain diagram. Figure 3-30 shows the CFRP laminate strip mounted in the Tinuis Olsen testing machine, which is connected to the data acquisition system.

Figure 3-30. Tension test setup: testing machine and data acquisition system.

CFRP has a brittle rupture failure mode. This was clear from the literature and the tension tests performed. Figure 3-31 shows the first signs of rupture of the outer fibers of the CFRP laminate specimen. As loading increased, more rupture occurred in the outer fibers (Figure 3-32), and successive popping sounds were heard.

A minor problem with the experimental setup was that the testing machine grips had some effect on the CFRP laminate specimen. The handles induced high stresses at the points of contact, causing an early rupture of the CFRP plates at the grips rather than the middle of the specimen. It was therefore concluded that the values obtained from the test results were to be used as a guide only, and that one should use the manufacturer's specifications for the analytical work. This assumption proved to be accurate, as would be shown in FE modeling presented in the following chapter. The stress strain curves of the CFRP laminates tested are shown in Figure 3-33, Figure 3-34, Figure 3-35, and Figure 3-36, where the average modulus of elasticity experimentally obtained is 145 GPa, which is comparable to the specifications value of 155 GPa; however, the ultimate stress observed was much less than the specifications due to the testing limitations faced. CFRP tension test results are summarized in Table 3-4.

Table 3-4. CFRP Tension Test Results

Tension Test #	1	2	3	4
Laminate Dimensions (mm)	100 x 1.40	100 x 1.40	50 x 1.40	100 x 1.40
Tensile modulus, E	148 GPa	141 GPa	141 GPa	144 GPa
Max Tensile strength, f_u	1295 MPa	1790 MPa	1535 MPa	1520 MPa

Figure 3-31. First signs of CFRP rupture: outer fibers ruptured.

Figure 3-32. Successive CFRP fiber rupture towards the specimen center.
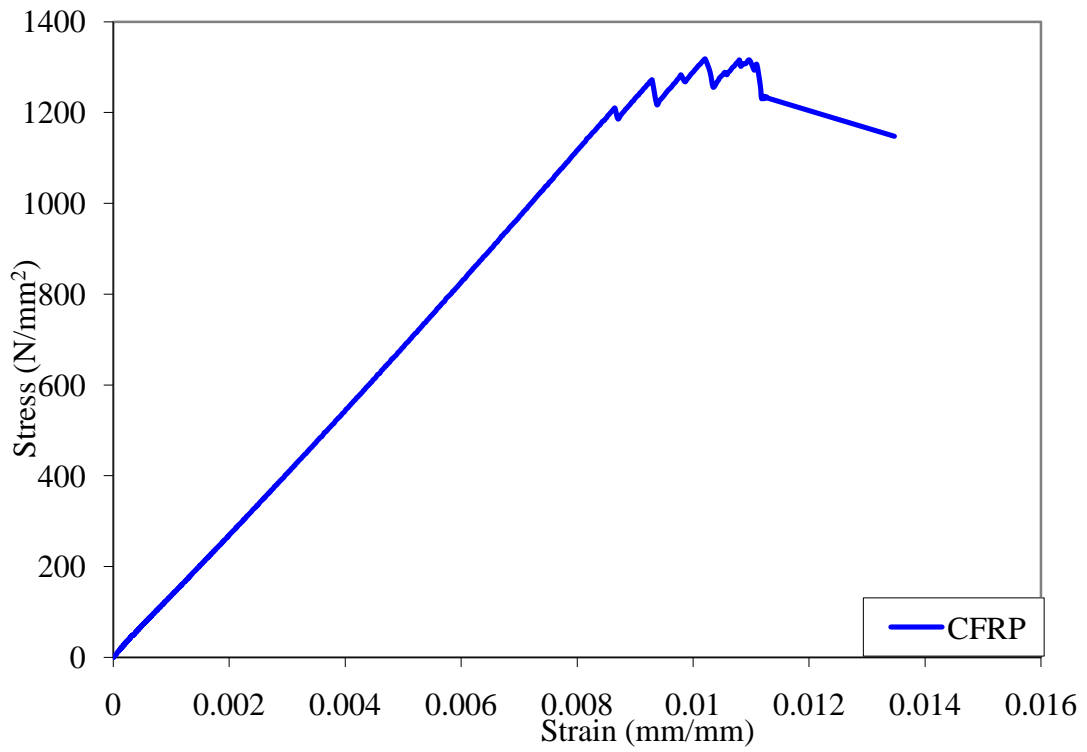
Figure 3-33. Stress-strain curve for CFRP Tension Test 1 – 100 mm x 1.40 mm.
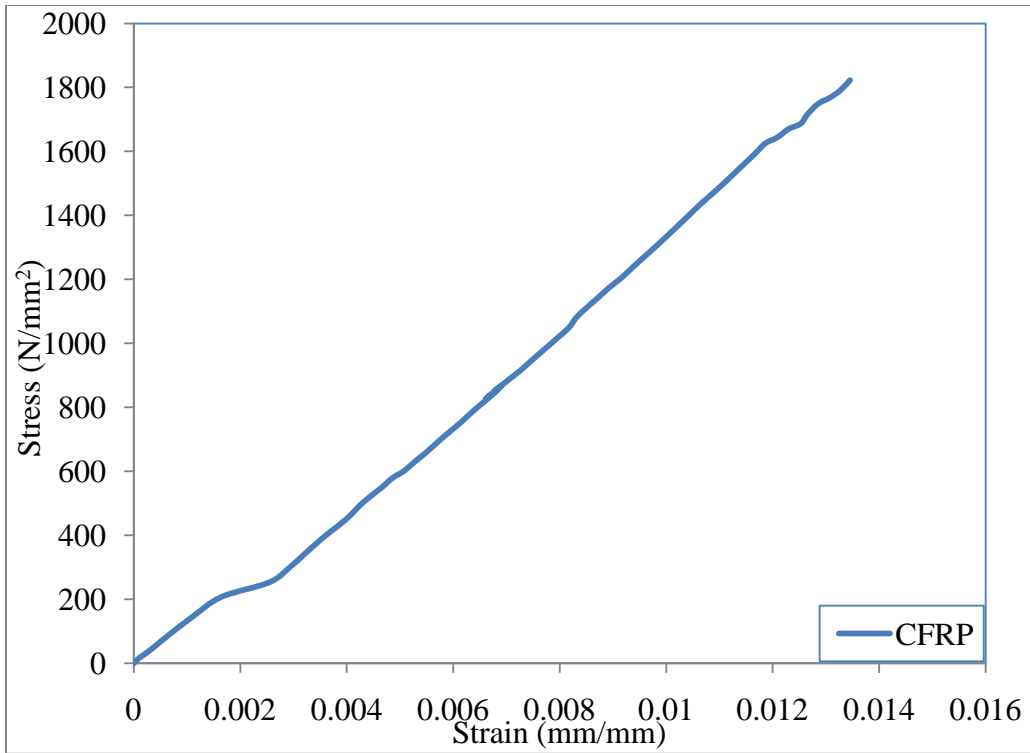
Figure 3-34. Stress-strain curve for CFRP Tension Test 2 – 100 mm x 1.40 mm.
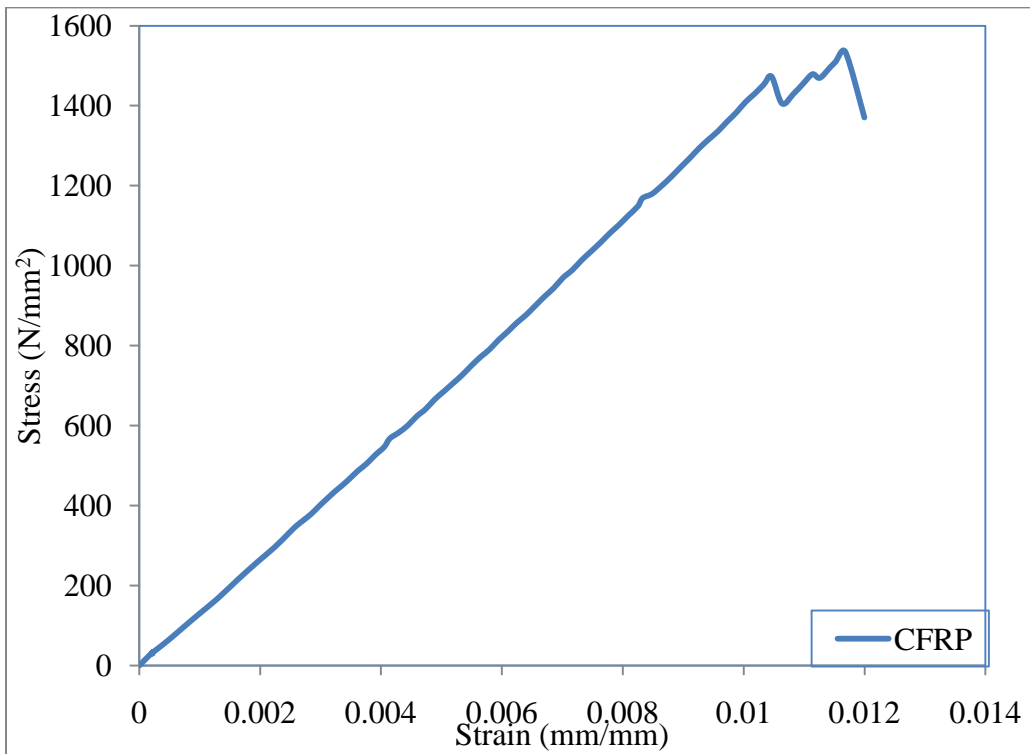
Figure 3-35. Stress-strain curve for CFRP Tension Test 3 – 50 mm x 1.40 mm.
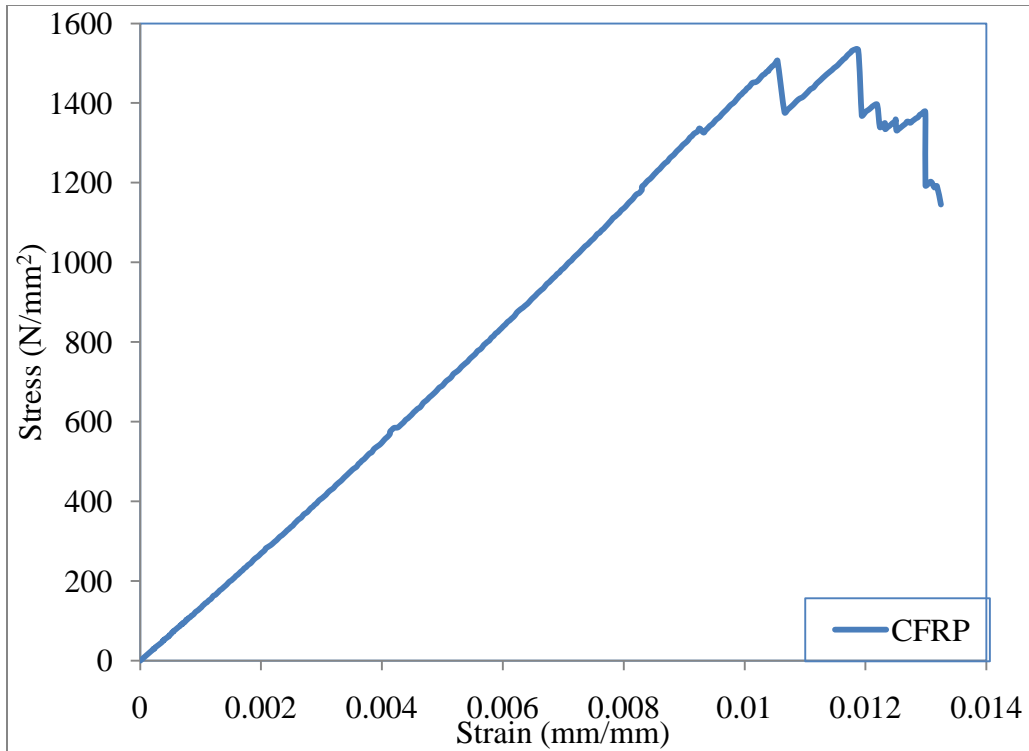
Figure 3-36. Stress-strain curve for CFRP Tension Test 4 – 100 mm x 1.40 mm.

The CFRP used in this study was not a high modulus CFRP but it was characterized by a relatively high strength compared that from other CFRP manufacturers. Table 3-5 compares the laminate properties of CFRP of similar thicknesses obtained from several manufacturers including Fyfe, Mitsubishi, and Epsilon. It is observed that even though CFRP from Fyfe has lower elasticity modulus as compared to Mitsubishi, the tensile strength of the Fyfe product is significantly higher than its counterparts.

Table 3-5. Laminate Properties of CFRP from Several Manufacturers Comparison

	(Fyfe, 2006)	Mitsubishi	Epsilon
Tensile modulus, E	155 GPa	229 GPa	460 GPa
Tensile strength, f_u	2790 MPa	1220 MPa	1530 MPa
Volumetric fiber content	68%	55%	70%
Laminate thickness (mm)	1.40-2.00	3.20	2.90-4.00

3.6 Summary

The chapter presents the experiments performed during the course of this research, starting with the tension tests performed on steel and CFRP specimens to obtain stiffness and strength

properties. The bulk of the experimental work was performed on five steel W200 x 19.3 (W8 x 13) beams topped by a steel plate that replaced the reinforced concrete deck. The chapter describes the steps executed in order to perform the tests. A summary of the results concludes this chapter.

At all times, the engineer / designer must understand the importance of achieving a good bond between the CFRP laminate and steel. To ensure a good bond, general CFRP installation steps can be summarized as follows:

- Prepare the steel surface using proper sand blasting techniques to obtain a white clean steel surface;
- Cut the CFRP and fiber fabric to the required lengths;
- Prepare wooden pieces to be used in the clamping process;
- Prepare enough C-clamps to use in the curing process;
- Clean the steel surface with rubbing alcohol and leave the surface to dry completely before proceeding to further steps;
- Apply the epoxy using the gun applicator;
- Distribute the epoxy using a trowel;
- Apply the fiber fabric layer to the steel surface;
- Add more epoxy as required;
- Install the CFRP laminate;
- Uniformly press on the CFRP laminate to ensure that the epoxy fills all of the voids under the laminate. The use of a clean, smooth cloth is recommended;
- Place the prepared wooden piece over the CFRP layer and use the clamps to apply uniform pressure along the CFRP length;
- Leave the CFRP to cure for at least 24 hours or as recommended by the epoxy manufacturer.

Section 4
Verification of FE Model

The chapter mainly describes the FE model built to simulate the steel beams tested experimentally in Chapter 3. Results from the verification models and the experimental results are compared in this chapter. The FE models are then used to perform the parametric study in Chapter 5.

4.1   Modeling Technique

A FE model was developed using the software package ABAQUS that was verified by the experimental program. ABAQUS and ANSYS were both considered during the research study by comparing both FE packages from the technical and GUI (graphical user interface) stand points. The technical comparison turned out that ABAQUS is much more capable of modeling fracture mechanics and contact problems through its enhanced solvers. The capabilities of ANSYS in fracture mechanics and contact options were satisfactory. From the GUI stand point, ABAQUS has a simple to use yet enhanced GUI, making it much more user friendly than the user menus in ANSYS. The basic program structure of ABAQUS is much more logical than the menu structure of ANSYS. The only advantage of ANSYS over ABAQUS is the number of users, due to its lower pricing.

Debonding and rupture of the CFRP plates is a geometrically nonlinear static problem that involves buckling or collapse behavior, where the load-displacement response represents a negative stiffness and the structure must release strain energy to remain in equilibrium. Several approaches are possible for modeling such behavior. One is to treat the buckling response dynamically, thus actually modeling the response with inertia effects imposed as the structure fails. Second, in some simple cases, a displacement control approach can provide a solution, even when the conjugate load (the reaction force) decreases as the displacement increases. A third approach would be to use dashpots to stabilize the structure during a static analysis. The fourth approach is the implementation of the modified Riks method, which provides static equilibrium during the unstable debonding phase of the response. This method is used for cases where the loading is proportional; that is, where the load magnitudes are governed by a single scalar parameter. The final fourth approach was the method used in this study.

4.2   Model Details

One begins modeling the experimental beams by defining the geometry. The beam together with the top plate and the CFRP layers were defined as parts. Furthermore, an adhesive layer between the CFRP plate and the lower surface of the steel beams' bottom flange had to be defined. Each part is first defined as a volume, which is then meshed into elements. The meshing size of each

part greatly depended in its relative size and the anticipated mode of failure. Element types and material properties were then specified and assigned to each corresponding part. Special element assignments were used for the CFRP laminate and adhesive layers, as will be demonstrated.

The meshing size for the steel parts was coarse due to the isotropic and ductile behavior of steel. The coarse mesh of the steel parts helped reduce the computing time. The CFRP plate and the adhesive layer had to be fine meshed to the anisotropic and brittle nature of the material, where a fine mesh would accurately predict the failure criteria defined by the material behavior, namely debonding and rupture. A coarse mesh for either the CFRP plate or the adhesive layer would have resulted in an unstable model with a non-converging solution. Since parts were meshed separately, no nodes were shared between adjacent parts. Therefore, contact surfaces had to be defined to create the bonding effect between parts. Surface constraints were used to tie the steel parts together (plate, top flange, web, and bottom flange) without any failure criteria defined, since full composite action controlled the actual behavior of the steel parts. These surface constraints made the meshing process simpler as opposed to attempting to fine mesh the parts to share common nodes at the interface. Further discussion on surface constraints is presented in the following section.

The loads were applied as unit loads at the third-point lengths of the beam, and a load proportionately factor (LPF) was calculated during the analysis of the model until failure criteria were reached. The nonlinear behavior of the steel and CFRP materials were defined in the model by the complete stress strain curves. Figure 4-1 shows an isometric view of the three-dimensional FE model developed, where each part was meshed separately. Surface constraints were defined to connect these parts together, without having connecting nodes between the parts, as previously discussed.

Figure 4-2 shows a full isometric view of the beam model. The applied loads can be seen at the third-point beam length on top of two transverse rigid parts. The rigid parts would ensure a uniform distribution of the concentrated line loads acting on the top plate, therefore avoiding local stress concentrations due to a point load acting at one particular node. Furthermore, the rigid part simulated the actual experimental setup discussed in Chapter 3.
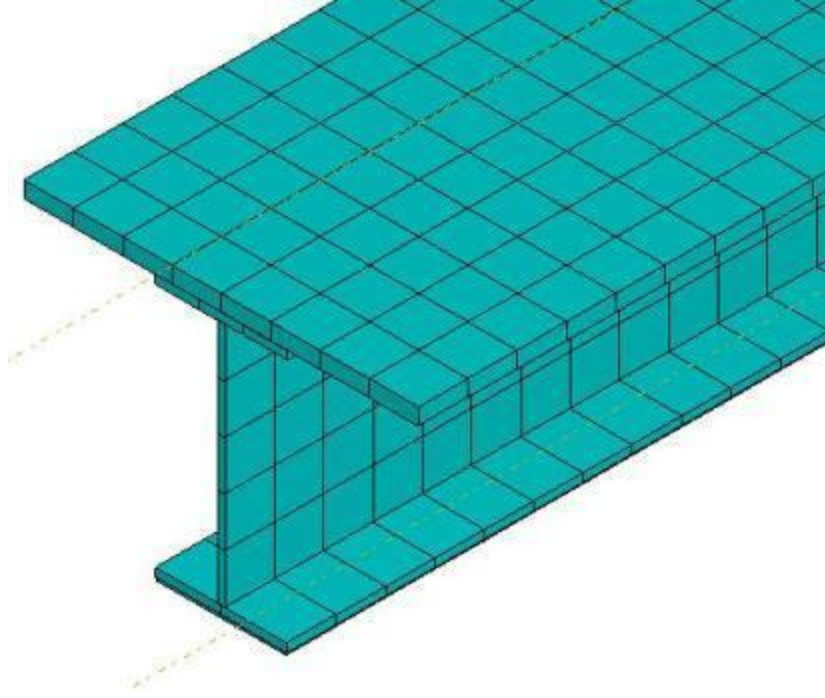
Figure 4-1. An isotropic view of the three-dimensional FE model.

Defining the concentrated load applied over time using the Riks method is presented in Figure 4-3. The magnitude and direction of the force on each of the two rigid parts was 500 N vertically downwards, which did add up to 1 kN, the unity loading for proper use of the Riks technique. The output of the Riks loading was a loading proportionality factor (LPF) and was read later in the output in kN. Figure 4-4 and Figure 4-5 present the boundary constraints defined for the hinged and roller supports, respectively.
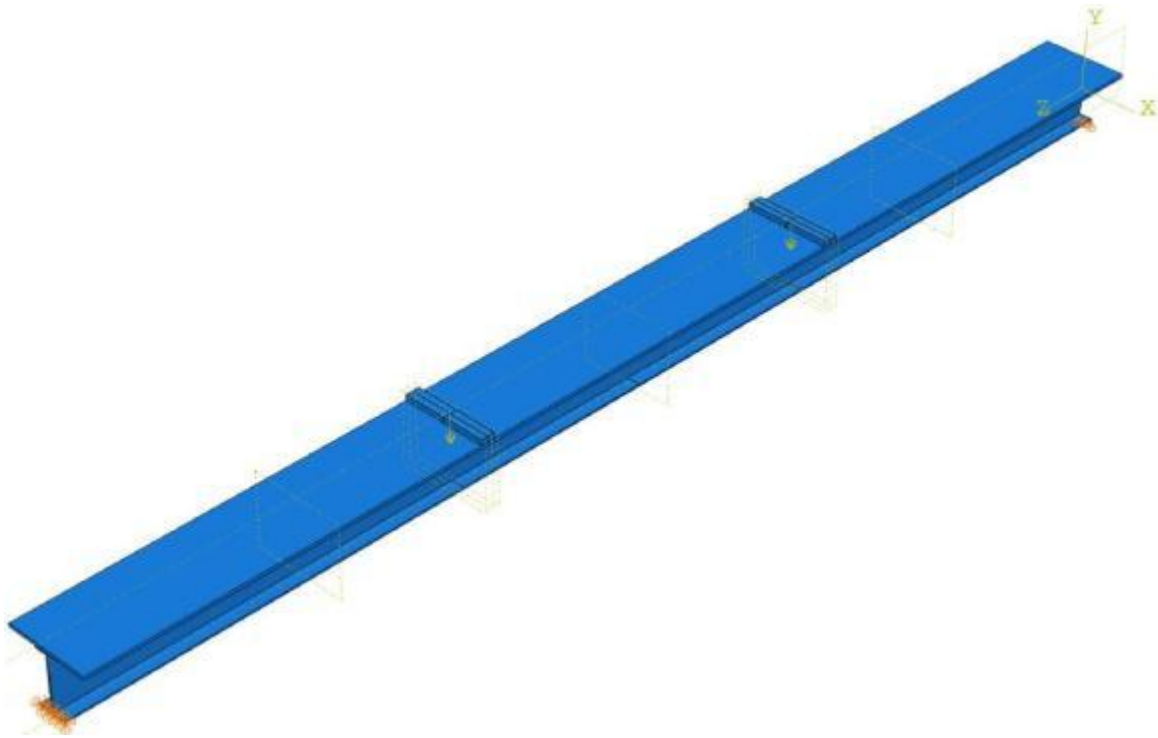
Figure 4-2. Isometric iiew of the beam model – loads shown.
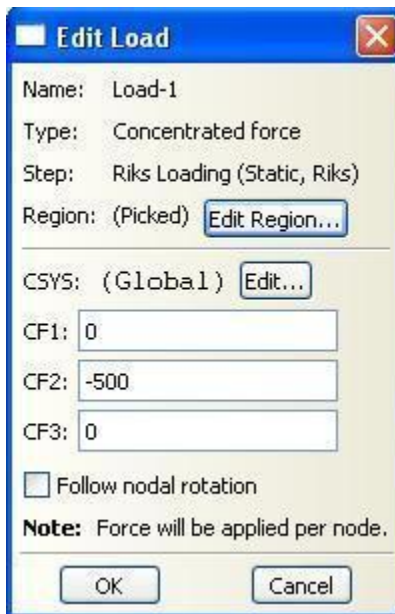
Figure 4-3. Concentrated load definition.
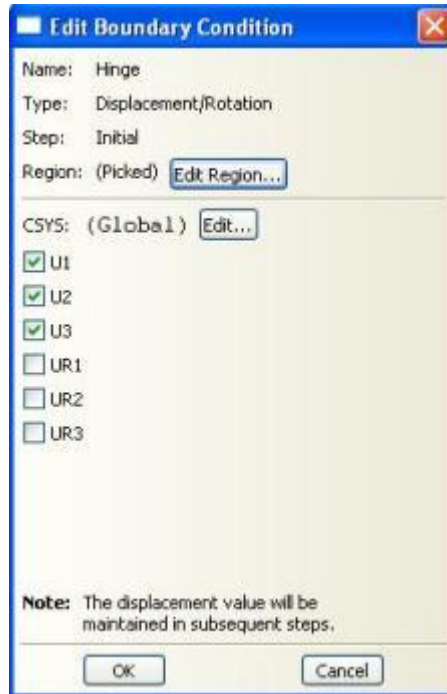
Figure 4-4. Boundary conditions – Hinged support.
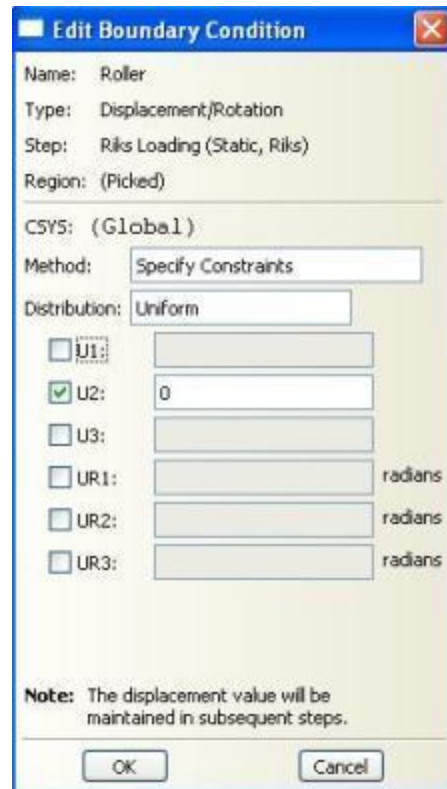
Figure 4-5. Boundary conditions – roller support.

4.3   Element Interaction Simulation and Special FE Models

Special FE models are discussed in this section to illustrate the steps taken to simulate correctly the interaction behavior between the various components of the composite beams.

4.3.1   Cohesive Elements and Adhesive Material Modeling

ABAQUS offers a damage model enabling the prediction of the onset of rupture and the modeling of damage evolution for elastic-brittle materials with anisotropic behavior, such as the CFRP laminates. The model is primarily intended to be used with fiber-reinforced materials since they typically exhibit such behavior. The damage model requires specification of the following: the undamaged response of the material that must be linearly elastic, a damage initiation criterion, and a damage evolution response where elements can be removed. Damage is characterized by the degradation of material stiffness. It plays an important role in the analysis of fiber-reinforced composite materials. Many such materials exhibit elastic-brittle behavior where damage is initiated without significant plastic deformation. Consequently, plasticity can be neglected when modeling the behavior of such materials. Four different modes of failure are considered: (1) fiber rupture in tension, (2) fiber buckling and kinking in compression, (3) matrix cracking under transverse tension and shearing, and (4) matrix crushing under transverse compression and shearing. In ABAQUS the onset of damage is determined by the initiation criteria proposed by Hashin (Hashin & Rotem, 1973); and (Hashin, 1980).

ABAQUS offers a library of cohesive elements to model the behavior of adhesive joints, interfaces in composites, and other situations where the integrity and strength of interfaces may be of interest. The cohesive element COH3D8 represented the epoxy used to bond the CFRP laminate to the steel beam. Modeling of cohesive elements consisted of choosing the appropriate element type, defining the initial geometry of the cohesive elements, and defining the mechanical constitutive behavior of the cohesive elements. The constitutive response of these elements depends on the specific application, namely continuum, gasket, and traction-separation. It is based on certain assumptions that the deformation and stress states are appropriate for each application area. For this model, traction-separation response was used to model the bond interface between the CFRP laminate and the steel beam. The modeling of bonded interfaces in composite materials often involves situations where the intermediate glue material is very thin and, for all practical purposes, may be considered to be of zero thickness. In three-dimensional problems the traction-separation-based model assumes three components of separation, one normal to the interface and two parallel to it, and the corresponding stress components are assumed to be active at a material point. Using the cohesive elements and adhesive material models, together with introducing the strain at which debonding was expected helped model the debonding behavior of the CFRP plate attached to the steel beam.

Modeling with cohesive elements consists of several steps. The first step is choosing the appropriate cohesive element type, including the cohesive elements in a finite element model, connecting them to other components, and understanding typical modeling issues that arise during modeling using cohesive elements. The second step is defining the initial geometry of the cohesive elements. Third, the mechanical constitutive behavior of the cohesive elements can be defined by (1) a continuum-based constitutive model; (2) a uniaxial stress-based constitutive

model, which is useful in modeling gaskets and/or single adhesive patches; or (3) a constitutive model specified directly in terms of traction versus separation. This study used the third behavior for cohesive elements, a three-dimensional traction separation model.

The cohesive elements could be used in areas of the model where it is expected that cracking would develop. It is not required that the model have initial cracking modeled. In fact, the precise locations where cracks initiate, as well as the evolution characteristics of such cracks, are determined as part of the solution. The cracks are restricted to propagate along the layer of cohesive elements and will not deflect into the surrounding material. Figure 4-6 shows a typical use of cohesive elements traction separation-based modeling, the debonding along a skin-stringer interface.
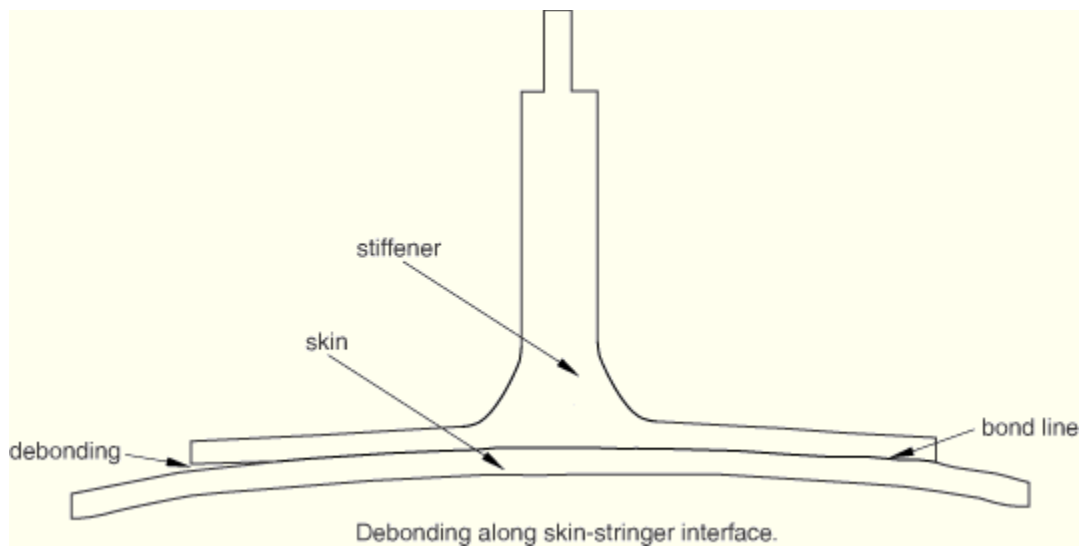
Figure 4-6. Debonding along a skin-stringer interface: typical situation for traction-separation-based modeling (*Abaqus Analysis User Manual*, 2007).

Figure 4-7 shows the form used in defining the cohesive elements in the model developed in this study. In essence, cohesive elements are used to model adhesives between two components, each of which may be deformable or rigid. They are used to model interfacial debonding using a cohesive zone framework.

Figure 4-7. Cohesive element definition form.

4.3.2 Mesh Tie Constraints

A surface-based tie constraint fully bonds two surfaces together for the duration of a simulation. It can be used only with surface-based constraint definitions. It can also be used to create a constraint on a surface so that it follows the motion of a three-dimensional beam. Surface-based constraints are useful for mesh refinement purposes, especially for three-dimensional problems, as they allow for rapid transitions in mesh density within the model. The idea behind surface constraints is to constrain each of the nodes on the slave surface to have the same motion as the point on the master surface to which it is closest. In addition, they eliminate the degrees of freedom of the slave surface nodes that are constrained, where possible.

Figure 4-8 shows the surface constraints definition form. The two surfaces to be constrained were predefined, then one surface was selected as a master surface, while the other was selected as a slave surface which would follow all of the translations and rotations of the master surface.
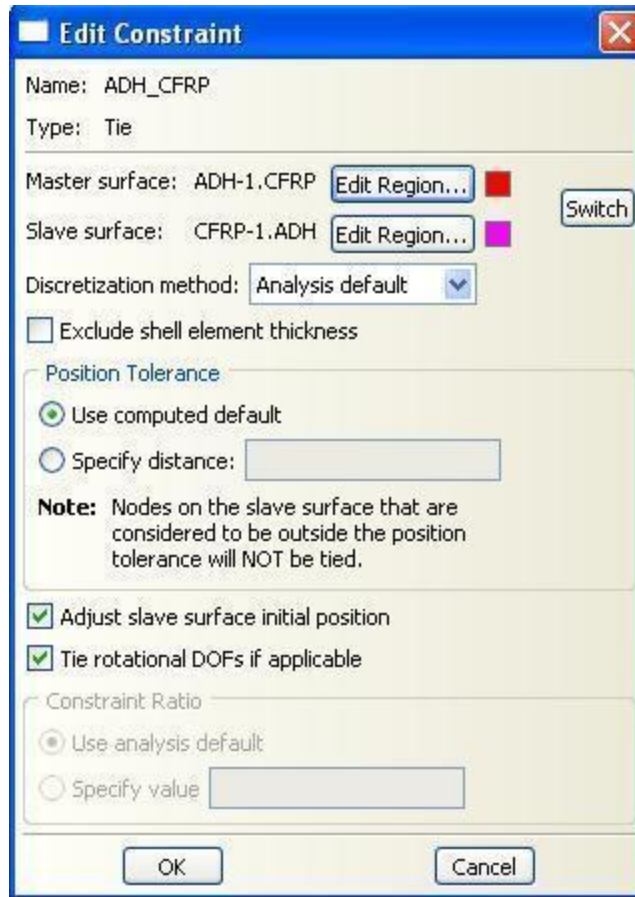
Figure 4-8. Surface constraints definition.

4.4 Compatibility of Steel Top Plate to Concrete Slab

The experimental program in Chapter 3 was performed using a steel top plate instead of a concrete slab. FE analysis was used to verify that the replacement was acceptable and compatible. A model with a concrete slab was built and compared to the models with a steel top plate.

4.4.1 Concrete

The smeared crack concrete model in ABAQUS was used to verify the compatibility of using a steel top plate to the typical concrete slab. The FE software provides a general capability for modeling reinforced concrete in all types of structures, including beams, trusses, shells, and solids The smeared crack concrete model is designed for applications in which the concrete is subjected to essentially monotonic straining at low confining pressures, which was the case with the four-point bending tests conducted. It consists of an isotropically hardening yield surface that is active when the stress is dominantly compressive and has an independent "crack detection surface" that determines if a point fails by cracking.

The smeared crack model uses oriented damaged elasticity concepts (smeared cracking) to describe the reversible part of the material's response after cracking failure. Reinforcement in concrete structures is typically provided by means of rebars, which are one-dimensional strain theory elements (rods) that can be defined singly or embedded in oriented surfaces. Rebars are typically used with metal plasticity models to describe the behavior of the rebar material and are superimposed on a mesh of standard element types used to model the concrete.

With this modeling approach, the concrete behavior was considered independently of the rebar. Effects associated with the rebar/concrete interface, such as bond slip and dowel action, are modeled approximately by introducing some "tension stiffening" into the concrete modeling to simulate load transfer across cracks through the rebar. Details regarding tension stiffening are provided in the following sections.

Defining the rebar can be tedious in complex problems, but it is important that this be done accurately since it may cause an analysis to fail due to a lack of reinforcement in key regions of a model. The composite section model built had the concrete section mainly in compression, but rebar was necessary to stabilize the solution and prevent early crack detection in the concrete section that would lead to inaccurate failure modes. This would be needed especially when the concrete was under tension stresses due to the upward shifting of the neutral axis from the steel-concrete interface to within the concrete slab as the loading increased. In this case, rebar would play an important role in carrying the tension forces, allowing the model to continue solving for the overall failure behavior.

The postfailure behavior for direct straining across cracks is modeled with tension stiffening, which allows one to define the strain-softening behavior for cracked concrete. This behavior also allows for the effects of the reinforcement interaction with concrete to be simulated in a simple manner. Tension stiffening is required in the concrete smeared cracking model. You can specify tension stiffening by means of a postfailure stress-strain relation or by applying a fracture energy cracking criterion.

4.4.1.1 Crack Detection

Cracking is assumed to occur when the stress reaches a failure surface that is called the "crack detection surface." This failure surface is a linear relationship between the equivalent pressure stress, p, and the Mises equivalent deviatoric stress, q, and is illustrated in Figure 4-9. When a crack has been detected, its orientation is stored for subsequent calculations. Subsequent cracking at the same point is restricted to being orthogonal to this direction, since stress components associated with an open crack are not included in the definition of the failure surface used for detecting the additional cracks.

Cracks are irrecoverable; they remain for the rest of the calculation (but may open and close). No more than three cracks can occur at any point (two in a plane stress case, one in a uniaxial stress case). Following crack detection, the crack affects the calculations because a damaged elasticity model is used. Oriented damaged elasticity is discussed in more detail in "An inelastic

constitutive model for concrete", Section 4.5.1 of the Abaqus Theory Manual *(Abaqus Analysis User Manual*, 2007).
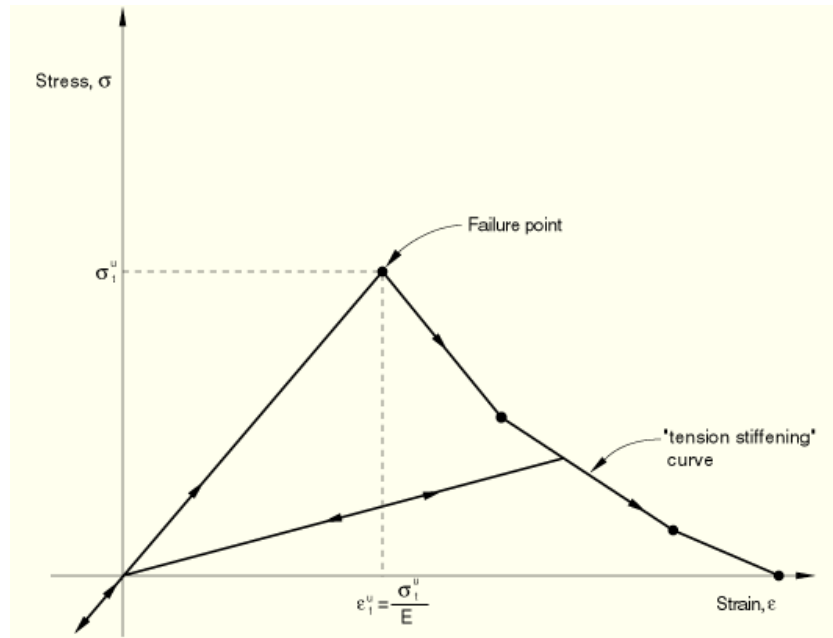
Figure 4-9. Tension stiffening model (*Abaqus Analysis User Manual*, 2007).

4.4.1.2 Fracture Energy Cracking Criterion

As discussed earlier, when there is no reinforcement in significant regions of a concrete model, the strain softening approach for defining tension stiffening may introduce unreasonable mesh sensitivity into the results. Crisfield (1986) discusses this issue and concludes that Hillerborg (1976) proposal is adequate to allay the concern for many practical purposes. Hillerborg defines the energy required to open a unit area of crack as a material parameter, using brittle fracture concepts. With this approach the concrete's brittle behavior is characterized by a stress-displacement response rather than a stress-strain response. Under tension a concrete specimen will crack across some section. After it has been pulled apart sufficiently for most of the stress to be removed (so that the elastic strain is small), its length will be determined primarily by the opening at the crack. The opening does not depend on the specimen's length (Figure 4-10).
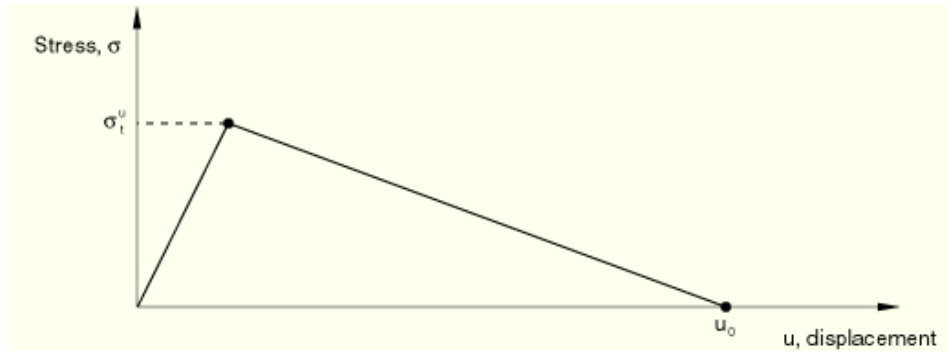
Figure 4-10. Fracture energy cracking model (*Abaqus Analysis User Manual,* 2007).

4.4.2 Compressive Behavior of the Concrete Model

The cracking and compressive responses of concrete that are incorporated in the concrete model are illustrated by the uniaxial response of a specimen shown in Figure 4-11. When concrete is loaded in compression, it initially exhibits elastic response. As the stress is increased, some non-recoverable (inelastic) straining occurs and the response of the material softens. An ultimate stress is reached, after which the material loses strength until it can no longer carry any stress. If the load is removed at some point after inelastic straining has occurred, the unloading response is softer than the initial elastic response: the elasticity has been damaged. This effect is ignored in the model, since we assume that the applications involve primarily monotonic straining, with only occasional, minor un-loadings. When a uniaxial concrete specimen is loaded in tension, it responds elastically until, at a stress that is typically 7%–10% of the ultimate compressive stress, cracks form so quickly that, even in the stiffest testing machines, it is very difficult to observe the actual behavior. The model assumes that cracking causes damage, in the sense that open cracks can be represented by a loss of elastic stiffness. It is also assumed that there is no permanent strain associated with cracking. This will allow cracks to close completely if the stress across them becomes compressive.
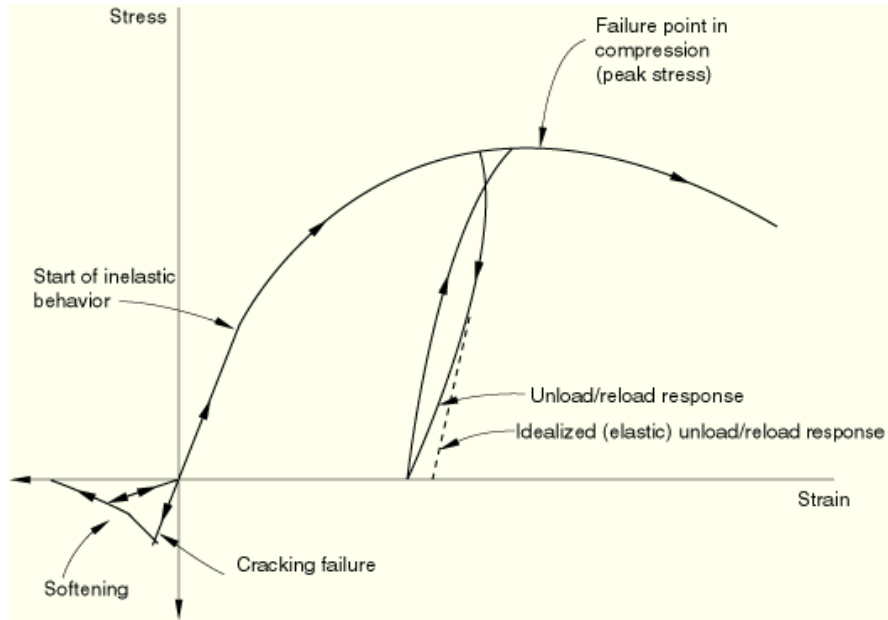
Figure 4-11. Uniaxial behavior of plain concrete (*Abaqus Analysis User Manual*, 2007).

4.5   Failure Modes in FE Models

Several modes of failure were programmed and defined in the ABAQUS FE models built to correctly develop a model that simulates the actual beams. In addition to modes of failure, the failure limits and material strength were also of great concern. In this section, the modes of failure anticipated, together with the material limits are discussed. The modes of failure taken into consideration were for (1) the steel beam, (2) the concrete slab, (3) the CFRP rupture, and (4) the CFRP debonding (epoxy failure).

4.5.1   Steel Beam Failure

Steel material was defined using its classical elastic and plastic properties. Elastic properties (Figure 4-12) were the Young's modulus, E = 185000 N/mm^2, and Poisson's ratio, ν = 0.3. The plastic material properties were specified as seen in Figure 4-13, where the data inputted starting from the yield point.
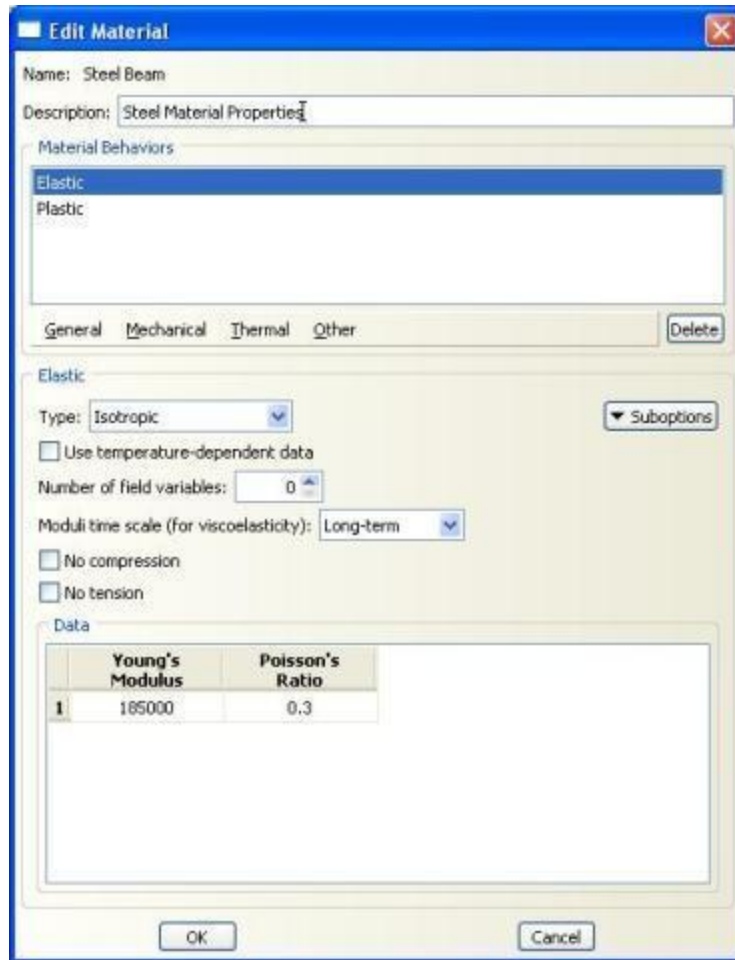
Figure 4-12. Steel elastic material properties.
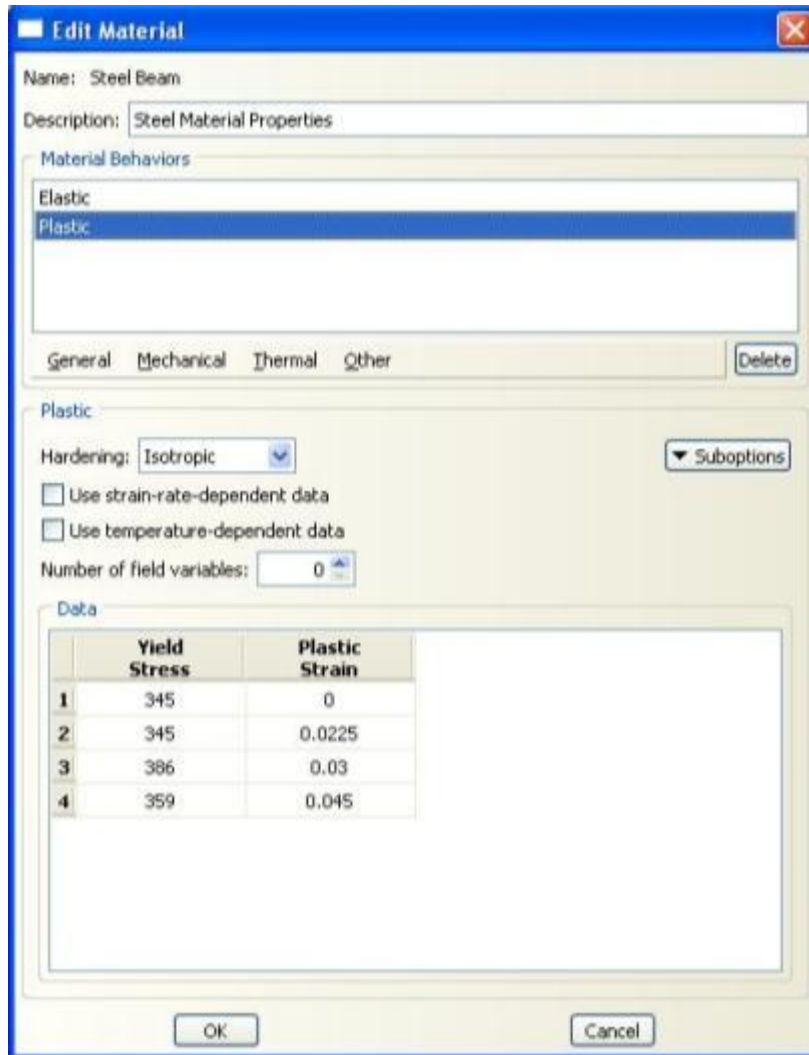
Figure 4-13. Steel plastic material properties.

4.5.2 Concrete Failure

Concrete material was defined using its classical elastic and plastic properties. Elastic properties (Figure 4-14) were the Young's modulus, $E = 18000$ N/mm^2, and poisson's ratio, $v = 0.15$.
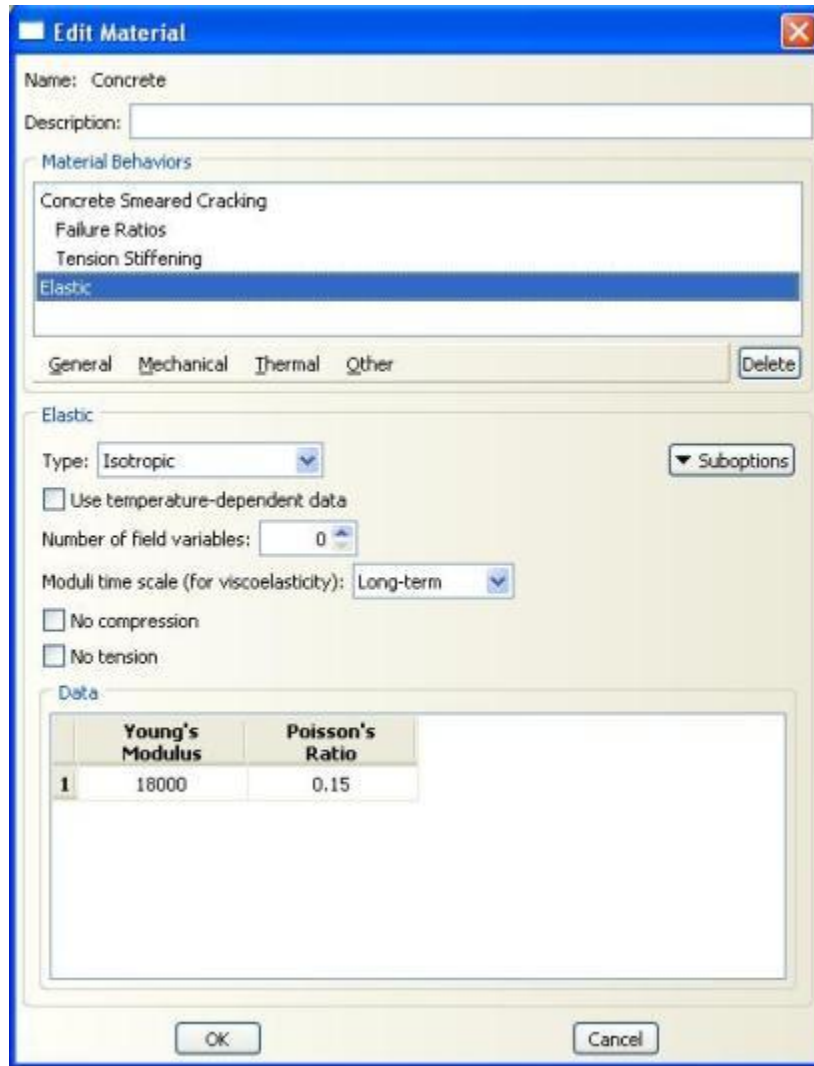
Figure 4-14. Concrete elastic material properties.

The concrete smeared cracking properties were specified as seen in Figure 4-15, where the data were inputted starting from the plastic point. The figure shows the values that were obtained from solved examples in the Abaqus reference manual (Abaqus Analysis User Manual, 2007). Concrete tension stiffening properties are shown in Figure 4-16.
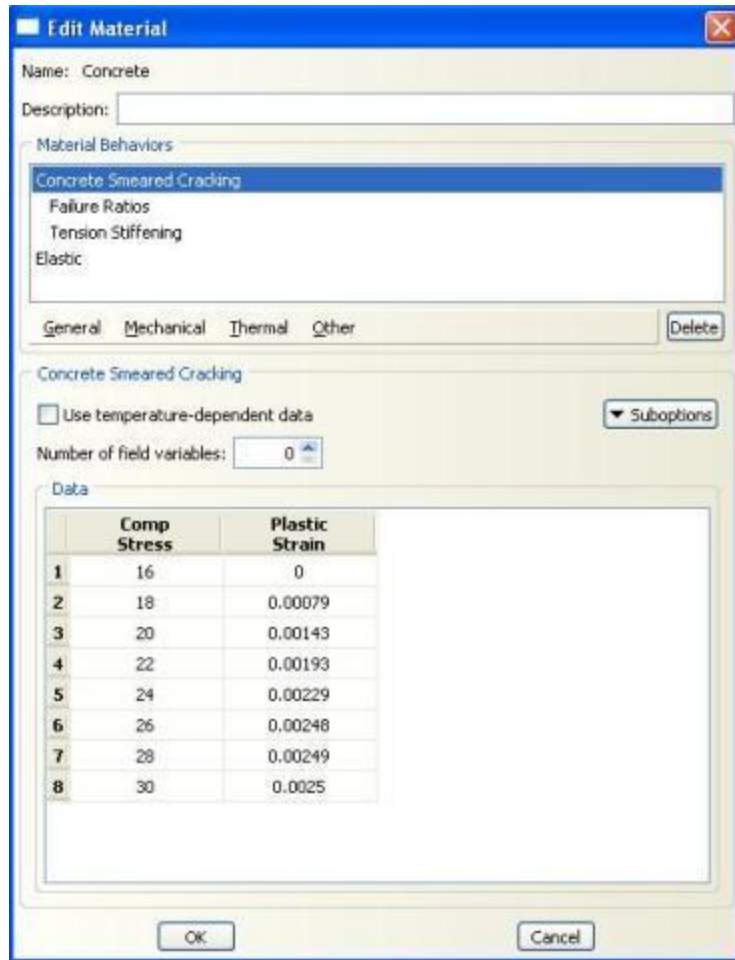
Figure 4-15. Concrete smeared cracking material properties.
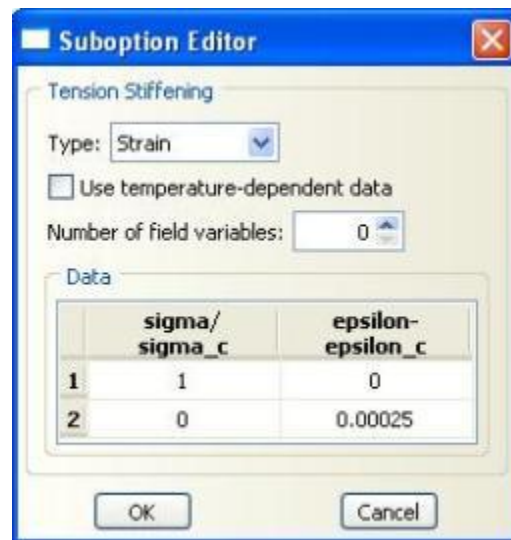
Figure 4-16. Concrete tension stiffening.

You can specify failure ratios to define the shape of the failure surface. Figure 4-17 shows the values that were obtained from solved examples in the Abaqus reference manual (*Abaqus Analysis User Manual*, 2007). Four failure ratios can be specified:

- The ratio of the ultimate biaxial compressive stress to the ultimate uniaxial compressive stress.
- The absolute value of the ratio of the uniaxial tensile stress at failure to the ultimate uniaxial compressive stress.
- The ratio of the magnitude of a principal component of plastic strain at ultimate stress in biaxial compression to the plastic strain at ultimate stress in uniaxial compression.
- The ratio of the tensile principal stress at cracking, in plane stress, when the other principal stress is at the ultimate compressive value, to the tensile cracking stress under uniaxial tension.
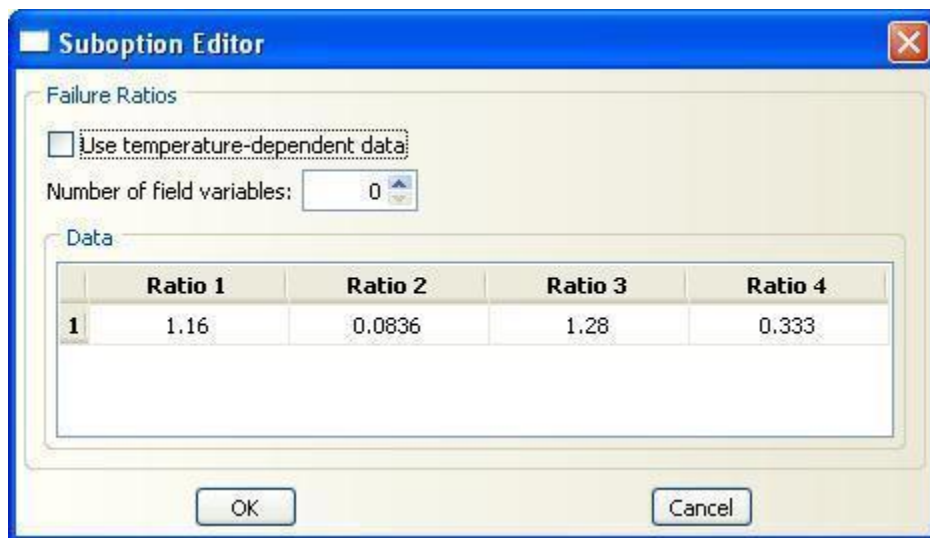
Figure 4-17. Concrete failure ratios.

4.5.3   CFRP Rupture

CFRP modeling in ABAQUS was done using Hashin models, as previously mentioned. The model has two main steps:

- Hashin Damage;
- Elastic material properties.

Figure 4-18 shows the window used for defining Hashin damage values that were obtained from the manufacturer, as well as tension test results and solved examples in the Abaqus reference manual (*Abaqus Analysis User Manual*, 2007). The values used were as follows:

- Longitudinal tensile strength = 3790 N/mm^2
- Longitudinal compressive strength = 2000 N/mm^2
- Transverse tensile strength = 1800 N/mm^2
- Transverse compressive strength = 1000 N/mm^2
- Longitudinal shear strength = 500 N/mm^2
- Transverse shear strength = 500 N/mm^2

Figure 4-19 shows the form used for defining damage evolution values. Values were obtained from solved examples in the Abaqus reference manual (*Abaqus Analysis User Manual*, 2007). The values used were as follows:

- Longitudinal tensile fracture energy = 50 kg.mm^2 / s^2 (μJ)
- Longitudinal compressive fracture energy = 50 kg.mm^2 / s^2 (μJ)
- Transverse tensile fracture energy = 10 kg.mm^2 / s^2 (μJ)
- Transverse compressive fracture energy = 10 kg.mm^2 / s^2 (μJ)

Figure 4-18. CFRP damage strength.
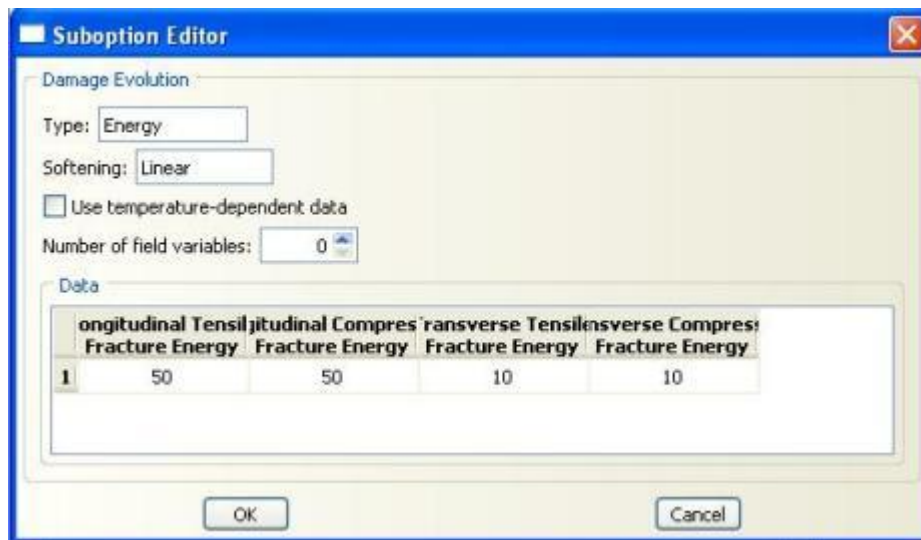
Figure 4-19. CFRP damage evolution.

Figure 4-20 shows the damage stabilization values used for the models. Values were also obtained from solved examples in the Abaqus reference manual (*Abaqus Analysis User Manual,* 2007). The values used were as follows:

- Viscosity coefficient in the longitudinal tensile direction = 0.001
- Viscosity coefficient in the longitudinal compressive direction = 0.001
- Viscosity coefficient in the transverse tensile direction = 0.005
- Viscosity coefficient in the transverse compressive direction = 0.005
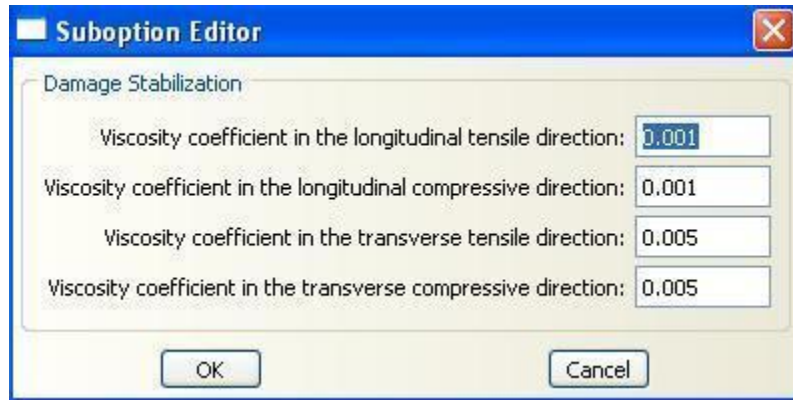
Figure 4-20. CFRP damage stabilization.

The CFRP elastic material properties are shown in Figure 4-21. Values were obtained from the manufacturer, tension test results, and solved examples in the Abaqus reference manual *(Abaqus Analysis User Manual,* 2007). The values used were as follows:

- E1 (Young's modulus in Longitudinal Direction) = 231000 N/mm^2
- E2 (Young's modulus in Transverse Direction) = 200000 N/mm^2
- v12 (Poisson's Ratio) = 0 N/mm^2
- G12 (Shear Modulus) = 600 N/mm^2
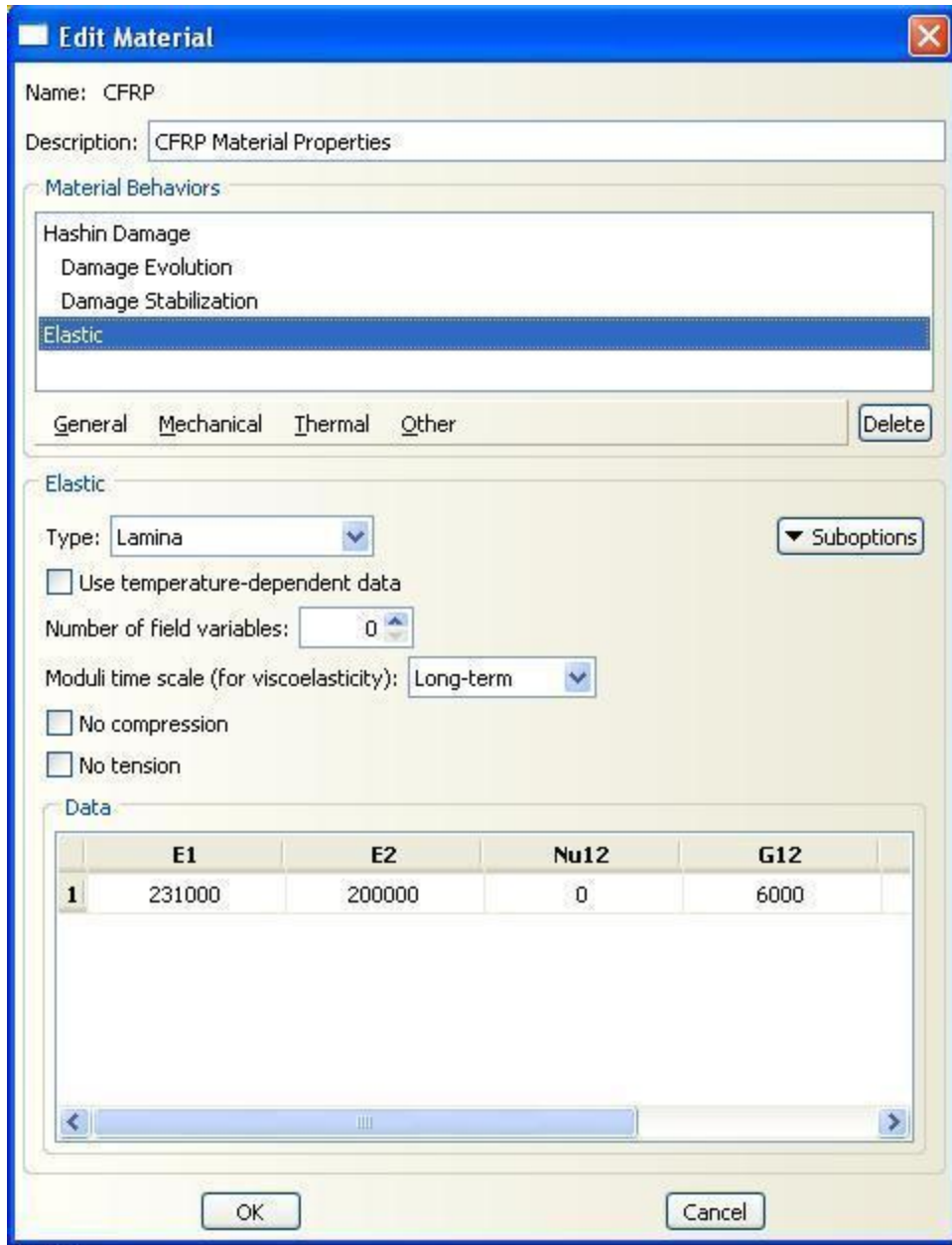
Figure 4-21. CFRP elastic material properties.

Figure 4-22 shows the definition of the CFRP section. The section was defined as a continuum homogeneous shell with CFRP material properties defined in Figure 4-18 to Figure 4-21. The only variable introduced in this form was the CFRP laminate thickness, which was shown to be 1.40 mm in this window. Different values were used for different models.
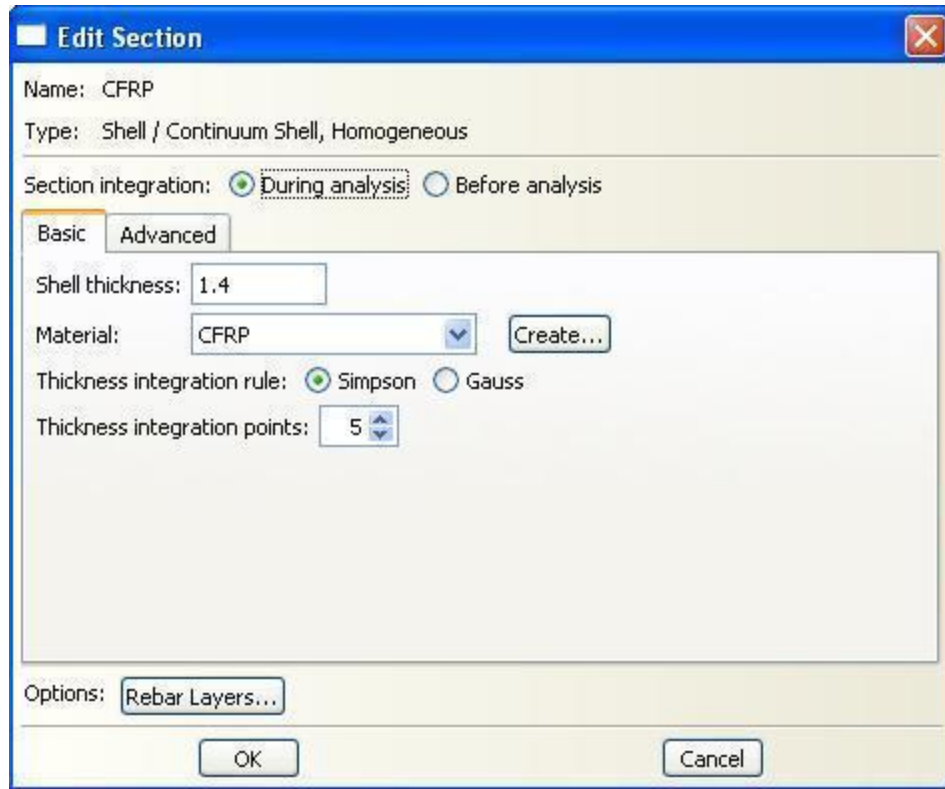
Figure 4-22. CFRP section definition.

4.5.4   CFRP Debonding – Epoxy Failure

Adhesive material (epoxy) was defined in the model to connect the CFRP laminate to the bottom flange of the steel beam. Adhesive definition is divided into two parts, the Quade damage and the elastic material properties. Values were obtained from the literature and solved examples in the Abaqus reference manual (*Abaqus Analysis User Manual*, 2007). Figure 4-23 shows the Quade damage definition of the adhesive elements. Data inputted in this form were the nominal strain values at which the epoxy layer looses its stiffness and starts failing:

- Nominal strain – Normal-only mode = 2.5e-5
- Nominal strain – Shear-only mode first direction = 6.65e-5
- Nominal strain – Shear-only mode second direction = 6.65e-5

A sub-option that was defined with the damage definition was the damage evolution option shown in Figure 4-24, which was the default value recommended by Abaqus *(Abaqus Analysis User Manual,* 2007). The adhesive elastic material properties are shown in Figure 4-25. Values were obtained from solved examples in the Abaqus reference manual *(Abaqus Analysis User Manual,* 2007). The values used were as follows:

- E (Young's modulus in Longitudinal Direction) = 200000 N/mm^2
- G1 (Shear Modulus in direction 1) = 75188 N/mm^2

- G2 (Shear Modulus in direction 2) = 75188 N/mm^2
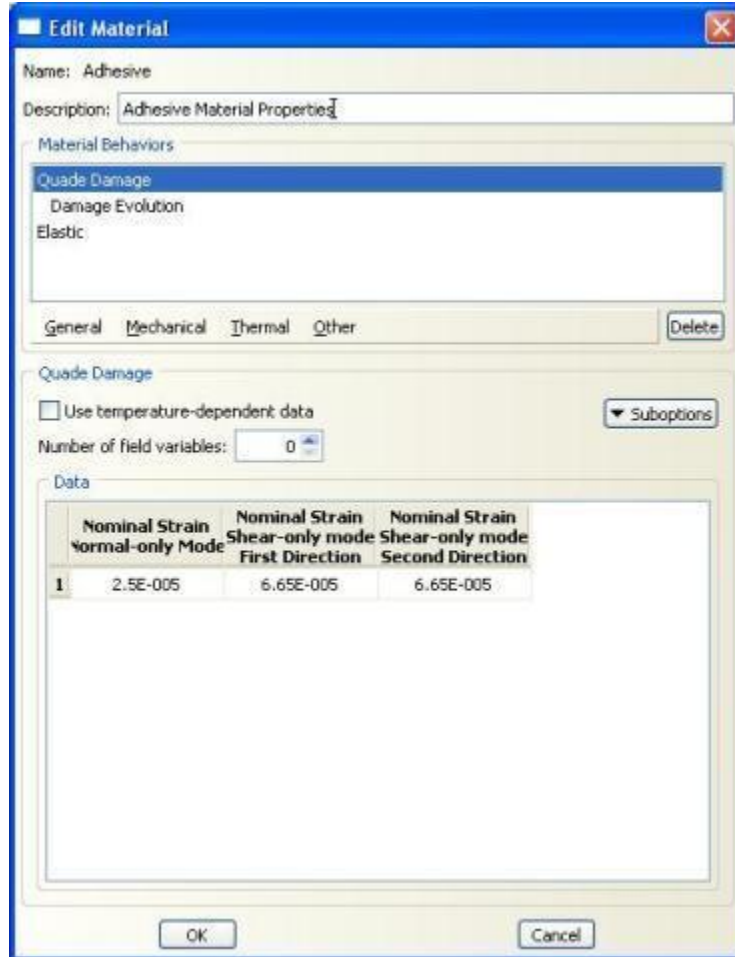
Figure 4-23. Epoxy damage properties.
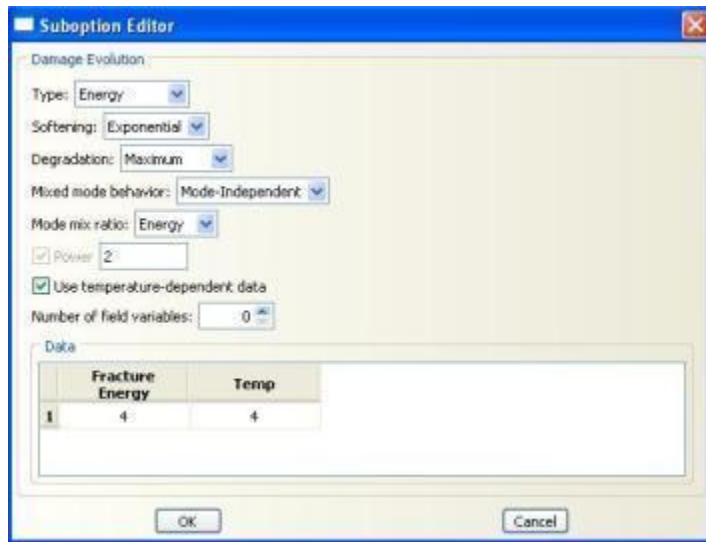
Figure 4-24. Epoxy damage evolution.
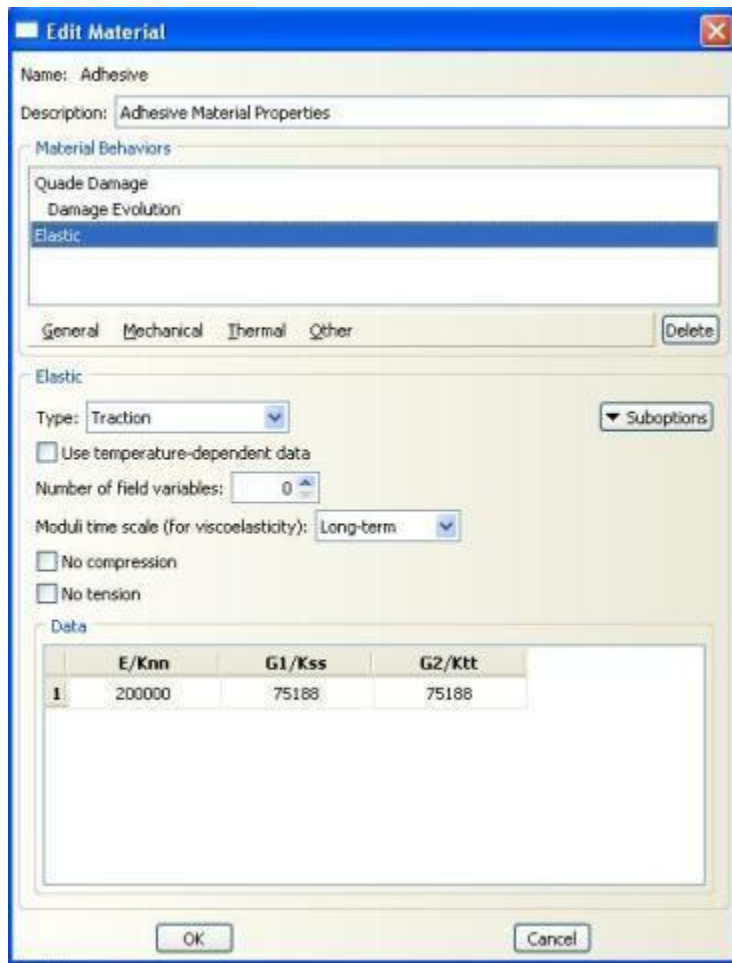
Figure 4-25. Epoxy elastic material properties.

4.6 Results

The verification of FE models built versus experimental work is presented in the following sections. Models with concrete deck versus models with the steel top plate are also compared to validate the assumption regarding replacement of the concrete deck with a steel plate.

4.6.1 Concrete Slab versus Steel Top Plate

The findings of the comparisons of the concrete slab and the steel top plate demonstrate that an excellent correlation exists between them. For all the different configurations of the CFRP strips tested, the models accurately predicted the debonding points, the ultimate load capacity, and deflections. Figure 4-26 through Figure 4-30 present the load-deflection curves obtained from the concrete-slab model and steel-plate model for Beams 1 through Beam 5. The curves show very good correlation between the two models, which indicates that replacing the concrete slab with a steel plate was successful. The concrete model was a little more stiff in the plastic zone at very high deflections.
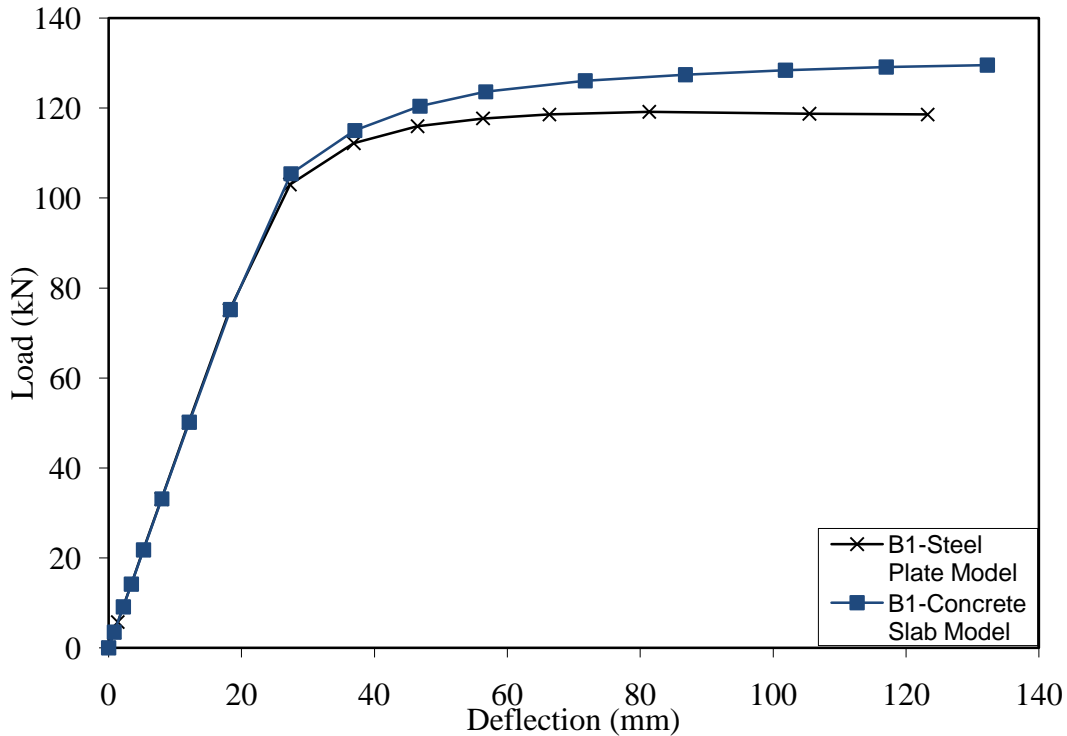
Figure 4-26. Load-deflection – steel plate vs. concrete slab – Beam 1.
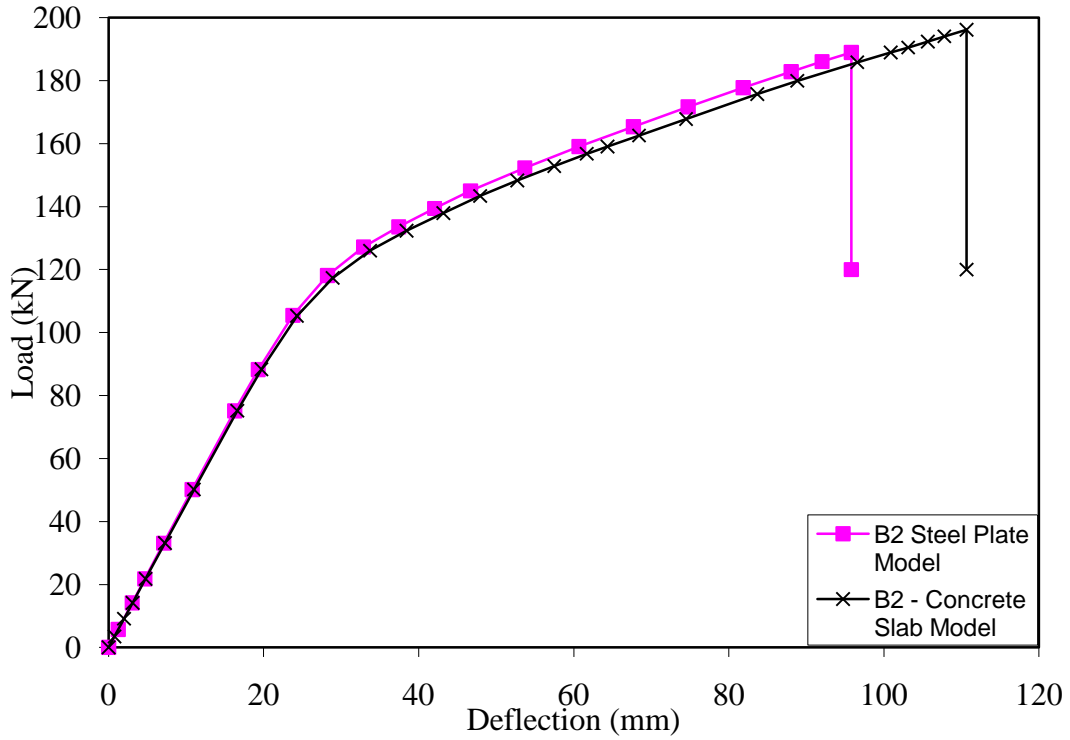
Figure 4-27. Load-deflection – steel plate vs. concrete slab – Beam 2.
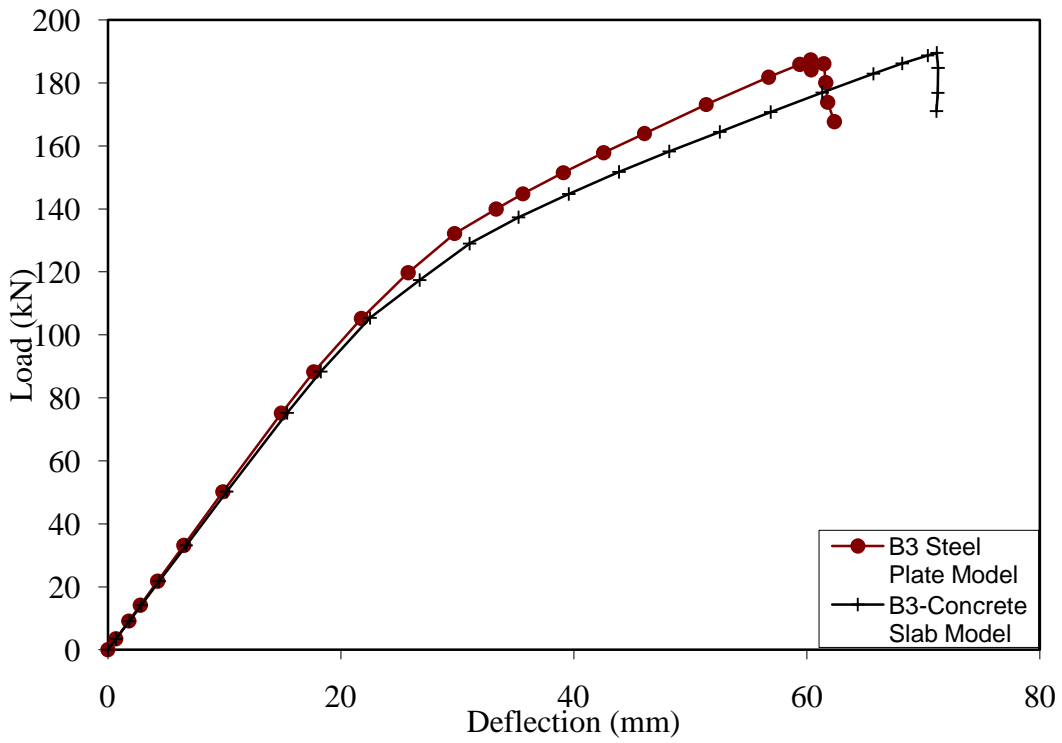
Figure 4-28. Load-deflection – steel plate vs. concrete slab – Beam 3.
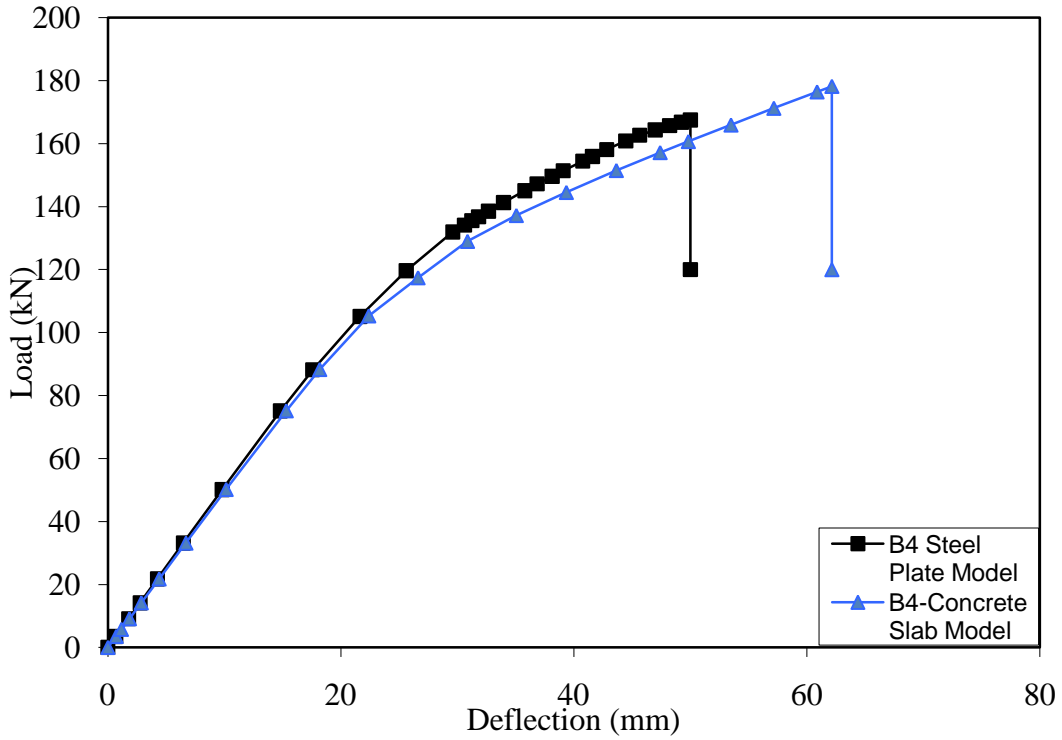
Figure 4-29. Load-deflection – Steel plate vs. concrete slab – Beam 4.
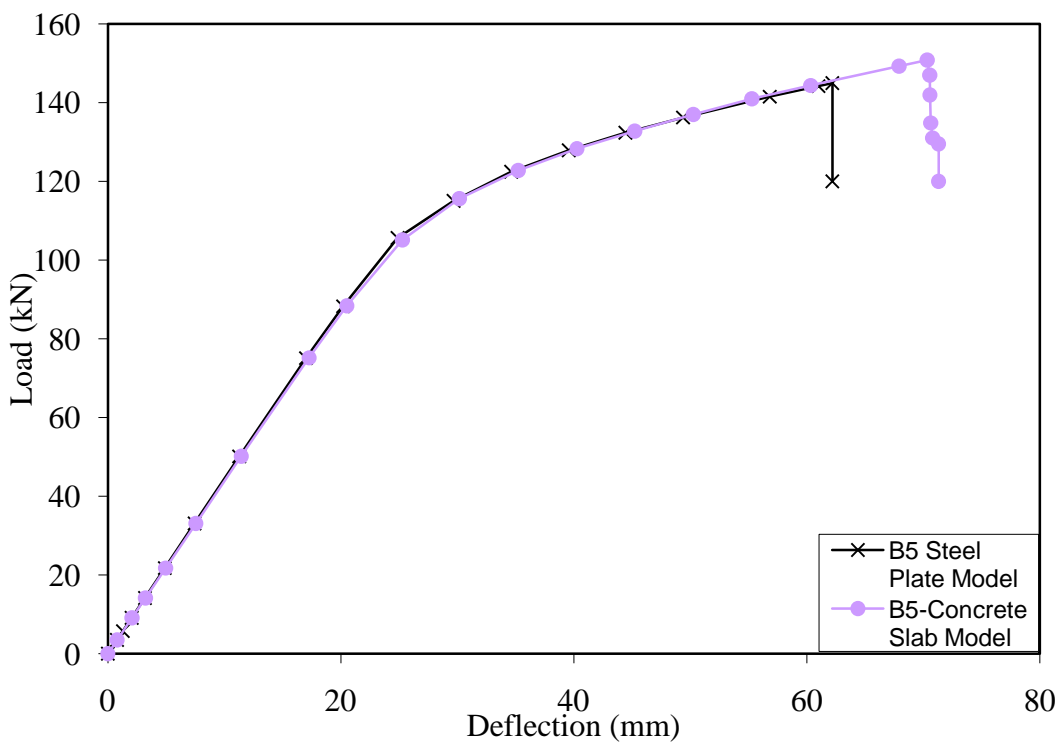
Figure 4-30. Load-deflection – steel plate vs. concrete slab – Beam 5.

69

4.6.2 Verification of FE Model by the Tested Beams

The verification of the FE models to the experimental tests is presented in this section. It was found that an excellent correlation exists between the experimentally tested steel beams and the FE models built. For all of the different configurations of the CFRP strips, the models accurately predicted the debonding points, the ultimate load capacity, and deflections. Strain comparison was also performed and showed a good correlation. This is observed in Figure 4-31 through Figure 4-34.
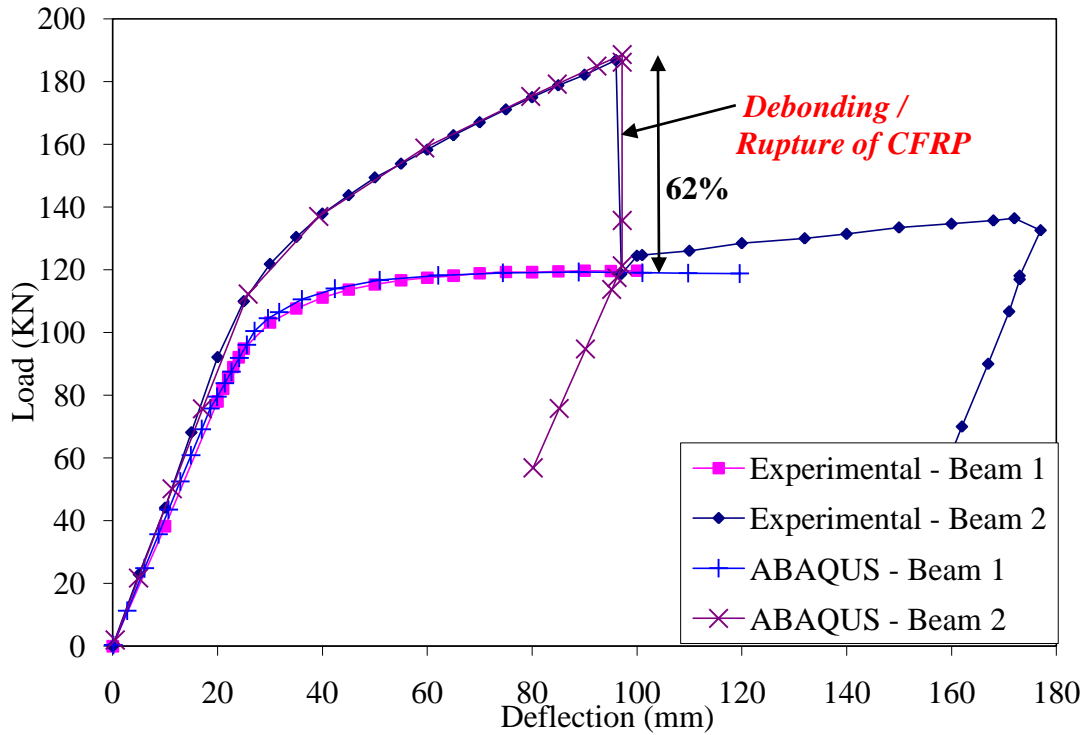
Figure 4-31. **Load-deflection curve for Beams 1 and 2 – experimental vs. Abaqus.**
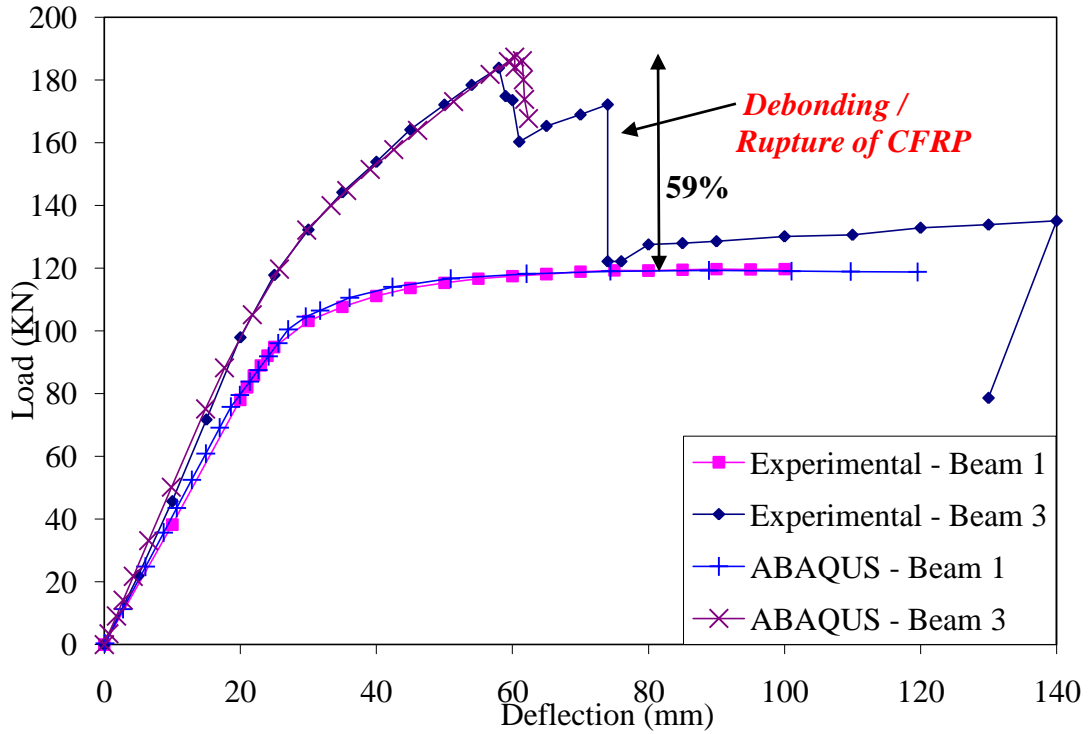
Figure 4-32. Load-deflection curve for Beams 1 and 3 – experimental vs. Abaqus.
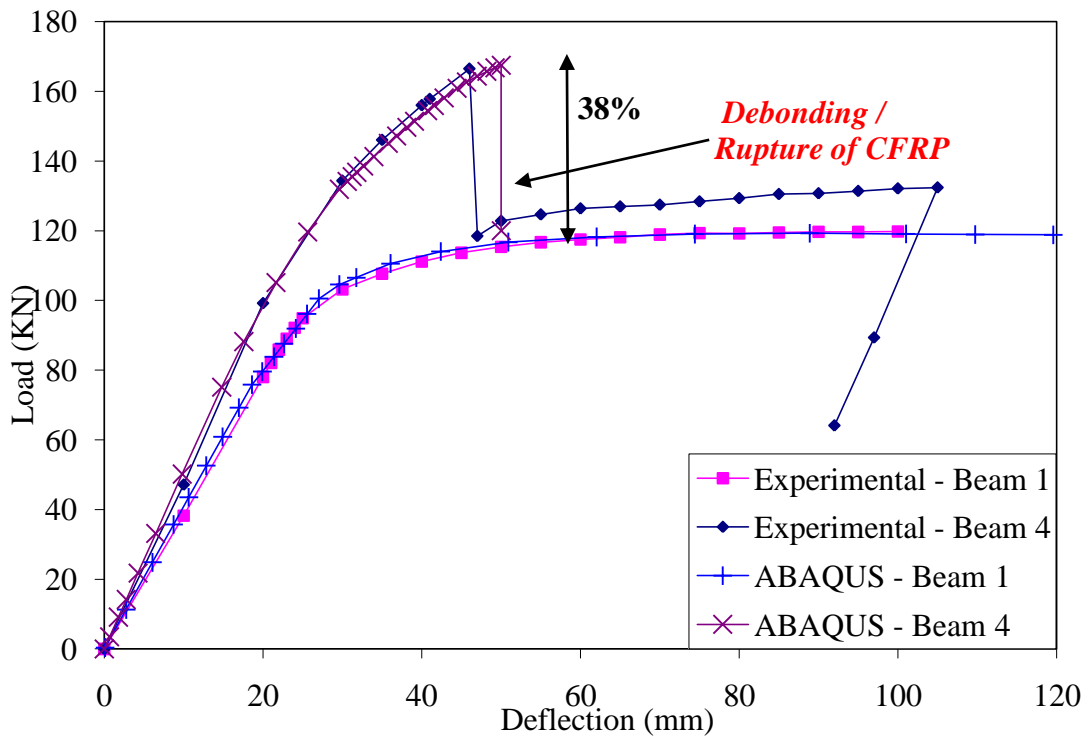
Figure 4-33. Load-deflection curve for Beams 1 and 4 – experimental vs. Abaqus.
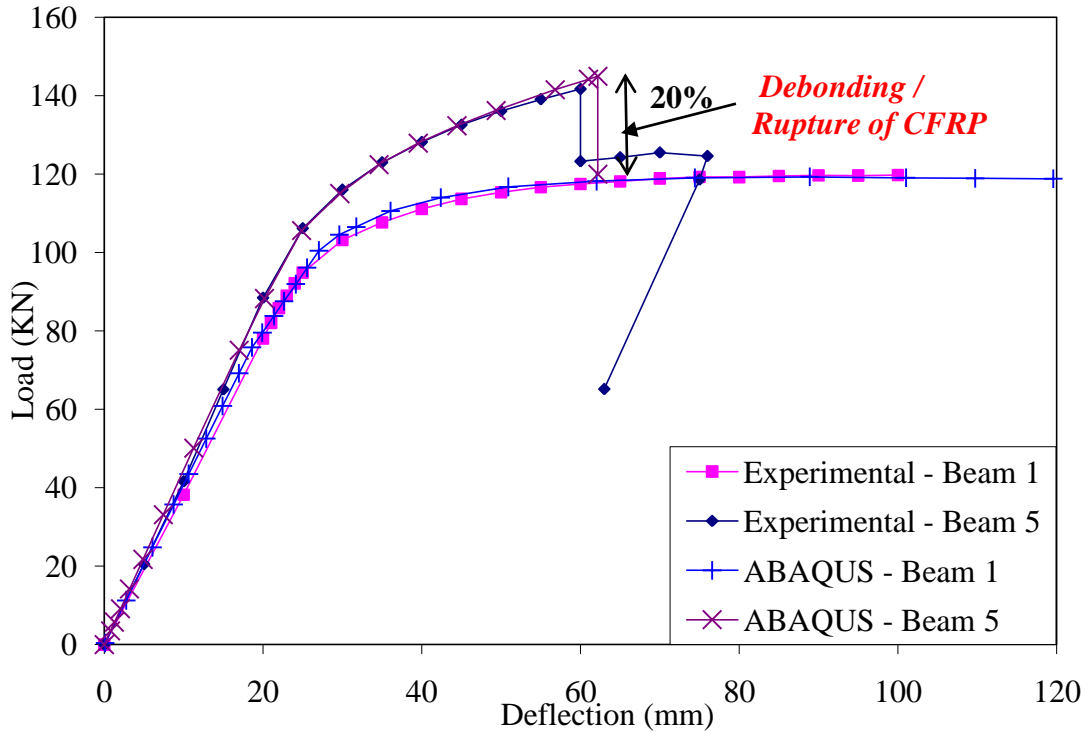
Figure 4-34. Load deflection curve for Beams 1 and 5 – experimental vs. Abaqus.

Based on all of these correlated models, a parametric study was performed, as shown in the following chapter, to test the sensitive parameters of steel beams strengthened using CFRP laminates.

4.6.3 Strain-Depth Verification

Strain-depth comparisons between the verification FE models and the experimental tests showed excellent correlation at the early loading stages, while strain readings started to deviate at the later stages. The strain-depth comparisons will be demonstrated in this section through a group of graphs (Figure 4-35, Figure 4-36, and Figure 4-37). Each graph shows three load levels at which the comparison occurs. Load steps are implied by ABAQUS load steps. That is why they do not exactly match the previous discussed load levels of 30%, 60%, and 90%.

Figure 4-35 shows the strain-depth variations of Beam 1. Three load stages were investigated: 33.11 kN, 75.40 kN, and 102.92 kN. Experimental results versus FE results show excellent correlation at all stages.

Figure 4-36 shows the strain-depth variations of Beam 2. Three load stages were investigated; 50.14 kN, 114.41 kN, and 159.89 kN. The comparison of experimental results versus FE results shows excellent correlation at early loading stages. Experimental strain readings exceed the FE strain reading at the 159.89 kN load level.

Figure 4-37 shows the strain-depth variations of Beam 3. Three load stages were investigated: 50.17 kN, 108.30 kN, and 160.06 kN. The comparison of experimental results versus FE results shows excellent correlation at the early loading stages. Experimental strain readings exceed the FE strain reading at the 160.06 kN load level.
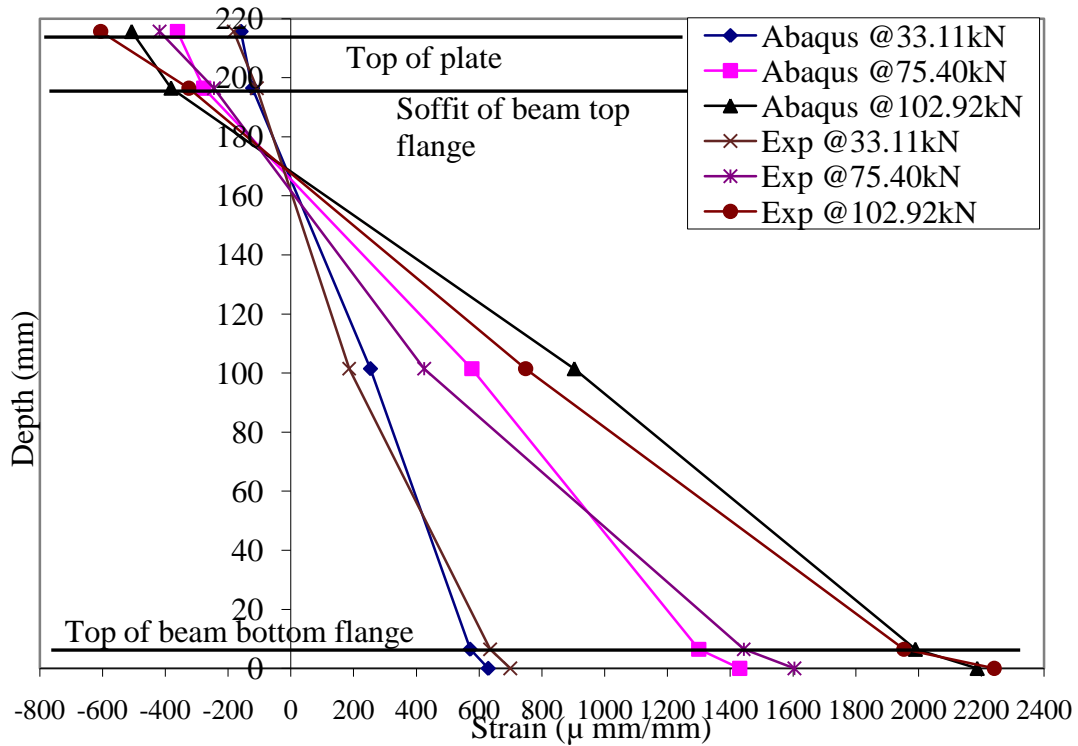
Figure 4-35. Beam depth-strain – experimental vs. Abaqus – Beam 1.
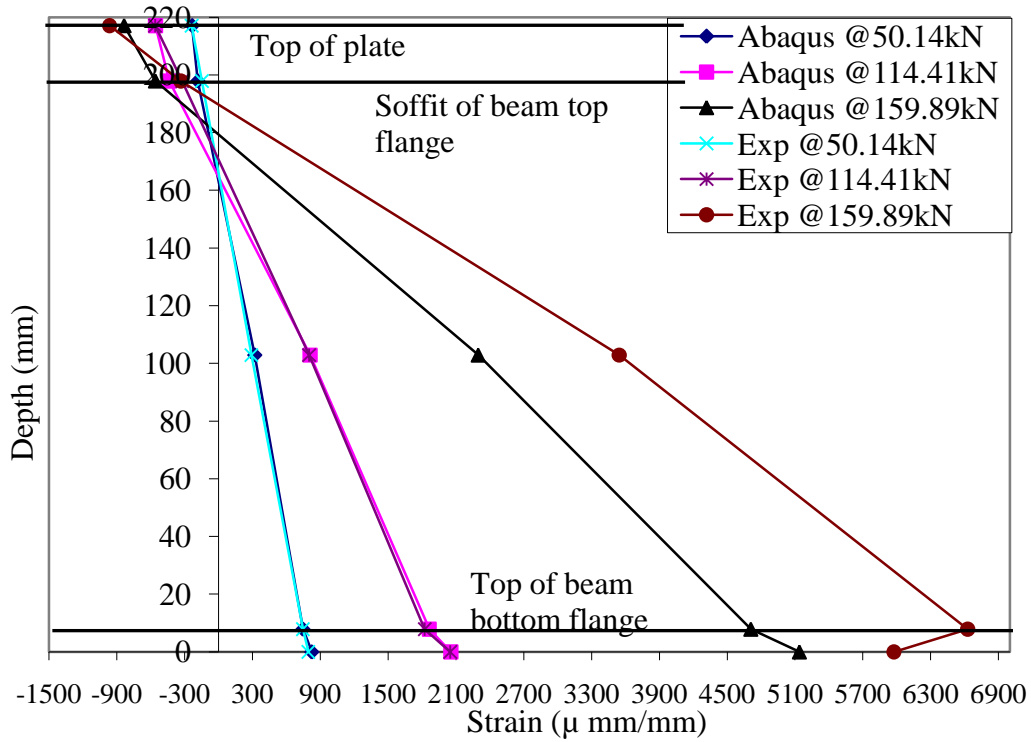
Figure 4-36. Beam depth-strain – experimental vs. Abaqus – Beam 2.
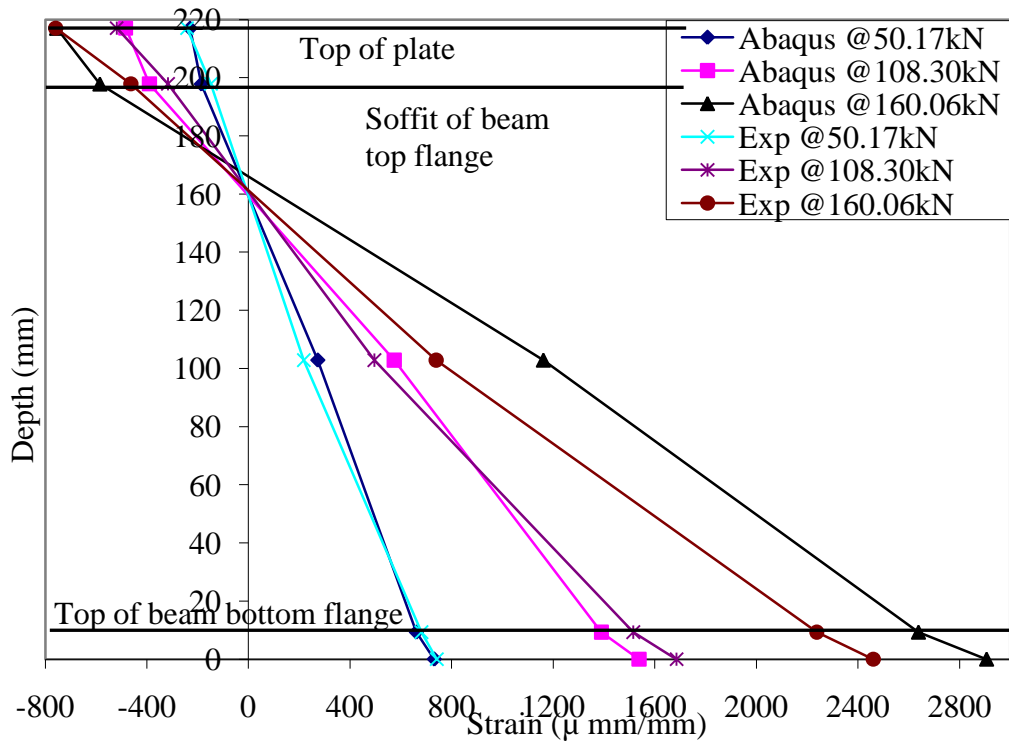
Figure 4-37. Beam depth-strain – experimental vs. Abaqus – Beam 3.

74

4.7 Summary

Verification of the FE model built to simulate the steel beams tested experimentally in Chapter 3 showed excellent correlation. Load-deflection curves were compared from both the verification models and the experimental results. Strain-depth curves were also compared. Results from the verification models and the experimental results were compared. The FE models were ready to perform the parametric study.

Section 5
Parametric Study

5.1   Introduction

While traditional retrofitting methods could be time consuming and uneconomical, an alternative repair method is suggested using CFRP laminate strips, providing engineers with a competitive solution that will increase the life-cycle of bridges repaired. The experimental work conducted showed that the method is effective and provided a reliable option to strengthen and rehabilitate steel girder bridges. Work in this chapter investigates the various parameters effecting its utilization. The study summarizes the extensive parametric FE analysis work conducted to strengthen steel beams using the novel CFRP laminate strips configurations.

The results of the parametric study demonstrated a significant gain in the beam's elastic and ultimate capacities. The ultimate gain of the beam greatly depends on the configuration of the CFRP laminates and the laminate's dimensions. The conclusion is that there are specific sensitive parameters controlling the effectiveness of the CFRP laminate rehabilitation technique. An adequate design of the rehabilitation method, which takes into consideration the effective parameters, would result in an effective design.

An extensive parametric study was conducted using the FE model developed in the previous chapter to investigate the sensitive parameters affecting the behavior of composite beams strengthened by CFRP plates. The parametric study involved the development of approximately 100 models, and through a process of elimination, the most effective parameters were established. Therefore, once a parameter is proved to be ineffective, it is eliminated from continued testing.

This chapter starts by introducing the parametric study table implemented, and results for each beam case were then discussed and analyzed. Finally, the results are presented with design recommendations for the structural engineer for an optimum design.

5.2   Parametric Study Program

The parametric study program was based on experimental and FE analysis work previously conducted (Salama & Abd-El-Meguid, 2007). Three small-scale steel beam models were developed to investigate the effectiveness of using different configurations of CFRP laminates to increase the strength and stiffness of steel highway bridge girders. Each beam had the same length and was loaded monotonically to failure using a four-point bending configuration separated equally. Uniform loading was investigated as an additional parameter. A schematic diagram of the cross-section of a typical modeled beam and the strain gages location is shown in

Figure 3-1. Figure 3-6 (a, b, c, & d) show the different CFRP configurations used for strengthening beams throughout the parametric study.

The W200 x 19.3 (W8 x 13), W310 x 38.7 (W12 x 26), and W410 x 53 (W16 x 36) steel beam sections proved to be the most appropriate based on the preliminary design criteria. Deeper beam sections were chosen in order to show that the CFRP rehabilitation is effective on any steel section when appropriately designed.

The factor that affected the beam selection was the span-to-depth ratio used for bridge design. Furthermore, steel bridges are composed of steel girders attached by shear connectors to the overlaying concrete slab. In the models developed, the concrete deck was replaced by a steel plate to control the experimental variation in concrete strength produced by different concrete batches. The steel plate was designed to have the neutral axis at the top flange of the steel beam, causing the beam to be mainly in tension and the plate in compression. The steel plate's width provided the beam with sufficient lateral support to avoid any lateral torsional buckling.

Preliminary design was done using an Excel spreadsheet with Visual Basic programming. The Visual Basic modules programmed are found in Appendix A and B. The sheet was divided into input (Table 5-1) and output phases (Table 5-2). The input sheet starts with the choice of the steel section where steel section properties are automatically extracted from stored section databases. Dimensions and material properties of the CFRP laminates and the steel top plate were the second input phase in the sheet. Loading was the final input phase in the sheet. Calculations are always automatically updated once an input changes. The output sheet (Table 5-2) starts by displaying the local stability and compactness of the chosen section. After all checks were performed, a message saying that the "section is compact" and "no instability" can be read. In the next output phase, the plastic neutral axis and the section plastic capacity were calculated for each step of the strengthening of the steel beam. The calculation of the plastic neutral axis included an iteration method, which is where the Visual Basic programming code was introduced. Plastic moment capacity was calculated using a Visual Basic module. Shear factor of safety was then calculated to ensure that the beam was only flexure governed, with no probability of failing in shear. Stresses and deflections were then displayed at the end of the spreadsheet.

Table 5-1. W200 x 19.3 – Input Data Sheet

SECTION DESIGN FOR EXPERIMENTAL TESTING				
input numbers in bold blue only				
Beam Dimensions				
Span=	**14.00**	ft	4.27	m	NO INSTABILITY
Beam Length=	15.00	ft	4.57	m	1.58
Lb=	**0.00**	ft	0.00	m	Flexure governed
Section=	**263**	W8X13	W200x19.3		
Beam Weight =	195	lb	89	kg	
Span/Depth Ratio=	21.03				
STEEL Section Properties					
A	3.84	in^2	24.77	cm^2	*section properties are*
d	7.99	in	20.29	cm	
tw	0.23	in	0.58	cm	*extractied from the*
tf	0.255	in	0.65	cm	
bf	4	in	10.16	cm	*tables based on the*
Ix-x	39.6	in^4	1648	cm^4	
Iy-y	2.73	in^4	114	cm^4	*selection done above.*
J	0.0871	in^4	4	cm^4	
Sx-x	9.91	in^3	162	cm^3	
Zx-x	11.4	in^3	187	cm^3	
ry	0.843	in	2.14	cm	
section weight	13.00	lb/ft	19.36	kg/m	
Elastic modulus (E)	2.90E+07	psi	2.04E+06	kg/cm^2	
Shear Modulus (G)	1.12E+07	psi	7.88E+05	kg/cm^2	
Yield stress	**50.0**	ksi	3.52	t/cm^2	
Residual stress	**10.0**	ksi	0.70	t/cm^2	
CFRP properties (added on the bottom face of the bottom flange)					
Width	3.94	in	**10.00**	cm	*O.K, Max is 10.16*
Thickness	0.06	in	**0.14**	cm	
Area	0.22	in^2	1.40	cm^2	
Equivalent area	0.15	in^2	0.96	cm^2	
Added inertia	6.20	in^4	257.89	cm^4	
Elastic modulus	2.00E+07	psi	**1.41E+06**	kg/cm^2	
Yield stress	**293.0**	ksi	20.62	t/cm^2	
CFRP properties (added on the top face of the bottom flange)					
Width	3.00	in	**7.62**	cm	*O.K, Max is 9.5758*
Thickness	0.06	in	**0.14**	cm	
Area	0.17	in^2	1.06	cm^2	
Equivalent area	0.11	in^2	0.73	cm^2	
Added inertia	4.72	in^4	196.51	cm^4	
Elastic modulus	2.00E+07	psi	**1.41E+06**	kg/cm^2	
Yield stress	**293.0**	ksi	20.62	t/cm^2	
Top plate properties (substituting the concrete slab)					
Width	12.00	in	**30.49**	cm	
Thickness	0.50	in	**1.27**	cm	
Area	6.00	in^2	38.72	cm^2	
Equivalent area	6.00	in^2	38.72	cm^2	
Added inertia	20.05	in^4	834.68	cm^4	
Elastic modulus	2.90E+07	psi	**2.04E+06**	kg/cm^2	
Yield stress	**50.0**	ksi	3.52	t/cm^2	
Point Loading					
Dist between loads =	**4.666666667**	ft	1.42	m	
Total Point Load =	**38300**	lb	17388.2	kg	

Table 5-2. W200 x 19.3 – Output Data Sheet

Output & Checks					
Width thickness ratio	λ	λ p	λ r		
Flange	7.84	9.15	22.35	Compact	
Web	29.9	90.55	137.27	Compact	
X1=	2336	ksi		**Section is Compact**	
X2=	0.00617	ksi^{-2}			
Lr=	8.51	ft			
Lp=	2.98	ft		**NO INSTABILITY**	
Applied Moment=	1082.2	kip.in	1247.9	t.cm	
Section	**Plastic NA (in)**	**Mn (kip.in)**	**F.O.S**	**Step Gain %**	
Steel Section only	3.97	555.3	0.51	0.00%	
Steel Section + Plate	0.41	820.9	0.76	47.82%	
Section + Plate+B_CFRP	0.46	1333.8	1.23	62.48%	
Section + Plate+2 CFRP	0.50	1707.5	1.58	28.01%	
Vn=	51.61	kips	23.43	ton	
Vu=	19.38	kips	8.80	ton	
Shear F.O.S=	**2.66**				
Stresses in steel plate					
f_{top}	-24177.71	psi	-1.70	t/cm^2	*SAFE*
Stresses in steel section					
f_{top}	-18359.80	psi	-1.29	t/cm^2	*SAFE*
f_{bottom}	74610.39	psi	5.25	t/cm^2	*UNSAFE*
q	10547.55	psi	0.742	t/cm^2	*SAFE*
Stresses in CFRP					
f_{bottom_Top}	49433.85	psi	3.48	t/cm^2	*SAFE*
f_{bottom_bottom}	51922.75	psi	3.65	t/cm^2	*SAFE*
P-Delta chart					
Load step	Load (kips)	Delta (Excel)			
0	0	0			
1	3830	0.1195			
2	7660	0.2390			
3	11490	0.3585			
4	15320	0.4780			
5	19150	0.5975			
6	22980	0.7170			
7	26810	0.8365			
8	30640	0.9559			
9	34470	1.0754			
10	38300	1.1949			

5.2.1 Flowchart Calculating Plastic Neutral Axis

```
                    ┌─────────────────┐
                    │      START      │
                    └─────────────────┘
                             │
                             ▼
   ╱─────────────────────────────────────────────────────╲
  ╱                   READ INPUT DATA                       ╲
 ╱        -Section Dimensions (D, B_F, T_W, T_F)             ╲
╱       -Plate Dimensions (Top_Plate_T, Top_Plate_W)          ╲
╲       -Top CFRP Dimensions (T_CFRP_T, T_CFRP_W)             ╱
 ╲   -Bottom CFRP Dimensions (B_CFRP_T, B_CFRP_W)           ╱
  ╲           -Steel Material Properties (FY)               ╱
   ╲          -CFRP Material Properties (CFRP_Y)           ╱
    ╲─────────────────────────────────────────────────╱
                             │
                             ▼
   ┌─────────────────────────────────────────────────────┐
   │              DEFINE AND ZERO ALL FORCES               │
   │          -Top plate force 1 (F_Top_Plate_1)           │
   │          -Top plate force 2 (F_Top_Plate_2)           │
   │          -Top flange force 1 (F_Top_Flange_1)         │
   │          -Top flange force 2 (F_Top_Flange_2)         │
   │                -Web force 1 (F_Web_1)                 │
   │                -Web force 2 (F_Web_2)                 │
   │            -Top CFRP force (F_CFRP_TOP)               │
   │        -Bottom flange force (F_Bottom_Flange)         │
   │        -Bottom CFRP force (F_CFRP_Bottom)             │
   └─────────────────────────────────────────────────────┘
                             │
                             ▼
              ┌──────────────────────────┐
              │     Plastic_NA = 0.0      │
              └──────────────────────────┘
                             │
                             ▼
  ⭕        ┌──────────────────────────────────────────┐
  5  ─────▶ │  Plastic_NA = Plastic_NA + 0.00001 x D   │
            └──────────────────────────────────────────┘
                             │
                             ▼
                           ⭕
                           1
```

```
        ( 1 )
          │
          ▼
     ╱╲
    ╱    ╲
   ╱ Plastic_NA < ╲        TRUE
  ╱  Top_Plate_T   ╲ ──────────────────────┐
   ╲              ╱                          │
    ╲            ╱                           ▼
     ╲        ╱    ┌─────────────────────────────────────────────────────────┐
       ╲    ╱      │ F_Top_Plate_1 = -Top_Plate_W * Plastic_NA * F_Y          │
        ╲╱         │ F_Top_Plate_2 = Top_Plate_W * (Top_Plate_T - Plastic_NA) *│
         │         │                 F_Y                                       │
         │         │ F_Top_Flange_1 = B_F * T_F * F_Y                          │
         │         │ F_Top_Flange_2 = 0                                        │
         │         │ F_Web_1 = (D - 2 * T_F) * T_W * F_Y                       │
         │         │ F_Web_2 = 0                                               │
         │         │ F_CFRP_TOP = T_CFRP_W * T_CFRP_T * CFRP_Y                 │
         │         │ F_Bottom_Flange = B_F * T_F * F_Y                         │
         │         │ F_CFRP_Bottom = B_CFRP_W * B_CFRP_T * CFRP_Y              │
         │         └─────────────────────────────────────────────────────────┘
  FALSE  │
         │
         ▼
       ╱╲
      ╱    ╲
     ╱ Plastic_NA < ╲          TRUE
    ╱ Top_Plate_T + T_F ╲ ──────────────────────┐
     ╲               ╱                            ▼
      ╲            ╱                            ( 2 )
        ╲    ╱
         ╲╱  FALSE
          │
          ▼
        ( 3 )
```

(2)

F_Top_Plate_1 = -Top_Plate_W * Top_Plate_T * F_Y
F_Top_Plate_2 = 0
F_Top_Flange_1 = -B_F * (Plastic_NA - Top_Plate_T) * F_Y
F_Top_Flange_2 = B_F * (Top_Plate_T + T_F - Plastic_NA) * F_Y
F_Web_1 = (D - 2 * T_F) * T_W * F_Y
F_Web_2 = 0
F_CFRP_TOP = T_CFRP_W * T_CFRP_T * CFRP_Y
F_Bottom_Flange = B_F * T_F * F_Y
F_CFRP_Bottom = B_CFRP_W * B_CFRP_T * CFRP_Y

(4)

(3)

F_Top_Plate_1 = -Top_Plate_W * Top_Plate_T * F_Y
F_Top_Plate_2 = 0
F_Top_Flange_1 = -B_F * T_F * F_Y
F_Top_Flange_2 = 0
F_Web_1 = -T_W * (Plastic_NA - Top_Plate_T - T_F) * F_Y
F_Web_2 = T_W * (D - 2 * T_F - Plastic_NA + Top_Plate_T + T_F) * F_Y
F_CFRP_TOP = T_CFRP_W * T_CFRP_T * CFRP_Y
F_Bottom_Flange = B_F * T_F * F_Y
F_CFRP_Bottom = B_CFRP_W * B_CFRP_T * CFRP_Y

(4)

```
          ( 4 )
           │
           ▼
┌──────────────────────────────────────────────────────────────────────┐
│ Sigma_Force = F_Top_Plate_1 + F_Top_Plate_2 + F_Top_Flange_1 + F_Top_Flange_2 + │
│      F_Web_1 + F_Web_2 + F_CFRP_TOP + F_Bottom_Flange + F_CFRP_Bottom   │
└──────────────────────────────────────────────────────────────────────┘
                              │
                              ▼
                   ╱◆╲
             Abs (Sigma_Force) >          TRUE
                  0.50              ────────────────►  ( 5 )
                   ╲◆╱
                    │
                    │ FALSE
                    ▼
          ╱────────────────────╲
         ╱  PRINT Plastic_NA     ╲
         ╲────────────────────────╲
                    │
                    ▼
              ┌──────────┐
              │   END    │
              └──────────┘
```

5.2.2 Flowchart Calculating Plastic Moment Capacity

```
                    ┌─────────────────────┐
                    │        START        │
                    └─────────────────────┘
                                │
                                ▼
        ╱─────────────────────────────────────────────────╲
       ╱              READ INPUT DATA                       ╲
      ╱       -Section Dimensions (D, B_F, T_W, T_F)         ╲
     ╱       -Plate Dimensions (Top_Plate_T, Top_Plate_W)     ╲
    ╱       -Top CFRP Dimensions (T_CFRP_T, T_CFRP_W)          ╲
   ╱      -Bottom CFRP Dimensions (B_CFRP_T, B_CFRP_W)          ╲
  ╱             -Steel Material Properties (FY)                  ╲
 ╱             -CFRP Material Properties (CFRP_Y)                 ╲
╱                -Plastic Neutral Axis (NA)                        ╲
```

```
        ┌─────────────────────────────────────────────────┐
        │           DEFINE AND ZERO ALL MOMENTS           │
        │          -Total plastic moment (M_Plastic)      │
        │          -Top plate moment 1 (M_Top_Plate_1)    │
        │          -Top plate moment 2 (M_Top_Plate_2)    │
        │          -Top flange moment 1 (M_Top_Flange_1)  │
        │          -Top flange moment 2 (M_Top_Flange_2)  │
        │             -Web moment 1 (M_Web_1)             │
        │             -Web moment 2 (M_Web_2)             │
        │          -Top CFRP moment (M_CFRP_TOP)          │
        │        -Bottom flange moment (M_Bottom_Flange)  │
        │       -Bottom CFRP moment (M_CFRP_Bottom)       │
        └─────────────────────────────────────────────────┘
                                │
                                ▼
                             ( 1 )
```

```
          ┌───┐
          │ 1 │
          └─┬─┘
            │
            ▼
        ╱─────────╲
       ╱  NA <     ╲          TRUE
      ╱  Top_Plate_T ╲─────────────────────┐
      ╲             ╱                       │
       ╲           ╱                        ▼
        ╲─────────╱
            │
          FALSE
```

M_Top_Plate_1 = Top_Plate_W * NA * F_Y * 0.5 * NA
M_Top_Plate_2 = Top_Plate_W * (Top_Plate_T - NA) * F_Y *
0.5 * (Top_Plate_T - NA)
M_Top_Flange_1 = B_F * T_F * F_Y * (Top_Plate_T - NA + 0.5
* T_F)
M_Top_Flange_2 = 0
M_Web_1 = (D - 2 * T_F) * T_W * F_Y * (Top_Plate_T - NA +
T_F + 0.5 * (D - 2 * T_F))
M_Web_2 = 0
M_CFRP_TOP = T_CFRP_W * T_CFRP_T * CFRP_Y *
(Top_Plate_T - NA + D - T_F - 0.5 * T_CFRP_T)
M_Bottom_Flange = B_F * T_F * F_Y * (Top_Plate_T - NA + D -
0.5 * T_F)
M_CFRP_Bottom = B_CFRP_W * B_CFRP_T * CFRP_Y *
(Top_Plate_T - NA + D + 0.5 * B_CFRP_T)

```
        ╱─────────────╲
       ╱ NA < Top_Plate_T + ╲       TRUE
      ╱       T_F           ╲──────────────────┐
      ╲                     ╱                   │
       ╲                   ╱                    ▼
        ╲─────────────────╱                   ┌───┐
              │                                │ 2 │
            FALSE                              └───┘
              │
              ▼
            ┌───┐
            │ 3 │
            └───┘
```

```
      ( 2 )
       │
       ▼
┌─────────────────────────────────────────────────────────────────────────┐
│  M_Top_Plate_1 = Top_Plate_W * Top_Plate_T * F_Y * (NA - 0.5 * Top_Plate_T) │
│                        M_Top_Plate_2 = 0                                    │
│   M_Top_Flange_1 = B_F * (NA - Top_Plate_T) * F_Y * 0.5 * (NA - Top_Plate_T) │
│ M_Top_Flange_2 = B_F * (Top_Plate_T + T_F - NA) * F_Y * 0.5 * (Top_Plate_T + T_F - NA) │
│  M_Web_1 = (D - 2 * T_F) * T_W * F_Y * (Top_Plate_T + T_F - NA + 0.5 * (D - 2 * T_F)) │
│                          M_Web_2 = 0                                        │
│ M_CFRP_TOP = T_CFRP_W * T_CFRP_T * CFRP_Y * (Top_Plate_T - NA + D - T_F - 0.5 * │
│                            T_CFRP_T)                                        │
│   M_Bottom_Flange = B_F * T_F * F_Y * (Top_Plate_T - NA + D - 0.5 * T_F)     │
│ M_CFRP_Bottom = B_CFRP_W * B_CFRP_T * CFRP_Y * (Top_Plate_T - NA + D + 0.5 * │
│                            B_CFRP_T)                                        │
└─────────────────────────────────────────────────────────────────────────┘
                             │
                             ▼
                          ( 4 )
```

```
                                    ( 3 )

┌─────────────────────────────────────────────────────────────────────────┐
│   M_Top_Plate_1 = Top_Plate_W * Top_Plate_T * F_Y * (NA - 0.5 * Top_Plate_T)  │
│                          M_Top_Plate_2 = 0                                 │
│         M_Top_Flange_1 = B_F * T_F * F_Y * (NA - Top_Plate_T - 0.5 * T_F)   │
│                          M_Top_Flange_2 = 0                                 │
│      M_Web_1 = T_W * (NA - Top_Plate_T - T_F) * F_Y * 0.5 * (NA - Top_Plate_T - T_F) │
│   M_Web_2 = T_W * (D - T_F - NA + Top_Plate_T) * F_Y * 0.5 * (D - T_F - NA + Top_Plate_T) │
│   M_CFRP_TOP = T_CFRP_W * T_CFRP_T * CFRP_Y * (D - T_F - NA + Top_Plate_T - 0.5 * │
│                              T_CFRP_T)                                      │
│        M_Bottom_Flange = B_F * T_F * F_Y * (D - 0.5 * T_F - NA + Top_Plate_T)   │
│   M_CFRP_Bottom = B_CFRP_W * B_CFRP_T * CFRP_Y * (D - NA + Top_Plate_T + 0.5 * │
│                              B_CFRP_T)                                      │
└─────────────────────────────────────────────────────────────────────────┘

                                    ( 4 )

┌─────────────────────────────────────────────────────────────────────────┐
│   M_Plastic = M_Top_Plate_1 + M_Top_Plate_2 + M_Top_Flange_1 + M_Top_Flange_2 + │
│      M_Web_1 + M_Web_2 + M_CFRP_TOP + M_Bottom_Flange + M_CFRP_Bottom        │
└─────────────────────────────────────────────────────────────────────────┘

                          / PRINT M_Plastic /

                          ┌──────────────┐
                          │     END      │
                          └──────────────┘
```

5.2.3   Effective Parameters

Parameters taken into consideration for the parametric study were CFRP laminate length, thickness, and configuration, and the beam cross section. The three different CFRP laminate lengths studied were defined relative to the length of the I-beam as a percentage value. The CFRP lengths tested were 60%, 75%, and 90% of the beam's total length. Three CFRP laminate thicknesses were tested: 1.40 mm (0.055 in), 2.00 mm (0.080 in), and 2.60 mm (0.105 in). Manufacturing companies of CFRP strips have standard widths and lengths of theses laminates, but they would typically be able to provide variations to those standards based on the consumer's request.

CFRP material properties for the parametric study were obtained from FYFE Company, the manufacturer of Tyfo$^{®}$ UC Composite Laminate Strip System. Values were also verified using experimental results shown in Chapter 3. The typical material properties of the laminate CFRP materials are; tensile modulus (E) of 155GPa, tensile Strength (F_u) of 2790MPa, rupture strain (ε_u) of 0.018, and volumetric fiber content of 68%.

5.2.4   Beam Designation

Beams developed for the study are shown in Table 5-3, Table 5-4, and Table 5-5. To help in the discussion of the beams, a unique designation system is provided for each beam with the following criteria:

- The letter "V" stands for beams verified with experimental results, and "P" stands for a model developed for the parametric study program.
- The first two digits after the letter designation represent the CFRP laminate length percentage compared to the total length of the beam; namely 60%, 75% and 90%.
- The following three digits represent the laminate thickness, for instance 055 would stand for 0.055 inches laminate thickness.
- The next two letters determine the CFRP configuration on each beam as shown in Figure 3-6 Such that "B4" represents 100 mm (4 in) wide laminate placed at the bottom face of the lower flange, "B2" represents a 50 mm (2 in) laminate width at the same location, "TB" represents two 100 mm (4 in) laminates placed at the top and bottom faces of the lower flange, and "BB" represents a two 100 mm (4 in) laminates placed at the bottom face of the lower flange.
- The last letter determines the load configuration, such that "T" stands for loading at third points of beam length, and "U" stands for uniform loading over the length of the beam.

As an example of beam designation, P75080B4T is a parametric study beam with a laminate length covering 75% of the length of the steel beam, having a thickness of 2.00 mm (0.080 in), placed at the bottom face of the lower flange and a width of 100 mm (4 in), and being loaded at third-points of the beam length. The control beam without laminates and loaded at third-points, would have a beam designation of P0000000T. This designation simplifies the comparison effort for 94 beams with varying parameters studied for each.

Table 5-3 shows the parametric study for beam section W200 x 19.3 loaded with a four-point loading configuration. The column titled "CFRP Config" indicates the configuration of eh laminates at the lower flange of the steel beam; "B" at bottom face, "B+T" at bottom and top faces, and "BB" double strips at bottom face. Table 5-4 shows the parametric study for beam section W200 x 19.3 loaded with a uniform loading configuration. Table 5-5 shows the parametric study for beam section W310 x 38.7 (Test # 75 – 84) and W410 x 53 (Test # 85 – 94) loaded with a four-point loading configuration. Number of tests was greatly reduced for these beams due to the elimination of parameters proven ineffective by previous tests.

Table 5-3. W200 x 19.3 Parametric Study Table – Four-Point Loading

Parameter Test #	CFRP Length	CFRP Thickness (in)	CFRP Width (in)	CFRP Config	Model Name
1	0%	0	0	0	V00000000T
2	75%	0.055	4	B	V75055B4T
3	75%	0.055	4+2+2	B+T	V75055TBT
4	75%	0.055	4+4	BB	V75055BBT
5	75%	0.055	2	B	V75055B2T
6	60%	0.055	4	B	P60055B4T
7	60%	0.055	4+2+2	B+T	P60055TBT
8	60%	0.055	4+4	BB	P60055BBT
9	60%	0.055	2	B	P60055B2T
10	90%	0.055	4	B	P90055B4T
11	90%	0.055	4+2+2	B+T	P90055TBT
12	90%	0.055	4+4	BB	P90055BBT
13	90%	0.055	2	B	P90055B2T
14	75%	0.08	4	B	P75080B4T
15	75%	0.08	4+2+2	B+T	P75080TBT
16	75%	0.08	4+4	BB	P75080BBT
17	75%	0.08	2	B	P75080B2T
18	60%	0.08	4	B	P60080B4T
19	60%	0.08	4+2+2	B+T	P60080TBT
20	60%	0.08	4+4	BB	P60080BBT
21	60%	0.08	2	B	P60080B2T
22	90%	0.08	4	B	P90080B4T
23	90%	0.08	4+2+2	B+T	P90080TBT
24	90%	0.08	4+4	BB	P90080BBT
25	90%	0.08	2	B	P90080B2T
26	75%	0.105	4	B	P75105B4T
27	75%	0.105	4+2+2	B+T	P75105TBT
28	75%	0.105	4+4	BB	P75105BBT
29	75%	0.105	2	B	P75105B2T
30	60%	0.105	4	B	P60105B4T
31	60%	0.105	4+2+2	B+T	P60105TBT
32	60%	0.105	4+4	BB	P60105BBT
33	60%	0.105	2	B	P60105B2T
34	90%	0.105	4	B	P90105B4T
35	90%	0.105	4+2+2	B+T	P90105TBT
36	90%	0.105	4+4	BB	P90105BBT
37	90%	0.105	2	B	P90105B2T

Table 5-4. W200 x 19.3 Parametric Study Table – Uniform Loading

Parameter Test #	CFRP Length	CFRP Thickness	CFRP Width	CFRP Config	Model Name
38	0%	0	0	0	P0000000U
39	75%	0.055	4	B	P60055B4U
40	75%	0.055	4+2+2	B+T	P60055TBU
41	75%	0.055	4+4	BB	P60055BBU
42	75%	0.055	2	B	P60055B2U
43	60%	0.055	4	B	P60055B4U
44	60%	0.055	4+2+2	B+T	P60055TBU
45	60%	0.055	4+4	BB	P60055BBU
46	60%	0.055	2	B	P60055B2U
47	90%	0.055	4	B	P90055B4U
48	90%	0.055	4+2+2	B+T	P90055TBU
49	90%	0.055	4+4	BB	P90055BBU
50	90%	0.055	2	B	P90055B2U
51	75%	0.08	4	B	P75080B4U
52	75%	0.08	4+2+2	B+T	P75080TBU
53	75%	0.08	4+4	BB	P75080BBU
54	75%	0.08	2	B	P75080B2U
55	60%	0.08	4	B	P60080B4U
56	60%	0.08	4+2+2	B+T	P60080TBU
57	60%	0.08	4+4	BB	P60080BBU
58	60%	0.08	2	B	P60080B2U
59	90%	0.08	4	B	P90080B4U
60	90%	0.08	4+2+2	B+T	P90080TBU
61	90%	0.08	4+4	BB	P90080BBU
62	90%	0.08	2	B	P90080B2U
63	75%	0.105	4	B	P75105B4U
64	75%	0.105	4+2+2	B+T	P75105TBU
65	75%	0.105	4+4	BB	P75105BBU
66	75%	0.105	2	B	P75105B2U
67	60%	0.105	4	B	P60105B4U
68	60%	0.105	4+2+2	B+T	P60105TBU
69	60%	0.105	4+4	BB	P60105BBU
70	60%	0.105	2	B	P60105B2U
71	90%	0.105	4	B	P90105B4U
72	90%	0.105	4+2+2	B+T	P90105TBU
73	90%	0.105	4+4	BB	P90105BBU
74	90%	0.105	2	B	P90105B2U

Table 5-5. W310 x 38.7 and W410 x 53 Parametric Study Table, Four-Point Loading

Parameter Test #	Beam Section	CFRP L	CFRP T	Model Name
75	W310x38.7	0%	0	P00000000T
76	W310x38.7	60%	0.055	P60055B4T
77	W310x38.7	60%	0.08	P60080B4T
78	W310x38.7	60%	0.105	P60105B4T
79	W310x38.7	75%	0.055	P75055B4T
80	W310x38.7	75%	0.08	P75080B4T
81	W310x38.7	75%	0.105	P75105B4T
82	W310x38.7	90%	0.055	P90055B4T
83	W310x38.7	90%	0.08	P90080B4T
84	W310x38.7	90%	0.105	P90105B4T
85	W410x53	0%	0	P00000000T
86	W410x53	60%	0.055	P60055B4T
87	W410x53	60%	0.08	P60080B4T
88	W410x53	60%	0.105	P60105B4T
89	W410x53	75%	0.055	P75055B4T
90	W410x53	75%	0.08	P75080B4T
91	W410x53	75%	0.105	P75105B4T
92	W410x53	90%	0.055	P90055B4T
93	W410x53	90%	0.08	P90080B4T
94	W410x53	90%	0.105	P90105B4T

5.3 Results

Comparison of the FE models was achieved through the load-deflection curves. Deflection was found at the midspan of the beam unless specified otherwise. Graphs are plotted for the main parameters found. The control beam curves (beams without CFRP laminates) are plotted in each graph to demonstrate the effectiveness of each parameter studied. Strength gain in both the elastic and plastic phases is summarized by tables after each figure and later in the chapter. The behavior of the beams was generally linear up to yielding point, becoming increasingly plastic until the debonding limit of the CFRP laminate.

5.3.1 CFRP Configuration

Figure 5-1 compares five plots for W200 x 19.3 beams acted upon by four-point loading with CFRP laminates covering 90% of the beams' length with thicknesses of 1.40 mm (0.055 in). The variable parameter was the laminate configurations. The control beam has the designation V0000000T, indicating that the beam was tested experimentally in the structural lab. Beam P90055B4T shows a significant increase in strength and displacement, hence is ductile in the plastic phase. Beam P90055TBT shows similar strength, but less displacement, hence less ductility. Beam P90055BBT shows less strength and ductility than the previous two beams. Beam P90055B2T shows the least strength gain, but similar displacement / ductility to beam P90055TBT. The laminate configuration is therefore a sensitive parameter, where the best configuration is that presented in Figure 3-1.

Table 5-6 show the increase in the load capacity and deflection limits of the strengthened beams at the elastic and ultimate loading points for W200 x 19.3 with CFRP 90% length and 1.40 mm thickness. The tables also provide the ductility ratio for each beam. The last two columns calculate the load gain at the elastic and ultimate loading points by comparing the strengthened beam to the non-strengthened control beam.

Table 5-6. W200 x 19.3 with CFRP 90% Length and 1.40 mm Thickness – Four-Point Loading

Model Name	Elastic		Ultimate		Ductility ratio	Load Gain	
	Deflection (mm)	Load (kN)	Deflection (mm)	Load (kN)		Elastic	Plastic
V00000000T	27	103	0	119	0.0		
P90055B4T	27	116	97	193	3.6	13%	62%
P90055TBT	27	124	60	187	2.2	20%	57%
P90055BBT	27	126	53	177	2.0	22%	48%
P90055B2T	27	109	62	145	2.3	6%	22%
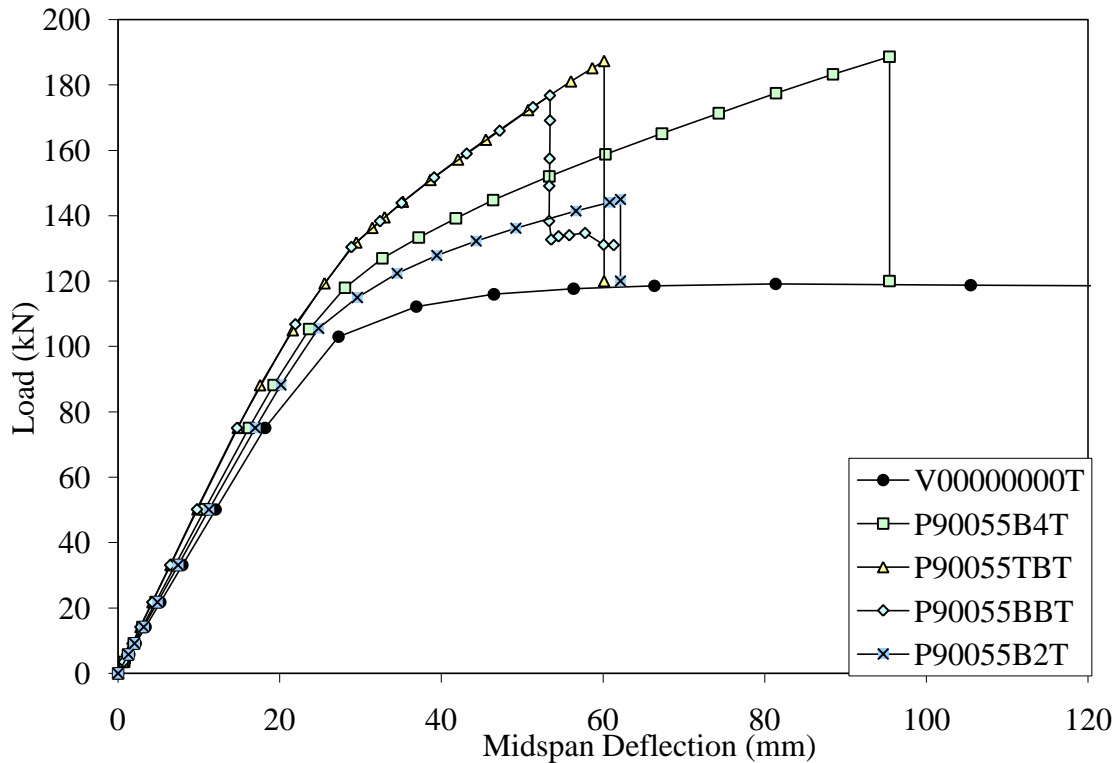
Figure 5-1 Beam W200 x 19.3 with CFRP 90% length and 1.40 mm thickness.

Figure 5-2 compares four plots of W200 x 19.3 beams acted upon by four-point loading with CFRP laminates covering 60% of the beam length with laminate thicknesses of 2.00 mm, each having a different CFRP laminate configuration. Beam P60080B4T shows an increase in strength and displacement; hence it is ductile in the plastic phase. However, note that CFRP

debonding or rupture did not occur, which otherwise would result in a sudden drop in the load deflection curve (as observed in other beams), indicating a typical plastic failure.

Table 5-7 shows the increase in the load capacity and deflection limits of the strengthened beams at the elastic and ultimate loading points for W200 x 19.3 with CFRP 60% length and 2.00 mm thickness. The tables also provide the ductility ratio for each beam. The last two columns calculate the load gain at the elastic and ultimate loading points by comparing the strengthened beam to the control non-strengthened beam.

Table 5-7. W200 x 19.3 with CFRP 60% Length and 2.00 mm Thickness – Four-Point Loading

Model Name	Elastic		Ultimate		Ductility ratio	Load Gain	
	Deflection (mm)	Load (kN)	Deflection (mm)	Load (kN)		Elastic	Plastic
P60080B4T	27	120	117	217	4.3	17%	82%
P60080TBT	27	128	59	180	2.2	24%	51%
P60080BBT	27	128	64	203	2.4	24%	71%
P60080B2T	27	110	66	157	2.4	7%	32%
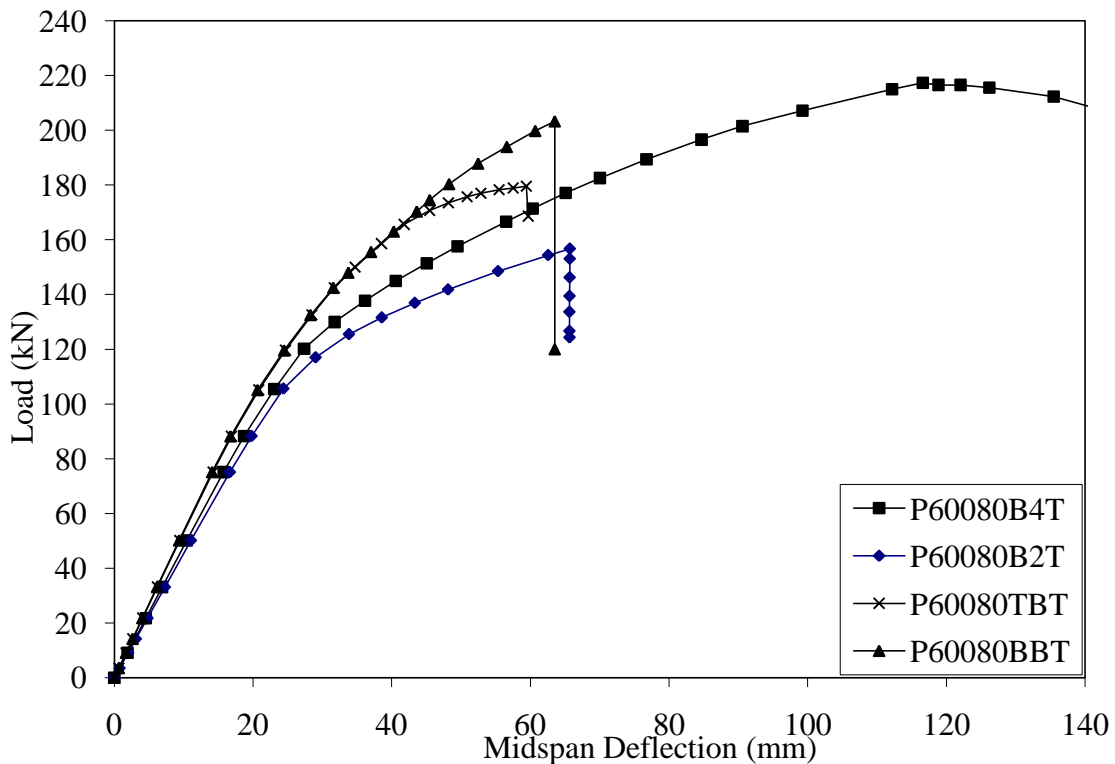
Figure 5-2. Beam W200 x 19.3 with CFRP 60% length and 2.00 mm thickness.

Figure 5-3 presents a finite element contour plot indicating a local failure of the beam just outside of the laminate zone, concluding that the development length of the laminate did not fully materialize. Beam P60080BBT shows less strength than beam P60080B4T, and less

displacement, hence less ductility. Beam P60080TBT has even less ductility, and Beam P60080B2T even less. It is therefore concluded that laminate configuration is a sensitive parameter even with different laminate dimensions.
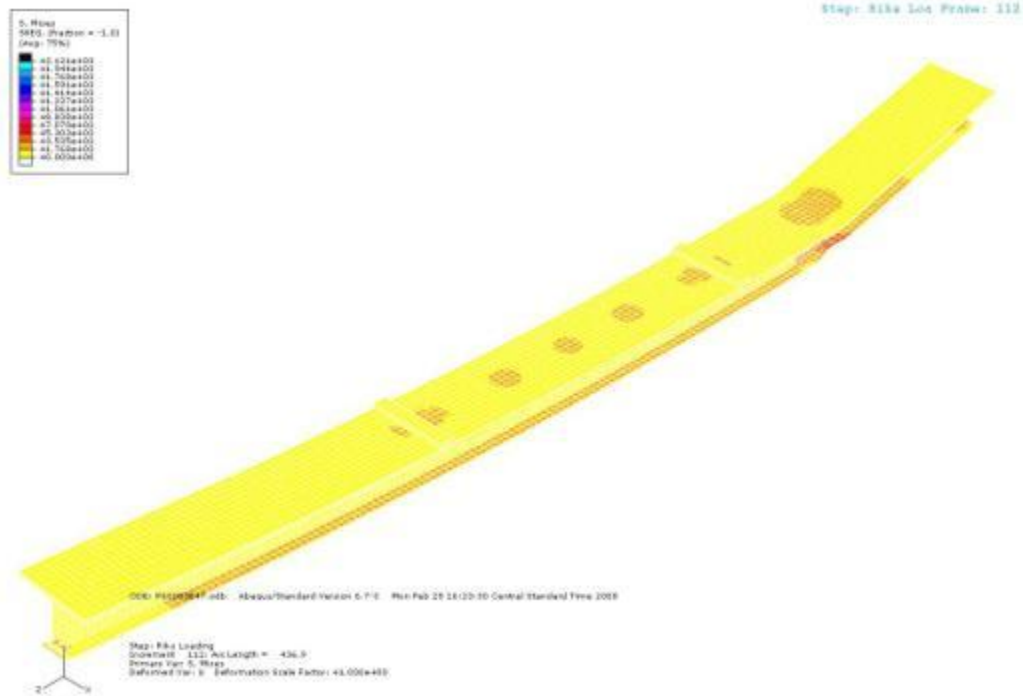
Figure 5-3. Beam P60080B4T failure outside the CFRP reinforced zone.

Figure 5-4 compares four W200 x 19.3 beams with CFRP laminates covering 60% of the beam length with a laminate thickness of 2.00 mm for different CFRP laminate configurations subject to uniform-loading. Beam P60080B4U shows an increase in strength and displacement, hence is ductile in the plastic phase, which is similar to P60080B4T (Figure 5-3). The load type did not change the ductility of the failure behavior of the beam.

Table 5-8 shows the increase in the load capacity and deflection limits of the strengthened beams at the elastic and ultimate loading points for W200 x 19.3 with CFRP 60% length and 2.00 mm thickness. The tables also provide the ductility ratio for each beam. The last two columns calculate the load gain at the elastic and ultimate loading points by comparing the strengthened beam to the control non-strengthened beam.

Table 5-8. W200 x 19.3 with CFRP 60% Length and 2.00 mm Thickness – Uniform Loading

Model Name	Elastic		Ultimate		Ductility ratio	Load Gain	
	Deflection (mm)	Load (kN)	Deflection (mm)	Load (kN)		Elastic	Plastic
P60080B4U	27	33	112	64	4.1	8%	72%
P60080TBU	27	35	69	49	2.5	14%	32%
P60080BBU	27	35	80	63	3.0	14%	71%
P60080B2U	27	33	68	49	2.5	6%	31%
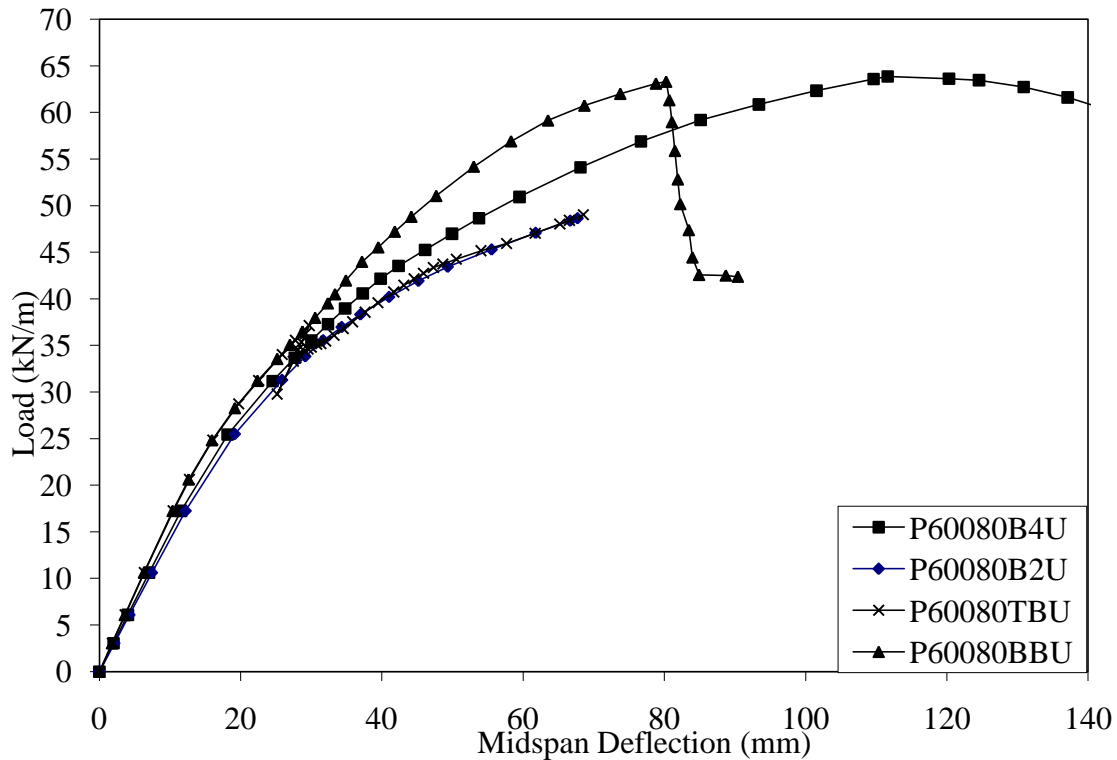
Figure 5-4. Beam W200 x 19.3 with CFRP 60% length and 2.00 mm thickness.

Figure 5-5 compares four W200 x 19.3 beams with CFRP laminates covering 75% of the beam length with a laminate thickness of 2.00 mm for different CFRP laminate configurations subject to uniform-loading. The behavior of the beams is similar to behavior presented in the previous graphs.

Table 5-9 shows the increase in the load capacity and deflection limits of the strengthened beams at the elastic and ultimate loading points for W200 x 19.3 with CFRP 75% length and 2.00 mm thickness. The tables also provide the ductility ratio for each beam. The last two columns calculate the load gain at the elastic and ultimate loading points by comparing the strengthened beam to the control non-strengthened beam.

Table 5-9. W200 x 19.3 with CFRP 75% Length and 2.00 mm Thickness – Uniform Loading

Model Name	Elastic		Ultimate		Ductility ratio	Load Gain	
	Deflection	Load	Deflection	Load		Elastic	Plastic
	(mm)	(kN)	(mm)	(kN)			
P75080B4U	27	33	109	68	4.0	8%	84%
P75080TBU	27	35	74	67	2.7	14%	81%
P75080BBU	27	35	67	63	2.5	14%	71%
P75080B2U	27	33	68	49	2.5	6%	31%
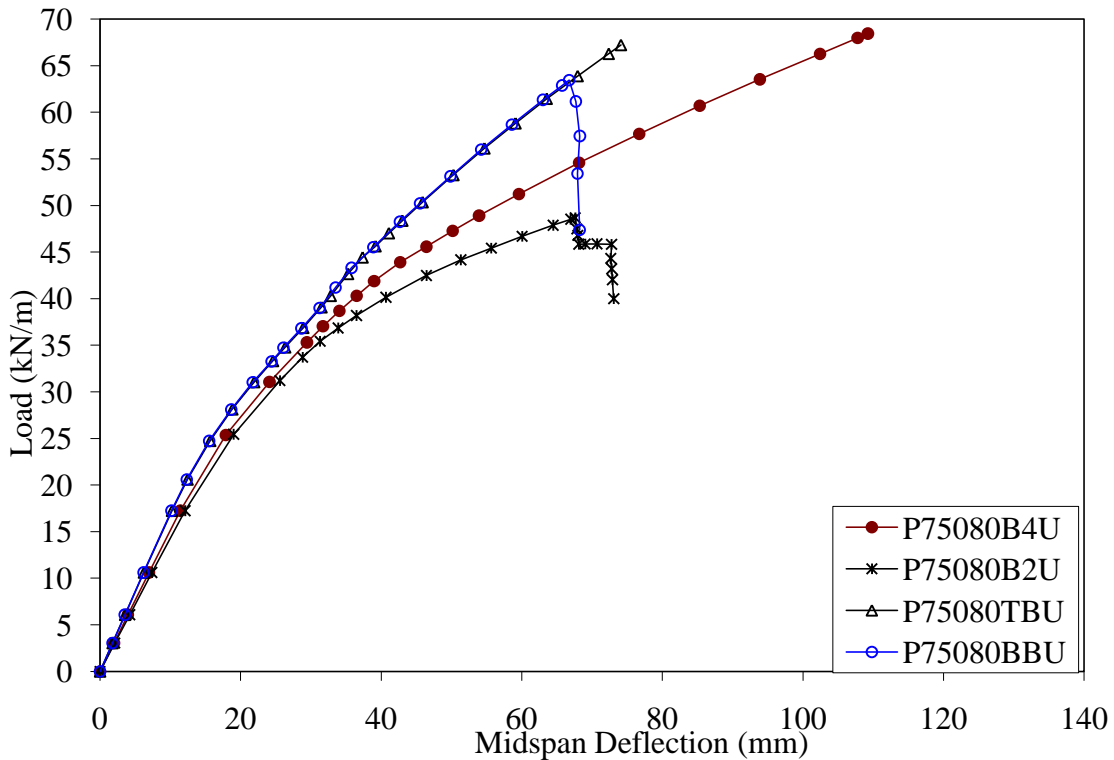
Figure 5-5. Beam W200 x 19.3 with CFRP 75% length and 2.00 mm thickness.

5.3.2 CFRP Thickness

Figure 5-6 compares four plots of W310 x 38.7 beams subjected to four-point loading having CFRP laminates covering 75% of the beam's length. The varying parameter was the laminate thickness, either 1.4 mm, 2.0 mm or 2.6 mm. The laminate configuration chosen for these beams is "B4", which denotes the presence of one laminate layer at the bottom face of the lower flange having a width of 100 mm (4 in). Beam P0000000T represents the control beam with no CFRP laminates reinforcing. Beam P75105B4T shows a significant increase in strength and displacement, hence is ductile in the plastic phase. Beam P75080B4T show less strength, and less displacement, and hence is less ductile. Beam P75055B4T has the least strength and displacement, and so less ductility than the beams P75105B4T and P75080B4T. The conclusion is that the laminate thickness is a sensitive parameter, where beam ductility increases as the laminate thickness increases. Refer to Table 5-15 for tabular results.
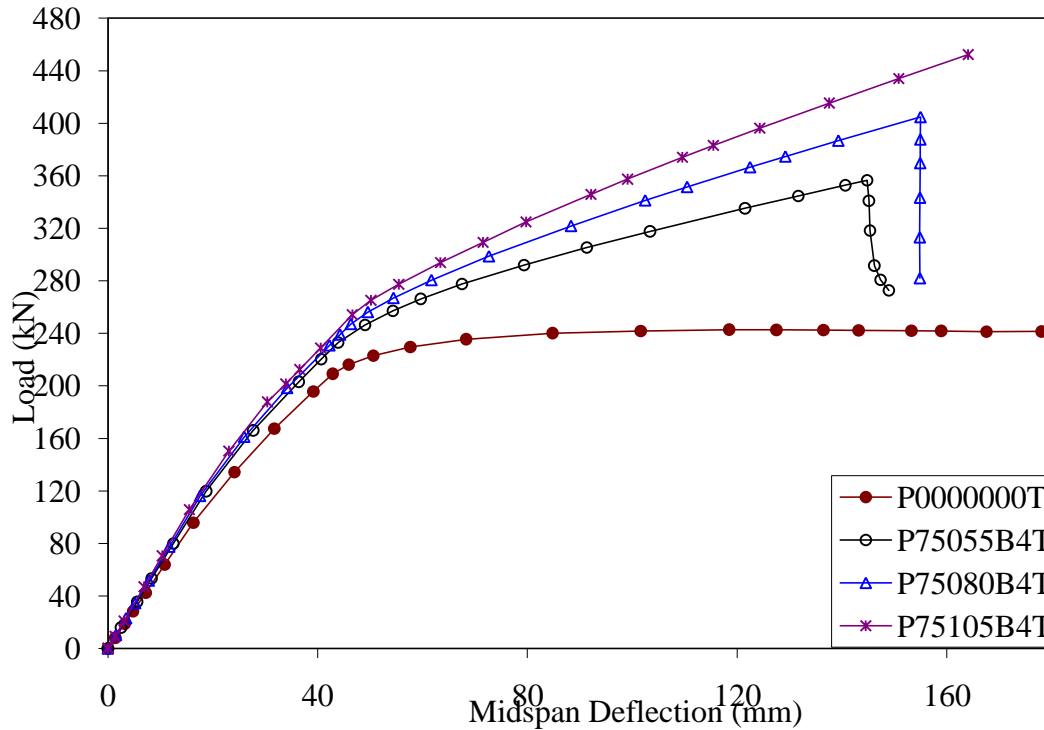
Figure 5-6. Beam W310 x 38.7 with CFRP 75% length and variable thickness.

5.3.3 CFRP Length

Figure 5-7 compares four plots of W200 x 19.3 beams subjected to four-point loading having CFRP laminates of 2.0 mm in thickness. The varying parameter was the laminate length, either 60%, 75% and 90%. The laminate configuration chosen for these beams is "B4", which denotes the presence of one laminate layer at the bottom face of the lower flange having a width of 100 mm (4 in). Beam V0000000T represents the control beam with no CFRP laminates reinforcing. Beams P75080B4T and P90080B4T show a significant increase in strength and displacement, and hence are ductile in the plastic phase. Beam P60080B4T show the same strength, but higher displacement with a different mode of failure. The beam with 60% CFRP laminate length failed outside the reinforced zone. The conclusion is that the laminate length is a sensitive parameter, where the maximum moment zone of the beam needs to be covered. Other than covering the maximum moment zone and adding sufficient debonding length, the CFRP laminate length parameter was not effective, as can be seen by comparing the behavior of beams P75080B4T and P90080B4T. Refer to Table 5-10 for tabular results.

Table 5-10. W200 x 19.3 Results Table, Four-Point Loading – CFRP Length Variable

Model Name	Elastic		Ultimate		Ductility ratio	Load Gain	
	Deflection (mm)	Load (kN)	Deflection (mm)	Load (kN)		Elastic	Plastic
V00000000T	27	103	0	119	0.0		
P75080B4T	27	120	104	219	3.9	17%	84%
P60080B4T	27	120	117	217	4.3	17%	82%
P90080B4T	27	120	104	219	3.8	17%	84%
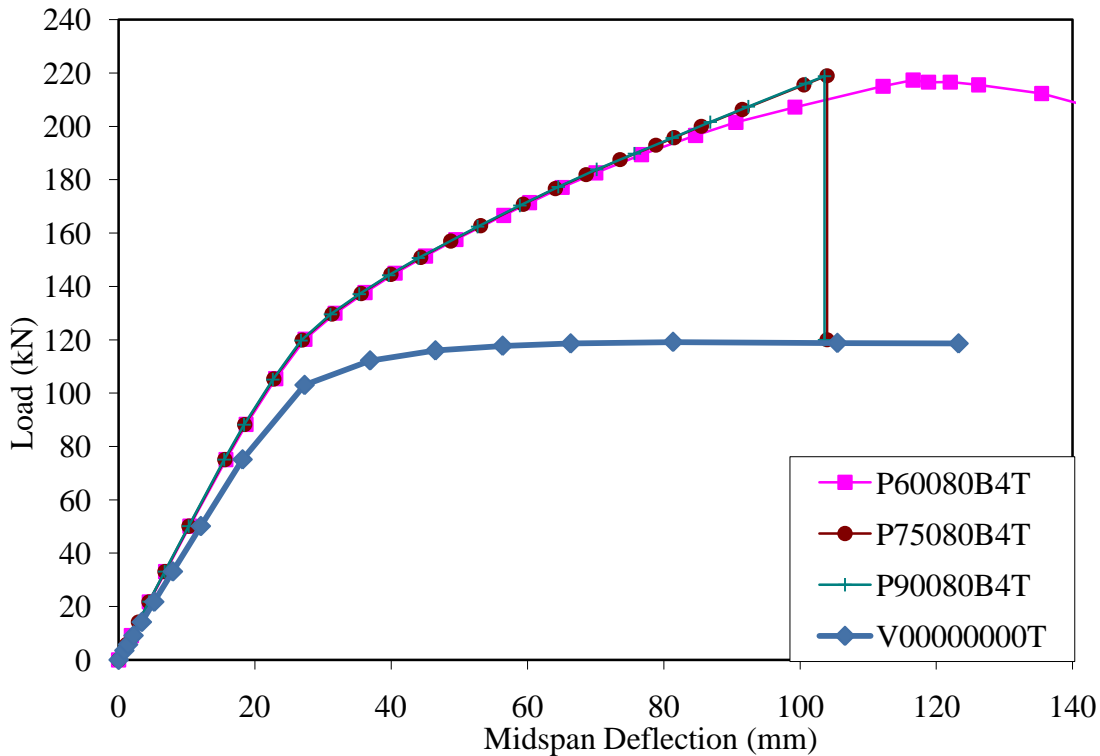
Figure 5-7. Beam W200 x 19.3 with CFRP 2.00 mm thickness and variable length.

5.3.4 *CFRP Width*

Figure 5-8 compares three plots of W200 x 19.3 beams subjected to four-point loading having CFRP laminates of 2.0 mm in thickness and CFRP laminate covering 75% of the beam length. The varying parameter was the laminate width of either 100 mm or 50 mm. The laminate configuration chosen for these beams was "B4" and "B2". B4 denotes the presence of one laminate layer at the bottom face of the lower flange having a width of 100 mm (4 in), while B2 denotes the presence of one laminate layer at the bottom face of the lower flange having a width of 50 mm (2 in). Beam V0000000T represents the control beam with no CFRP laminates reinforcing. Beam P75080B4T shows a significant increase in strength and displacement, hence is ductile in the plastic phase. Beam P75080B2T shows much less strength and lower displacement. The conclusion is that the laminate width is a sensitive parameter, where it is recommended to cover the whole flange width. Refer to Table 5-11 for tabular results.

Table 5-11. W200 x 19.3 Results Table, Four-Point Loading – CFRP Width Variable

Model Name	Elastic		Ultimate		Ductility ratio	Load Gain	
	Deflection (mm)	Load (kN)	Deflection (mm)	Load (kN)		Elastic	Plastic
V00000000T	27	103	0	119	0.0		
P75080B4T	27	120	104	219	3.9	17%	84%
P75080B2T	27	110	62	154	2.3	7%	29%
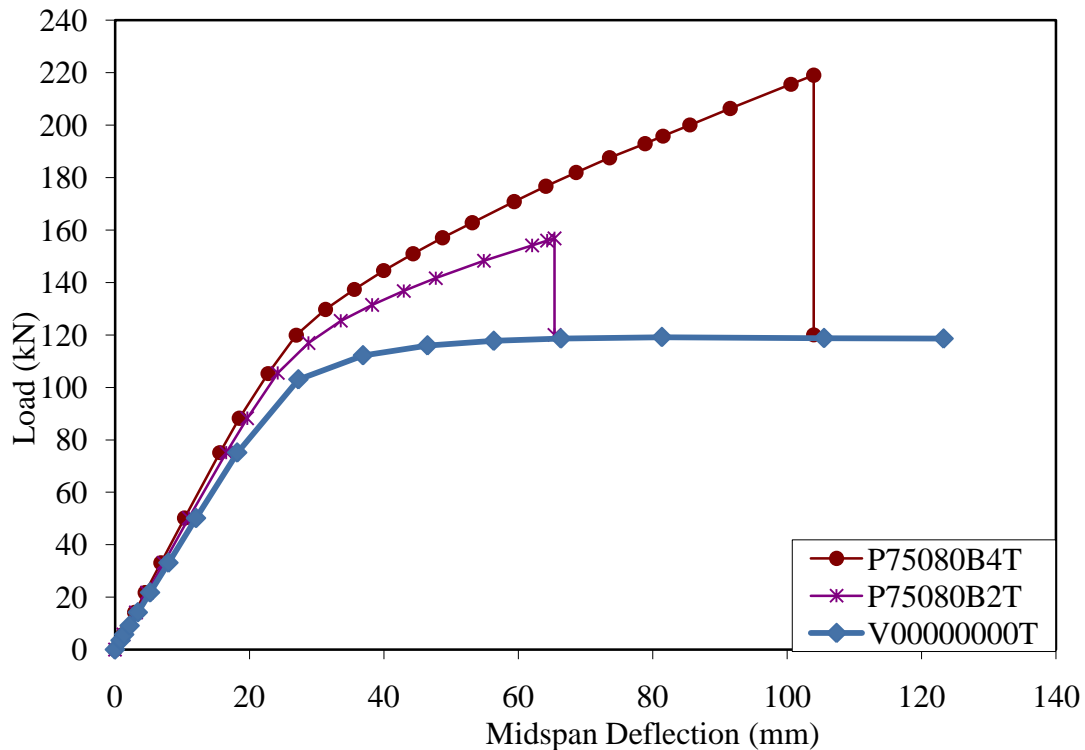
Figure 5-8. Beam W200 x 19.3 with CFRP 75% Length with variable CFRP laminate width.

5.3.5 *CFRP Manufacturer*

Figure 5-9 compares four plots of W200 x 19.3 beams subjected to four-point loading with CFRP laminates covering 75% of the beam's length. The varying parameter was the CFRP laminate manufacturer, either Fyfe, Epsilon, or Mitsubishi. The laminate configuration chosen for these beams is "B4", which denotes the presence of one laminate layer at the bottom face of the lower flange having a width of 100 mm (4 in). Beam W200 x 19.3 reinforced with Fyfe CFRP shows a significant increase in strength and displacement, hence is ductile in the plastic phase. Beam W200 x 19.3 reinforced with Mitsubishi CFRP shows less strength but similar stiffness and less displacement, hence is less ductile. Beam W200 x 19.3 reinforced with Epsilon CFRP has the least strength and displacement / ductility than the other two beams. The conclusion is that the laminate material properties are sensitive parameters, where beam ductility increases as the ultimate laminate strength increases, and laminate stiffness decreases. Table 5-12

shows the change in stiffness in beam W200 x 19.3 stiffness rehabilitated by CFRP from different manufacturers. Increasing the elastic modulus from 200 GPa to 460 GPa, a 130% increase only increases the beam stiffness from 5.02 kN/mm to 5.48 kN/mm, a 9.2% increase. This proves that the CFRP elastic modulus is a non-effective parameter within the elastic modulus range of (155 GPa – 230 GPa). A slight increase in the overall beam stiffness was noticed (9.2 %) when the elastic modulus was increased to more than double the original value.

Table 5-12. W200 x 19.3 Beam Stiffness Comparison with CFRP from Different Manufacturers

	(Fyfe, 2006)	Mitsubishi	Epsilon
Tensile modulus, E	155 GPa	229 GPa	460 GPa
Tensile strength, f_u	2790 MPa	1220 MPa	1530 MPa
Beam Stiffness, kN/mm	5.02	5.02	5.48
Laminate thickness (mm)	1.40-2.00	3.20	2.90-4.00
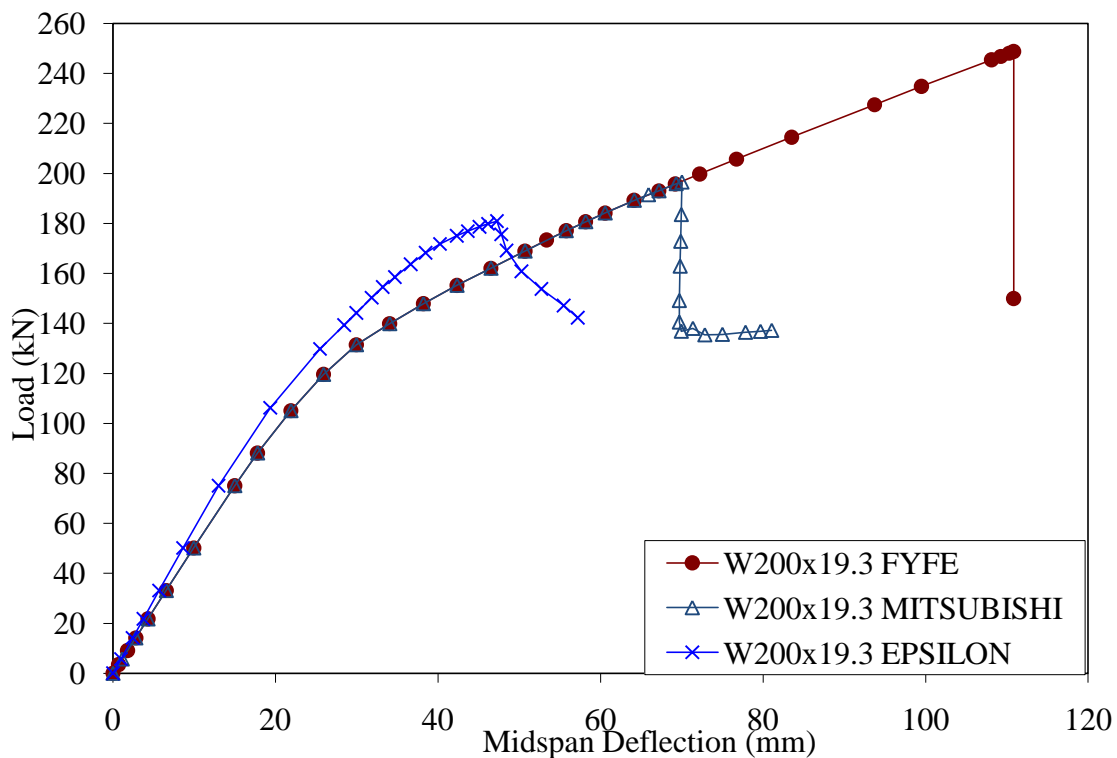
Figure 5-9. Beam W200 x 19.3 with CFRP 75% length from different manufacturers.

5.3.6 CFRP Elastic Modulus

Three models were executed to test the effectiveness of the CFRP elastic modulus on the behavior of the modeled beam. Figure 5-10 shows the load deflection curves of the modeled

beams. It can be noticed that the beams with E = 148 GPa and E = 200 GPa were identical, while the beam with the higher young's modulus value, E = 460 GPa, showed a slight increase in stiffness (8%) but with much less displacement and hence ductility.
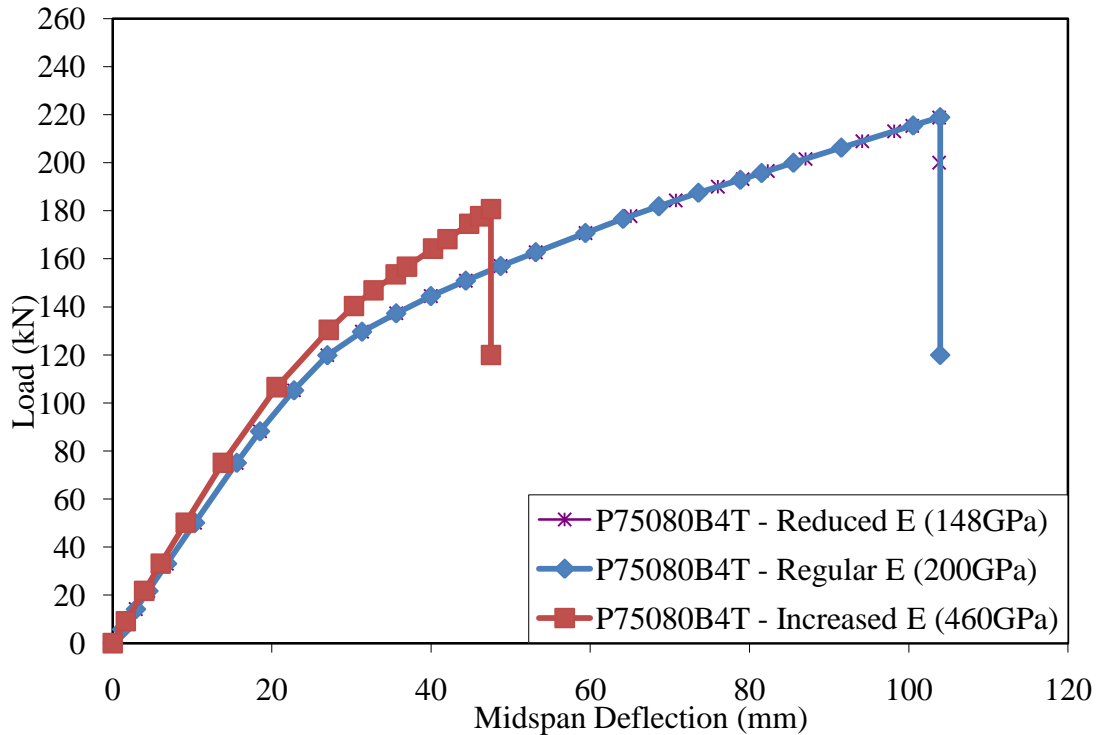
Figure 5-10. Beam W200 x 19.3 with different CFRP Young's modulus.

5.3.7 Results Summary

Results of all of the parametric studies are summarized in Table 5-13 through Table 5-16. The tables show the increase in the load capacity and deflection limits of the strengthened beams at the elastic and ultimate loading points. The tables also provide the ductility ratio for each beam. The last two columns calculate the load gain at the elastic and ultimate loading points by comparing the strengthened beam to the control non-strengthened beam.

5.4 Conclusions

The study presented the findings of an extensive parametric study program to develop a CFRP laminate system for flexural strengthening of steel beams. The effectiveness of the strengthening system was demonstrated, and the detailed behavior of the strengthened beams was examined. Results proved the effectiveness of CFRP thickness and laminate configuration as an important design parameter. CFRP laminate length proved to be of less effect as long as it covered the maximum moment zone. The laminate length parameter was less effective in case of four-point loading configuration as compared to uniform loading.

Overall, the research findings demonstrate the effectiveness of externally bonded CFRP laminates for the strengthening and repair of steel structures and bridges.

Table 5-13 summarizes the results for beam W200 x 19.3 (W8 x 13) subjected to four-point loading. The following could be concluded from the table:

- Beams with similar configuration and equal CFRP thicknesses tend to give the same load gain in both the elastic and plastic stages even if the CFRP length is changed, indicating that CFRP length is not an effective parameter.
- The main concern in regards to laminate length is that it needs to be sufficiently long to ensure proper development length. This becomes a main concern for thick laminates, such as that observed for a model having a laminate thickness of 2.40 mm (0.105 in) and covering only 60% of the beams length.
- As compared to the control beam, the elastic load range gain varied from 5% to 32%, the plastic load range gain varied from 21% to 109%, and the ductility ratio varied from 1.60 to 4.30.

From the results in Table 5-13 and the conclusions listed above, the CFRP laminate thickness proves to be of great effect, while the laminate length is of less significance for four-point loading as long as maximum moment zone is covered adequately. The CFRP laminate configuration proved to be an effective rehabilitation parameter for all beams.

Table 5-14 summarizes the results for the W200 x 19.3 (W8 x 13) beams subjected to uniform loading; the following could be concluded from the table:

- CFRP laminate length is effective in all beams, especially those with higher CFRP thicknesses. This is due to the spreading out of the load and the failure of the beam outside the reinforced zone.
- As compared to the control beam, the elastic load range gain varied from 2% to 19%, the plastic load range gain varied from 12% to 110%, and the ductility ratio varied from 1.30 to 4.40.

Based on the table results and these conclusions, the CFRP laminate thickness proved to be of great effect. The laminate length is of more significance to the case of uniform loading configuration.

Table 5-15 summarizes the results for the W310 x 38.7 (W12 x 26) beams subject to four-point loading; the following could be concluded from the table:

- Beams with similar configuration and CFRP thickness tend to give the same load gain in both the elastic and plastic stages; therefore, the CFRP length is not effective.
- As compared to the control beam, the elastic load range gain varied from 7% to 16%, the plastic load range gain varied from 47% to 87%, and the ductility ratio varied from 4.58 to 5.82.

From the table results and these conclusions, the CFRP laminate thickness proves to be of great effect, while the laminate length is of less significance in the case of four-point loading.

Table 5-16 summarizes the results for the W410 x 53 (W16 x 36) beams subject to four-point loading. The following could be concluded from the table:

- Beams with similar configuration and CFRP thickness tend to give the same load gain in both the elastic and plastic stages; therefore, the CFRP length is not effective.
- As compared to the control beam, the elastic load range gain varied from 3.5% to 10.5%, the plastic load range gain varied from 37% to 70%, and the ductility ratio varied from 3.55 to 4.11.

From the results in Table 5-15 and Table 5-16 and from these conclusions, the CFRP laminate thickness proves to be of great effect, while the laminate length is of less significance to the case of four-point loading configuration. Results prove that the rehabilitation technique is effective for deeper beams.

Table 5-13. W200 x 19.3 Results Table, Four-Point Loading

Model Name	Elastic		Ultimate		Ductility ratio	Load Gain	
	Deflection (mm)	Load (kN)	Deflection (mm)	Load (kN)		Elastic	Plastic
V00000000T	27	103	0	119	0.0		
V75055B4T	27	116	97	193	3.6	13%	62%
V75055TBT	27	124	60	187	2.2	20%	57%
V75055BBT	27	126	54	177	2.0	22%	48%
V75055B2T	27	109	62	145	2.3	6%	22%
P60055B4T	27	116	97	189	3.6	13%	58%
P60055TBT	27	124	51	168	1.9	20%	41%
P60055BBT	27	124	54	177	2.0	20%	48%
P60055B2T	27	109	62	145	2.3	6%	22%
P90055B4T	27	116	97	189	3.6	13%	58%
P90055TBT	27	124	60	187	2.2	20%	57%
P90055BBT	27	124	53	177	2.0	20%	48%
P90055B2T	27	109	62	145	2.3	6%	22%
P75080B4T	27	120	104	219	3.9	17%	84%
P75080TBT	27	128	55	181	2.0	24%	52%
P75080BBT	27	128	60	204	2.2	24%	71%
P75080B2T	27	110	62	154	2.3	7%	29%
P60080B4T	27	120	117	217	4.3	17%	82%
P60080TBT	27	128	59	180	2.2	24%	51%
P60080BBT	27	128	64	203	2.4	24%	71%
P60080B2T	27	110	66	157	2.4	7%	32%
P90080B4T	27	120	104	219	3.8	17%	84%
P90080TBT	27	128	59	203	2.2	24%	70%
P90080BBT	27	128	59	203	2.2	24%	70%
P90080B2T	27	110	64	155	2.4	7%	30%
P75105B4T	27	125	111	249	4.1	21%	109%
P75105TBT	27	136	44	177	1.6	32%	49%
P75105BBT	27	136	53	187	2.0	32%	57%
P75105B2T	27	117	68	169	2.5	14%	41%
P60105B4T	27	125	109	217	4.0	21%	82%
P60105TBT	27	136	54	182	2.0	32%	52%
P60105BBT	27	136	43	179	1.6	32%	50%
P60105B2T	27	117	69	168	2.5	14%	41%
P90105B4T	27	125	111	249	4.1	21%	109%
P90105TBT	27	136	56	210	2.1	32%	76%
P90105BBT	27	136	64	230	2.4	32%	93%
P90105B2T	27	117	68	169	2.5	14%	41%

Table 5-14. W200 x 19.3 Results Table, Uniform Loading

Model Name	Elastic		Ultimate		Ductility ratio	Load Gain	
	Deflection (mm)	Load (kN)	Deflection (mm)	Load (kN)		Elastic	Plastic
P0000000U	27	31	0	37	0.0		
P75055B4U	27	33	99	59	3.7	6%	59%
P75055TBU	27	34	66	58	2.5	9%	57%
P75055BBU	27	34	60	55	2.2	9%	48%
P75055B2U	27	31	63	45	2.3	2%	21%
P60055B4U	27	33	102	59	3.8	6%	59%
P60055TBU	27	34	70	58	2.6	9%	56%
P60055BBU	27	34	61	55	2.3	9%	48%
P60055B2U	27	31	62	45	2.3	2%	20%
P90055B4U	27	33	99	59	3.7	6%	59%
P90055TBU	27	34	47	48	1.7	9%	30%
P90055BBU	27	34	36	42	1.3	9%	12%
P90055B2U	27	31	63	45	2.3	2%	21%
P75080B4U	27	33	109	68	4.0	8%	84%
P75080TBU	27	35	74	67	2.7	14%	81%
P75080BBU	27	35	67	63	2.5	14%	71%
P75080B2U	27	33	68	49	2.5	6%	31%
P60080B4U	27	33	112	64	4.1	8%	72%
P60080TBU	27	35	69	49	2.5	14%	32%
P60080BBU	27	35	80	63	3.0	14%	71%
P60080B2U	27	33	68	49	2.5	6%	31%
P90080B4U	27	33	109	69	4.0	8%	85%
P90080TBU	27	35	74	67	2.7	14%	81%
P90080BBU	27	35	66	63	2.5	14%	70%
P90080B2U	27	33	67	49	2.5	6%	31%
P75105B4U	27	34	118	78	4.4	11%	110%
P75105TBU	27	37	81	76	3.0	19%	105%
P75105BBU	27	37	74	72	2.7	19%	94%
P75105B2U	27	32	72	52	2.7	4%	41%
P60105B4U	27	34	102	64	3.8	11%	72%
P60105TBU	27	37	80	64	3.0	19%	74%
P60105BBU	27	37	80	64	3.0	19%	74%
P60105B2U	27	32	73	52	2.7	4%	41%
P90105B4U	27	34	95	69	3.5	11%	85%
P90105TBU	27	37	80	76	3.0	19%	105%
P90105BBU	27	37	73	72	2.7	19%	94%
P90105B2U	27	32	71	52	2.6	4%	41%

Table 5-15. W310 x 38.7 Results Table, Four-Point Loading

Model Name	Elastic		Ultimate		Ductility ratio	Load Gain	
	Deflection (mm)	Load (kN)	Deflection (mm)	Load (kN)		Elastic	Plastic
P00000000T	32	167	0	242	0.0		
P60055B4T	32	180	145	356	4.6	8%	47%
P60080B4T	32	185	158	405	5.0	10%	67%
P60105B4T	32	190	185	446	5.8	13%	84%
P75055B4T	32	184	145	357	4.6	10%	47%
P75080B4T	32	189	155	405	4.9	13%	67%
P75105B4T	32	194	164	452	5.2	16%	87%
P90055B4T	32	187	144	356	4.6	12%	47%
P90080B4T	32	191	154	404	4.8	14%	67%
P90105B4T	32	194	164	453	5.2	16%	87%

Table 5-16. W410 x 53 Results Table, Four-Point Loading

Model Name	Elastic		Ultimate		Ductility ratio	Load Gain	
	Deflection (mm)	Load (kN)	Deflection (mm)	Load (kN)		Elastic	Plastic
P00000000T	50	270	0	324	0.0		
P60055B4T	50	282	181	447	3.6	5%	38%
P60080B4T	50	287	193	499	3.8	6%	54%
P60105B4T	50	290	208	551	4.1	8%	70%
P75055B4T	50	280	180	447	3.6	4%	38%
P75080B4T	50	290	191	499	3.8	8%	54%
P75105B4T	50	298	202	551	4.0	11%	70%
P90055B4T	50	280	179	447	3.6	4%	38%
P90080B4T	50	290	191	499	3.8	8%	54%
P90105B4T	50	298	202	551	4.0	11%	70%

5.5 Recommendations

Based on the parametric study, the following recommendation should be considered while strengthening steel beams using CFRP laminates:

- The CFRP laminate length should cover at least 75% of the beam length.
- Other modes of failure should always be checked.
- The best CFRP configuration is the configuration covering the bottom face of the bottom flange.
- CFRP thickness is an effective parameter, and shall be chosen according to the designers' required strength.
- CFRP Young's modulus is not a very effective parameter.
- CFRP ultimate strength is much more effective.

Section 6
Bridge Design Rehabilitation Guidelines

6.1 Background

The wide range of uses of CFRP in infrastructures such as bridges was discussed in the previous chapters, as well as the experimental testing and FE analysis. This chapter presents the utilization of CFRP plates to strengthen steel girders for bridges through an analytical approach. It should be noted that CFRP laminates was not installed onto bridges.

6.2 Scope

FE models were developed for a typical steel bridge. The FE model would then include the CFRP laminates to predict the behavior of the bridge after strengthening. The bridge was a steel girder bridge topped by a reinforced concrete deck slab.

6.3 Finite Element Bridge Modeling

A steel girder bridge model was built using the SAP 2000 FE package. The model's details, in terms of structural properties, material properties, and loading data, will be introduced in the following sections.

6.3.1 Bridge Description

The bridge is a steel girder bridge topped by a reinforced concrete deck slab. The bridge has four lanes with a total ADT of 31,980 and a truck percentage of 17%. The bridge has three simply supported spans with a total bridge length of 52.6 m. The bridge has no skew angle with the abutments or piers.

6.3.2 Bridge Modeling

A FE model was built to simulate the behavior of the bridge. Grillage analysis was the basis of the FE model; frame elements were used to model both the girders and the slab. The deck was virtually modeled as a grid of longitudinal and transverse beams. The grillage simulates the bridge closely by having the frame members coincide with the center lines of the girders. Diaphragms are represented by transverse elements that coincide with the midspan of the slab; otherwise, transverse elements are equally spaced throughout the bridge length with spacing of one-quarter to one-eighths of the effective span length. These specifications for grillage analysis and behavior follow the guidelines set by Hambly in his book "Bridge Deck Behavior" (Hambly, 1976).

Girders used in the bridge were built-up steel girders (Figure 6-1). Dimensions of the bridge and girder spacing are given in a cross-sectional view of the bridge (Figure 6-2). The figure also shows the lane positions with reference to the nearest girders. Figure 6-1 shows the girder dimensions and the section's dimensional properties used in the FE analysis.
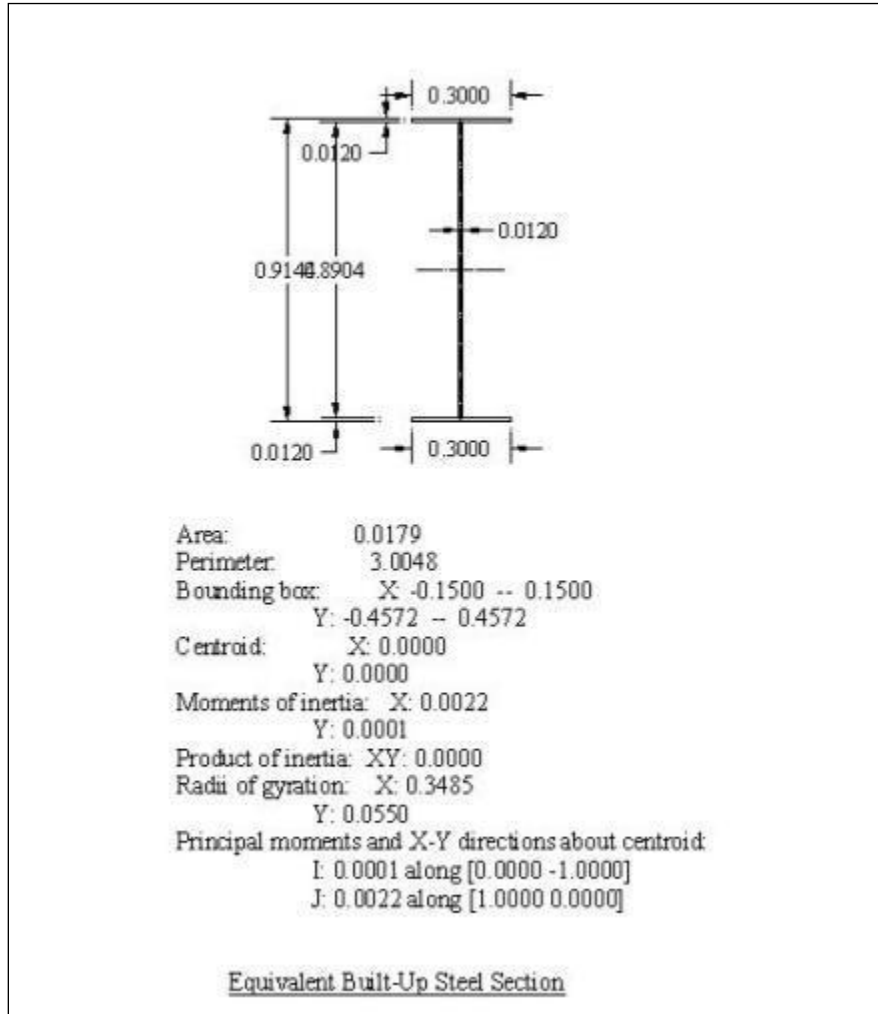
Figure 6-1. Steel Girder Dimensions and Area Properties
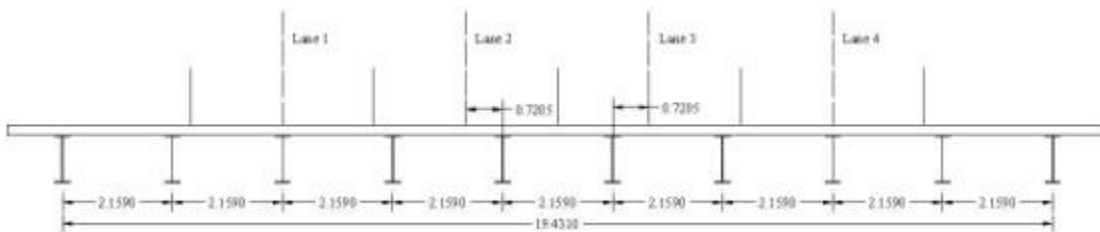
Figure 6-2. Bridge cross section and lane positions.

Figure 6-3 displays the gross composite section properties of the girder with the overlaying slab. The slab width used in the analysis was obtained according to the AASHTO code criteria (1998). The flexural moment of inertia of each grillage member is calculated about the centroid of the section it represents. The section properties of transverse grillage members represents only the slab, except for the mid-transverse grillage members, which represent the diaphragm in addition to the slab.
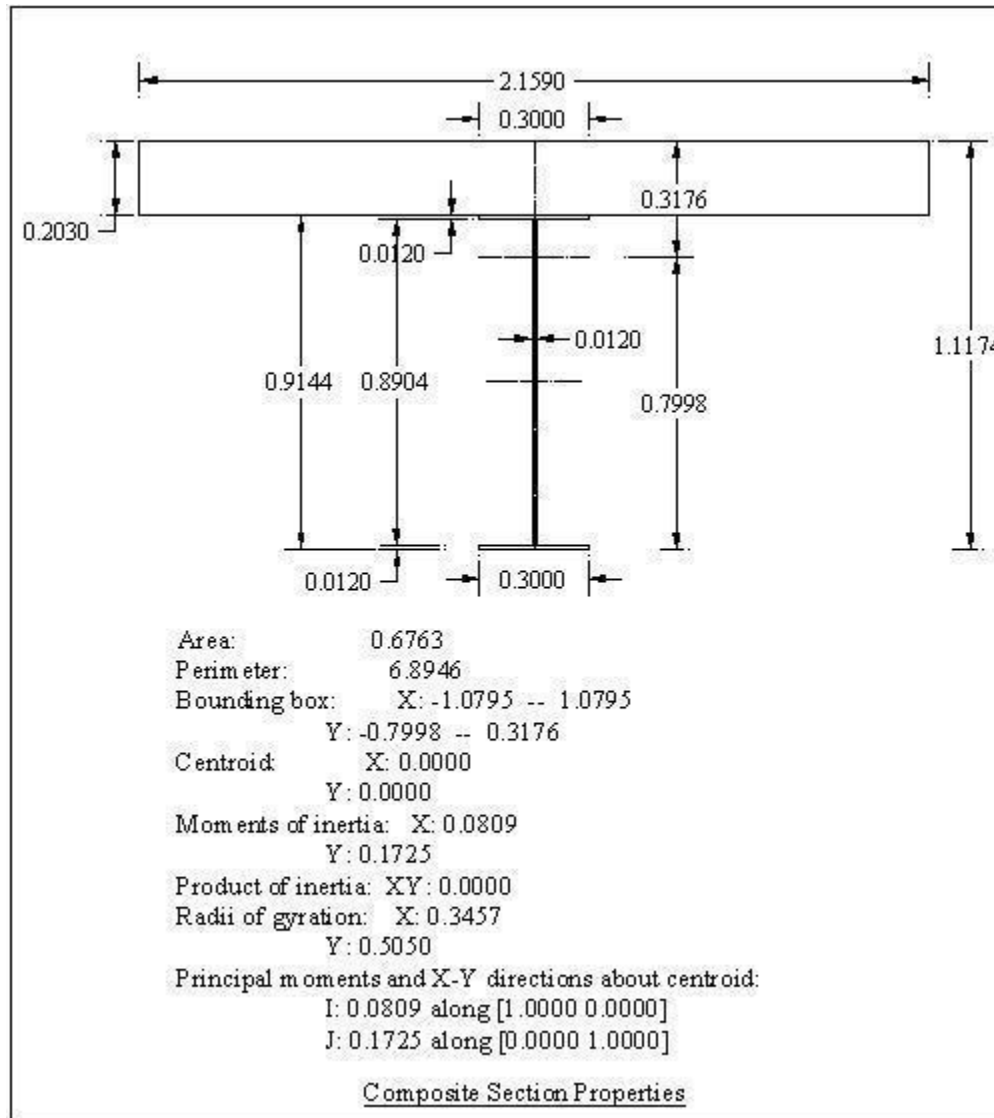
Figure 6-3. Composite section dimensions and area properties.

FE using SAP2000 analysis (SAP 2000, 2008) directly provides moment values as part of the results output. The moment readings will be the comparison basis for the bridge before and after strengthening with CFRP. Another strain comparison was also provided. The moment to strain conversion was used to convert the SAP 2000 moment readings to strain. The moment to strain equation used was

$$\varepsilon = \frac{My}{EI}$$

6.3.3 Bridge Loading

Ten auxiliary trucks were used for loading the bridge model. Table 6-1 shows the data for the 10 trucks analyzed, including the number of axles and the static weight for each truck.

Table 6-1. Truck Loading Data

Truck	Number of Axles	Lane	Gross weight (kN)
1	5	2	335.1
2	5	3	359.6
3	5	3	351.4
4	5	2	356.1
5	5	3	336.0
6	6	1	321.2
7	5	3	334.7
8	5	3	341.8
9	5	2	344.5
10	5	1	299.3

6.3.4 Utilizing the FE Model to Evaluate Rehabilitation using CFRP

The FE model is then used to apply CFRP laminates on the bridge girders. Strain values were expected to drop, as seen in Figure 6-4 to Figure 6-13 showing the strain reduction obtained from the FE analysis due to applying CFRP to the bridge girders. The FE model can be applied on steel bridge girders or prestressed concrete girders.
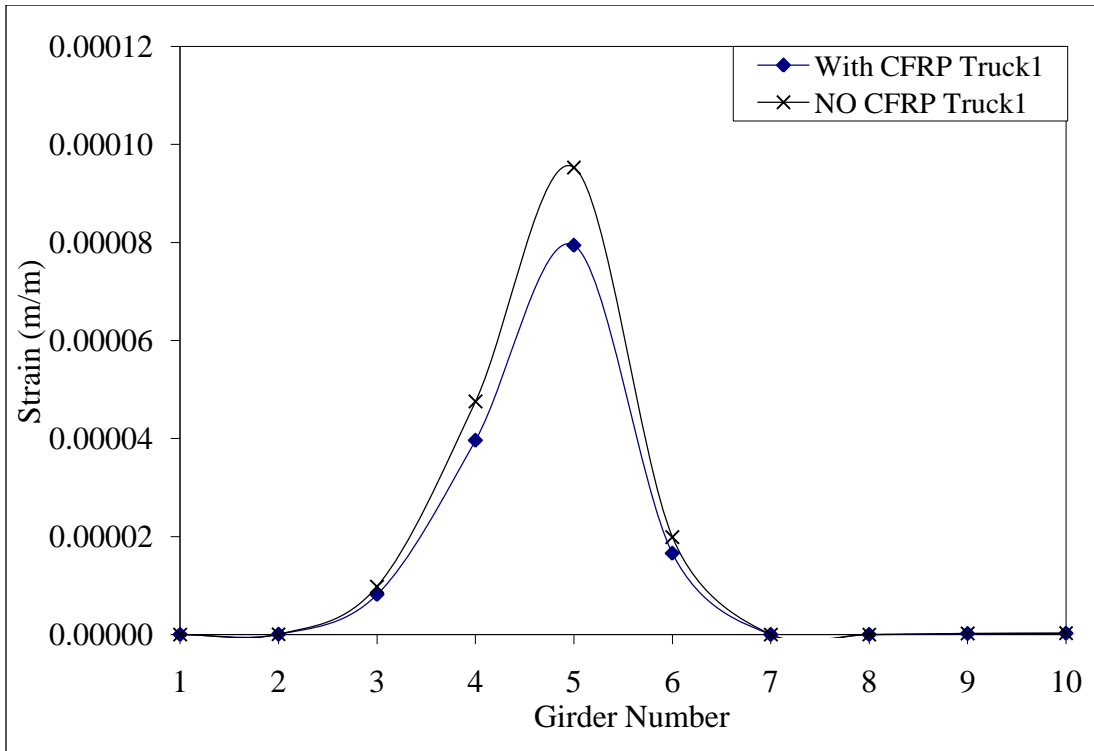
Figure 6-4. Strain reduction after rehabilitation with CFRP – Truck 1.
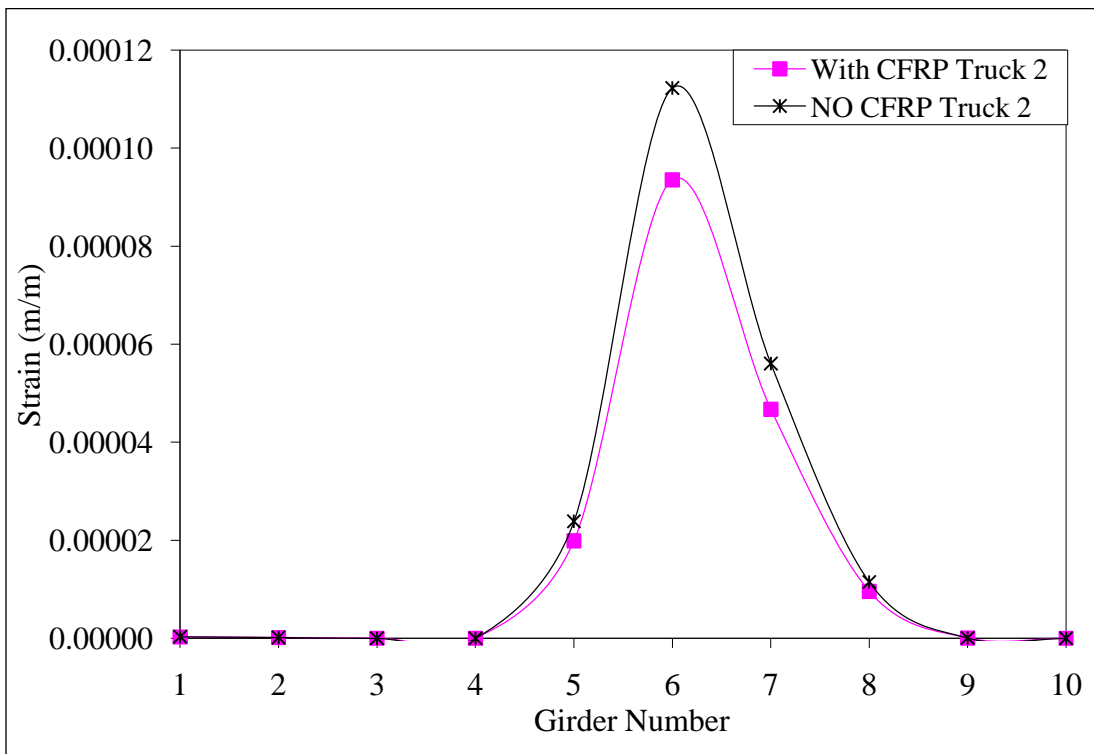
Figure 6-5. Strain reduction after rehabilitation with CFRP – Truck 2.

111
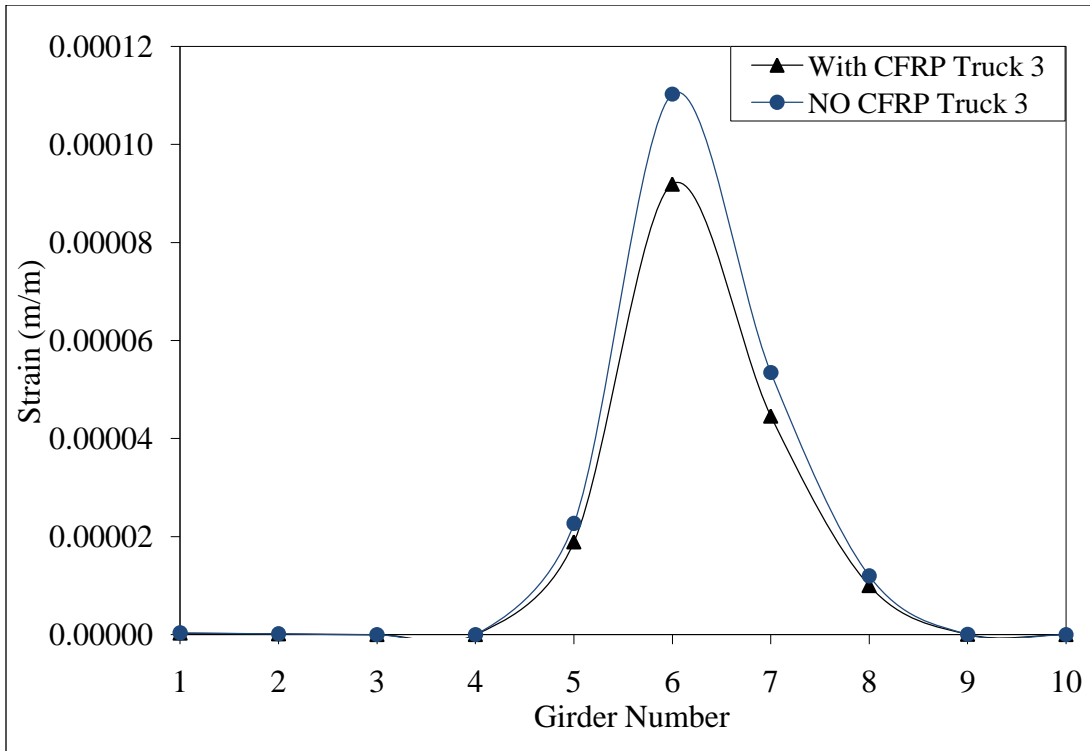
Figure 6-6. Strain reduction after rehabilitation with CFRP – Truck 3.
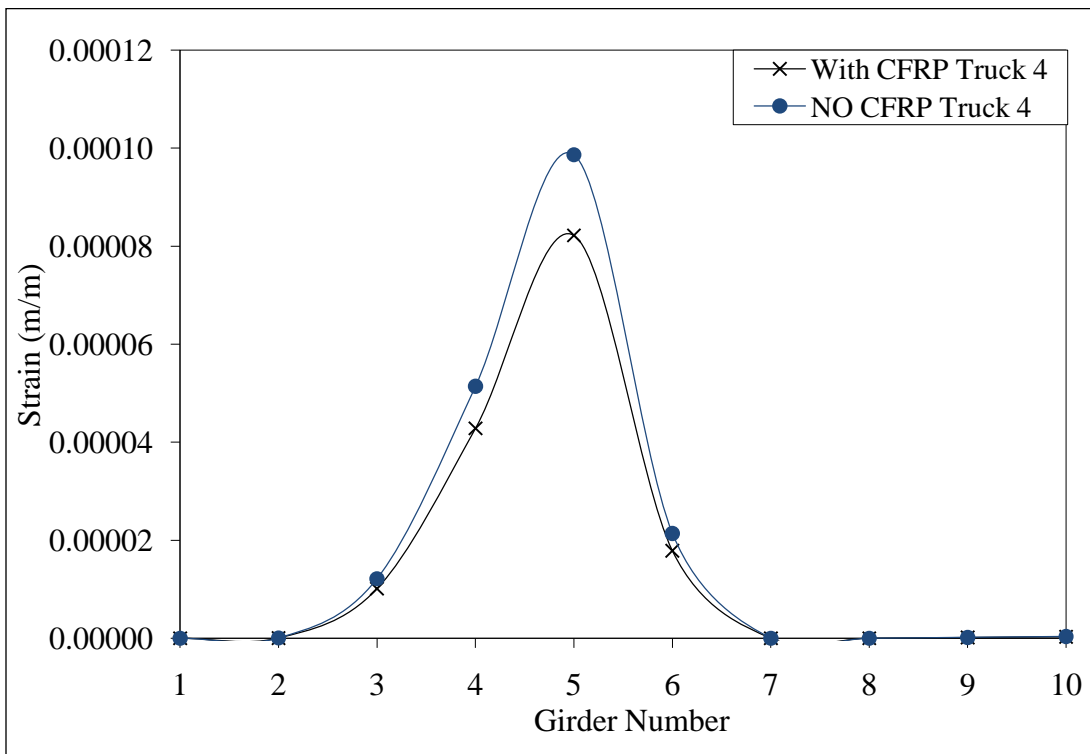
Figure 6-7. Strain reduction after rehabilitation with CFRP – Truck 4.

112
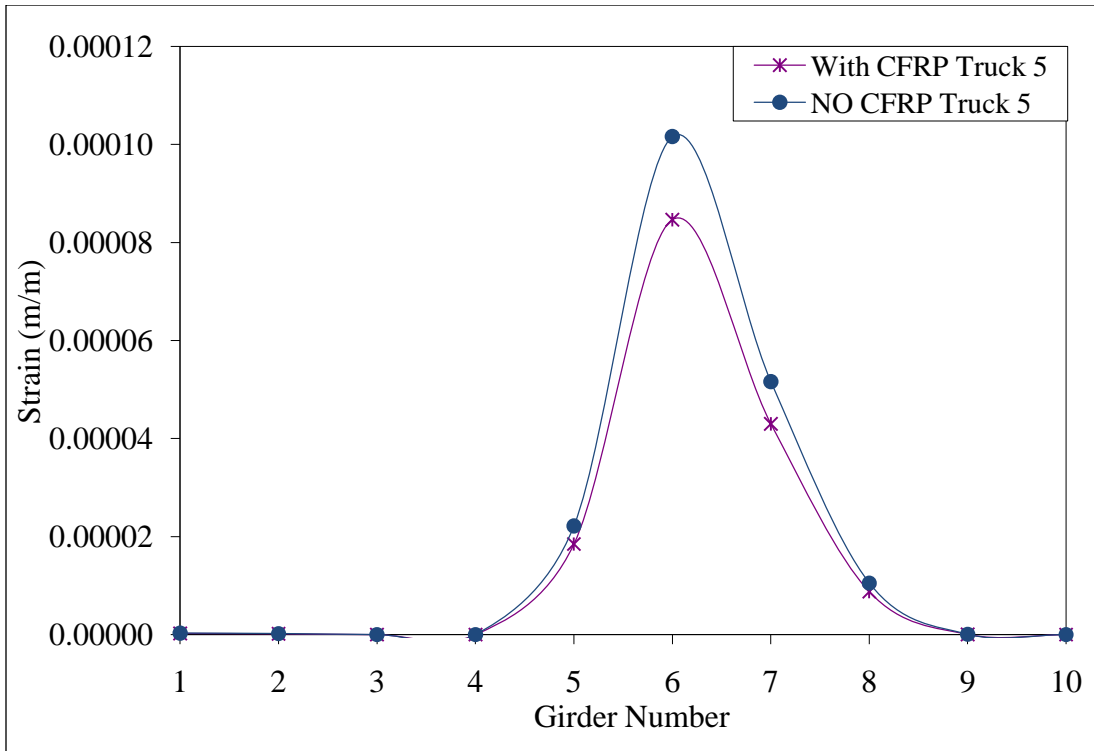
Figure 6-8. Strain reduction after rehabilitation with CFRP – Truck 5.
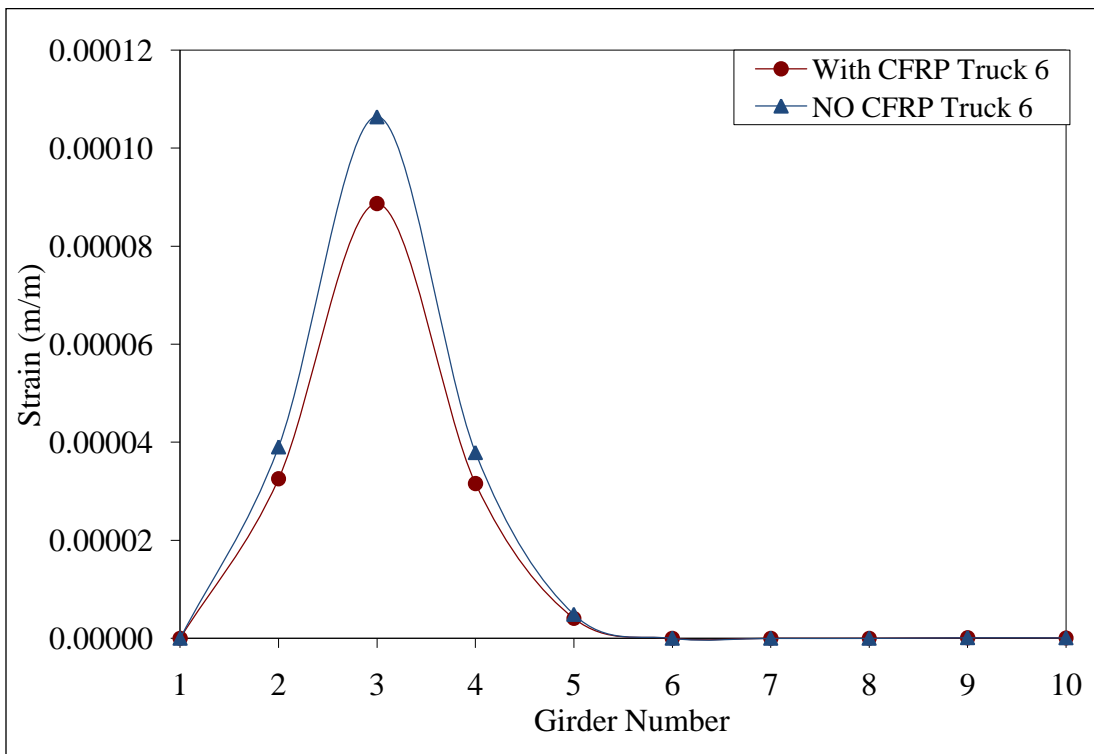
Figure 6-9. Strain reduction after rehabilitation with CFRP – Truck 6.

113
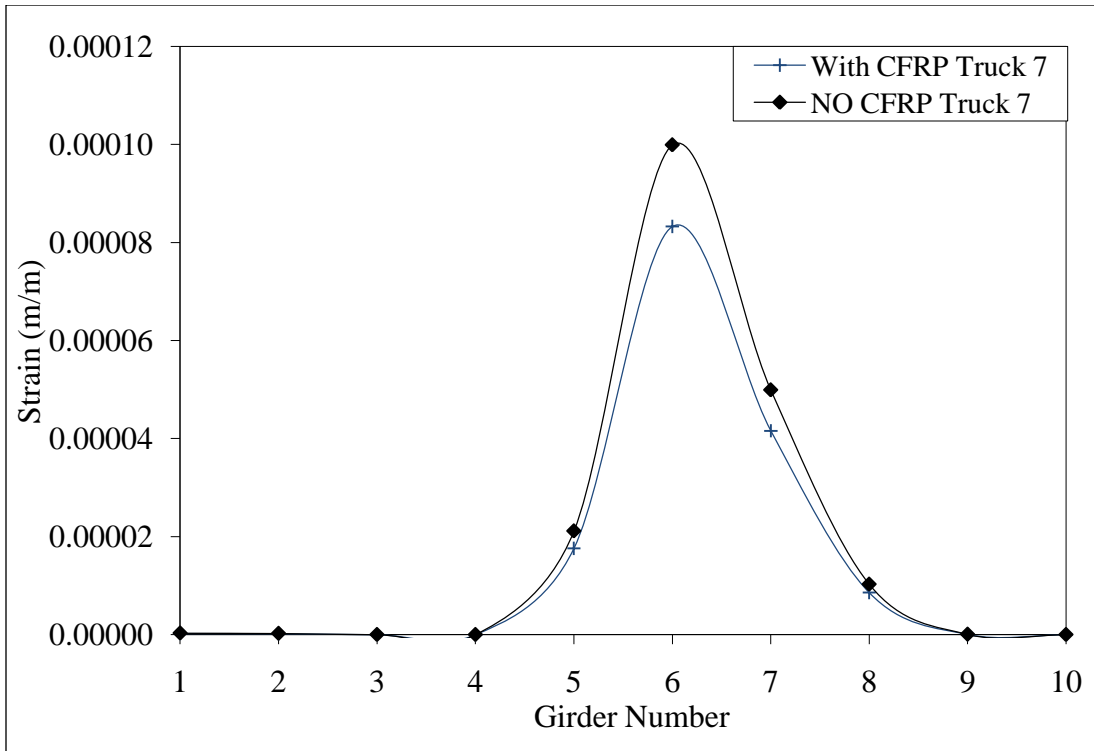
Figure 6-10. Strain reduction after rehabilitation with CFRP – Truck 7.
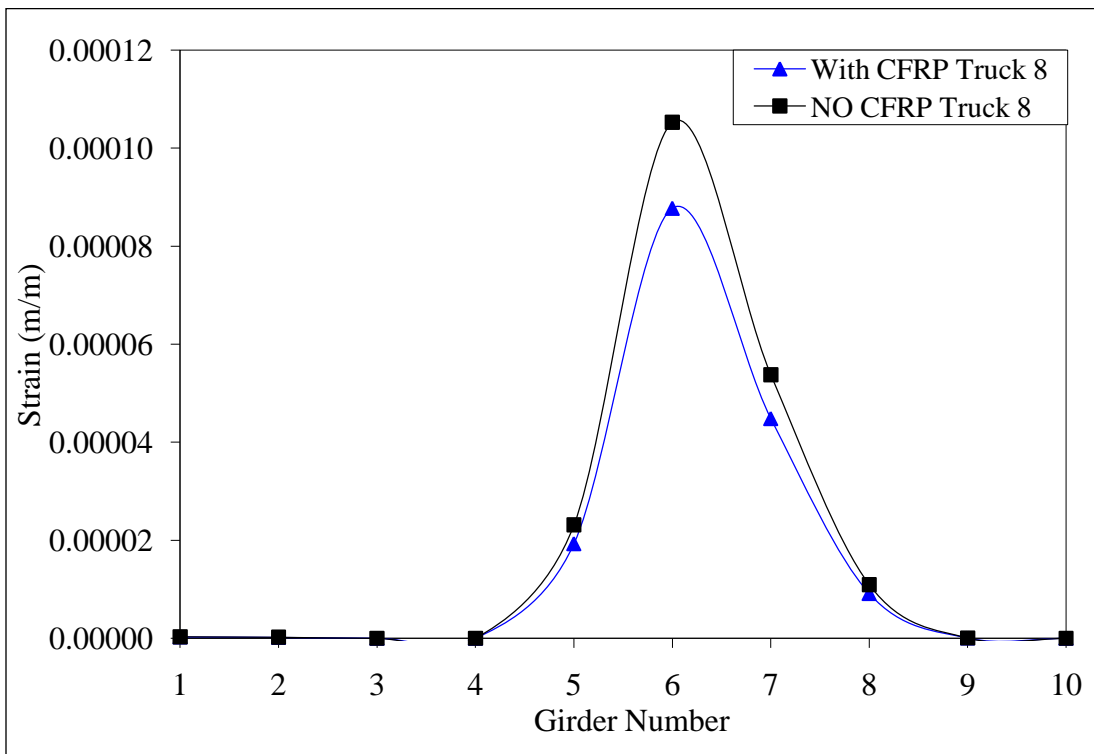
Figure 6-11. Strain reduction after rehabilitation with CFRP – Truck 8.

114
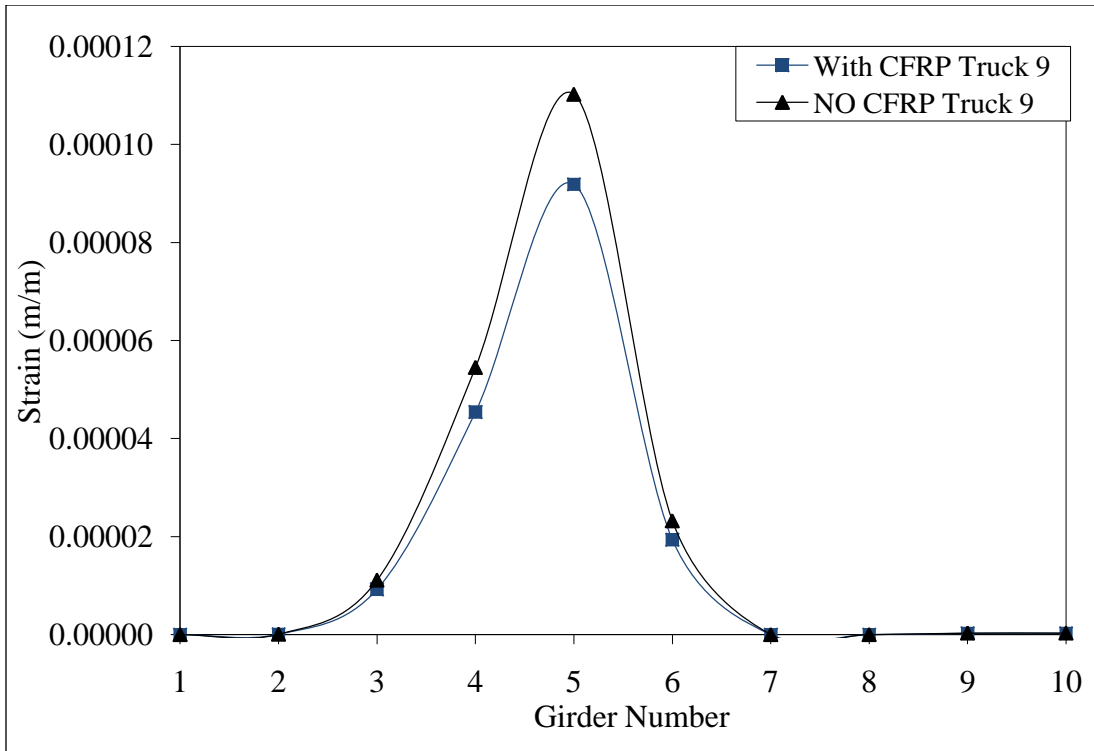
Figure 6-12. Strain reduction after rehabilitation with CFRP – Truck 9.
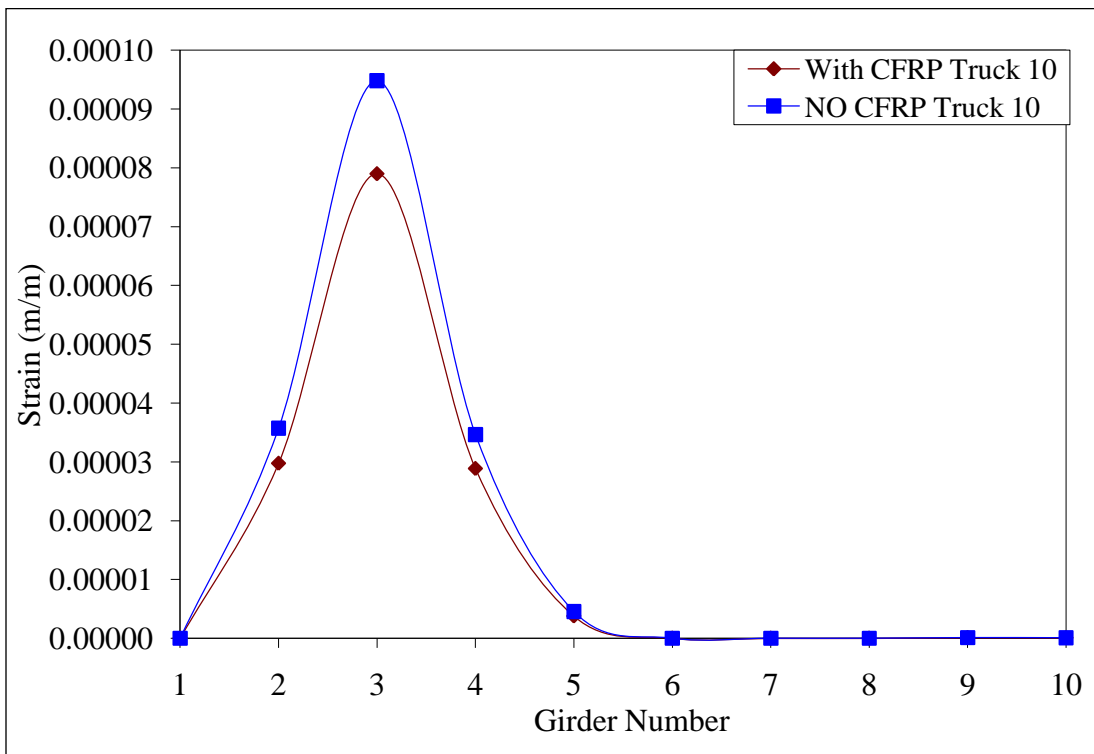
Figure 6-13. Strain reduction after rehabilitation with CFRP – Truck 10.

Using the same FE model, truck loading was then increased with the aim of reaching the same stress level in steel before rehabilitation. Models were executed once again, and moment values were extracted for all girders and displayed in Figure 6-14 to Figure 6-23. Moments from the original truck loading are also shown in the figures for comparison. The moment increase was found to average 20%, which in turn increased the posting load limit by 20%.
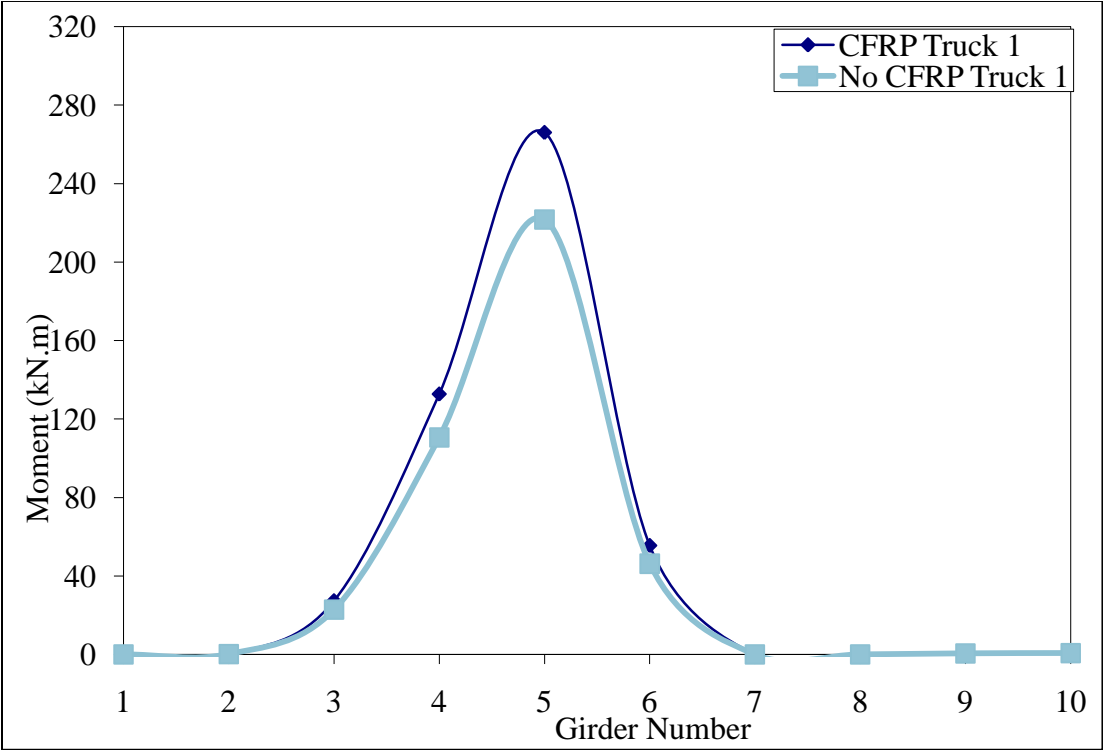
Figure 6-14. Moment increase after rehabilitation with CFRP – Truck 1.
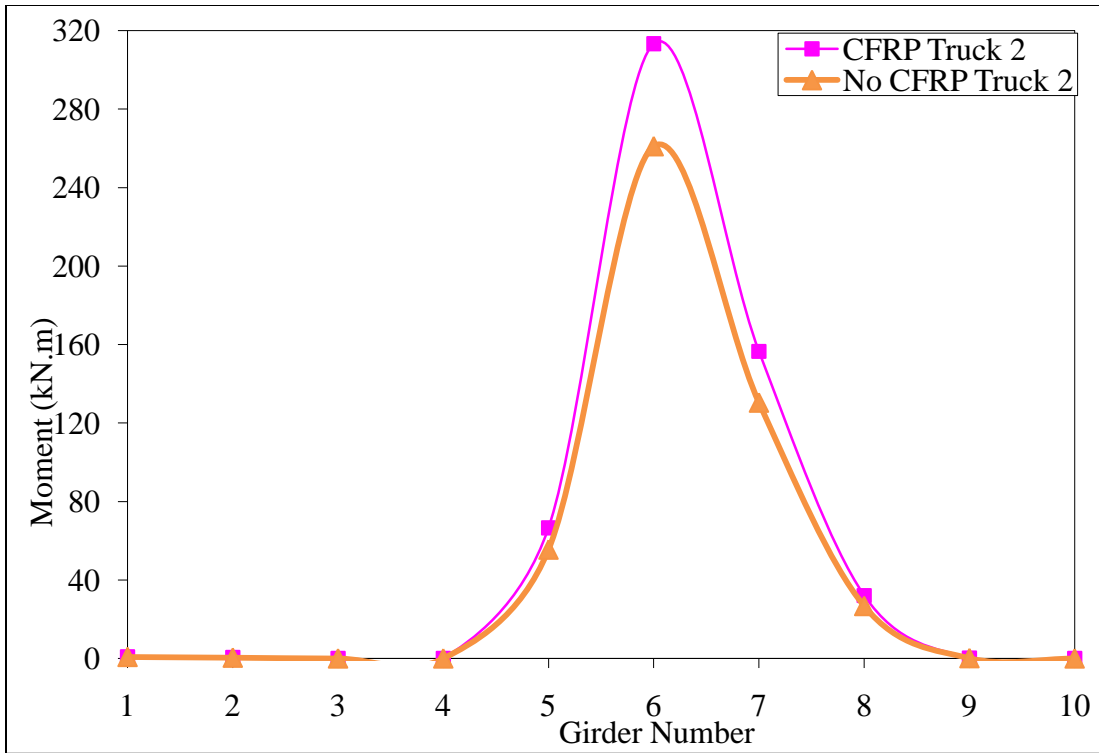
Figure 6-15. Moment increase after rehabilitation with CFRP – Truck 2.
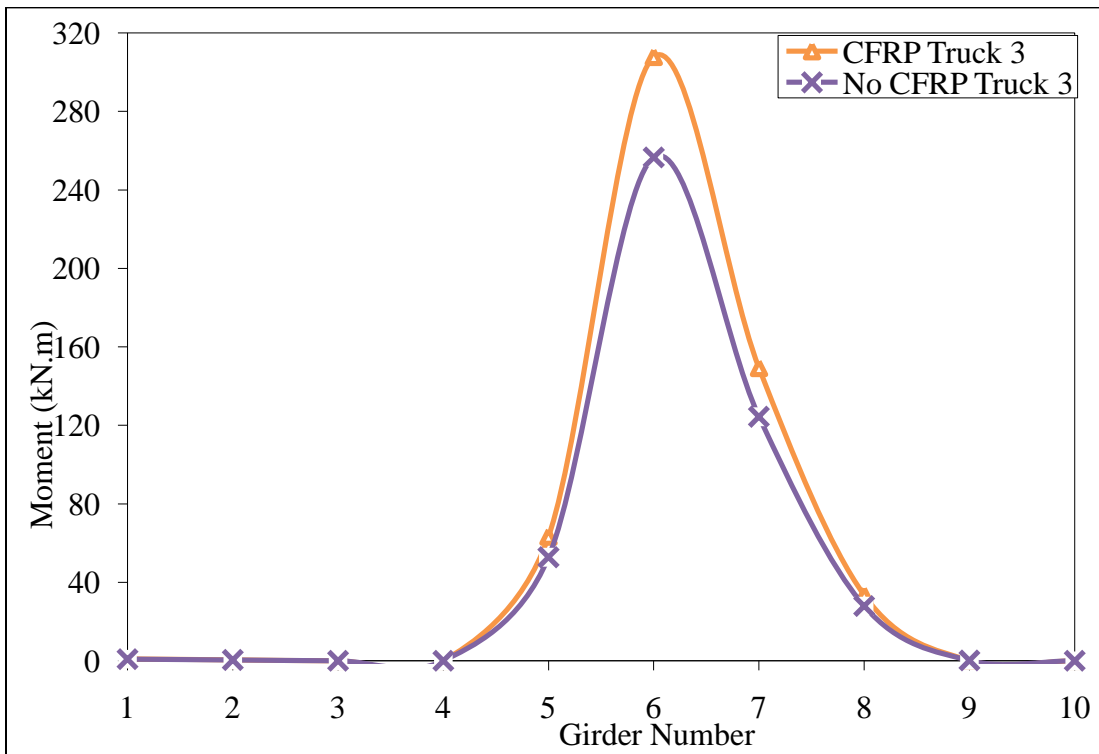
Figure 6-16. Moment increase after rehabilitation with CFRP – Truck 3.

117
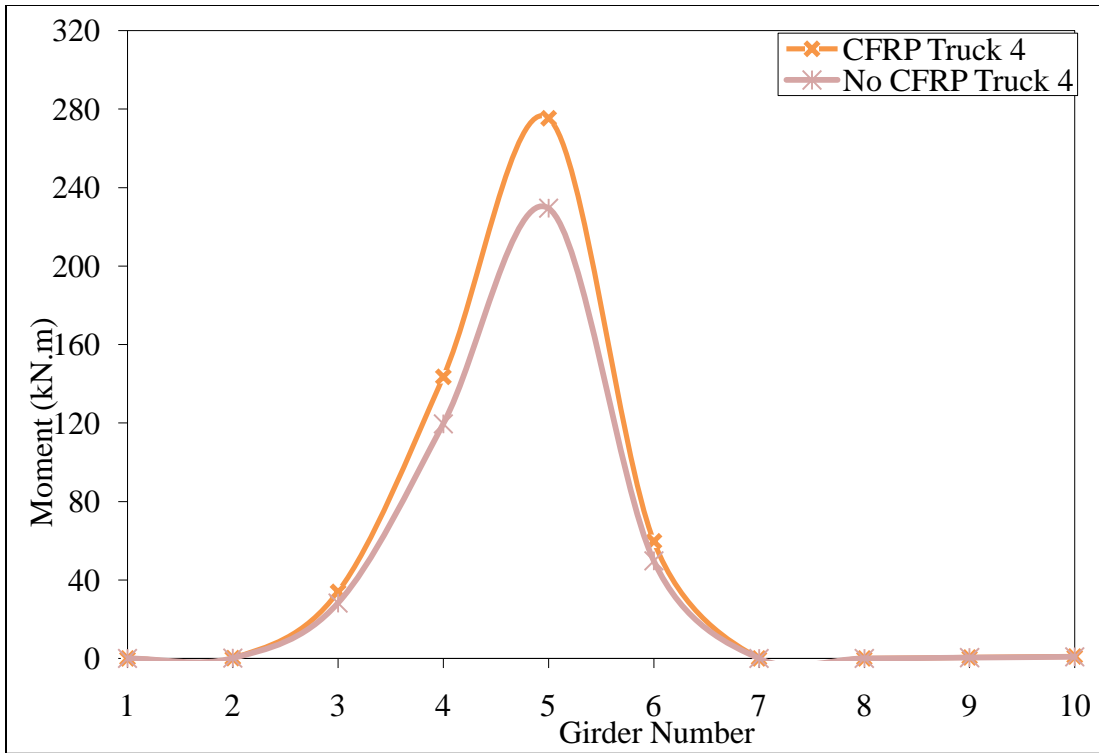
Figure 6-17. Moment increase after rehabilitation with CFRP – Truck 4.
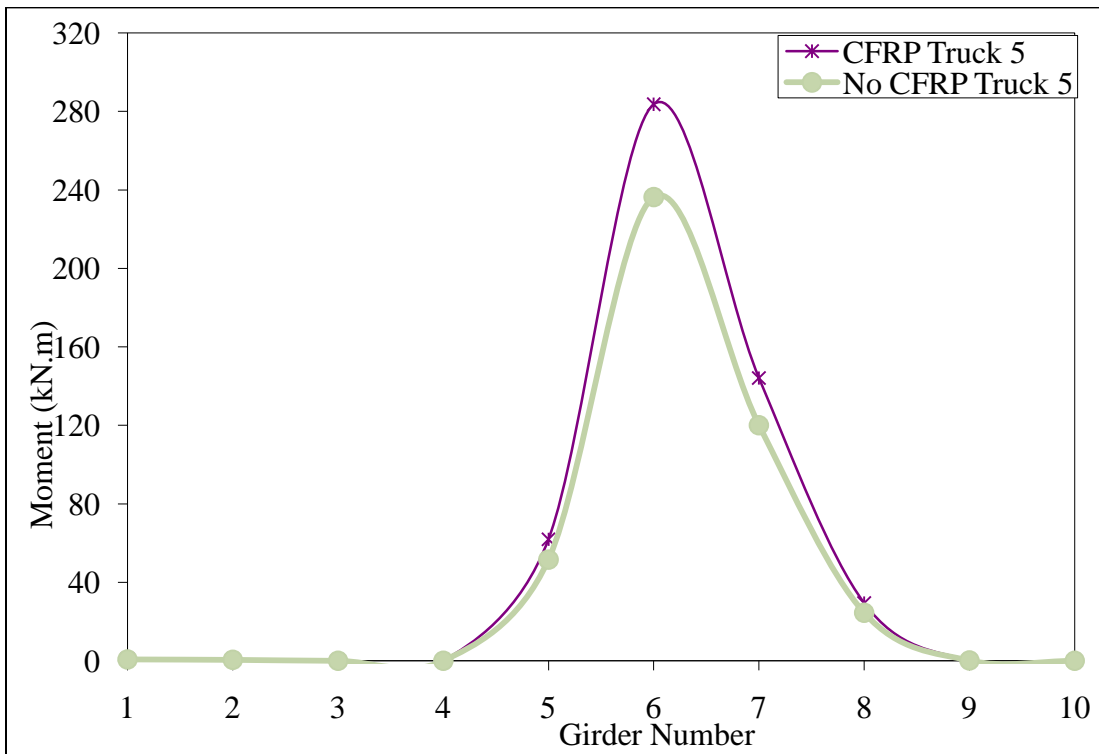
Figure 6-18. Moment increase after rehabilitation with CFRP – Truck 5.
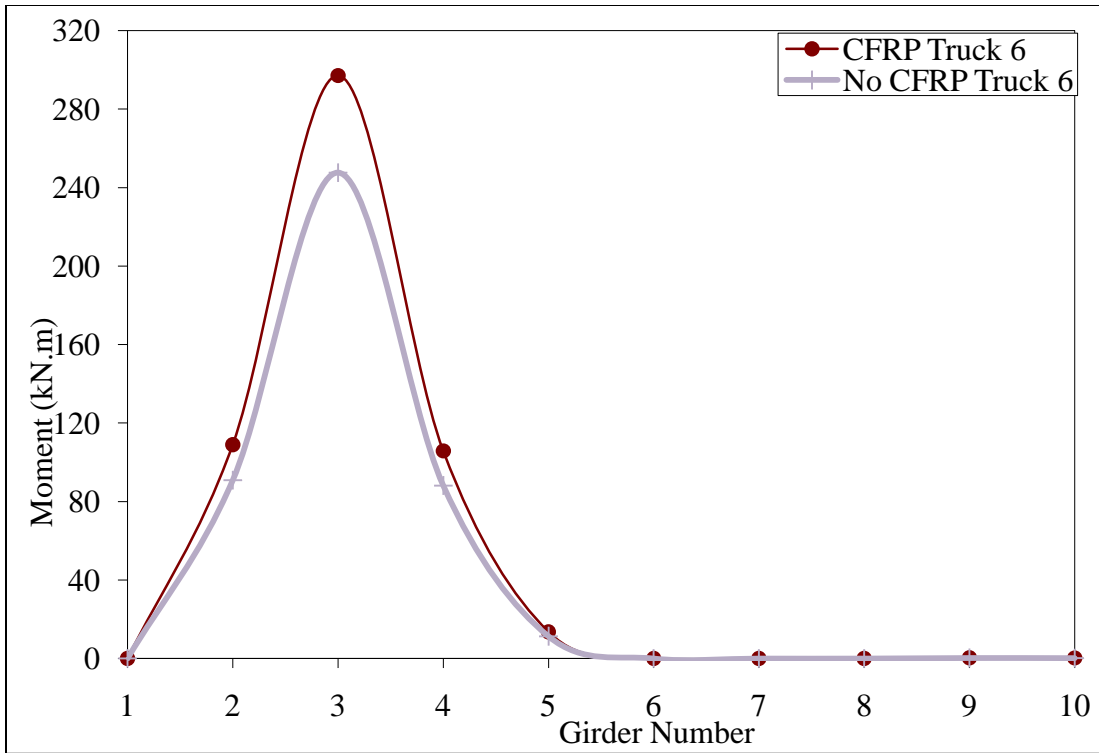
Figure 6-19. Moment increase after rehabilitation with CFRP – Truck 6.
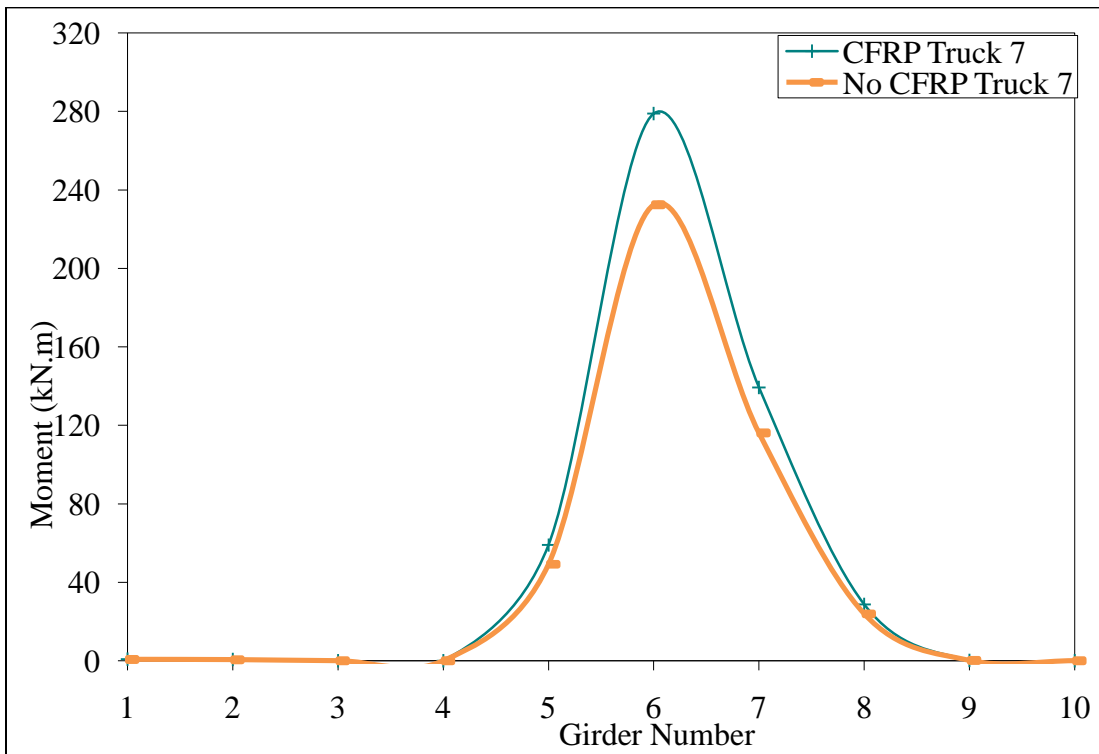
Figure 6-20. Moment increase after rehabilitation with CFRP – Truck 7.

119
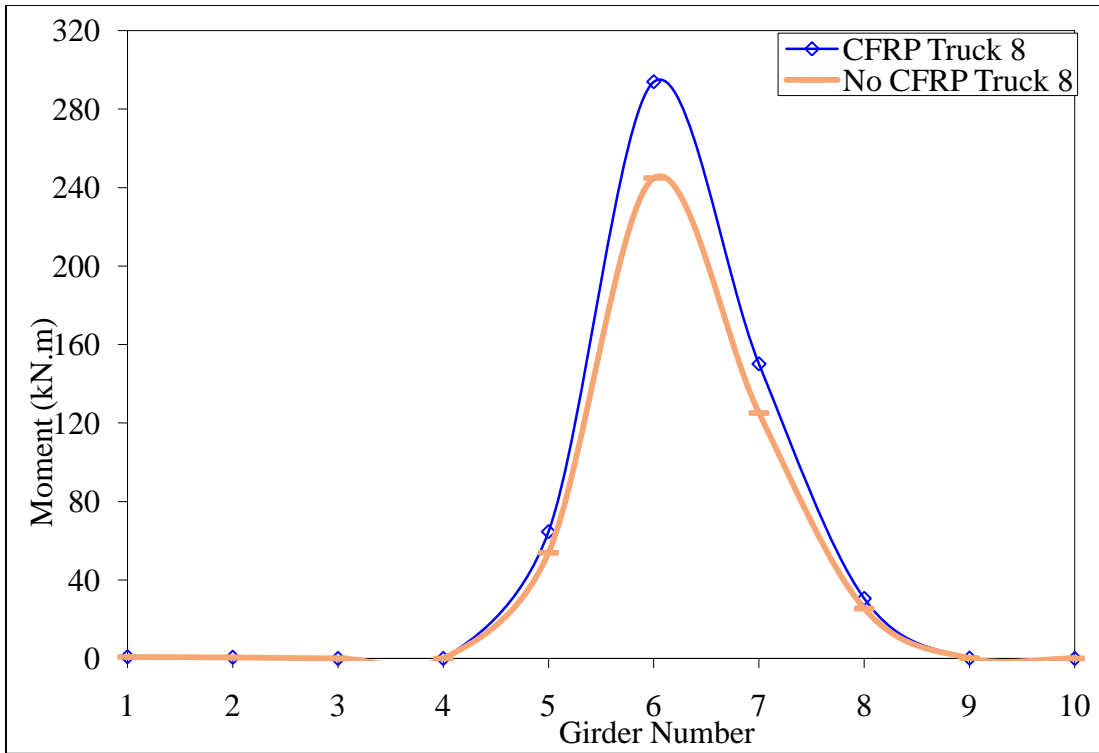
Figure 6-21. Moment increase after rehabilitation with CFRP – Truck 8.
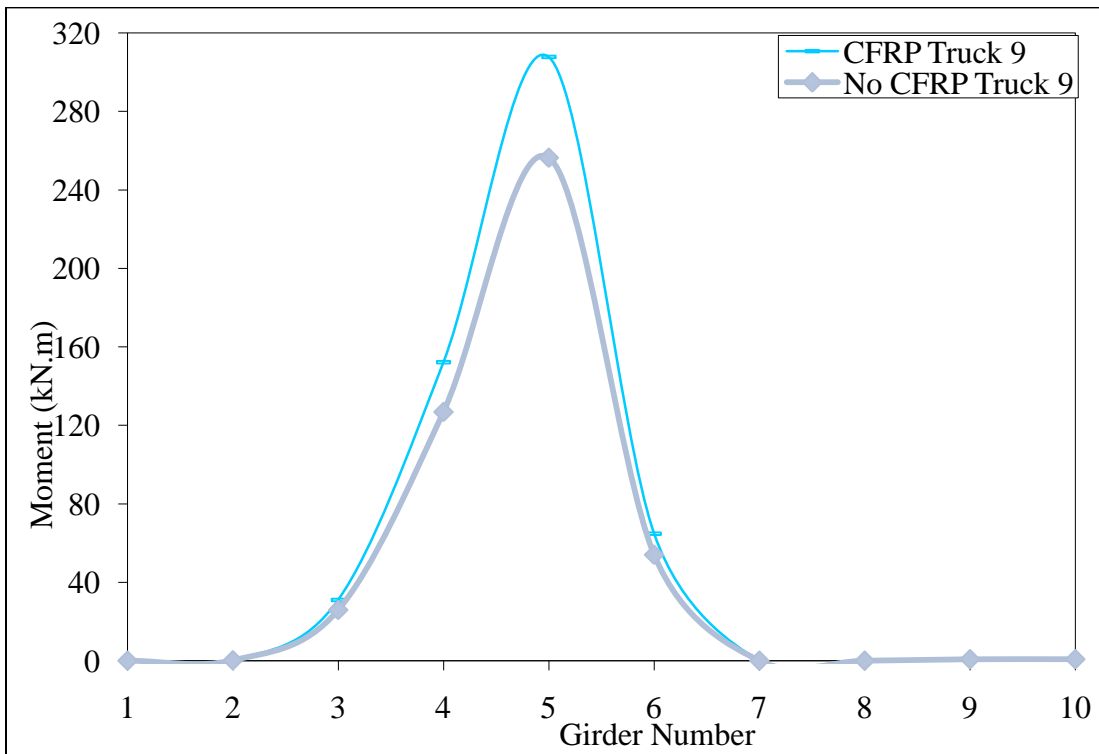
Figure 6-22. Moment increase after rehabilitation with CFRP – Truck 9.
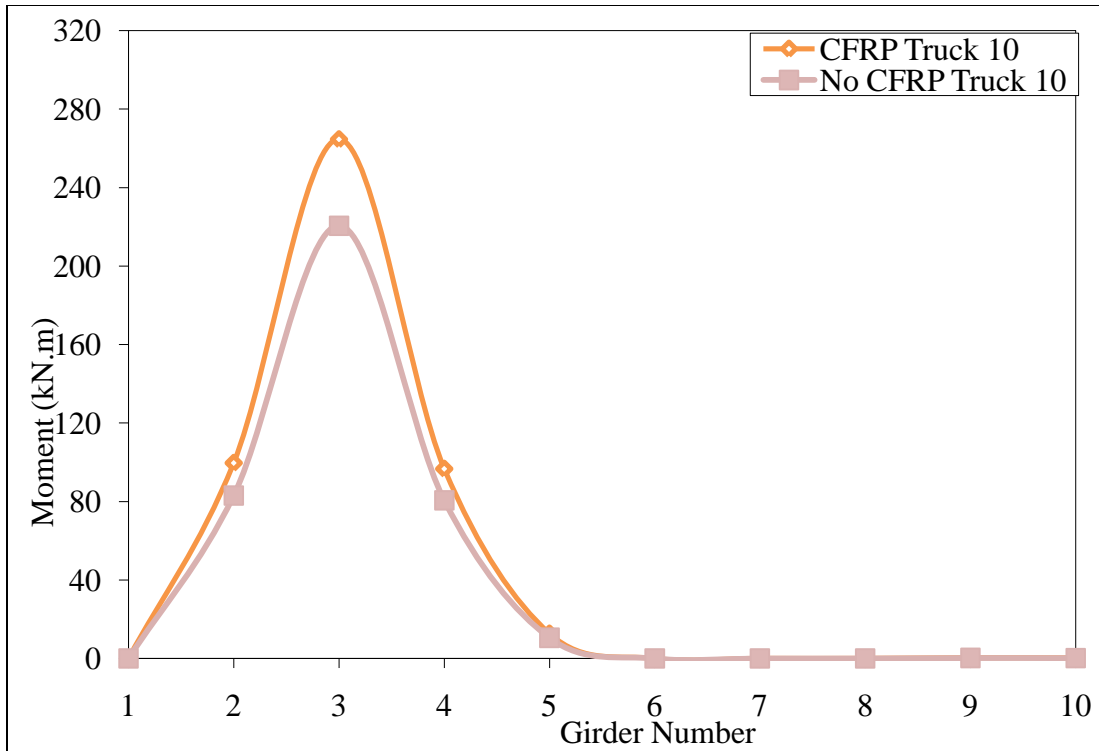
Figure 6-23. Moment increase after rehabilitation with CFRP – Truck 10.

6.4 Steel Bridge Girder – Solved Example

This section presents a design example of a steel girder bridge strengthened using CFRP laminates. Recommendations for the bridge design engineer will then be summarized. All the calculations are based on AASHTO LRFD bridge design specifications (1998). Equations and design limits used in this section are those implemented in the design Excel spreadsheet presented previously in Chapter 5.

First, a steel bridge will be designed without CFRP laminates. The same bridge would then be analyzed after being strengthened using CFRP. This example would show the significant increase to the load-carrying capacity of the bridge due to this technique. A complete design check was performed to ensure the bridge enhanced safety after rehabilitation.

The bridge designed is a simple-span composite rolled-steel-beam bridge shown in Figure 6-24 and Figure 6-25 with 10.5 m span. The design live load applied was HL-93. Roadway width is 13,420 mm from curb to curb, and the future top wearing surface is 75 mm thick bituminous overlay. The concrete strength, f_c', is 30 MPa, the steel reinforcement is M270 of grade Gr250.

6.4.1 Develop General Section

The bridge is to carry interstate traffic over a normally small stream that is subject to high water flows during the rainy season.

6.4.2 Develop Typical Section and Design Basis

6.4.2.1 I-Girder [A6.10.1]

Design flexural members for:

- Strength limit state;
- Service limit state;
- Fatigue and fracture limit state for details;
- Fatigue requirements for web;
- Constructability;
- Member proportions of flexural components:

$$0.1 \leq \frac{I_{yc}}{I_y} \leq 0.9$$
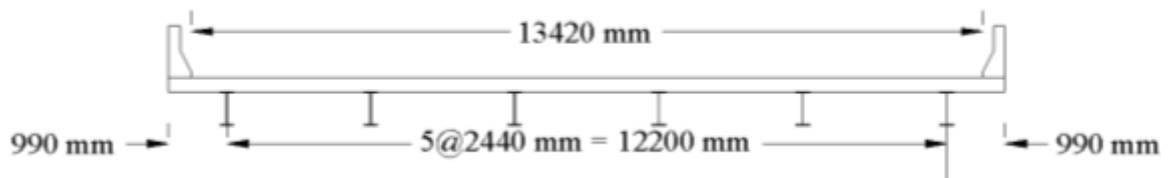
Figure 6-24. Bridge example – bridge cross section.
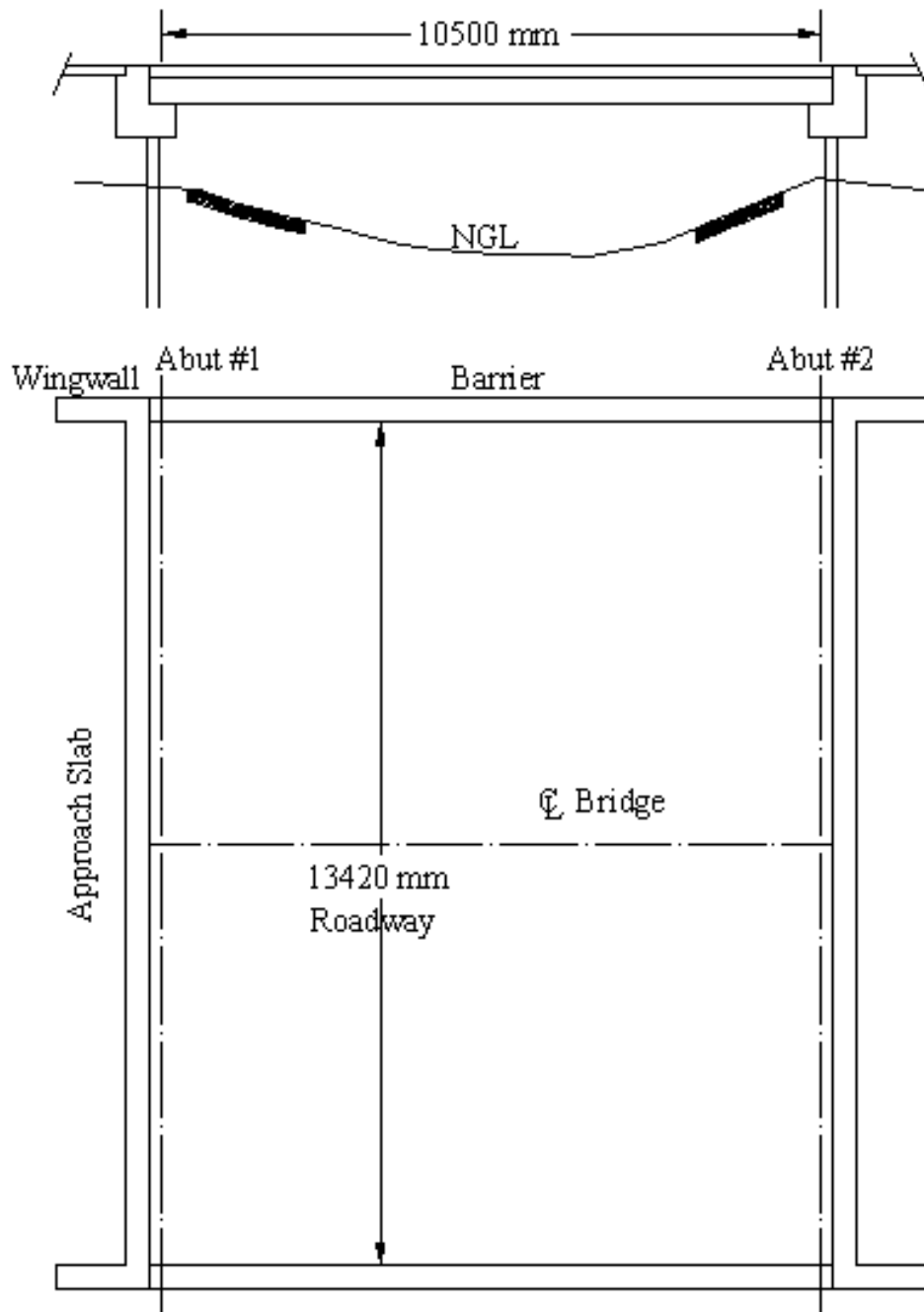
Figure 6-25. Bridge example – (a) general elevation and (b) plan view.

6.4.2.2 Elastic Analysis or Inelastic Analysis [A6.10.2.2]

Elastic analysis will be performed. The span is simply supported, thus moment redistribution is not used.

6.4.2.3 Homogeneous or Hybrid [A6.10.5.4]

Rolled beams are homogeneous (the flanges and web are the same material and strength). For homogeneous sections, the hybrid factor, R_h, shall be taken as 1.0. For compression flanges, if either a longitudinal stiffener is provided or the following equation is satisfied, then the load shedding factor R_b shall be taken as 1.0.

$$\frac{2D_c}{t_w} \leq \lambda_b \sqrt{\frac{E}{f_c}}$$

Otherwise,

$$R_b = 1 - \left(\frac{a_r}{1200 + 300a_r}\right)\left(\frac{2D_c}{t_w} - \lambda_b \sqrt{\frac{E}{f_c}}\right)$$

For which

$$a_r = \frac{2D_c t_w}{A_{fc}}$$

For tension flanges, R_b shall be taken as 1.0.

6.4.3   Design Conventionally Reinforced Concrete Deck

The deck design will not be included in this design as it has no influence on the rehabilitation of steel girders using CFRP.

6.4.4   Select Resistance Factors

Strength Limit state   Φ   [A6.5.4.2]

Flexure   1.00

Shear   1.00

Non-strength limit states   1.00   [A1.3.2.1]

6.4.5   Select Load Modifiers

Load modifiers are summarized in Table 6-2 with references to AASHTO.

Table 6-2. LRFD Load Modifiers

		Strength	Service	Fatigue
Ductility, η_D	[A1.3.3]	0.95	1.0	1.0
Redundancy, η_R	[A1.3.4]	0.95	1.0	1.0
Importance, η_I	[A1.3.5]	1.05	N/A	N/A
$\eta = \eta_D \eta_R \eta_I$	[A1.3.2.1]	0.95	1.0	1.0

6.4.6   Select Applicable Load Combinations

Strength I Limit State

$$U = \eta[1.25DC + 1.50DW + 1.75(LL + IM) + 1.0FR + \gamma_{TG}TG]$$

Service I Limit State

$$U = 1.0(DC + DW) + 1.0(LL + IM) + 0.3(WS + WL) + 1.0FR$$

Fatigue and Fracture Limit State

$$U = 0.75(LL + IM)$$

6.4.7   Calculate Live Load Force Effects [A3.6.1.1.1]

Select number of lanes: [A3.6.1.1.1]

$$N_L = INT\left(\frac{w}{3600}\right) = INT\left(\frac{13420}{3600}\right) = 3$$

Multiple presence factor: (Table 4.6) [A3.6.1.1.2]. Refer to Table 6-3.

Table 6-3. Multiple Presence Factors

No. of loaded lanes	m
1	1.20
2	1.00
3	0.85

Dynamic load allowance: (Table 4.7) [A3.6.2.1]. Refer to Table 6-4.

Table 6-4. Dynamic Load Allowance Factors

Component	IM (%)
Deck joints	75
Fatigue	15
All other	33

Distribution factors for moment: [A4.6.2.2.2] Cross-section type (a) (Table 2.2), S = 2440 mm, L = 10500 mm. assume for preliminary design,

$$\frac{K_g}{Lt_s^3} = 1.0$$

Interior beams (Table 6.5) [Table A4.6.2.2.2b-1]. One design lane loaded:

$$mg_M^{SI} = 0.06 + \left(\frac{S}{4300}\right)^{0.4} \left(\frac{S}{L}\right)^{0.3} \left(\frac{K_g}{Lt_s^3}\right)^{0.1}$$

$$mg_M^{SI} = 0.06 + \left(\frac{2440}{4300}\right)^{0.4} \left(\frac{2440}{10500}\right)^{0.3} (1.00)^{0.1} = 0.575$$

Two design lanes loaded:

$$mg_M^{MI} = 0.075 + \left(\frac{S}{2900}\right)^{0.6} \left(\frac{S}{L}\right)^{0.2} \left(\frac{K_g}{Lt_s^3}\right)^{0.1}$$

$$mg_M^{SI} = 0.075 + \left(\frac{2440}{2900}\right)^{0.6} \left(\frac{2440}{10500}\right)^{0.2} (1.00)^{0.1} = 0.748$$

The two design lanes loaded governs.

Exterior beams (Table 6.5) [Table A4.6.2.2.2d-1]. One design lane loaded – lever rule. Refer to Figure 6-26.

$$R = \frac{P}{2}\left(\frac{650 + 2450}{2440}\right) = 0.635P$$

$$mg_M^{SE} = 0.635$$

$$mg_M^{SE} = 1.2(0.635) = 0.762, governs$$

Two or more design lanes loaded:

$$d_e = 990 - 380 = 610mm$$

$$e = 0.77 + \frac{d_e}{2800} = 0.77 + \frac{610}{2800} = 0.988 < 1.0$$

Use $e = 1.0$

$$mg_M^{ME} = e \, mg_M^{MI} = 0.748$$
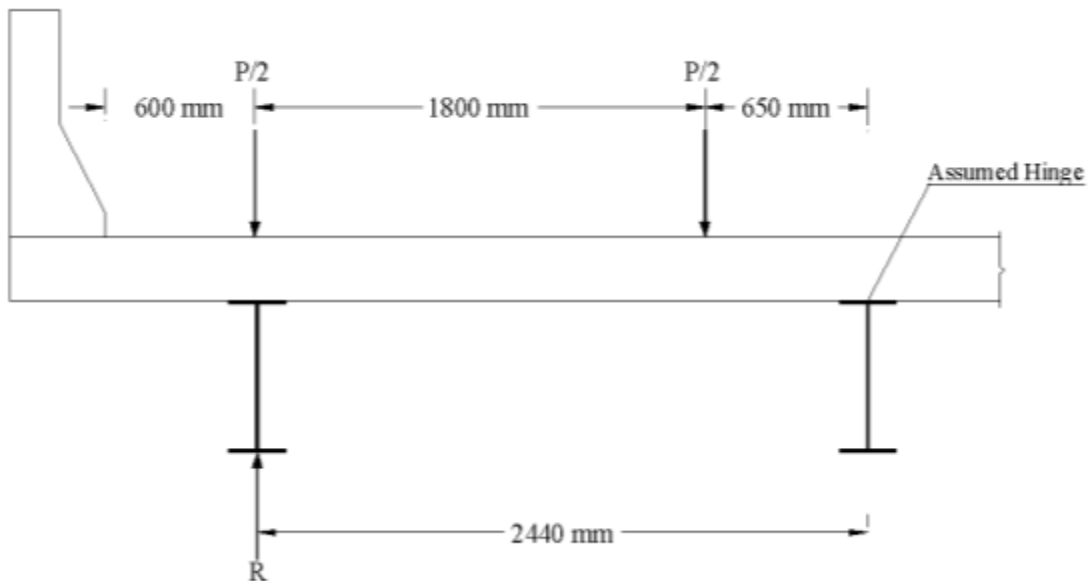
Figure 6-26. Lever rule for determination of distribution factor for moment in exterior beam, one lane loaded.

Distributed live load moments

$$M_{LL+IM} = mg \left[(M_{Tr} \text{ or } M_{Ta}) \left(1 + \frac{IM}{100} \right) + M_{Ln} \right]$$

$$M_{Tr} = 145(2.625) + (145 + 35)(0.475) = 466 \, kN.m$$

$$M_{Ta} = 110(2.625 + 2.025) = 512 \, kN.m, governs$$

The absolute moment due to the tandem actually occurs under the wheel closest to the resultant when the cg of the wheels on the span and the critical wheel are equidistant from the centerline of the span. For this span, the absolute maximum moment is 513 kN.m. However, the value of 512 kN.m is used because moments due to other loads are maximum at the centerline and thus can be added to the tandem load moment. Refer to Figure 6-27 for the truck, tandem, and lane load locations for maximum moment at 105 (midspan)

$$M_{Ln} = \frac{9.3(10.5)^2}{8} = 128 \ kN.m$$

Interior Beams

$$M_{LL+IM} = 0.748[(512)(1.33) + 128] = 605 \ kN.m$$

Exterior Beams

$$M_{LL+IM} = 0.762[(512)(1.33) + 128] = 616 \ kN.m$$
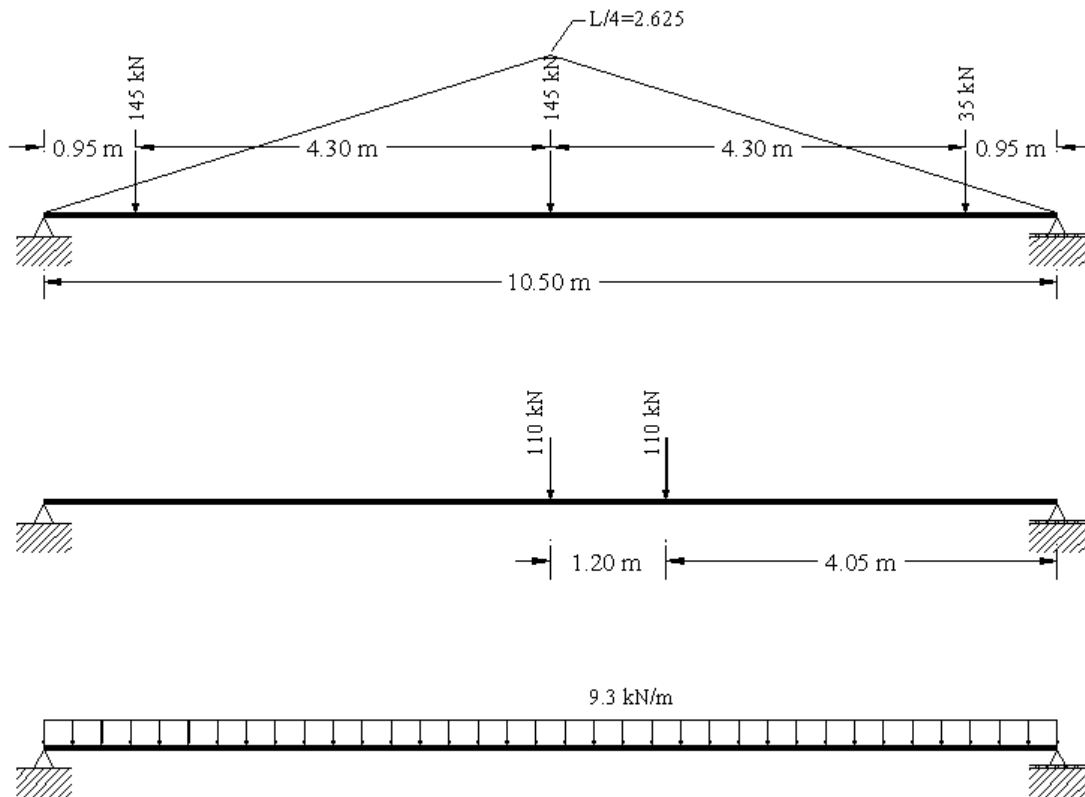
Figure 6-27. Truck, tandem, and lane load placement for maximum moment at Location 105.

Distribution factors for shear [A4.6.2.2.3] Cross-section type (a) (Table 2.2)

Interior beams (Table 6.5) [Table A4.6.2.2.3a-1], one design lane loaded

$$mg_V^{SI} = 0.36 + \left(\frac{S}{7600}\right) = 0.36 + \left(\frac{2440}{7600}\right) = 0.681$$

Two design lanes loaded

$$mg_V^{MI} = 0.20 + \left(\frac{S}{3600}\right) - \left(\frac{S}{10500}\right)^{2.0} = 0.20 + \left(\frac{2440}{3600}\right) - \left(\frac{2440}{10500}\right)^{2.0} = 0.826$$

The two design lanes loaded factor governs.

Exterior beams (Table 6.5) [Table A4.6.2.2.3b-1] One design lane loaded

$$mg_V^{SE} = 0.762, governs$$

Two or more design lanes loaded

$$d_e = 610mm$$

$$e = 0.60 + \frac{d_e}{3000} = 0.60 + \frac{610}{3000} = 0.803$$

$$mg_V^{ME} = e \; mg_V^{MI} = (0.803)(0.826) = 0.663$$

Distributed live load for shears. Figure 6-28 shows the truck, tandem, and lane load positions for maximum shear at span end (location 100).

$$V_{LL+IM} = mg\left[(V_{Tr} \; or \; V_{Ta})\left(1 + \frac{IM}{100}\right) + V_{Ln}\right]$$

$$V_{Tr} = 145(1 + 0.590) + (35)(0.181) = 237 \; kN, governs$$

$$V_{Ta} = 110(1 + 0.886) = 207 \; kN$$

$$V_{Ln} = \frac{9.3(10.5)}{8} = 49 \; kN$$
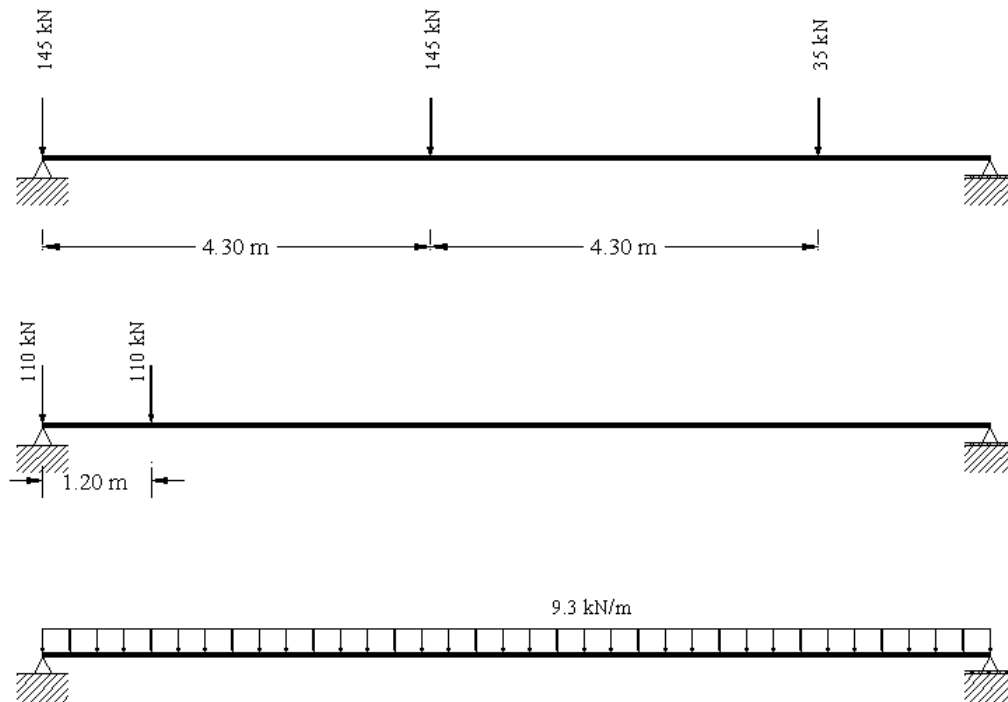
Figure 6-28. Truck, tandem, and lane load placement for maximum shear at Location 100.

Interior Beams

$$V_{LL+IM} = 0.826[(237)(1.33) + 49] = 301 \; kN$$

Exterior Beams

$$V_{LL+IM} = 0.762[(237)(1.33) + 49] = 278 \; kN$$

Reactions to substructure

The following reactions are per design lane without any distribution factors

$$R_{100} = V_{100} = 1.33V_{Tr} + V_{Ln} = 1.33(237) + 49 = 364 \; kN/lane$$

6.4.8 Calculate Force Effects from Other Loads

- D1 = dead load of structural components and their attachments, acting on the non-composite section
- D2 = future wearing surface

- D3 = barriers that have a cross-sectional area of 197 312 mm^2

A 50 mm x 300 mm average concrete haunch at each girder is used to account for camber and unshored construction.

Assume a beam weight of 1.5 kN/m.

For a uniformly distributed load, w,

$$M_{105} = 13.78w$$

$$V_{100} = 5.25w$$

Interior girders

D1   *Deck Slab* $(2400)(10^{-9})(9.81)(205)(2440) = 11.78\ kN/m$

     Girder $= 1.5\ kN/m$

     Haunch $(2400)(10^{-9})(9.81)(300)(50) = 0.35\ kN/m$

$$w_{D1}^I = 13.63\ kN/m$$

D2 75 mm bituminous paving

$$w_{D2}^I = (2250)(9.81)(10^{-9})(75)(2440) = 4.04\ kN/m$$

D3 Barriers, one-sixth share

$$w_{D3}^I = \frac{2(197312)(2400)(9.81)}{6(10^9)} = 1.55\ kN/m$$

Table 6-5 summarizes the un-factored moments and shear at critical section for interior girders.

Table 6-5. Interior Girder Un-factored Moments and Shears

Load Type	W (kN/m)	Moment (kN.m) M_{105}	Shear (kN) V_{100}
D1	13.63	188	72
D2	4.04	56	21
D3	1.55	21	8
LL + IM	N/A	605	301

Exterior girders

D1   *Deck Slab* $(2400)(10^{-9})(9.81)[(230)(990) + (205)(1220) = 11.25 \, kN/m$

   Girder $= 1.5 \, kN/m$

   Haunch $(2400)(10^{-9})(9.81)(300)(50) = 0.35 \, kN/m$

$$w_{D1}^I = 13.10 \, kN/m$$

D2 75 mm bituminous paving

$$w_{D2}^I = (2250)(9.81)(10^{-9})(75)(1220 + 990 - 380) = 3.03 \, kN/m$$

D3 Barriers, one-sixth share

$$w_{D3}^I = \frac{2(197312)(2400)(9.81)}{6(10^9)} = 1.55 \, kN/m$$

Table 6-6 summarizes the un-factored moments and shear at critical section for exterior girders.

Table 6-6. Exterior Girder Un-factored Moments and Shears

Load Type	W (kN/m)	Moment (kN.m) M_{105}	Shear (kN) V_{100}
D1	13.10	181	69
D2	3.03	42	16
D3	1.55	21	8
LL + IM	N/A	616	278

6.4.9   Design Required Sections

6.4.9.1 Strength Limit State

Interior beam – factored shear and moment

$$U = \eta[1.25D1 + 1.50D2 + 1.25D3 + 1.75(LL + IM)]$$

$$V_u = 0.95[1.25(72) + 1.50(21) + 1.25(8) + 1.75(301)] = 625 \, kN$$

$$M_u = 0.95[1.25(188) + 1.50(56) + 1.25(21) + 1.75(605)] = 1334 \, kN.m$$

Exterior beam – factored shear and moment

$$V_u = 0.95[1.25(69) + 1.50(16) + 1.25(8) + 1.75(278)] = 576\ kN$$

$$M_u = 0.95[1.25(181) + 1.50(42) + 1.25(21) + 1.75(616)] = 1324\ kN.m$$

6.4.9.2 Loading and Concrete Placement Sequence [A6.10.5.1.1a]

Case 1   Weight of girder and slab (D1). Supported by steel girder alone.

Case 2 Superimposed dead load (FWS, curbs, and railings) (D2 and D3). Supported by long-term composite section.

Case 3 live load plus impact (LL+IM). Supported by short-term composite section.

6.4.9.3 Determine Effective Flange Width [A4.6.2.6]

For interior girders. The effective flange width is the least of:

- One-quarter of the average span length
- Twelve times the average thickness of the slab, plus the greater of the web thickness or one-half the width of the top flange of the girder
- Average spacing of adjacent girders

Assume the girder top flange is 200 mm wide

$$b_i = min \begin{bmatrix} (0.25)(10500) = 2625mm \\ (12)(190) + \dfrac{200}{2} = 2380mm \\ 2440mm \end{bmatrix}$$

Therefore, b_i = 2380 mm

For exterior girders the effective flange width is one-half the effective flange width of the adjacent interior girder, plus the least of:

- One-eighth of the average span length
- Six times the average thickness of the slab, plus the greater of the web thickness or one-half the width of the top flange of the girder

The width of the overhang

$$b_e = \frac{b_i}{2} + min \begin{bmatrix} (0.125)(10500) = 1313mm \\ (6)(190) + \dfrac{200}{4} = 1190mm \\ 990mm \end{bmatrix}$$

Therefore,

$$b_e = \frac{b_i}{2} + 990 = \frac{2380}{2} + 990 = 2180mm$$

6.4.9.4 Modular Ratio

$For\, f_c' = 30MPa,\ n = 8\ [A6.10.5.1.1b]$

6.4.9.5 Cover Plates

For economy, the lightest and shallowest beam with the largest cover plate possible gives the best design. The length of the cover plate, L_{cp}, must satisfy [A6.10.9]

$$L_{cp} \geq 2d_s + 900$$

Where d_s = depth of the steel section (mm)

6.4.9.6 Trial Section Properties

6.4.9.6.1 Steel Section at Midspan.

Try W610x101 with 10 mm x 200 mm cover plate. Properties of W610x101 are taken from AISC. The calculations for the steel section properties are summarized in Table 6-7 and shown in Figure 6-29.

Component	A	y	Ay	$y - \overline{y}$	$A(y - \overline{y})^2$	I_0
Beam	12900	$\dfrac{603}{2} = 301.5$	3.899×10^6	-41.4	21.8×10^6	764×10^6
Cover Plate	2000	603+5=608	1.216×10^6	265.4	140.9×10^6	17×10^3
Σ	14900		5.105×10^6		162.7×10^6	764×10^6

Table 6-7. Steel Section Properties
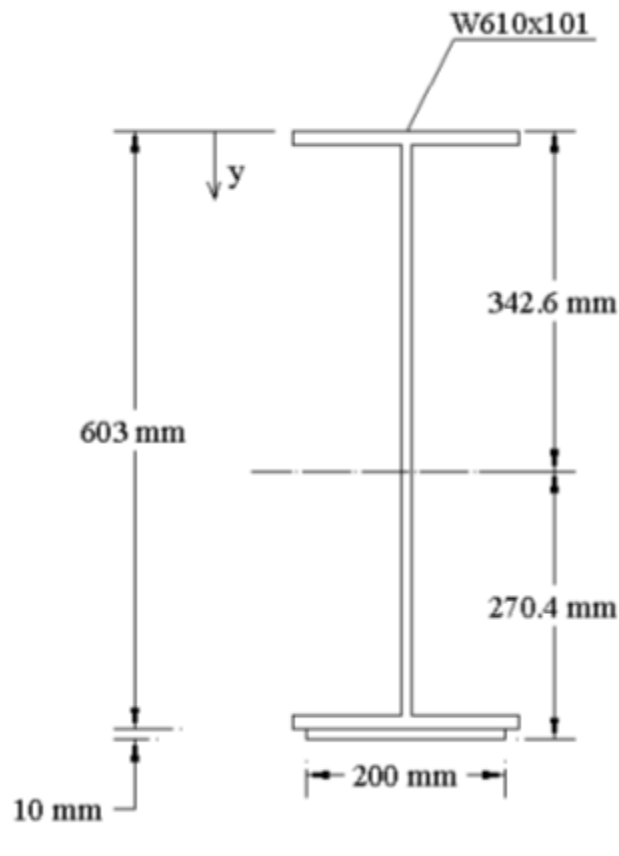
Figure 6-29. Steel section at midspan.

$$I_x = (162.7 \times 10^6) + (764 \times 10^6) = 926.7 \times 10^6 \ mm^4$$

$$\bar{y} = \frac{\sum Ay}{\sum A} = \frac{5.105 \times 10^6}{14900} = 342.6 \ mm$$

$$y_t = -342.6 \ mm \qquad y_b = 613 - 342.6 = 270.4 \ mm$$

$$S_t = \frac{I_x}{y_t} = \frac{926.7 \times 10^6}{-342.6} = -2.705 \times 10^6 \ mm^3$$

$$S_b = \frac{I_x}{y_b} = \frac{926.7 \times 10^6}{270.4} = 3.427 \times 10^6 \ mm^3$$

(Note: positive *y* is downward from centroid of section)

135

6.4.9.6.2 Composite Section, n = 8, at Midspan.

Figure 6-30 shows the composite section with a haunch of 25 mm, a net slab thickness (without 15 mm sacrificial wearing surface) of 190 mm, and an effective width of 2380 mm The composite section properties calculations are summarized in Table 6-8.
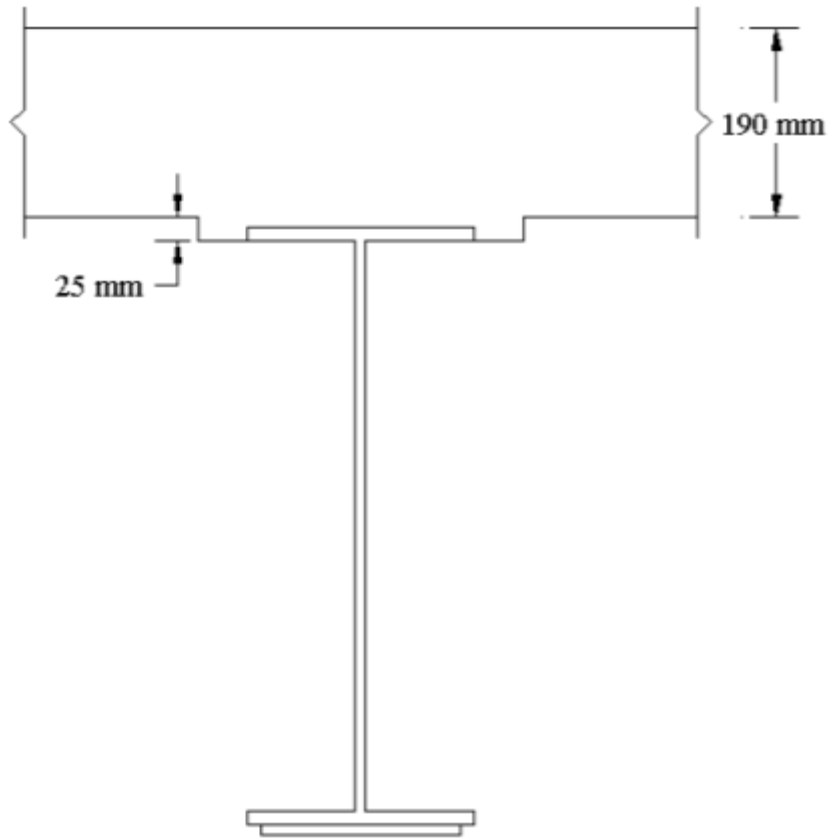
Figure 6-30. Composite section at midspan.

$$I_x = (2523 \times 10^6) + (1097 \times 10^6) = 3620 \times 10^6 \ mm^4$$

$$\bar{y} = \frac{\sum Ay}{\sum A} = \frac{-1.678 \times 10^6}{71425} = -23.5 \ mm$$

$$y_t = 23.5 \ mm \qquad y_b = 613 + 23.5 = 636.5 \ mm$$

$$S_t = \frac{I_x}{y_t} = \frac{3620 \times 10^6}{23.5} = 154 \times 10^6 \ mm^3$$

$$S_b = \frac{I_x}{y_b} = \frac{3620 \times 10^6}{636.5} = 5.69 \times 10^6 \ mm^3$$

6.4.9.6.3 Composite Section, 3n = 24, at Midspan.

The composite section properties calculations, reduced for the effect of creep in the concrete slab, are summarized in Table 6-9.

$$I_x = (1780 \times 10^6) + (983.4 \times 10^6) = 2763.4 \times 10^6 \ mm^4$$

$$\bar{y} = \frac{\sum Ay}{\sum A} = \frac{2.844 \times 10^6}{33742} = 84.3 \ mm$$

$$y_t = -84.3 \ mm \qquad y_b = 613 - 84.3 = 528.7 \ mm$$

$$S_t = \frac{I_x}{y_t} = \frac{2763.4 \times 10^6}{-84.3} = -32.78 \times 10^6 \ mm^3$$

$$S_b = \frac{I_x}{y_b} = \frac{2763.4 \times 10^6}{528.7} = 5.227 \times 10^6 \ mm^3$$

Table 6-8. Short-Term Composite Section Properties, n=8, b$_i$ = 2380 mm

Component	A	y	Ay	$y - \bar{y}$	$A(y - \bar{y})^2$	I$_0$
Concrete (b$_i$ x t$_s$/n)[a]	56525	$-25 - \frac{190}{2}$ $= -120$	-6.783x10^6	-96.5	526x10^6	170x10^6
Steel	14900	342.6	5.105x10^6	366.1	1997x10^6	927x10^6
Σ	71425		-1.678x10^6		2523x10^6	1097x10^6

[a] The parameter b_i is used because interior girders control the moment design

6.4.9.7 Member Proportions [A6.10.1.1]

$$0.1 \leq \frac{I_{yc}}{I_y} \leq 0.9$$

$$I_y = (29.5 \times 10^6) + \frac{1}{12}(10)(200^3) = 36.17 \times 10^6 \ mm^4$$

$$I_{yc} = \frac{1}{12}(14.9)(200^3) = 14.72 \times 10^6 \ mm^4$$

$$0.1 < \frac{I_{yc}}{I_y} = \frac{14.72 \times 10^6}{36.17 \times 10^6} = 0.407 < 0.9, \ \ OK$$

Fatigue Induced by Web Flexure [A6.10.4.3]

$$\frac{2D_c}{t_w} = \frac{2(342.6)}{10.5} = 65.3 < 5.76 \sqrt{\frac{E}{F_{yc}}} = 5.76 \sqrt{\frac{200000}{250}} = 162.9$$

Therefore, f_{cf} must be less than $R_h F_{yc}$, where

f_{cf} = maximum compressive elastic flexural stress in the compression flange due to the un-factored permanent load and twice the fatigue loading [A6.10.4.2].

The un-factored moment at location 105 due to the fatigue loading was calculated and found to be 397 kN.m. The value given in Table 6-10 for M_{LL+IM} is twice the positive moment value with load factor and without multiple presence.
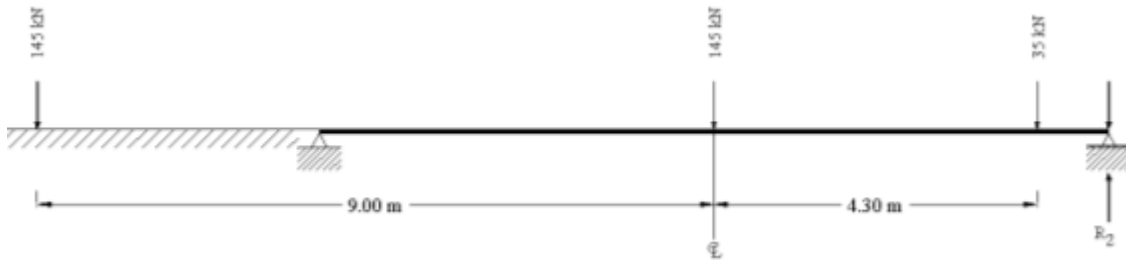
Figure 6-31. Fatigue truck placement for maximum moment.

$$M_{LL+IM} = 2(0.75)(1.15)(0.748)(397)/1.2 = 427 \ kN.m$$

Table 6-9. Long-Term Composite Section Properties, 3n=24

Component	A	y	Ay	$y - \bar{y}$	$A(y - \bar{y})^2$	I_0
Concrete $(b_i \times t_s/3n)^a$	18842	−120	-2.261x10^6	-204.3	786x10^6	56.7x10^6
Steel	14900	342.6	5.105x10^6	258.3	994x10^6	926.7x10^6
Σ	33742		2.844x10^6		1780x10^6	983.4x10^6

^{a} The parameter b_i is used because interior girders control the moment design

138

Table 6-10. Maximum Flexural Stress in the Web for Positive Flexure (Interior Girder)

Load	M_{D1}	M_{D2}	M_{D3}	M_{LL+IM}	S_t Steel	S_t Composite	Stress (MPa)
D1	188				-2.705×10^6		-69.5
D2		56				-32.78×10^6	-1.7
D3			21			-32.78×10^6	-0.6
LL+IM				427		154.0×10^6	2.8
Total							-69.0

$$f_{cf} = 69.0 \ MPa < 250 \ MPa, \quad OK$$

6.4.9.8 Stresses

Stresses in top and bottom of girder for strength limit state are given in Table 6-11 and Table 6-12. Yielding has occurred in the bottom flange.

Table 6-11. Compressive Stresses in Top of Steel Beam Due to Factored Loading (Interior Girder)

Load	M_{D1}	M_{D2}	M_{D3}	M_{LL+IM}	S_t Steel	S_t Composite	Stress (MPa)
D1	235				-2.705×10^6		-86.9
D2		84				-32.78×10^6	-2.6
D3			26			-32.78×10^6	-0.8
LL+IM				1059		154.0×10^6	6.9
Total							-83.4
						$\eta = 0.95$	-79.2

Table 6-12. Tensile Stresses in Bottom of Steel Beam Due to Factored Loading

Load	M_{D1}	M_{D2}	M_{D3}	M_{LL+IM}	S_b Steel	S_b Composite	Stress (MPa)
D1	235				3.427×10^6		68.6
D2		84				5.277×10^6	16.1
D3			26			5.277×10^6	5.0
LL+IM				1059		5.69×10^6	186.1
Total							275.8
						$\eta = 0.95$	262.0

6.4.9.9 Determine if Section is Compact

Web Slenderness (Table 8.16) [A6.10.5.2.2c]

$$\frac{2D_{cp}}{t_w} \leq 3.76 \sqrt{\frac{E}{F_{yc}}}$$

Number of bars in top of slab in effective width $= \dfrac{b_i}{bar\ spacing} = \dfrac{2290}{250} = 10\ No.\ 10\ bars$

Number of bars in bottom slab $== \dfrac{2290}{250} = 7\ No.\ 15\ bars$

Plastic Forces Assume PNA is in slab above bottom bars (c<156 mm)

Top Reinforcement, $P_{rt} = F_{yr}A_{rt} = (400)(10)(100)(10^{-3}) = 400\ kN$

Concrete Slab, $P_s = 0.85 f_c' a b_i = 0.85(30)(2290)(10^{-3})a = 58\ a$

Bottom Reinforcement, $P_{rb} = F_{yr}A_{rb} = (400)(7)(200)(10^{-3}) = 560\ kN$

Beam, $T_{bm} = (AF_y)_{bm} = (12900)(250)(10^{-3}) = 3225\ kN$

Cover Plate, $T_{cp} = (AF_y)_{cp} = (10)(200)(250)(10^{-3}) = 500\ kN$

Plastic Neutral Axis PNA

$$C = T$$

$$400 + 58a = 560 + 3225 + 500$$

$$a = 67.0\ mm, \quad \beta_1 = 0.85 - \frac{2}{7}(0.05) = 0.836$$

$$c = \frac{a}{\beta_1} = \frac{67.0}{0.836} = 80.1\ mm < 156\ mm, \quad OK$$

Because the PNA is not in the web, D_{cp} shall be taken equal to 0, the web slenderness requirement is satisfied [A6.10.5.1.4b], the section is classified as compact, and $M_n = M_p$.

Calculate Plastic Moment M_p by summing moments about PNA:

Top Reinforcement: $400(c - d') = 400(80.1 - 76.95)(10^{-3}) = 1.3\ kN.m$

Slab: $58a\left(c - \frac{a}{2}\right) = 58(91.4)\left(80.1 - \frac{91.4}{2}\right)(10^{-3}) = 182\ kN.m$

Bottom reinforcement: $560(d - c) = 560(156 - 80.1)(10^{-3}) = 43 \ kN.m$

Beam: $3225(205 + 25 + 603/2 - 80.1)(10^{-3}) = 1456 \ kN.m$

Cover Plate: $500(205 + 25 + 603 + 5 - 80.1)(10^{-3}) = 379 \ kN.m$

$$M_p = 1.3 + 182 + 43 + 1456 + 379 = 2061 \ kN.m$$

$$\emptyset M_p = 1.0(2061) = 2061 \ kN.m > M_u = 1334 \ kN.m, \ \ OK$$

6.4.9.9.1 Compression Flange Slenderness [A6.10.5.2.2c].

No requirement at strength limit state for compact composite I-sections in positive flexure (Table 8.16) [Table A6.10.5.2.1-1]

6.4.9.9.2 Compression Flange Bracing.

No requirement at strength limit state for compact composite I-sections in positive flexure (Table 8.16) [Table A6.10.5.2.1-1]

6.4.9.9.3 Calculate Flexural Resistance [A6.10.5.2.2a].

For simple spans, the nominal flexural resistance is taken as

$$M_n = M_p = 2061 \ kN.m$$

$$M_r = \emptyset_f M_n = 1.0(2061) = 2061 \ kN.m > M_u = 1334 \ kN.m, \ \ OK$$

6.4.9.9.4 Check Positive Flexure Ductility [A6.10.5.2.2b].

As calculated in Table 6-11 and Table 6-12, the moment due to the factored loads results in stresses of 79.2 and 262.0 MPa in the top and bottom flanges, respectively. Because the bottom flange elastic stress exceeds the yield strength of the flange (250 MPa), the section must satisfy

$$D_p \leq \frac{d + t_s + t_h}{7.5}$$

Where

D_p = distance from the top of the slab to the neutral axis at the plastic moment = 80.1 mm

d = depth of the steel section = 603 mm

t_s = thickness of the concrete slab = 205 mm

t_h = thickness of the concrete haunch = 25 mm

$$\frac{d + t_s + t_h}{7.5} = \frac{603 + 205 + 25}{7.5} = 111 \; mm > D_p = 80.1 \; mm, \;\; OK$$

Therefore, all requirements for flexure have been satisfied.

6.4.9.10   Shear Design

For beams with un-stiffened web (Table 8.19) [A6.10.7.2]

$$V_r = \emptyset_v V_n = 1.00 V_n$$

$$\frac{D}{t_w} = \frac{d - 2t_f}{t_w} = \frac{603 - 2(14.9)}{10.50} = 54.6$$

$$2.46 \sqrt{\frac{E}{F_{yw}}} = 2.46 \sqrt{\frac{200000}{250}} = 69.6 > 54.6$$

Therefore,

$$V_n = V_p = 0.58 F_{yw} D t_w = 0.58(250)(573.2)(10.50) = 873 \; kN$$

$$V_r = 1.00 V_n = 873 \; kN > V_u = 625 \; kN$$

(factored shear in interior beam), OK

Bearing Stiffener design [A6.10.8.2]

$$0.85 \emptyset_b V_n = 0.75(1.0)(873) = 655 \; kN > V_u = 625 \; kN$$

The bearing stiffeners are not required.

6.4.10 Dimension and Detail Requirements

6.4.10.1 Material Thickness [A6.7.3].

Bracing and cross frames shall not be less than 8 mm in thickness. Web thickness of rolled beams shall not be less than 7 mm.

$$t_w = 10.5\ mm > 7\ mm, \quad OK$$

6.4.10.2 Optional Deflection Control [A2.5.2.6.2].

Allowable service load deflection

$$\leq \frac{1}{800}\ span = \frac{10500}{800} = 13\ mm$$

From [A3.6.1.3.2], deflection is taken as the larger of:

- That resulting from the design truck alone.
- That resulting from 25% of the design truck taken together with the design lane load.

The distribution factor for deflection may be taken as the number of lanes divided by the number of beams, because all design lanes should be loaded, and all supporting components should be assumed to deflect equally.

$$DF = \frac{No.\ lanes}{No.\ beams} = \frac{3}{6} = 0.5$$

Deflection resulting from design truck alone, Figure 6-32.
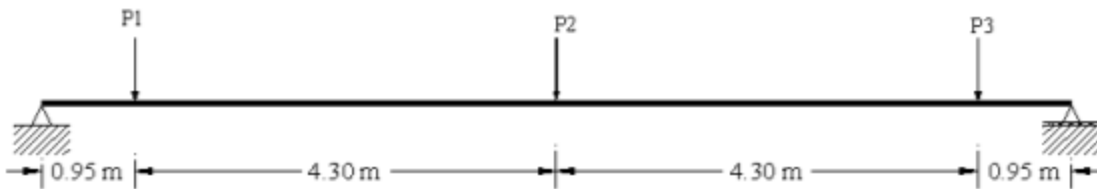
Figure 6-32. Truck placement for maximum deflection.

$$P_1 = P_2 = 0.5(145)\left(1 + \frac{IM}{100}\right) = 0.5(145)(1.33) = 96.4\ kN$$

$$P_3 = 0.5(35)(1.33) = 23.3 \, kN$$

The deflection at any point, Δ_x, due to a point load P can be found from AISC manual, refer to Figure 6-33, for $x \leq a$

$$\Delta_x = \frac{Pbx}{6EIL}(L^2 - b^2 - x^2)$$
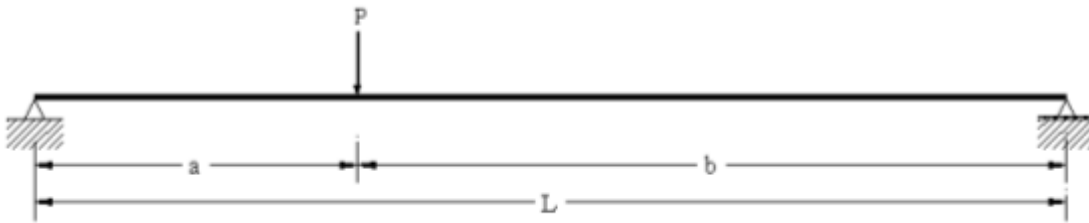
Figure 6-33. General placement of point load *P*.

The maximum deflection (located at center) of a simply supported span, due to a concentrated load at the center of the span, can be found from the AISC. Refer to Figure 6-34:

$$\Delta_{CL} = \frac{PL^3}{48EI}$$

Figure 6-34. Point load *P* at center of span.

$$\Delta_{CLTr} = \Delta_{P1} + \Delta_{P2} + \Delta_{P3}$$

$$= \frac{(P_1 + P_3)(0.95)\left(\frac{10.5}{2}\right)(10^9)}{6(200000)(3620 \times 10^6)(10.5)} \times \left[(10.5)^2 - (0.95)^2 - (\frac{10.5}{2})^2\right]$$

$$+ \frac{P_2(10.5)^3(10^9)}{48(200000)(3620 \times 10^6)} = (P_1 + P_3)(215.8 \times 10^{-3}) + P_2(804 \times 10^{-3})$$

$$= 4.2 \, mm$$

Deflection resulting from 25% design truck together with the design lane load

$$\Delta_{CL25\%Tr} = 0.25(4.2) = 1.1\ mm$$

The deflection due to lane load can be found from the AISC:

$$\Delta_{max} = \frac{5wL^4}{384EI}$$

$$\Delta_{CL\ Ln} = \frac{5(0.5)(9.3)(10500)^4}{384(200000)(3620 \times 10^6)} = 0.85\ mm$$

$$\Delta_{CL} = \Delta_{CL25\%Tr} + \Delta_{CL\ Ln} = 1.1 + 0.85 = 2\ mm$$

$$\therefore \Delta_{CL\ Tr} = 4.2\ mm\ \ controls$$

$$\Delta_{CL} = 4.2\ mm < \Delta_{all} = 13\ mm,\ \ OK$$

6.4.10.3   Service Limit State Control of Permanent Deflections [A6.10.3]

For both flanges of composite sections

$$f_f \leq 0.95 R_h F_{yf} = 0.95(1.0)(250) = 238\ MPa$$

Where

f_f = elastic flange stress caused by the factored loading

The maximum Service II moment, which occurs at Location 105 in the interior beam, is due to un-factored dead loads D1, D2, and D3, and the factored live load, 1.3(LL+IM), taken from Table 6-5. The stresses calculated from these moments are given in Table 6-13 and Table 6-14.

$$max\ f_f = 207.9\ Mpa < 238\ Mpa,\ \ OK$$

Table 6-13. Stresses in Top of Flange of Steel Beam Due to Service II Moments

Load	M_{D1}	M_{D2}	M_{D3}	M_{LL+IM}	S_b Steel	S_b Composite	Stress (MPa)
D1	188				-2.705×10^6		-69.5
D2		56				-32.78×10^6	-1.7
D3			21			-32.78×10^6	-0.6
LL+IM				787		154.0×10^6	5.1
Total							-66.7

Table 6-14. Stresses in Bottom Flange of Steel Beam Due to Service II Moments

Load	M_{D1}	M_{D2}	M_{D3}	M_{LL+IM}	S_b Steel	S_b Composite	Stress (MPa)
D1	188				3.427×10^6		54.9
D2		56				5.277×10^6	10.7
D3			21			5.277×10^6	4.0
LL+IM				787		5.69×10^6	138.3
Total							207.9

6.4.10.4   Check Construction Requirements, (Dead Load Camber)

The centerline deflection due to a uniform load on a simply support span is:

$$\Delta_{CL} = \frac{5}{384}\frac{w_D L^4}{EI} = \frac{5}{384}\frac{w_D (10500)^4}{200000\, I} = (791.3 \times 10^6)\frac{w_D}{I}$$

By substituting the dead loads from Table 6-5 and Table 6-6, the centerline deflections are calculated in Table 6-15 and Table 6-16. Use a 12 mm camber on all beams.

Table 6-15. Exterior Beam Deflection Due to Dead Loads

Load Type	Load, w (N/mm)	I (mm^4)	Δ_{CL} (mm)
D1	13.10	926.7×10^6	11
D2	3.03	2763.4×10^6	0.9
D3	1.55	2763.4×10^6	0.5
Total			12.4

Table 6-16. Interior Beam Deflection Due to Dead Loads

Load Type	Load, w (N/mm)	I (mm^4)	Δ_{CL} (mm)
D1	13.63	926.7×10^6	12
D2	4.04	2763.4×10^6	1.2
D3	1.55	2763.4×10^6	0.5
Total			13.7

6.4.10.5   Check Fatigue [A6.5.3]

$$(\Delta F)_n = \frac{1}{2}(\Delta F)_{TH} = 82.5 \; MPa$$

The maximum stress range is assumed to be twice the live load stress range due to the passage of the fatigue load. However, the stress range need not be multiplied by two because the fatigue resistance is divided by two.

$$M_{LL+IM} = 290 \; kN.m$$

$$M_{fatigue} = 217 \; kN.m$$

$$f = \frac{M}{S_b} = \frac{217 \times 10^6}{5.69 \times 10^6} = 38 \; MPa < 82.5 \; Mpa, \quad OK$$

where S_b is the section modulus for the short-term composite section, calculated before.

6.4.10.6   Shear Connectors [A6.10.7.4]

Shear connectors must be provided throughout the length of the span for simple span composite bridges. Use 19 mm diameter studs, 100 mm high. The ratio of height to diameter is:

$$\frac{100}{19} = 5.26 > 4, \quad OK \; [A6.10.7.4.1a]$$

6.5 Steel Bridge Girder Strengthened using CFRP – Solved Example

The steel bridge girder example from the previous section will be used as the basis of this example. Sections affected by the addition of the CFRP laminate will only be included below. CFRP properties are taken to be the same as mentioned in Chapter 3. Tensile modulus = 155 GPa, and the tensile strength = 2790MPa.

6.5.1 Design Required Sections

The same design procedure followed in the previous example still apply to this section.

6.5.1.1 Section Properties

6.5.1.1.1 Steel Section at Midspan.

Using the W610x101 with the 10 mm x 200 mm cover plate with an additional 10 mm x 200 mm CFRP laminate.

First, a Young's modulus ratio n_{CFRP} will be calculated:

$$n_{CFRP} = \frac{E_{CFRP}}{E_{Steel}} = \frac{155}{200} = 0.775$$

Properties of W610x101 are taken from AISC. The calculations for the steel and CFRP section properties are summarized in Table 6-17 and shown in Figure 6-35. The CFRP area will be reduced by multiplying the actual physical area by n_{CFRP}.

Table 6-17. Section Properties (Steel + CFRP)

Component	A	y	Ay	$y - \bar{y}$	$A(y - \bar{y})^2$	I_0
Beam	12900	$\frac{603}{2} = 301.5$	3.899×10^6	-67.0	58.0×10^6	764×10^6
Cover Plate	2000	603+5=608	1.216×10^6	239.4	114.6×10^6	17×10^3
CFRP	1550	613+5=618	0.95×10^6	249.4	96.4×10^6	1615
Σ	16450		6.063×10^6		269.11×10^6	764×10^6
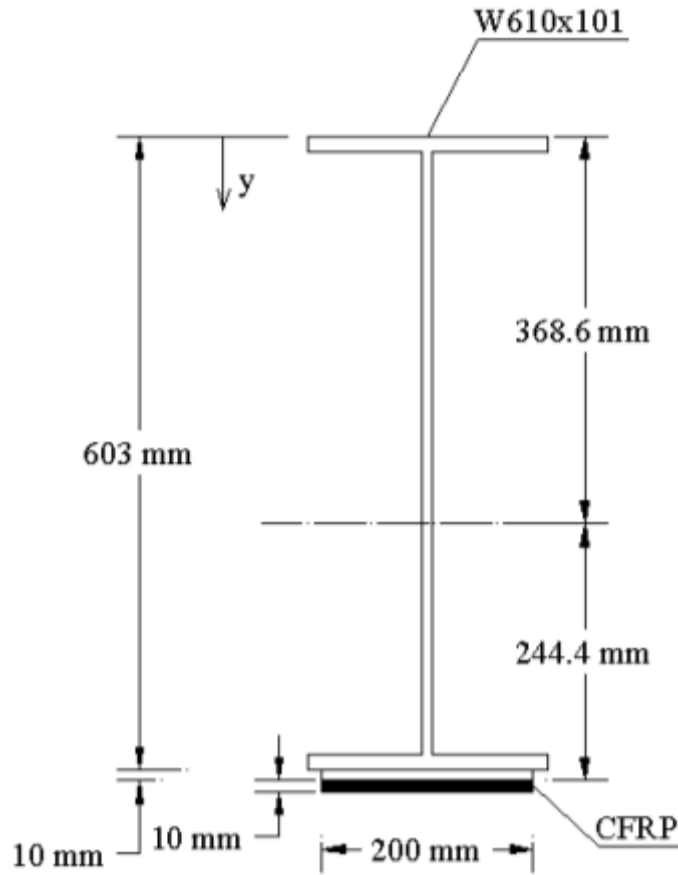
Figure 6-35. Steel section with CFRP at midspan.

$$I_x = (269.11 \times 10^6) + (764 \times 10^6) = 1030 \times 10^6 \ mm^4$$

$$\bar{y} = \frac{\sum Ay}{\sum A} = \frac{6.063 \times 10^6}{16450} = 368.58 \ mm$$

$$y_t = -368.58 \ mm \qquad y_b = 613 - 368.58 = 234.41 \ mm$$

$$S_t = \frac{I_x}{y_t} = \frac{1030 \times 10^6}{-368.58} = -2.802 \times 10^6 \ mm^3$$

$$S_b = \frac{I_x}{y_b} = \frac{1030 \times 10^6}{234.41} = 4.407 \times 10^6 \ mm^3$$

$$Increase \ in \ Section \ Inertia = \frac{(1030 \times 10^6 - 926.7 \times 10^6) \ mm^4}{926.7 \times 10^6 \ mm^4} \times 100 = 11\%$$

$$Increase\ in\ Section\ Modulus = \frac{(4.407 \times 10^6 - 3.427 \times 10^6)\ mm^3}{3.427 \times 10^6\ mm^3} = 28.6\%$$

Note that the inertia, I_x increased by only 11%, while the increase in the bottom section modulus, S_b, was 28.6%. This is due to the fact that the neutral axis was shifted downwards, which greatly affects the S_b, which leads to the increase of section capacity. The top section modulus, S_b, remained almost the same, which means no extra stresses will be seen at the compression zone (concrete deck or top flange). This is also one of the benefits of the CFRP rehabilitation system.

(Note: positive y is downward from centroid of section)

6.5.1.1.2 Composite Section.

The composite section shown in Figure 6-36 shows the composite section with a haunch of 25 mm, a net slab thickness (without 15 mm sacrificial wearing surface) of 190 mm, and an effective width of 2380 mm, in addition to the 10 mm CFRP laminate. The composite section properties calculations are summarized in Table 6-18 and Table 6-19.

$$I_x = (3041 \times 10^6) + (1200 \times 10^6) = 4241.86 \times 10^6\ mm^4$$

$$\bar{y} = \frac{\sum Ay}{\sum A} = \frac{-0.719 \times 10^6}{72975} = -9.86\ mm$$

$$y_t = 9.86\ mm \qquad y_b = 613 + 9.86 = 622.86\ mm$$

$$S_t = \frac{I_x}{y_t} = \frac{4241.86 \times 10^6}{9.86} = 430.2 \times 10^6\ mm^3$$

$$S_b = \frac{I_x}{y_b} = \frac{4241.86 \times 10^6}{622.86} = 6.81 \times 10^6\ mm^3$$

Table 6-18. Short-Term Composite Section Properties, n=8, b_i = 2380 mm

Component	A	y	Ay	$y - \bar{y}$	$A(y - \bar{y})^2$	I_0
Concrete (b_i x t_s/n)[a]	56525	$-25 - \frac{190}{2}$ $= -120$	-6.783x10^6	-110.1	685x10^6	170x10^6
Steel	16450	368.6	6.063x10^6	378.46	2356x10^6	1030x10^6
$\sum$	72975		-0.719x10^6		3041x10^6	1200x10^6

[a] The parameter b_i is used because interior girders control the moment design
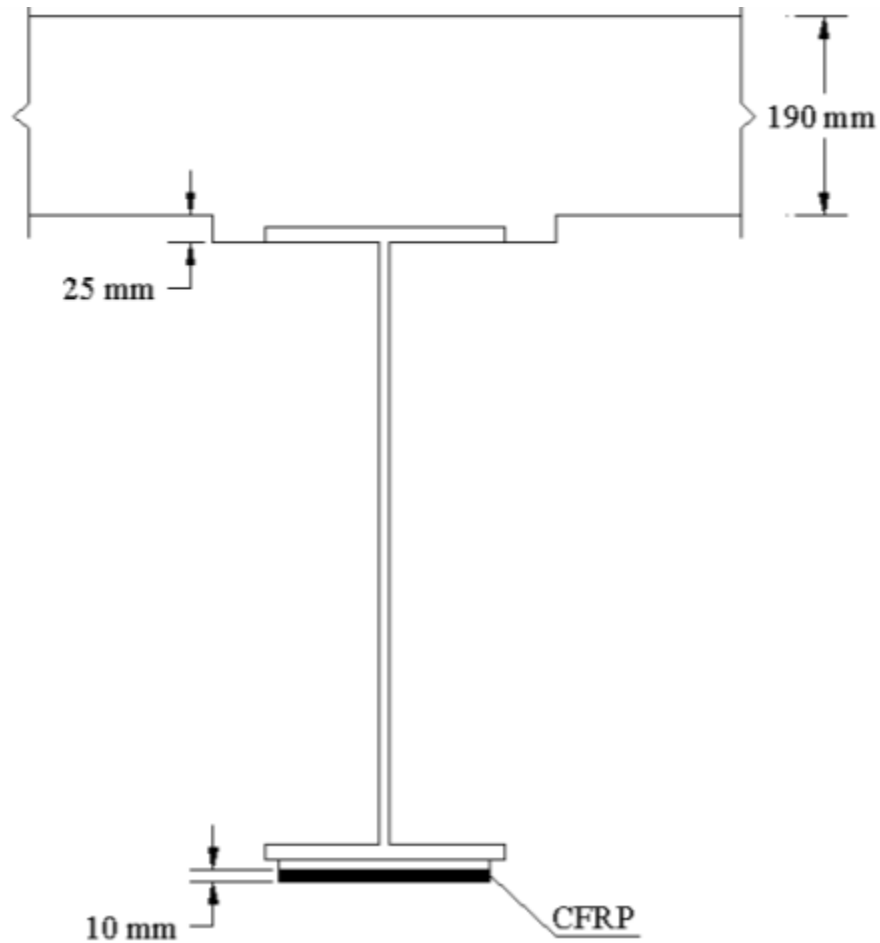
Figure 6-36. Composite steel section with CFRP at midspan.

$$I_x = (2096.6 \times 10^6) + (1200 \times 10^6) = 3296.6 \times 10^6 \ mm^4$$

$$\bar{y} = \frac{\sum Ay}{\sum A} = \frac{3.802 \times 10^6}{35292} = 107.74 \ mm$$

$$y_t = -107.74 \ mm \qquad y_b = 613 - 107.74 = 505.26 \ mm$$

$$S_t = \frac{I_x}{y_t} = \frac{3296.6 \times 10^6}{-107.74} = -30.6 \times 10^6 \ mm^3$$

$$S_b = \frac{I_x}{y_b} = \frac{3296.6 \times 10^6}{505.26} = 6.52 \times 10^6 \ mm^3$$

Reconsidering the long-term composite action, the increase in inertia and section modulus is recalculated:

$$Increase\ in\ Section\ Inertia = \frac{(3296.6 \times 10^6 - 2763.4 \times 10^6)\ mm^4}{2763.4 \times 10^6\ mm^4} \times 100 = 19.3\%$$

$$Increase\ in\ Section\ Modulus = \frac{(6.52 \times 10^6 - 5.69 \times 10^6)\ mm^3}{5.69 \times 10^6\ mm^3} = 14.6\%$$

Table 6-19. Long-Term Composite Section Properties, 3n=24

Component	A	y	Ay	$y - \bar{y}$	$A(y - \bar{y})^2$	I_0
Concrete (b$_i$ x t$_s$/3n)[a]	18842	$-25 - \frac{190}{2}$ $= -120$	-2.26x10^6	-227.7	977.26x10^6	170x10^6
Steel+CFRP	16450	368.6	6.064x10^6	260.86	1119.4x10^6	1030x10^6
Σ	35292		3.802x10^6		2096.6x10^6	1200x10^6

[a] The parameter b_i is used because interior girders control the moment design

Table 6-20. Maximum Flexural Stress in the Web for Positive Flexure (Interior Girder)

Load	M$_{D1}$	M$_{D2}$	M$_{D3}$	M$_{LL+IM}$	S$_t$ Steel	S$_t$ Composite	Stress (MPa)
D1	188				-2.802x10^6		-67.09
D2		56				-30.6 x10^6	-1.83
D3			21			-30.6 x10^6	-0.69
LL+IM				427		430.2x10^6	0.99
Total							-68.62

$$f_{cf} = 71.0\ MPa < 250\ MPa,\ \ OK$$

6.5.1.2 Stresses

Stresses in top and bottom of girder for strength limit state are given in Table 6-21 and Table 6-22. Yielding has occurred in the bottom flange.

Table 6-21. Compressive Stresses in Top of Steel Beam Due to Factored Loading (Interior Girder)

Load	M_{D1}	M_{D2}	M_{D3}	M_{LL+IM}	S_t Steel	S_t Composite	Stress (MPa)
D1	235				-2.802×10^6		-83.87
D2		84				-30.6×10^6	-2.75
D3			26			-30.6×10^6	-0.85
LL+IM				1059		430.2×10^6	2.46
Total							-85.0
						$\eta=0.95$	-80.75

Table 6-22. Tensile Stresses in Bottom of Steel Beam Due to Factored Loading

Load	M_{D1}	M_{D2}	M_{D3}	M_{LL+IM}	S_b Steel	S_b Composite	Stress (MPa)
D1	235				4.407×10^6		53.32
D2		84				6.52×10^6	12.88
D3			26			6.52×10^6	4.0
LL+IM				1059		6.81×10^6	155.51
Total							225.7
						$\eta=0.95$	214.41

Deflection resulting from design truck alone, Figure 6-32.

$$P_1 = P_2 = 0.5(145)\left(1 + \frac{IM}{100}\right) = 0.5(145)(1.33) = 96.4 \; kN$$

$$P_3 = 0.5(35)(1.33) = 23.3 \; kN$$

The deflection at any point, Δ_x, due to a point load P can be found from AISC manual, refer to Figure 6-33, for $x \leq a$

$$\Delta_x = \frac{Pbx}{6EIL}(L^2 - b^2 - x^2)$$

The maximum deflection (located at center) of a simply supported span, due to a concentrated load at the center of the span, can be found from the AISC. Refer to Figure 6-34:

$$\Delta_{CL} = \frac{PL^3}{48EI}$$

$$\Delta_{CLTr} = \Delta_{P1} + \Delta_{P2} + \Delta_{P3}$$

$$= \frac{(P_1 + P_3)(0.95)\left(\frac{10.5}{2}\right)(10^9)}{6(200000)(4241.86 \times 10^6)(10.5)} \times \left[(10.5)^2 - (0.95)^2 - (\frac{10.5}{2})^2\right]$$

$$+ \frac{P_2(10.5)^3(10^9)}{48(200000)(4241.86 \times 10^6)} = (P_1 + P_3)(215.8 \times 10^{-3}) + P_2(804 \times 10^{-3})$$

$$= 3.55 \; mm$$

Deflection resulting from 25% design truck together with the design lane load

$$\Delta_{CL25\%Tr} = 0.25(3.55) = 0.89 \; mm$$

The deflection due to lane load can be found from the AISC:

$$\Delta_{max} = \frac{5wL^4}{384EI}$$

$$\Delta_{CL\,Ln} = \frac{5(0.5)(9.3)(10500)^4}{384(200000)(4241.86 \times 10^6)} = 0.72 \; mm$$

$$\Delta_{CL} = \Delta_{CL25\%Tr} + \Delta_{CL\,Ln} = 0.89 + 0.72 = 1.61 \; mm$$

$$\therefore \Delta_{CL\,Tr} = 3.55 \; mm \quad controls$$

$$\Delta_{CL} = 3.55 \; mm < \Delta_{all} = 13 \; mm, \quad OK$$

Service Limit State Control of Permanent Deflections [A6.10.3]. For both flanges of composite sections

$$f_f \leq 0.95 R_h F_{yf} = 0.95(1.0)(250) = 238 \; MPa$$

Where

f_f = elastic flange stress caused by the factored loading

154

The maximum Service II moment, which occurs at Location 105 in the interior beam, is due to un-factored dead loads D1, D2, and D3, and the factored live load, 1.3(LL+IM), taken from Table 6-5. The stresses calculated from these moments are given in Table 6-23 and Table 6-24.

$$max\, f_f = 170\ Mpa < 238\ Mpa,\ \ OK$$

Table 6-23. Stresses in Top of Flange of Steel Beam Due to Service II Moments

Load	M_{D1}	M_{D2}	M_{D3}	M_{LL+IM}	S_b Steel	S_b Composite	Stress (MPa)
D1	188				-2.705×10^6		-67.1
D2		56				-30.6×10^6	-1.8
D3			21			-30.6×10^6	-0.7
LL+IM				787		430.2×10^6	1.8
Total							-67.8

Table 6-24. Stresses in Bottom Flange of Steel Beam Due to Service II Moments

Load	M_{D1}	M_{D2}	M_{D3}	M_{LL+IM}	S_b Steel	S_b Composite	Stress (MPa)
D1	188				3.427×10^6		42.7
D2		56				6.52×10^6	8.6
D3			21			6.52×10^6	3.2
LL+IM				787		6.81×10^6	115.6
Total							170

6.5.1.3 Check Construction Requirements, (Dead Load Camber)

The centerline deflection due to a uniform load on a simply support span is:

$$\Delta_{CL} = \frac{5}{384}\frac{w_D L^4}{EI} = \frac{5}{384}\frac{w_D (10500)^4}{200000\ I} = (791.3 \times 10^6)\frac{w_D}{I}$$

By substituting the dead loads from Table 6-5 and Table 6-6, the centerline deflections are calculated in Table 6-25 and Table 6-26. Use a 12 mm camber on all beams.

Table 6-25. Exterior Beam Deflection Due to Dead Loads

Load Type	Load, w (N/mm)	I (mm^4)	Δ_{CL} (mm)
D1	13.10	1030×10^6	9.9
D2	3.03	3296.6×10^6	0.8
D3	1.55	3296.6×10^6	0.4
Total			11.1

Table 6-26. Interior Beam Deflection Due to Dead Loads

Load Type	Load, w (N/mm)	I (mm⁴)	Δ_{CL} (mm)
D1	13.63	1030 x 10⁶	10.8
D2	4.04	3296.6 x 10⁶	1.0
D3	1.55	3296.6 x 10⁶	0.4
Total			12.2

6.5.1.4 Check Fatigue [A6.5.3]

$$(\Delta F)_n = \frac{1}{2}(\Delta F)_{TH} = 82.5\ MPa$$

The maximum stress range is assumed to be twice the live load stress range due to the passage of the fatigue load. However, the stress range need not be multiplied by two because the fatigue resistance is divided by two.

$$M_{LL+IM} = 290\ kN.m$$

$$M_{fatigue} = 217\ kN.m$$

$$f = \frac{M}{S_b} = \frac{217 \times 10^6}{6.52 \times 10^6} = 33\ MPa < 82.5\ Mpa,\quad OK$$

where S_b is the section modulus calculated before for the short-term composite section.

6.6 CFRP Contribution to Steel Bridge Girders

In this section, a comparison between both solved examples in sections 6.5 and 6.6 will be provided. The contribution of the CFRP laminate added to the steel girder will be discussed. Change in the section inertia and section modulus will be discussed thoroughly. The effect of the CFRP laminate on stresses as well as fatigue stresses will be pointed out, and finally, the effect on the girder deflections.

6.6.1   Section Inertia and Modulus

6.6.1.1 Steel Section Properties

The increase in section properties due to adding the CFRP laminate was significant. Comparing the steel girder without the concrete slab, before and after adding the CFRP laminate, the comparison is as follows:

- Section inertia without CFRP laminate; $I_x = 926.7 \times 10^6 \ mm^4$
- Section inertia with CFRP laminate; $I_x = 1030 \times 10^6 \ mm^4$
- The increase in section inertia due to CFRP laminate = 11.2%

The increase in section modulus (bottom fibers) due to adding the CFRP laminate was more significant due to the shifting of the neutral axis downwards when adding a CFRP laminate. Comparing the steel girder without the concrete slab, before and after adding the CFRP laminate, the comparison is as follows:

- Section modulus without CFRP laminate; $S_b = 3.427 \times 10^6 \ mm^3$
- Section modulus with CFRP laminate; $S_b = 4.407 \times 10^6 \ mm^3$
- The increase in section modulus due to CFRP laminate = 28.6%

The increase in section modulus (top fibers) due to adding the CFRP laminate was not significant due to the shifting of the neutral axis downwards when adding a CFRP laminate. The top section modulus is not of great importance in the rehabilitation process due its generally low stress levels. Comparing the steel girder without the concrete slab, before and after adding the CFRP laminate, the comparison is as follows:

- Section modulus without CFRP laminate; $S_t = -2.705 \times 10^6 \ mm^3$
- Section modulus with CFRP laminate; $S_t = -2.802 \times 10^6 \ mm^3$
- The increase in section modulus due to CFRP laminate = 3.5%

6.6.1.2 Composite Section Properties

The increase in section properties due to adding the CFRP laminate was also significant. Comparing the composite steel girder, before and after adding the CFRP laminate, the comparison is as follows:

- Section inertia without CFRP laminate; $I_x = 2763.4 \times 10^6 \ mm^4$
- Section inertia with CFRP laminate; $I_x = 3296.6 \times 10^6 \ mm^4$
- The increase in section inertia due to CFRP laminate = 19.2%

The increase in section modulus (bottom fibers) due to adding the CFRP laminate was more significant due to the shifting of the neutral axis downwards when adding a CFRP laminate.

Comparing the composite steel girder, before and after adding the CFRP laminate, the comparison is as follows:

- Section modulus without CFRP laminate; $S_b = 5.227 \times 10^6 \ mm^3$
- Section modulus with CFRP laminate; $S_b = 6.52 \times 10^6 \ mm^3$
- The increase in section modulus due to CFRP laminate $= 24.7\%$

A decrease in section modulus (top fibers) due to adding the CFRP laminate was noticed and was not significant due to the shifting of the neutral axis downwards when adding a CFRP laminate. The top section modulus is not of great importance in the rehabilitation process due its generally low stress levels. Comparing the composite steel girder, before and after adding the CFRP laminate, the comparison is as follows:

- Section modulus without CFRP laminate; $S_t = -32.78 \times 10^6 \ mm^3$
- Section modulus with CFRP laminate; $S_t = -30.6 \times 10^6 \ mm^3$
- The increase in section modulus due to CFRP laminate $= -6.6\%$

6.6.2 Stresses

The decrease in bottom tensile stresses due to factored loading after adding the CFRP laminate was significant. Comparing the composite steel girder, before and after adding the CFRP laminate, the comparison is as follows:

- Tensile stresses without CFRP laminate; $\sigma_b = 262 \ MPa$
- Tensile stresses with CFRP laminate; $\sigma_b = 214.41 \ MPa$
- The decrease in tensile stresses due to CFRP laminate $= 22.2\%$

The decrease in bottom tensile stresses due to Service II loading after adding the CFRP laminate was also significant. Comparing the composite steel girder, before and after adding the CFRP laminate, the comparison is as follows:

- Tensile stresses without CFRP laminate; $\sigma_b = 207.9 \ MPa$
- Tensile stresses with CFRP laminate; $\sigma_b = 170 \ MPa$
- The decrease in tensile stresses due to CFRP laminate $= 22.2\%$

6.6.3 Fatigue Stresses

The decrease in fatigue stress range after adding the CFRP laminate was significant. Comparing the composite steel girder, before and after adding the CFRP laminate, the comparison is as follows:

- Fatigue stress range without CFRP laminate; $\Delta f = 33 \ MPa$
- Fatigue stress range with CFRP laminate; $\Delta f = 38 \ MPa$
- The decrease in fatigue stress range due to CFRP laminate $= 15.2\%$

6.6.4 Deflections

The decrease in deflections due to factored loading after adding the CFRP laminate was significant. Comparing the interior composite steel girder, before and after adding the CFRP laminate, the comparison is as follows:

- Deflections without CFRP laminate; $\Delta = 13.7\ mm$
- Deflections with CFRP laminate; $\Delta = 12.2\ mm$
- The decrease in deflections due to CFRP laminate $= 9.5\%$

Comparing the exterior composite steel girder, before and after adding the CFRP laminate, the comparison is as follows:

- Deflections without CFRP laminate; $\Delta = 12.4\ mm$
- Deflections with CFRP laminate; $\Delta = 11.1\ mm$

The decrease in deflections due to CFRP laminate $= 10.5\%$

6.7 Design Guidelines

Steel girders strengthened by CFRP laminates have several potential modes of failure, such as rupture of CFRP laminates, debonding of CFRP laminates, crushing of the concrete, or web failure due to shear. The design guidelines proposed here are mainly concerned by the first two modes of failure, as the latest two can be check using AASHTO equations.

Installation of CFRP laminates can increase the elastic stiffness of a steel girder leading to the reduction in the elastic strain in the tension flange of the girder as compared to an unstrengthened girder at the same load level. Due to these two effects, the live load capacity of a steel girder can be increased using externally bonded CFRP laminates. The following section presents a proposed design philosophy and procedure that can be used to design the CFRP strengthening for steel–concrete composite flexural girders to achieve a desired increase of the live load level of the girder.

- Develop general bridge section;
- Develop typical section and design basis;
- Design conventionally reinforced concrete deck;
- Select appropriate resistance factors [A6.5.4.2];
- Select load modifiers [A1.3.3], [A1.3.4], [A1.3.5];
- Select applicable load combinations;
- Calculate live load force effects [A3.6.1.1.1];
- Calculate force effects from other loads;
- Choose CFRP thickness, width, and length;
- Choose a CFRP configuration (B4 recommended). It is also recommended to cover the whole flange width;

- CFRP length should cover the maximum moment zone in addition to the development lengths;
- CFRP length should cover at least 75% of the girder length;
- Calculate section properties for steel girders with CFRP laminates;
- Design required sections;
- Check flexural stresses for interior and exterior girders;
- Check for deflections;
- Check for fatigue stresses.

6.8   Summary

This chapter discussed two topics: first, simulation work of a typical composite steel concrete bridge using FE models. The models were then used in the evaluation process of the proposed rehabilitation technique using CFRP laminates.

The second part of the chapter was to evaluate the strengthening of steel girder bridges using CFRP plates through solved AASHTO bridge examples. This includes the gain in strength, section modulus, and stiffness of the bridge girders. The reduction of the deflections and the fatigue stress ranges are also discussed. Design guidelines for rehabilitating steel bridges using CFRP were also introduced at the end of the chapter.

Section 7
Summary, Conclusions, and Future Research

7.1 Summary

This research presented the findings of an experimental testing program and finite element parametric study to develop a CFRP laminate system for flexural strengthening of steel beams and steel bridge girders. Based on the experimental findings, a detailed and accurate finite element model was developed to facilitate proper simulation and analysis of the composite steel beams strengthened by CFRP laminates. Several CFRP configurations were presented, and a comparison between all configurations showed the advantages and disadvantages of each configuration. The effectiveness of the strengthening system was demonstrated and the detailed behavior of the strengthened beams was examined.

Consequently, a bridge FE model was developed using SAP 2000. The model was strengthened by CFRP, which enhanced its behavior significantly (20% increase in flexural capacity). The research findings demonstrated the effectiveness of externally bonded CFRP laminates for strengthening and repair of steel structures and bridges.

Throughout the literature review, several rehabilitation techniques were discussed. A historical background was presented on the evolution of the rehabilitation methods, which lead to the use of FRP. Very few studies investigated the rehabilitation using CFRP on steel bridge girders in the USA. All of these studies were either theoretical, or still in the experimentation phase. The current use of CFRP in concrete structural applications was presented. It showed a significant impact on flexural behavior, fatigue, deflection, and column confinement.

The research work in this study presented an experimental program that involved four-point loading tests conducted on five composite beams strengthened by CFRP laminates. An Excel spreadsheet with embedded Visual Basic programming was developed to design steel beams strengthened with CFRP laminates. The Visual Basic modules were developed to calculate the plastic neutral axis location, the plastic moment capacity, and the beam deflections.

Tension testing of steel and CFRP specimens was also conducted to obtain their accurate material properties that were then used for the FE model. The study described the steps executed on order to perform the experimental tests successfully.

The process of developing the FE model conducted using the FE software package ABAQUS. The model had to account for the anisotropic behavior of the CFRP and the adhesive properties of the epoxy that attached the CFRP to the steel beam. Verification of the FE model developed was achieved by comparing the analytical results to the experimental data. A very good correlation was found; therefore, the model was used to develop a parametric study.

An extensive parametric study using the FE model was performed to determine the sensitive parameters affecting the CFRP rehabilitation process. A hundred models were built and executed using the FE program. Parameters investigated were CFRP laminate length, thickness, and configuration. Beam loading, and the steel beam cross-section size were also variable. Results were presented in the form of load deflection charts and in the form of summarized tables showing the strength gain in both the elastic and plastic load range.

In chapter 6, "Bridge Design: Rehabilitation Guidelines", two main topics were discussed. First, the simulation work of a typical composite steel concrete bridge is discussed. The model also showed a significant improvement to the bridges behavior when using CFRP. Second, an example of a bridge designed using the AASHTO code strengthened using CFRP laminates is presented. The chapter concludes by comparing the behavior of the bridge designed with and without CFRP plates. The comparison showed significant improvements in strength, section modulus (increase of 28.6%), stiffness (increase of 11.2%), as well as fatigue (decrease of 15.2%) and deflection responses (decrease of 10.5%). Finally, design guidelines are provided at the end of the chapter.

7.2 Conclusion

Conclusions drawn from this research study can be summarized as follows:

- Steel beams reinforced with CFRP laminates showed a significant increase in flexural capacity reaching 62%, and the beams exhibited satisfactory ductile behavior before laminate debonding.
- Debonding occurred after yielding of the steel beam signifying that bonding was effective during the elastic stage (in the design range of beams and girders).
- At debonding (in the plastic region) it was observed that the beam did not develop a plastic hinge at the point of maximum moment, rather it behaved like the control beam (unreinforced by CFRP) with similar strength and ductility.
- Proper CFRP laminate configuration is essential for maximum gain in enhancing the beams, behavior. Increasing the CFRP laminates does not necessarily enhance the steel beam behavior.
- Substituting the concrete slab with a steel plate is a valid assumption for the experimental work and was verified by FE models.
- FE models using ABAQUS were accurate in predicting the load deflection curve and debonding load.
- The FE models were able to predict the strain versus depth curves for all tested beams.
- The parametric study using the FE model developed showed that the sensitive parameters affecting steel beams reinforced by CFRP laminates are CFRP laminate thickness, CFRP Young's modulus, and CFRP ultimate laminate strength.
- The CFRP laminate length is not an effective parameter as long as the maximum moment zone is covered and appropriate development length is satisfied. Based

on the analytical work, it is recommended that the CFRP laminate length be not less than 75% of the girder length.
- It is recommended that the CFRP laminate width should cover the whole beam soffit.
- The SAP2000 model would be a useful tool for structural engineers to strengthen and/or rehabilitate bridges using CFRP plates.

7.3 Future Research

This research work studied the flexural enhancement of steel beams reinforced with CFRP laminates. The experimental application of the CFRP plates was conducted in the laboratory only. Future research would implement this rehabilitation method on a real bridge, and field testing should be done to evaluate the actual effect on a full-scale bridge structure.

Furthermore, the main mode of failure of steel beams reinforced with CFRP laminates was debonding. Further investigation and experimentation could be performed using different types of adhesives, which may significantly reduce or eliminate the debonding mode of failure.

Section 8
References

AASHTO. (1998). *AASHTO LRFD Bridge Design Specifications.* Washington, D.C.: American Association of State Highway and Transportation Officials.

Abaqus Analysis User Manual. (2007).

ACI Committee, 4. (2003). ACI 440.1R-03, Guide for the Design and Construction of Concrete Reinforced with FRP Bars.

Al-Emrani, M., & Kliger, R. (2006). Experimental and Numerical Investigation of the Behaviour and Strength of Composite Steel-CFRP Members. *Advances in Structural Engineering , 9* (6), 819-831.

Al-Saidy, A. H. (2001). Structural Behaviour of Composite Beams Strengthened/Reparies with Carbon Fiber Reinforced Polymer Plates. Ames, Iowa: Iowa State University.

Al-Saidy, A. H., Klaiber, F. W., & Wipf, T. J. (2004). Repair of steel composite beams with carbon fiber-reinforced plates. *Journal of Composites for Construction, ASCE , 8* (2), 163-172.

Atadero, Lee, L., & Karbhari, V. (2005). Consideration of material variability in reliability analysis of FRP strengthened bridge decks. *Journal of Composite Structures , 70*, 430-443.

Baker, A. (1997). Growth characterization of fatigue cracks repaired with adhesively bonded boron/epoxy composite. (pp. 117-128). Sydney, Australia: Advances in Fracture Research: Proc., 9th Int. Conf. on Fracture.

Basseti, A. N. (2000). Fatigue life extension of riveted bridge members using prestressed carbon fiber composites. *Steel Structures of 2000's, ECCS* , 11-13.

Boyd, C. B. (1997). *A Load-Deflection Study of Fiber Reinforced Plastics as Reinforcement in Concrete Bridge Decks.* Thesis, Virginia Polytechnic Institute and State University, Civil Engineering, Blacksburg, Virginia.

Burgoyne, J. (1999). Advanced Composites in Civil Engineering in Europe. *University of Cambridge.*

Crisfield, M. (1986). Snap-through and snap-back response in concrete structures and the dangers of under-integration. *International Journal for Numerical Methods in Engineering , 22*, 751-767.

Dawood, M. (2005). Fundamental Behaviour of Steel-Concrete Composite beams Strengthened with High Modulus Carbon Reinforced Polymer Materials. Master's Thesis, North Carolina State University, Raleigh, North Carolina.

Deeks, A. J., & Hao, H. (2004). *Development of Mechanics of Structures and Materials.* Perth, Australia: CRC Press.

El Damatty, A. A., Abushagur, M., & Youssef, M. A. (2005). Rehabilitation of Composite Steel Bridges Using GFRP Plates. *Applied Composite Materials, Springer 2005 , 12*, 309-325.

Farhey, D. N., Naghavi, R., Levi, A., Thakur, A. M., Pickett, M. A., Nims, D. K., et al. (2000). Deterioration Assessment And Rehabilitation Design of Existing Steel Bridge. *Journal of Bridge Engineering , 5* (1), 39-48.

Hambly, E. C. (1976). *Bridge Deck Behaviour.* Edinburgh: Chapman and Hall, Ltd.

Hashin, Z. (1980). Failure Criteria for Unidirectional Fiber Composites. *Journal of Applied Mechanics , 47*, 329-334.

Hashin, Z., & Rotem, A. (1973). A Fatigue Criterion for Fiber-Reinforced Materials. *Journal of Composite Materials , 7*, 448-464.

Hillerborg, A. M. (1976). Analysis of crack formation and crack growth in concrete by means of fracture mechanics and finite elements. *Cement Concrete Research , 6*, 773-782.

Jones, R. (1998). Guide to Short Fiber Reinforced Plastics. *Chernow Editorial Services .*

Jones, S. C., & Civjan, S. A. (2003). Application of Fiber Reinforced Polymer Overlays to Extend Steel Fatigue Life. *Journal of Composites for Construction, ASCE , 7*, 331-338.

Karbhari, V. (2005). Building materials for the renewal of civil infrastructure. *Journal of Reinforced Plastics , 49*, 14-25.

Lenwari, A., Thepchatri, T., & Albrecht, P. (2006). Debonding strength of steel beams strengthened with CFRP plates. *Journal of Composites for Construction, ASCE , 10*, 69-78.

Lenwari, A., Thepchatri, T., & Albrecht, P. (2005). Flexural Response of Steel Beams Strengthened with Partial-Length CFRP Plates. *Journal of Composites for Construction, ASCE , 9*, 296-303.

Liu, X., Silva, P., & Nanni, A. (2001). Rehabilitation of Steel Bridge Members with FRP Composite Materials. *Composites in Construction , 613-617.*

McRae, S., & Ramey, G. E. (2003). Rehabilitation of Bridge Superstructures via the addition of Girder Lines I: Theoretical Considerations. *Practice Periodical on Structural Design and Construction , 8* (3), 164-171.

Mertz, D. R., & Gillespie, J. W. (1996). Rehabilitation of steel girders through the application of advance composite materials. Washington D.C: Transportation Research Board.

Naito, C. (2005, May/June). Anchorage of Reinforced Concrete Parapets on Glass Fiber Reinforced Polymer Bridge Decks. *Journal of Composites for Construction, ASCE , 247-254.*

Nezamian, A., & Setunge, S. (2007, September/October). Case Study of Application of FRP Composites in Strengthening the Reinforced Concrete Headstock of a Bridge Structure. *Journal of Composites for Construction, ASCE , 531-544.*

Nozaka, K., Sheild, C., & Hajjar, J. (2005). Design of a test specimen to assess the effective bond length of carbon fiber reinforced polymer strips bonded to fatigued steel bridge girders. *Journal of Composites for Construction, ASCE , 9*, 304-312.

Nozaka, K., Sheild, C., & Hajjar, J. (2005). Effective Bond Length of Carbon-Fiber-Reinforced Polymer Strips Bonded to Fatigued Steel Bridge I-Girders. *Journal of Bridge Engineering, ASCE , 10* (2), 195-205.

Okeil, A. M., El-Tawil, S., & Shahawy, M. (2002, September/October). Flexural Reliability of Reinforced Concrete Bridge Girders Strengthened with Carbon Fiber-Reinforced Polymer Laminates. *Journal of Bridge Engineering, ASCE* , 290-299.

Pantelides, C. P., Cercone, L., & Policelli, F. (2004, January/February). Development of a Specification for Bridge Seismic Retrofit with Carbon Fiber Reinforced Polymer Composites. *Journal of Composites for Construction, ASCE* , 88-96.

Phares, B. M., Wipf, T. J., Klaiber, F. W., Abu-Hawash, A., & Lee, Y.-S. (2003). Strengthening of Steel Girder Bridges Using FRP. Ames, Iowa: Proceedings of the 2003 Mid-Continent Transportation Research Symposium.

QuakeWrap. (2008). Retrieved October 23, 2008, from QuakeWrap: www.quakewrap.com

Ramey, G. E., & Wright, R. L. (1997, August). Bridge Deterioration rates and durability-longetivity performance. *Practice Periodical on Structural Design and Construction , 2* (3), pp. 98-104.

Salama, T., & Abd-El-Meguid, A. S. (2007). Experimentation and Finite Element Analysis of Steel Beams Strengthened by CFRP Laminates. *Proceedings of the 87th Annual Meetings of Transportation Research Board.* Washington D.C.: Transportation Research Board.

SAP 2000. (2008).

Schnerch, D. M. (2007). Proposed design guidelines for strengthening of steel bridges with FRP materials. *Construction and Building Materials , 21* (5), 1001-1010.

Schnerch, D. (2005). Strengthening of steel structures with high modulus carbon fiber reinforced polymer (CFRP) materials. PhD dissertation, North Carolina State University, Raleigh, North Carolina.

Sen, R., Libby, L., & Mullins, G. (2001). Strengthening steel bridge sections using CFRP laminates. *Composites Part B: Engineering , 39*, 309-322.

Shalaby, A. M. (2007). *Development of a New Spun Concrete Pole Reinforced with Carbon Fiber Reinforced Polymer Bars.* Dissertation, University of Alabama at Birmingham, Civil, Construction and Environmental Engineering Department.

Stallings, J. M., Tedesco, J. W., El-Mihilmy, M., & McCauley, M. (2000, May). Field Performance of FRP Bridge Repairs. *Journal of Bridge Engineering* , 107-113.

Stoll, F., Saliba, J. E., & Laura, E. C. (2000). Experimental study of CFRP- prestressed high strength concrete bridge beams. *Journal of Composite Structures , 49*, 191-200.

Swaminathan, S., Pagano, N. J., & Ghosh, S. (2006). Analysis of Interfacial Debonding in Three-Dimensional Composite Microstructures. *Journal of Engineering Materials and Technology , 128*, 96-106.

Tavakkolizadeh, M., & Saadatmanesh, H. (2003). Strengthening of steel-concrete composite girders using carbon fiber reinforced polymer sheets. *Journal of Structural Engineering, ASCE, 129* (1), 30-40.

Wipf, T. J., Phares, B. M., Klaiber, F. W., & Lee, Y. S. (2003). *Evaluation of Post-tension Strengthened Steel Girder Bridge Using FRP Bars.* Iowa: Center for Transportation Research and Education, Bridge Engineering Center, Iowa State University.

Wipf, T., Phares, B., Klaiber, F., Al-Saidy, A., & Lee, Y. (2005, July). Strengthening Steel Girder Bridges with Carbon Fiber-Reinforced Polymer Plates. *Journal of the Transportation Research Board* , 435-447.

Appendices

Appendix A: Plastic Neutral Axis Calculations

```
Function Plastic_NA(Top_Plate_W, Top_Plate_T, D, B_F, T_F, T_W, T_CFRP_W, T_CFRP_T,
B_CFRP_W, B_CFRP_T, F_Y, CFRP_Y) As Double
        Sigma_Force = 0
        Plastic_NA = 0
        F_Top_Plate_1 = 0
        F_Top_Plate_2 = 0
        F_Top_Flange_1 = 0
        F_Top_Flange_2 = 0
        F_Web_1 = 0
        F_Web_2 = 0
        F_CFRP_TOP = 0
        F_Bottom_Flange = 0
        F_CFRP_Bottom = 0

10    Plastic_NA = Plastic_NA + 0.00001 * D

    If Plastic_NA < Top_Plate_T Then                           ' plastic NA in top plate
        F_Top_Plate_1 = -Top_Plate_W * Plastic_NA * F_Y
        F_Top_Plate_2 = Top_Plate_W * (Top_Plate_T - Plastic_NA) * F_Y
        F_Top_Flange_1 = B_F * T_F * F_Y
        F_Top_Flange_2 = 0
        F_Web_1 = (D - 2 * T_F) * T_W * F_Y
        F_Web_2 = 0
        F_CFRP_TOP = T_CFRP_W * T_CFRP_T * CFRP_Y
        F_Bottom_Flange = B_F * T_F * F_Y
        F_CFRP_Bottom = B_CFRP_W * B_CFRP_T * CFRP_Y
    Else
        If Plastic_NA > Top_Plate_T And Plastic_NA < (Top_Plate_T + T_F) Then   ' plastic NA
in top flange
            F_Top_Plate_1 = -Top_Plate_W * Top_Plate_T * F_Y
            F_Top_Plate_2 = 0
            F_Top_Flange_1 = -B_F * (Plastic_NA - Top_Plate_T) * F_Y
            F_Top_Flange_2 = B_F * (Top_Plate_T + T_F - Plastic_NA) * F_Y
            F_Web_1 = (D - 2 * T_F) * T_W * F_Y
            F_Web_2 = 0
            F_CFRP_TOP = T_CFRP_W * T_CFRP_T * CFRP_Y
            F_Bottom_Flange = B_F * T_F * F_Y
            F_CFRP_Bottom = B_CFRP_W * B_CFRP_T * CFRP_Y
        Else                                                     ' plastic NA in Web
            F_Top_Plate_1 = -Top_Plate_W * Top_Plate_T * F_Y
            F_Top_Plate_2 = 0
            F_Top_Flange_1 = -B_F * T_F * F_Y
            F_Top_Flange_2 = 0
```

```
        F_Web_1 = -T_W * (Plastic_NA - Top_Plate_T - T_F) * F_Y
        F_Web_2 = T_W * (D - 2 * T_F - Plastic_NA + Top_Plate_T + T_F) * F_Y
        F_CFRP_TOP = T_CFRP_W * T_CFRP_T * CFRP_Y
        F_Bottom_Flange = B_F * T_F * F_Y
        F_CFRP_Bottom = B_CFRP_W * B_CFRP_T * CFRP_Y
    End If
  End If

  Sigma_Force = F_Top_Plate_1 + F_Top_Plate_2 + F_Top_Flange_1 + F_Top_Flange_2 +
F_Web_1 + F_Web_2 + F_CFRP_TOP + F_Bottom_Flange + F_CFRP_Bottom
  If Abs(Sigma_Force) > 0.5 Then GoTo 10

  End Function
```

Appendix B: Plastic Moment Capacity Calculations

```
Function M_Plastic(Top_Plate_W, Top_Plate_T, D, B_F, T_F, T_W, T_CFRP_W, T_CFRP_T,
B_CFRP_W, B_CFRP_T, F_Y, CFRP_Y, NA) As Single
      M_Plastic = 0
      M_Top_Plate_1 = 0
      M_Top_Plate_2 = 0
      M_Top_Flange_1 = 0
      M_Top_Flange_2 = 0
      M_Web_1 = 0
      M_Web_2 = 0
      M_CFRP_TOP = 0
      M_Bottom_Flange = 0
      M_CFRP_Bottom = 0

   If NA < Top_Plate_T Then                                  ' plastic NA in top plate
      M_Top_Plate_1 = Top_Plate_W * NA * F_Y * 0.5 * NA
      M_Top_Plate_2 = Top_Plate_W * (Top_Plate_T - NA) * F_Y * 0.5 * (Top_Plate_T -
NA)
      M_Top_Flange_1 = B_F * T_F * F_Y * (Top_Plate_T - NA + 0.5 * T_F)
      M_Top_Flange_2 = 0
      M_Web_1 = (D - 2 * T_F) * T_W * F_Y * (Top_Plate_T - NA + T_F + 0.5 * (D - 2 *
T_F))
      M_Web_2 = 0
      M_CFRP_TOP = T_CFRP_W * T_CFRP_T * CFRP_Y * (Top_Plate_T - NA + D - T_F - 0.5
* T_CFRP_T)
      M_Bottom_Flange = B_F * T_F * F_Y * (Top_Plate_T - NA + D - 0.5 * T_F)
      M_CFRP_Bottom = B_CFRP_W * B_CFRP_T * CFRP_Y * (Top_Plate_T - NA + D + 0.5
* B_CFRP_T)
    Else
      If NA > Top_Plate_T And NA < (Top_Plate_T + T_F) Then   ' plastic NA in top flange
         M_Top_Plate_1 = Top_Plate_W * Top_Plate_T * F_Y * (NA - 0.5 * Top_Plate_T)
         M_Top_Plate_2 = 0
         M_Top_Flange_1 = B_F * (NA - Top_Plate_T) * F_Y * 0.5 * (NA - Top_Plate_T)
         M_Top_Flange_2 = B_F * (Top_Plate_T + T_F - NA) * F_Y * 0.5 * (Top_Plate_T +
T_F - NA)
         M_Web_1 = (D - 2 * T_F) * T_W * F_Y * (Top_Plate_T + T_F - NA + 0.5 * (D - 2 *
T_F))
         M_Web_2 = 0
         M_CFRP_TOP = T_CFRP_W * T_CFRP_T * CFRP_Y * (Top_Plate_T - NA + D - T_F -
0.5 * T_CFRP_T)
         M_Bottom_Flange = B_F * T_F * F_Y * (Top_Plate_T - NA + D - 0.5 * T_F)
         M_CFRP_Bottom = B_CFRP_W * B_CFRP_T * CFRP_Y * (Top_Plate_T - NA + D +
0.5 * B_CFRP_T)
      Else                                                    ' plastic NA in Web
```

```
        M_Top_Plate_1 = Top_Plate_W * Top_Plate_T * F_Y * (NA - 0.5 * Top_Plate_T)
        M_Top_Plate_2 = 0
        M_Top_Flange_1 = B_F * T_F * F_Y * (NA - Top_Plate_T - 0.5 * T_F)
        M_Top_Flange_2 = 0
        M_Web_1 = T_W * (NA - Top_Plate_T - T_F) * F_Y * 0.5 * (NA - Top_Plate_T -
T_F)
        M_Web_2 = T_W * (D - T_F - NA + Top_Plate_T) * F_Y * 0.5 * (D - T_F - NA +
Top_Plate_T)
        M_CFRP_TOP = T_CFRP_W * T_CFRP_T * CFRP_Y * (D - T_F - NA + Top_Plate_T -
0.5 * T_CFRP_T)
        M_Bottom_Flange = B_F * T_F * F_Y * (D - 0.5 * T_F - NA + Top_Plate_T)
        M_CFRP_Bottom = B_CFRP_W * B_CFRP_T * CFRP_Y * (D - NA + Top_Plate_T +
0.5 * B_CFRP_T)
      End If
   End If

   M_Plastic = M_Top_Plate_1 + M_Top_Plate_2 + M_Top_Flange_1 + M_Top_Flange_2 +
M_Web_1 + M_Web_2 + M_CFRP_TOP + M_Bottom_Flange + M_CFRP_Bottom

End Function
```